Durham E-Theses

The mass-dependent stable osmium isotope system - Method development and application to high-temperature systems

NANNE, JOSEFINE,AGNES,MARIA

How to cite:

NANNE, JOSEFINE,AGNES,MARIA (2018) *The mass-dependent stable osmium isotope system - Method development and application to high-temperature systems*, Durham theses, Durham University. Available at Durham E-Theses Online: http://etheses.dur.ac.uk/12649/

Use policy

The Mass-dependent Stable Osmium Isotope System

Method development and application to high-temperature systems

Josefine Agnes Maria (Fienke) Nanne

A thesis submitted in partial fulfilment of the requirements for the degree of:

DOCTOR OF PHILOSOPHY

at Durham University, UK

Supervisory Team

Dr. Helen M. Williams, currently at the University of Cambridge
Dr. Marc-Alban Millet, currently at Cardiff University
Prof. Kevin W. Burton
Dr. Chris W. Dale

- ABSTRACT -

Josefine A.M. Nanne – The stable osmium isotope system.

This PhD thesis reports the development and application of a new geochemical tool; stable isotopes of osmium (Os) and their mass-dependent fractionation. Osmium is of interest because it holds some very specific characteristics (e.g. highly siderophile, refractory, chalcophile under mantle conditions) that makes it of interest for examining key processes in geo- and cosmo- sciences. Previous studies have explored the abundance of Os, the radiogenic Os isotopes, and mass-independent Os anomalies. However, no previous study has explored the stable isotopes of Os in a mass-dependent manner. The first objective of this thesis, which will be presented in chapter 2, was to develop a method that is capable of resolving variations in Os stable isotopes. After a method was developed that has been shown to provide high precision and reproducible stable Os isotope compositions, it was applied to various rock types to examine key and current questions within geosciences. Specifically, focus was put on examining the abundance of highly siderophile elements in the Earth's mantle and an attempt was made to unravel the processes associated with metal core crystallization. To this end, the stable Os isotope composition of chondrites, Earth's mantle samples, and iron meteorites have been constrained. The outcome of these studies is presented in chapters 3 and 4. Chondrite data show that the bulk solar nebula composition holds a homogeneous composition. Earth's mantle samples are on average similar to chondrites, which is consistent with the late veneer model for Earth's highly siderophile element budget. Iron meteorites yield significant stable Os isotope variation, showing that planetary core solidification generates significant stable Os isotope variability. The latter provides new insights in the crystallization history of planetary cores, showing the strong potential of mass-dependent Os isotopes as a new geochemical tool.

TABLE OF CONTENTS

CHAPTER 1   1

Introduction

CHAPTER 2   17

High Precision Osmium Stable Isotope Measurements by Double Spike MC−ICP−MS and N−TIMS.

CHAPTER 3   61

The Osmium Stable Isotope Composition of Chondrites and Earth's Mantle

Implications for Planetary Formation and Differentiation

CHAPTER 4   101

The Osmium Stable Isotope Compositions of Magmatic Iron Meteorites

Implications for Planetary Core Evolution

CHAPTER 5   137

Synthesis and Outlook

LIST OF FIGURES

CHAPTER 4

CHAPTER 5

No Figures.

LIST OF TABLES

CHAPTER 1

No Tables.

CHAPTER 2

CHAPTER 3

CHAPTER 4

CHAPTER 5

No Tables.

DECLARATION

I declare that the work presented in this thesis, submitted for the degree of Doctor of Philosophy at Durham University, is the result of my own original research. I have clearly indicated, when appropriate, the contributions of colleagues and have made every effort to acknowledge all collaborative work. To the best of my knowledge, this thesis is distinct from any previously submitted or published work at this University or any other institution.

Josefine A. M. Nanne

Durham University

August, 2017

ACKNOWLEDGEMENTS

Such a project cannot be tackled alone, and luckily I did not have to. To all the people involved I would like to say a big "THANK YOU!".

A big "Thank you" goes of course to my supervisors and co-authors for their support, scientific insight, encouragement and advice throughout. I am very grateful that I could always knock on their doors for questions and for discussing data. Helen, thank you for allowing me to be part of a great team. Marc, thank you for your inspiring enthusiasm. Kevin, thank you for looking at problems with a clear and simple view. Geoff, thank you for maintaining a great lab. Chris, thank you for looking at written pieces with a lot of detail.

Next to my supervisors, I would like to thank my internal reviewers, Jeroen van Hunen and Madeleine Humphreys for keeping me on track. Thank you for providing me with a clear focus on the progress of my PhD and preventing me from getting carried away in gathering more and more data. I would also like to thank all the admin staff for their support.

In the lab I had to tackle various new techniques for which I have received valuable help from Dave Selby, Adam Sproson, Eddy Dempsey, Alice du Vivier, and Jo Peterkin (great music as well). Chris Ottley is thanked for tackling problems with my "friend" the HPA machine, Ian Chaplin for sample preparation, and Steven Lishman and his team for cutting of iron meteorites. Thanks a lot for your support.

In order to keep my mind "healthy" and "balanced", I have a lot of thanks for a few incredible groups. Thanks to everyone of Newcastle Vikings Handball Club, Durham Choral Society, and of course Ustinov Womens Football Club (GO UNICORNS!). Not only was it great to be part of these groups, I am also very lucky to have received a lot of support from friends and family. To my 214 Family and friends at Ustinov, thank you for providing me with a warm home to get back to after a long day at work. A big thanks also goes to all the people at work that have made the department an enjoyable environment to work in. Definitely not to forget, I would like to thank my friends at "home" for coming to visit me and being there when I needed a break. And then suddenly, there was a new family to be part of – the Cosmo-isotopes of Münster. The move to Germany and the end of my thesis has certainly been made easier by you guys – thanks! Also the patience of Thorsten Kleine is very much appreciated.

– CHAPTER 1 –

Introduction

PREFACE

Recent years have seen rapid advances in stable isotope geochemistry, with more and more elements being investigated. The novel elements, as well as the more traditional (C-H-O-N-S), have provided a wealth of information that has led to a better understanding of many bio-, geo-, and cosmo-logical processes. In this thesis, the potential of osmium stable isotopes to examine questions in geo- and cosmo-chemistry is explored.

This chapter provides general background information about the main research areas of this thesis: stable isotope geochemistry and the element osmium. Subsequently, the contribution of this thesis to these research areas is outlined with discussion of the various objectives that will be addressed. Finally, the relevance of each chapter to the overall research goals of this thesis will be explained and the contributions of co-authors are clarified.

CONTENT CHAPTER 1

1. RESEARCH AREAS

1.1 STABLE ISOTOPES

1.1.1 History and Current Stage of Research

Stable isotope geochemistry found its origin in the 1930-40's when the first instruments capable of detecting individual isotopes were developed. The first elements analysed were the light isotopes; H, C, N, O, and S, for which variations in stable isotope compositions are large and, as such, easier to detect. They are referred to as "traditional" stable isotopes. With time, techniques and instruments have seen dramatic advances, in particular since the advent of multi-collector inductively coupled plasma mass spectrometry (MC-ICP-MS; Halliday et al., 1995), allowing for the detection of ever smaller isotope variations. This has led to a significant expansion of the field of stable isotope research (**Figure 1-1**) as changes in isotope composition even for some of the heaviest elements could be observed (e.g., U - Stirling et al., 2007; Tl - Rehkämper and Halliday, 1999). Discoveries of natural mass-dependent isotope fractionation in these so-called "non-traditional" stable isotopes, benefiting from their different geochemical behaviour, have provided new, unique ways by which to examine geo-, cosmo-, and bio-chemical processes. Recently, the current stage of research for a large range of non-traditional elements has been reviewed in a publication of RIMG by Teng et al. (2017) and was previously summarized by Johnson et al. (2004).

Figure 1-1 Periodic table in which "traditional" stable isotopes are highlighted in yellow and "non-traditional" isotopes are indicated in blue, clearly showing the large expansion of the stable isotope field. Osmium, indicated in purple, has until this study not been considered in terms of mass-dependent isotope fractionation.

1.1.2 Theoretical Background

Isotope fractionation refers to the difference in isotope composition between various compounds or phases that can result from equilibrium or non-equilibrium ("kinetic") processes. The theoretical background behind equilibrium, mass-dependent, stable isotope fractionation was established by Bigeleisen and Mayer (1947) and Urey (1947). The theory predicts that the extent of isotope fractionation is proportional to the isotopic mass difference and it shows that fractionation arises from differences in vibrational energy levels of constituent atoms. As such, fractionation is driven by changes in the bonding environment with the heavier isotopes preferring stiffer bonds related to an high force constant. Chemical reactions or phase changes cause a change in the bonding environment which, consequently, results in preferential partitioning of heavy isotopes relative to light isotopes between specific environments. Parameters controlling the type of bonding are, for example, the oxidation or coordination state where the isotopically heavier species are, generally, associated with a lower coordination and higher oxidation states of the element of interest (e.g., Schauble, 2004). This dependency is used to place constraints on the conditions under which processes have taken place. Kinetic fractionation refers to processes where the effective transport is unidirectional due to differences in reaction or transport rate. Common processes that show this behaviour are diffusion, evaporation, and condensation. The reaction rate or rate of change, and hence the degree to which isotopes are fractionated, is controlled by physical parameters such as temperature, pressure, and oxygen fugacity.

1.1.3 Determination of Mass-dependent Isotope Compositions

Isotope measurements are performed by mass-spectrometry and, consequently, are subject to instrumental mass fractionation. This induced fractionation should be corrected in order to derive the natural fractionation. The most commonly used correction method is sample-standard (smp-std) bracketing (ssb), whereby measurements of unknown samples are intercalated with measurements of a reference standard. The stable isotope composition is then calculated as the difference between the measured isotope ratio of the sample and that of the average of the bracketing standards. The assumption made here is that instrumental mass bias is identical for sample and standard. However, the presence of residual chemical matrices in samples can lead to inaccurate results. To quantify the uncertainty, additional analyses are required which is time consuming. Doping samples with an element that exhibits similar mass bias behaviour to the element of interest is another method that can correct for instrumental mass fractionation. The assumption made in this case is that the doped element fractionates in an identical manner to the element of interest, with the extent of isotope fractionation depending purely on isotope mass. In the case of radiogenic isotopes, the ratio of two stable non-radiogenic isotopes can be used to correct for instrumental mass fractionation. However, this approach uses a constant stable isotope ratio and, consequently, corrects for both natural and induced stable isotope fractionation. In order to avoid this and resolve natural stable isotope fractionation from instrumental mass fractionation effects, the double spike (DS) technique can be employed (Dodson, 1963). The key advantage of this technique is that the isotope ratios of a measurement are used to constrain instrumental mass bias
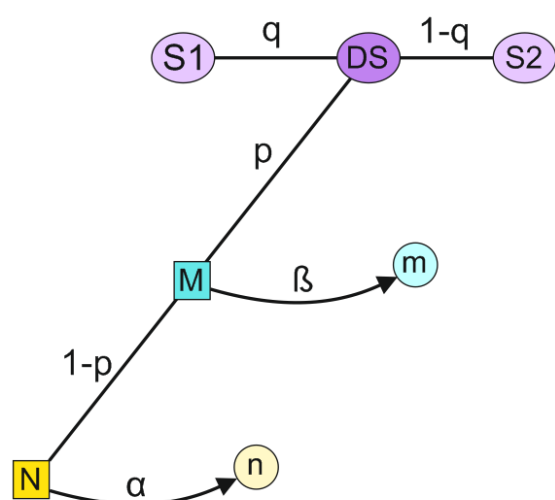
Figure 1-2 Schematic diagram showing the parameters involved in the double spike technique. It illustrates how the double spike (DS), which is composed by mixing two single spikes (S1 and S2) in the most optimal proportions (q to $1-q$), is mixed with the sample of interest (N) in relative quantities "p" and "$1-p$", to end up with a mixture (M). It, furthermore, illustrates that if this mixture is analysed by aid of mass spectrometry, the isotopic composition is changed by induced mass fractionation (β) to "m", similar as that the sample has been influenced by natural fractionation (α). The fractionation can only be expressed as a relative measure, and as such "n" represents the composition of the reference material to which isotopic composition of the natural sample is compared. Figure adjusted after Rudge et al. (2009).

explicitly for the sample examined. The DS method is, therefore, more robust to variable instrumental conditions and does not rely on assumptions of similar fractionation behaviour which, in the case of residual matrix effects, is especially hard to assess by smp-std bracketing. Furthermore, the DS method does not require the presence of a well-established isotope ratio, and if the DS is added prior to sample digestion, any fractionation taking place during digestion and chemical separation can be corrected for. This is impossible using the other two methods and a 100% yield or no fractionation has to be assumed. The DS technique is, therefore, ideally suited and commonly used to study non-traditional stable isotope systems (e.g., Siebert et al., 2001; Millet et al., 2012; Creech et al., 2013; Hopp et al., 2016).

The technique works as follows, the sample is mixed with a tracer enriched in two isotopes of an element in a known ratio; the double spike. Complete spike-sample equilibration is required. By assuming that the sample and standard of reference are related to each other by mass-dependent fractionation following an exponential law, it is possible to calculate the instrumental mass bias from mass spectrometry data, thereby deriving the natural fraction (**Figure 1-2**). Parameters required to accomplish the calculations are (1) the measured sample-DS mixture composition; (2) the composition of the reference standard and double spike; (3) the natural logarithm of the ratio of the isotopic masses. These parameters are taken as input values for a non-linear equation that can be resolved by iterative methods (e.g., Rudge et al., 2009). As the equation contains three unknowns, three isotope ratios are required to resolve the unknown parameters.

1.1.4 Notation of Stable Isotope Compositions

The magnitude of mass-dependent isotope fractionation is often limited and as such is reported, most commonly, in parts per thousand, or per mil (‰). The variation of a sample is expressed relative to a standard of reference following an equation of this format:

$$\delta^{i/j}Os_{std} = \left(\frac{R_{sample}}{R_{standard}} - 1\right) * 1000$$

, where R is the isotopic ratio of interest for the sample measured and the standard solution used for reference, and i and j are the isotopic masses used in this ratio.

1.2 THE ELEMENT OSMIUM

1.2.1 Discovery of Osmium

The element osmium (Os) was discovered by S Tennant in 1803 and is named after the Greek "Osme" meaning odour. With time, Os was found to comprise seven naturally occurring isotopes, ^{184}Os, ^{186}Os, ^{187}Os, ^{188}Os, ^{189}Os, ^{190}Os, ^{192}Os, with relative isotopic abundances of 0.02%, 1.59%, 1.96%, 13.24%, 16.15%, 26.26%, 40.78% (de Laeter et al., 2003). The six major isotopes of osmium were first reported by Aston in 1931 (Aston, 1931) and the rare isotope, ^{184}Os, was discovered by Nier in 1937 (Nier, 1937). Two Os isotopes are radiogenic, ^{187}Os isotope which is formed by beta decay of ^{187}Re ($t_{1/2}$= 41.6 Ga; Smoliar et al., 1996; Selby et al., 2007) and ^{186}Os which is produced from ^{190}Pt via alpha emission ($t_{1/2}$= 449.4 Ga; Walker et al., 1997). Recently, the potential alpha decay of ^{184}Os to ^{180}W has been discussed (Peters et al., 2014; Cook et al., 2015).

1.2.2 Characteristics of Osmium

Osmium is a Group VIII transition element and one of the Platinum Group Elements (PGE; Ru, Rh, Pd, Os, Ir and Pt). The PGE tend to exist in metallic state or bond with chalcogens (S, Se, Te) or pnictogens (P, As, Sb, Bi). Following the Goldschmidt element geochemical characteristic classification, osmium is a highly siderophile element (HSE). This means that Os has a strong tendency to partition into metallic iron relative to silicate phases, the hydrosphere, or the atmosphere. The HSE are highly refractory, which for Os is reflected in a melting point of 3306 K and a 50% condensation temperature of 1812 K (at 10^{-4} atm; Lodders, 2003). Osmium also displays chalcophile behaviour, and tends to strongly partition into sulphide melts and sulphide minerals. During mantle melting it behaves as a compatible element – primarily due to its affinity for sulphide – and is, therefore, preferentially retained in the melting residue, i.e., in the mantle relative to the crust. Osmium can form compounds with variable oxidation states of +8, +6, +4, +3, +2, 0, and -2. In natural geological systems, it is most stable as 0, and +4.

1.2.3 Determination of Osmium Isotope Ratios

The first osmium isotopic measurements were accomplished in the 1980's and focused on the [187]Re-[187]Os isotope system (e.g., Allègre and Luck, 1980; Luck et al., 1980). Techniques utilized included secondary ion mass spectrometry (SIMS) and resonance ionization mass spectrometry (RIMS). Inductively coupled plasma mass spectrometry (ICPMS) also proved to be an ideal technique to efficiently ionize Os (e.g., Russ et al., 1987) and became more common after optimizing the introduction system (e.g., Pearson and Woodland, 2000; Schoenberg et al., 2000). The high ionization potentials of Os (8.7 eV) prevents formation of positively charged metallic ions at the temperatures typically attainable by thermal ionization mass spectrometry. In 1991, the discovery was made that Os could be very efficiently ionised in the form of oxide anions, OsO_3^-, by negative thermal ionization mass spectrometry (N-TIMS; Creaser et al., 1991; Völkening et al., 1991). This technique significantly improved measurement precision and allowed for a larger range of materials to be investigated. In parallel, analytical improvements were made in the digestion techniques, with important implications for the full chemical equilibration between spike and sample (e.g., Shirey and Walker, 1998), and advances in chemical separation techniques (Cohen and Waters, 1996; Birck et al., 1997). These advances were of particular interest for utilizing the Pt-Os decay system as variations in radiogenic [186]Os are substantially smaller than for radiogenic [187]Os.

1.2.4 Use of Osmium in Geoscience

The highly siderophile characteristic of Os has made it a key tracer of planetary accretion and differentiation processes. Another key aspect of Os are the decay systems, Re-Os and Pt-Os, which have been utilized as geochronometers and source tracers for studying geological and cosmological processes. To give a better idea of the wide variety of topics for which Os data has been key, a few of the numerous studies will be outlined below.

Experimental studies have shown that fractionation between Re-Os and Pt-Os takes place during metal-silicate segregation (e.g., Brenan et al., 2005; Brenan and McDonough, 2009). This behaviour has been used to understand the HSE abundance of the Earth's mantle (e.g., Brenan and McDonough, 2009; Maier et al., 2009). One important hypothesis to originate from these studies is the "Late Veneer" hypothesis (Kimura et al., 1974), which will be addressed in Chapter 3. This hypothesis originates from the observation that the HSE abundance of the Earth's mantle is inconsistent with experimentally determined metal-silicate differentiation coefficients. Key observations that support the hypothesis are a similar [187]Re-[187]Os and [190]Pt -[186]Os isotopic evolution for chondrites as for the Earth's primitive upper mantle (e.g., Meisel et al., 2001; Brandon et al., 2006). Fractionation, of Re and Pt relative to Os, also takes place during fractional crystallization of a metallic core. As a result, the [187]Re-[187]Os and [190]Pt -[186]Os decay systems have been utilized for dating the crystallization of asteroidal cores (e.g., Hirt et al., 1963; Smoliar et al., 1996; Cook et al., 2004; McCoy et al., 2011). A further process that fractionates Re from Os is mantle melting, with Os being highly compatible whereas Re is

behaving incompatible. Mantle melting is one of the dominant processes governing the distribution of these elements between the Earth's crust and mantle (Burton et al., 2002). Pearson et al. (2007) showed that mantle depletion events are related to peaks in the generation of continental crust, which supports models of continental growth that result from large-scale mantle melting events. Other studies have shown that additional Os isotopic evidence for ancient melting events can be derived from single sulphide grains (Burton et al., 2000; Harvey, 2005). This is because sulphides, which have a strong control on the osmium budget of mantle rocks (e.g., Lorand and Luguet, 2016), can be effectively shielded from diffusion processes by their silicate hosts (Burton et al., 1999). In addition to mantle melting and melt extraction processes, recycling of oceanic crust and/or lithosphere following subduction contributes greatly to the chemical heterogeneity of the mantle. Previous studies have examined the behaviour of the Re-Os system during subduction (Brandon et al., 1996; Suzuki et al., 2011), and the implications for crustal recycling (Dale et al., 2007). Contrary to previously assumptions of Os immobility, it seems that under oxidizing conditions Os behaves as a mobile element and as such can be transferred in to the mantle wedge (Brandon et al., 1996; Suzuki et al., 2011). Another observation that is in contrast with the generally assumed immobile and compatible behaviour of Os, is the mobilization of Os during metasomatism as a result of chemical reaction of melt or fluid percolation through the mantle (e.g., Handler et al., 1999; Büchl et al., 2002). It is evident that, in order to interpret variations in abundance and more precise use of the Re-Os decay system, a better understanding of the behaviour of osmium during Earth processes is required. This understanding, moreover, is essential for obtaining a primitive signature of the silicate portion of Earth. Apart from the radiogenic isotopes, some studies have focussed on mass-independent stable isotopic anomalies (e.g., Yokoyama et al., 2007). Contrary to other isotope systems (e.g., Mo –Dauphas et al., 2002; Burkhardt et al., 2011; Ru –Chen et al., 2010), no anomalies are observed on a bulk rock scale. However, acid leachates and residues of chondrites have been shown to preserve Os isotope anomalies hosted in presolar grains and of nucleosynthetic origin (Yokoyama et al., 2007; Reisberg et al., 2009; Yokoyama et al., 2010).

In this thesis, the focus is placed on the application of stable Os isotopes to high-temperature processes. It must, however, be noted that Os is also an interesting element for examining a multitude of low-temperature geological processes. For example, radiogenic Os isotopes have been used to trace anthropogenic inputs to costal sediments (e.g., Esser and Turekian, 1993) and provide an excellent record of palaeo-oceanographic changes (e.g., Burton et al., 1999; Peucker-Ehrenbrink and Ravizza, 2000; Cohen, 2004). This has led, amongst others, to a better understanding of ocean circulation (e.g., Du Vivier et al., 2014), volcanism (e.g., Ravizza and Peucker-Ehrenbrink, 2003), and continental weathering (e.g., Ravizza et al., 2001) through time. In industry, Os is used as a biosensor for food quality control (e.g., Antiochia et al., 2013) and for clinical diagnostic procedures (e.g., Jeon et al., 2013). Furthermore, it is used as a catalyst in chemical processes and for the production of very hard alloys. Understanding the formation of ore deposits is, therefore, of high economic interest and as such intensively studied (e.g., Barnes and Ripley, 2016).

2. THESIS OBJECTIVES

The main aim of this thesis has been to explore the potential that stable osmium isotopes hold to investigate geo- and cosmological processes. In order to do this, the first objective that had to be realised was to:

    (1)   Develop analytical techniques capable of resolving variations in stable osmium isotope compositions.

Considering the relatively large mass difference (~2%) between the abundant heavy and light Os isotopes, coupled with the capacity of this element to possess various redox states, osmium has the potential to exhibit significant stable isotope variations. The high mass of Os isotopes means that isotope variations will be limited, even more so when investigating high-temperature processes. That it is still worthwhile to do so, is shown by the observation of mass-dependent stable isotope fractionation for other high-mass elements. Using the different technical developments, outlined above, to our advantage, it is now possible to measure and resolve variations of the magnitude that might exist in the natural environment.

With the development of this new method for measuring Os stable isotopes, the next step was to actually explore the potential of this novel system. In this thesis, focus has been placed on two key high-temperature processes in geo- and cosmo-sciences, i.e., planetary differentiation and subsequent core evolution. More specifically, this thesis has addressed:

    (2)   The origin of the highly siderophile element (HSE) budget of the Earth's mantle.

    (3)   The processes associated with the crystallization of planetary, metallic cores.

The highly siderophile characteristic of Os, combined with its refractory and immobile behaviour, makes it a powerful element for the investigation of these processes. A more detailed reasoning for the investigation of these topics is provided in the relevant chapters.

3. THESIS OUTLINE

This thesis comprises three research chapters each representing an individual study that addresses one of the objectives described above. A final chapter summarizes the main conclusions and returns to the overall objectives of this thesis. The following sections provide a synopsis of Chapter 2-5 and describe how they relate to the overall thesis research aims. In case of co-authors, their contributions will be clarified. Other support that was provided along the way has been acknowledged at the end of each chapter.

Chapter 2 – The first data chapter outlines the work that has been accomplished to set-up the methodology that enables osmium stable isotope measurements at high precision. This involved combining state-of-the-art chemical and analytical techniques specifically for the measurement of osmium stable isotopes. Various tests will be discussed that were accomplished to demonstrate the robustness of the method against any potential sources of inaccuracy, using various reference solutions and geological materials. These analyses were also used to assess the reproducibility, precision, and accuracy that can be achieved for these Os isotope

measurements. Finally, the first stable Os isotope data for geological materials are presented and an estimate of the upper mantle value of the Earth is provided.

An adjusted version of this chapter has been published in *Journal of Analytical Atomic Spectrometry*. Co-authors are; M.-A. Millet, K.W. Burton, C.W. Dale, G.M. Nowell., and H.M. Williams. After publication, an addendum has been added to this chapter that resolves the lower $^{186}Os/^{188}Os$ data. Together with Marc-Alban Millet and Helen Williams I formulated the Os double spike. Chris Dale provided assistance during the first chemical and analytical procedures, and Geoff Nowell gave guidance during analytical work. The calculations for the optimal double spike composition as well as for the double spike calibration were performed by Marc-Alban Millet. All sample processing, analyses, data filtering and processing were accomplished by myself, in parts in collaboration with Marc-Alban Millet. I wrote the manuscript in its entirety and compiled figures, which was subsequently improved by comments of all co-authors.

Chapter 3 – Chapter 3 presents the first ever study to utilize stable Os isotopes and relates to the second objective of this study; investigation of the HSE budget of the Earth's mantle. To this end, a diverse range of chondrites, primitive meteorites that are thought to resemble building blocks of planetary bodies, and a suite of different terrestrial mantle samples have been characterized in terms of their stable Os isotope composition. Since we are dealing with a newly developed method, extra attention was paid to assess data quality. Subsequently, the behaviour of stable Os isotopes within the different groups is discussed. Finally, the implications for the origin of Earth's HSE abundance will be addressed.

The aim is to submit an adjusted version of this chapter to Geochimica et Cosmochimica Acta. Co-authors on this paper will be; M.-A. Millet, K.W. Burton, C.W. Dale, J. Harvey, H.M. Williams. I have been involved in all sample processing, data collection and data processing. Marc-Alban Millet has arranged meteoritic material from the Field Museum, Chicago, and was involved in processing and analysing some of the chondrite samples. Jason Harvey provided terrestrial sample materials and Kevin Burton some chondrite samples. All co-authors have contributed to data interpretation. The chapter was written and figures were compiled by myself, which subsequently was improved by constructive comments of all co-authors.

Chapter 4 – In Chapter 4, the stable osmium isotope compositions of magmatic iron meteorites, Fe-Ni alloys that sample the cores of differentiated planetary bodies, are presented. It is shown that iron meteorites possess resolvable variations in their Os stable isotope composition. By modelling the potential effect of metal fractional crystallization on the stable Os isotope composition, arguments are provided for mixing of early and late crystallized components during solidification of planetary cores. In order to publish this data chapter as a journal paper, more data will need to be obtained.

Chapter 5 - In the final chapter, Chapter 5, all work presented in this thesis will be summarized. The main conclusions are highlighted and discussed in the context of the main objectives of this study. Where more research is thought to be required, this will be discussed and suggestions will be made to improve the current stage of research. Furthermore, potentially rewarding future research topics will be considered.

REFERENCES

Allègre, C. J., and Luck, J.-M., 1980, Osmium isotopes as petrogenetic and geological tracers: Earth and Planetary Science Letters, v. 48, no. 1, p. 148-154.

Antiochia, R., Vinci, G., and Gorton, L., 2013, Rapid and direct determination of fructose in food: a new osmium-polymer mediated biosensor: Food chemistry, v. 140, no. 4, p. 742-747.

Aston, F. W., 1931, Constitution of Osmium and Ruthenium: Nature, v. 127, p. 233.

Barnes, S.-J., and Ripley, E. M., 2016, Highly siderophile and strongly chalcophile elements in magmatic ore deposits: Reviews in Mineralogy and Geochemistry, v. 81, no. 1, p. 725-774.

Bigeleisen, J., and Mayer, M. G., 1947, Calculation of equilibrium constants for isotopic exchange reactions: The Journal of Chemical Physics, v. 15, no. 5, p. 261-267.

Birck, J. L., Barman, M. R., and Capmas, F., 1997, Re-Os Isotopic Measurements at the Femtomole Level in Natural Samples: Geostandards Newsletter, v. 21, no. 1, p. 19-27.

Brandon, A. D., Creaser, R. A., Shirey, S. B., and Carlson, R. W., 1996, Osmium recycling in subduction zones: Science, v. 272, no. 5263, p. 861-863.

Brandon, A. D., Walker, R. J., and Puchtel, I. S., 2006, Platinum–osmium isotope evolution of the Earth's mantle: Constraints from chondrites and Os-rich alloys: Geochimica et Cosmochimica Acta, v. 70, no. 8, p. 2093-2103.

Brenan, J. M., and McDonough, W. F., 2009, Core formation and metal-silicate fractionation of osmium and iridium from gold: Nature Geosci, v. 2, no. 11, p. 798-801.

Brenan, J. M., McDonough, W. F., and Ash, R., 2005, An experimental study of the solubility and partitioning of iridium, osmium and gold between olivine and silicate melt: Earth and Planetary Science Letters, v. 237, no. 3, p. 855-872.

Büchl, A., Brügmann, G., Batanova, V. G., Münker, C., and Hofmann, A. W., 2002, Melt percolation monitored by Os isotopes and HSE abundances: a case study from the mantle section of the Troodos Ophiolite: Earth and Planetary Science Letters, v. 204, no. 3, p. 385-402.

Burkhardt, C., Kleine, T., Oberli, F., Pack, A., Bourdon, B., and Wieler, R., 2011, Molybdenum isotope anomalies in meteorites: Constraints on solar nebula evolution and origin of the Earth: Earth and Planetary Science Letters, v. 312, no. 3–4, p. 390-400.

Burton, K., Schiano, P., Birck, J.-L., Allegre, C., Rehkämper, M., Halliday, A., and Dawson, J., 2000, The distribution and behaviour of rhenium and osmium amongst mantle minerals and the age of the lithospheric mantle beneath Tanzania: Earth and Planetary Science Letters, v. 183, no. 1, p. 93-106.

Burton, K. W., Gannoun, A., Birck, J.-L., Allègre, C. J., Schiano, P., Clocchiatti, R., and Alard, O., 2002, The compatibility of rhenium and osmium in natural olivine and their behaviour during mantle melting and basalt genesis: Earth and Planetary Science Letters, v. 198, no. 1, p. 63-76.

Burton, K. W., Schiano, P., Birck, J.-L., and Allègre, C. J., 1999, Osmium isotope disequilibrium between mantle minerals in a spinel-lherzolite: Earth and Planetary Science Letters, v. 172, no. 3, p. 311-322.

Chen, J. H., Papanastassiou, D. A., and Wasserburg, G. J., 2010, Ruthenium endemic isotope effects in chondrites and differentiated meteorites: Geochimica et Cosmochimica Acta, v. 74, no. 13, p. 3851-3862.

Cohen, A. S., 2004, The rhenium–osmium isotope system: applications to geochronological and palaeoenvironmental problems: Journal of the geological Society, v. 161, no. 4, p. 729-734.

Cohen, A. S., and Waters, F. G., 1996, Separation of osmium from geological materials by solvent extraction for analysis by thermal ionisation mass spectrometry: Analytica Chimica Acta, v. 332, no. 2, p. 269-275.

Cook, D. L., Kruijer, T. S., Leya, I., and Kleine, T., 2015, Reply to comment by Peters et al.(2015) on" Cosmogenic 180W variations in meteorites and re-assessment of a possible 184Os-180W decay system": Geochimica et cosmochimica acta, v. 169, p. 240-243.

Cook, D. L., Walker, R. J., Horan, M. F., Wasson, J. T., and Morgan, J. W., 2004, Pt-Re-Os systematics of group IIAB and IIIAB iron meteorites 1: Geochimica et Cosmochimica Acta, v. 68, no. 6, p. 1413-1431.

Creaser, R. A., Papanastassiou, D. A., and Wasserburg, G. J., 1991, Negative thermal ion mass spectrometry of osmium, rhenium and iridium: Geochimica et Cosmochimica Acta, v. 55, no. 1, p. 397-401.

Creech, J. B., Baker, J. A., Handler, M. R., Schiller, M., and Bizzarro, M., 2013, Platinum stable isotope ratio measurements by double-spike multiple collector ICPMS: Journal of Analytical Atomic Spectrometry, v. 28, no. 6, p. 853-865.

Dale, C. W., Gannoun, A., Burton, K. W., Argles, T. W., and Parkinson, I. J., 2007, Rhenium–osmium isotope and elemental behaviour during subduction of oceanic crust and the implications for mantle recycling: Earth and Planetary Science Letters, v. 253, no. 1, p. 211-225.

Dauphas, N., Marty, B., and Reisberg, L., 2002, Molybdenum evidence for inherited planetary scale isotope heterogeneity of the protosolar nebula: The Astrophysical Journal, v. 565, no. 1, p. 640.

de Laeter, J. R., Böhlke, J. K., De Bièvre, P., Hidaka, H., Peiser, H., Rosman, K., and Taylor, P., 2003, Atomic weights of the elements. Review 2000 (IUPAC Technical Report): Pure and applied chemistry, v. 75, no. 6, p. 683-800.

Dodson, M. H., 1963, A theorethical study of the use of international standards for precise isotopic analysis by the surface ionisation technique: Part I - General first-order algebraic solutions: Journal of Scientific Instruments, v. 40, p. 289-295.

Du Vivier, A. D., Selby, D., Sageman, B. B., Jarvis, I., Gröcke, D. R., and Voigt, S., 2014, Marine 187 Os/188 Os isotope stratigraphy reveals the interaction of volcanism and ocean circulation during Oceanic Anoxic Event 2: Earth and Planetary Science Letters, v. 389, p. 23-33.

Esser, B. K., and Turekian, K. K., 1993, Anthropogenic osmium in coastal deposits: Environmental Science & Technology, v. 27, no. 13, p. 2719-2724.

Halliday, A. N., Lee, D.-C., Christensen, J. N., Walder, A. J., Freedman, P. A., Jones, C. E., Hall, C. M., Yi, W., and Teagle, D., 1995, Recent developments in inductively coupled plasma magnetic sector multiple collector mass spectrometry: International Journal of Mass Spectrometry and Ion Processes, v. 146, p. 21-33.

Handler, M. R., Bennett, V. C., and Dreibus, G., 1999, Evidence from correlated Ir/Os and Cu/S for late-stage Os mobility in peridotite xenoliths: Implications for Re-Os systematics: Geology, v. 27, no. 1, p. 75-78.

Harvey, J., Sulphides in the sub-continental lithospheric mantle (SCLM): unravelling the effects of melt depletion and metasomatism using Re-Os isotopes, in Proceedings Geophysical Research Abstracts2005, Volume 7, p. 03658.

Hirt, B., Herr, W., and Hoffmeister, W., 1963, Age determinations by the rhenium-osmium method: Radioactive Dating, p. 35-43.

Hopp, T., Fischer-Godde, M., and Kleine, T., 2016, Ruthenium stable isotope measurements by double spike MC-ICPMS: Journal of Analytical Atomic Spectrometry, v. 31, no. 7, p. 1515-1526.

Jeon, W. Y., Choi, Y. B., and Kim, H. H., 2013, Homogeneous Electrochemical Detection of Hippuric Acid in Urine Based on the Osmium–Antigen Conjugate: ChemPhysChem, v. 14, no. 10, p. 2331-2337.

Johnson, C. M., Beard, B. L., Albarède, F., and Union, C. G., 2004, Geochemistry of non-traditional stable isotopes, Mineralogical Society of America Washington, DC.

Kimura, K., Lewis, R. S., and Anders, E., 1974, Distribution of gold and rhenium between nickel-iron and silicate melts: implications for the abundance of siderophile elements on the Earth and Moon: Geochimica et Cosmochimica Acta, v. 38, no. 5, p. 683-701.

Lodders, K., 2003, Solar system abundances and condensation temperatures of the elements: The Astrophysical Journal, v. 591, no. 2, p. 1220.

Lorand, J.-P., and Luguet, A., 2016, Chalcophile and siderophile elements in mantle rocks: Trace elements controlled by trace minerals: Reviews in Mineralogy and Geochemistry, v. 81, no. 1, p. 441-488.

Luck, J.-M., Birck, J.-L., and Allegre, C.-J., 1980, 187Re–187Os systematics in meteorites: early chronology of the Solar System and age of the Galaxy.

Maier, W. D., Barnes, S. J., Campbell, I. H., Fiorentini, M. L., Peltonen, P., Barnes, S.-J., and Smithies, R. H., 2009, Progressive mixing of meteoritic veneer into the early Earth/'s deep mantle: Nature, v. 460, no. 7255, p. 620-623.

McCoy, T., Walker, R., Goldstein, J., Yang, J., McDonough, W., Rumble, D., Chabot, N., Ash, R., Corrigan, C., and Michael, J., 2011, Group IVA irons: New constraints on the crystallization and cooling history of an asteroidal core with a complex history: Geochimica et Cosmochimica Acta, v. 75, no. 22, p. 6821-6843.

Meisel, T., Walker, R. J., Irving, A. J., and Lorand, J.-P., 2001, Osmium isotopic compositions of mantle xenoliths: a global perspective: Geochimica et Cosmochimica Acta, v. 65, no. 8, p. 1311-1323.

Millet, M.-A., Baker, J. A., and Payne, C. E., 2012, Ultra-precise stable Fe isotope measurements by high resolution multiple-collector inductively coupled plasma mass spectrometry with ^{57}Fe–^{58}Fe double spike: Chemical Geology, v. 304, p. 18-25.

Nier, A. O., 1937, The isotopic constitution of osmium: Physical Review, v. 52, no. 8, p. 885.

Pearson, D., and Woodland, S., 2000, Solvent extraction/anion exchange separation and determination of PGEs (Os, Ir, Pt, Pd, Ru) and Re–Os isotopes in geological samples by isotope dilution ICP-MS: Chemical Geology, v. 165, no. 1, p. 87-107.

Pearson, D. G., Parman, S. W., and Nowell, G. M., 2007, A link between large mantle melting events and continent growth seen in osmium isotopes: Nature, v. 449, no. 7159, p. 202-205.

Peters, S. T. M., Münker, C., Becker, H., and Schulz, T., 2014, Alpha-decay of 184Os revealed by radiogenic 180W in meteorites: Half life determination and viability as geochronometer: Earth and Planetary Science Letters, v. 391, p. 69-76.

Peucker-Ehrenbrink, B., and Ravizza, G., 2000, The marine osmium isotope record: Terra Nova, v. 12, no. 5, p. 205-219.

Ravizza, G., Norris, R. N., Blusztajn, J., and Aubry, M. P., 2001, An osmium isotope excursion associated with the Late Paleocene thermal maximum: Evidence of intensified chemical weathering: Paleoceanography, v. 16, no. 2, p. 155-163.

Ravizza, G., and Peucker-Ehrenbrink, B., 2003, Chemostratigraphic Evidence of Deccan Volcanism from the Marine Osmium Isotope Record: Science, v. 302, no. 5649, p. 1392-1395.

Rehkämper, M., and Halliday, A. N., 1999, The precise measurement of Tl isotopic compositions by MC-ICPMS: Application to the analysis of geological materials and meteorites: Geochimica et Cosmochimica Acta, v. 63, no. 6, p. 935-944.

Reisberg, L., Dauphas, N., Luguet, A., Pearson, D., Gallino, R., and Zimmermann, C., 2009, Nucleosynthetic osmium isotope anomalies in acid leachates of the Murchison meteorite: Earth and Planetary Science Letters, v. 277, no. 3, p. 334-344.

Rudge, J. F., Reynolds, B. C., and Bourdon, B., 2009, The double spike toolbox: Chemical Geology, v. 265, no. 3–4, p. 420-431.

Russ, G. P., Bazan, J. M., and Date, A. R., 1987, Osmium isotopic ratio measurements by inductively coupled plasma source mass spectrometry: Analytical Chemistry, v. 59, no. 7, p. 984-989.

Schauble, E. A., 2004, Applying stable Isotope fractionation theory to new systems: Reviews in Mineralogy and Geochemistry, v. 55, p. 65-111.

Schoenberg, R., Nägler, T. F., and Kramers, J. D., 2000, Precise Os isotope ratio and Re–Os isotope dilution measurements down to the picogram level using multicollector inductively coupled plasma mass spectrometry: International Journal of Mass Spectrometry, v. 197, no. 1, p. 85-94.

Selby, D., Creaser, R. A., Stein, H. J., Markey, R. J., and Hannah, J. L., 2007, Assessment of the 187 Re decay constant by cross calibration of Re–Os molybdenite and U–Pb zircon chronometers in magmatic ore systems: Geochimica et Cosmochimica Acta, v. 71, no. 8, p. 1999-2013.

Shirey, S. B., and Walker, R. J., 1998, The Re-Os isotope system in cosmochemistry and high-temperature geochemistry: Annual Review of Earth and Planetary Sciences, v. 26, no. 1, p. 423-500.

Siebert, C., Nägler, T. F., and Kramers, J. D., 2001, Determination of molybdenum isotope fractionation by double-spike multicollector inductively coupled plasma mass spectrometry: Geochemistry, Geophysics, Geosystems, v. 2, no. 7, p. 1032.

Smoliar, M. I., Walker, R. J., and Morgan, J. W., 1996, Re-Os Ages of Group IIA, IIIA, IVA, and IVB Iron Meteorites: Science, v. 271, no. 5252, p. 1099-1102.

Stirling, C. H., Andersen, M. B., Potter, E.-K., and Halliday, A. N., 2007, Low-temperature isotopic fractionation of uranium: Earth and Planetary Science Letters, v. 264, no. 1–2, p. 208-225.

Suzuki, K., Senda, R., and Shimizu, K., 2011, Osmium behavior in a subduction system elucidated from chromian spinel in Bonin Island beach sands: Geology, v. 39, no. 11, p. 999-1002.

Teng, F.-Z., Dauphas, N., and Watkins, J. M., 2017, Non-Traditional Stable Isotopes: Retrospective and Prospective: Reviews in Mineralogy and Geochemistry, v. 82, no. 1, p. 1-26.

Urey, H. C., 1947, The thermodynamic properties of isotopic substances: Journal of the Chemical Society (Resumed), p. 562-581.

Völkening, J., Walczyk, T., and G Heumann, K., 1991, Osmium isotope ratio determinations by negative thermal ionization mass spectrometry: International Journal of Mass Spectrometry and Ion Processes, v. 105, no. 2, p. 147-159.

Walker, R. J., Morgan, J. W., Beary, E. S., Smoliar, M. I., Czamanske, G. K., and Horan, M. F., 1997, Applications of the ^{190}Pt-^{186}Os isotope system to geochemistry and cosmochemistry: Geochimica et Cosmochimica Acta, v. 61, no. 22, p. 4799-4807.

Yokoyama, T., Alexander, C. M. D., and Walker, R. J., 2010, Osmium isotope anomalies in chondrites: results for acid residues and related leachates: Earth and Planetary Science Letters, v. 291, no. 1, p. 48-59.

Yokoyama, T., Rai, V. K., Alexander, C. M. D., Lewis, R. S., Carlson, R. W., Shirey, S. B., Thiemens, M. H., and Walker, R. J., 2007, Osmium isotope evidence for uniform distribution of s-and r-process components in the early solar system: Earth and Planetary Science Letters, v. 259, no. 3, p. 567-58

– CHAPTER 2 –

High Precision Osmium Stable Isotope Measurements by
Double Spike MC-ICP-MS and N-TIMS.

1.   Department of Earth Sciences, Durham University,
     Science Labs, South Road, Durham DH1 3LE, United Kingdom.

§   *Present address:* Institut für Planetologie, University of Münster,
     Wilhelm-Klemm-Str. 10, 48149 Münster, Germany.

$ *Present address:* School of Earth and Ocean Sciences, Cardiff University,
     Main building, Park Place, Cardiff CF10 3AT, United Kingdom.

▢   *Present address:* Department of Earth Sciences, The University of Cambridge,
     Downing Street, Cambridge CB2 3EQ, United Kingdom.

After publication an addendum has been added to this thesis Chapter to resolve the lower $^{186}Os/^{188}Os$ data.

ABSTRACT

Osmium stable isotopes provide a new, potentially powerful tool with which to investigate a diverse range of geological processes including planetary formation, ore-genesis and weathering. In this paper, we present a new technique for high precision measurement of osmium (Os) stable isotope ratios by both Multiple- Collector Inductively Coupled Plasma Mass Spectrometry (MC-ICP-MS) and Negative ion Thermal Ionisation Mass Spectrometry (N-TIMS). We use a ^{188}Os–^{190}Os double spike, composed of 61% ^{188}Os and 39% ^{190}Os, to correct for mass dependent fractionation resulting from sample preparation and isotope measurement, with the ideal spike to sample ratio being 55 : 45. Isotope ratios are expressed as δ^{190}Os which is the per mil deviation in the measured ^{190}Os/^{188}Os ratio relative to isotope reference material DROsS. Repeated analyses of double spiked DROsS for both MC-ICP-MS (n = 80 cycles) and N-TIMS (n = 280 cycles) show that an internal precision of 0.01–0.02‰ on δ^{190}Os (2 se) can be attained, with a long-term reproducibility of 0.02‰ and 0.03‰ (2 sd; n = 91 and 83, respectively). The better reproducibility on MC-ICP-MS than on N-TIMS is, predominantly, due to measurement at higher beam intensities (11–18 V with consumption of ~200 ng natural Os vs. 2–18 V with consumption of 2.3–45 ng natural Os, respectively). In addition to stable isotope compositions, our method allows for simultaneous measurement of ^{187}Os/^{188}Os and ^{186}Os/^{188}Os ratios with a precision of <40 ppm (2 se; 80 cycles for MC-ICP-MS and 280 cycles for N-TIMS) and an external reproducibility of 123–268 ppm and 234–361 ppm (2 sd; n = 91 for MC-ICP-MS and n = 83 for N-TIMS), respectively. We demonstrate that a similar precision and reproducibility can be obtained for other pure Os solutions as well as for geological materials. Furthermore, with a range of analytical tests we evaluate and demonstrate the robustness of our method with regards to residual matrix effects and interference correction, signal intensity and on-peak zero on MC-ICP-MS, and the effect of oxygen corrections and isobaric interference on N-TIMS. Finally, we report the first Os stable isotope compositions for geological reference materials, including mantle peridotites and chromitites, and one ordinary chondrite.

CONTENT CHAPTER 2

1. INTRODUCTION

Osmium (Os) has two radiogenic isotopes ([186]Os and [187]Os) and five naturally occurring stable isotopes: [184]Os, [188]Os, [189]Os, [190]Os, and [192]Os, with relative abundances of 0.02 %, 13.21 %, 16.11 %, 26.21 %, and 40.74 %, respectively. Osmium is a refractory and highly siderophile (Fe-loving) element and is, therefore, of considerable interest in the study of planetary differentiation and formation of Earth's metallic core. It is also a chalcophile (S-loving) element, and strongly partitions into sulphides. Consequently, Os behaves compatibly during mantle melting, where sulphide remains as a residual phase in the source. Taking advantage of the chemical properties of Os and the differences in behaviour between Re, Pt and Os, the [187]Re-[187]Os and [190]Pt-[186]Os decay systems have become important chronometers and tracers in both high and low-temperature geochemistry (e.g., Shirey and Walker, 1998; Carlson, 2005). More specifically, these radiogenic isotope systems have been used to study early solar system dynamics (e.g., Meisel et al., 1996; Walker et al., 2002, planetary differentiation processes (e.g., Brandon et al., 1998; Walker, 2009), mantle heterogeneity (e.g., Snow and Reisberg, 1995; Meibom et al., 2002), crustal growth and recycling (e.g., Brandon et al., 1996; Dale et al., 2007; Pearson et al., 2007), economic mineralization in ore deposits (e.g., Stein et al., 1998), and the nature of weathering processes associated with brief climatic excursions (e.g., Pegram et al., 1992; Peucker-Ehrenbrink and Ravizza, 2000; Burton, 2006). However, despite the potential to use stable Os isotopes to investigate these same processes, thus far this system remains unexplored.

A potential limitation for the use of Os stable isotopes in geochemistry is the small range of natural variation expected for high-mass elements. This is compounded by the very low abundance of Os in most terrestrial samples. However, recent advances in mass spectrometry and development of new techniques for stable isotope measurement have led to the discovery of significant and systematic stable isotope fractionation for high-mass stable isotope systems in both high and low-temperature environments (Rehkämper et al., 2002; Nielsen et al., 2006a; Nielsen et al., 2006b; Stirling et al., 2007; Brennecka et al., 2010; Creech et al., 2013; Creech et al., 2014). This suggests that Os stable isotope variations may be measurable if a suitable high precision analytical method can be developed.

Additional complications that must be addressed in order to successfully measure Os stable isotopes include the non-quantitative recovery of Os during sample processing (typically 60-80 %; Shen et al., 1996; Birck et al., 1997) and instrumental mass bias (MC-ICP-MS) or mass fractionation (N-TIMS) during measurement. Such fractionation can be overcome by the use of a double spike (DS; Dodson, 1963). This approach has been shown to reliably account for mass-dependent stable isotope fractionation that can occur during all steps of sample processing (i.e., digestion, chemical separation and mass spectrometry; Galer, 1999; Millet et al., 2012; Creech et al., 2013).

In this paper, we present a new method for measurement of high-precision stable Os isotope ratios using a [188]Os-[190]Os double spike by both plasma source (MC-ICP-MS) and negative thermal ionisation mass spectrometry (N-TIMS). Method development on both machines allows for analysis of sample materials over a broad range of Os concentrations (>1 ppb) at precisions of 0.01-0.02‰ in δ^{190}Os (2 se; 80 cycles for MC-ICP-MS

and 280 cycles for N-TIMS). In addition, we show that the method allows for simultaneous collection of stable isotopes and radiogenic isotope ratios, $^{187}Os/^{188}Os$ and $^{186}Os/^{188}Os$, at a precision of <40 ppm (2 se; 80 cycles for MC-ICP-MS and 280 cycles for N-TIMS). We show the robustness, precision and accuracy of our method through a range of analytical tests and repeated measurements of pure Os solutions and geological materials. Finally, data is presented for a variety of geological materials.

2. OSMIUM DOUBLE SPIKE METHODOLOGY

2.1 OSMIUM DOUBLE SPIKE DESIGN

The double spike (DS) approach requires four stable isotopes that are related to each other by mass-dependent stable isotope fractionation. For Os we can use ^{188}Os, ^{189}Os, ^{190}Os, and ^{192}Os. Departures from mass-dependent fractionation, either due to cosmogenic effects or nucleosynthetic anomalies, have not been detected in terrestrial samples but have been reported for extra-terrestrial materials. Components of carbonaceous chondrites display mass independent Os isotopic anomalies although homogeneity is shown at the bulk meteoritic scale (e.g., Brandon et al., 2005, Yokoyama et al., 2007, Yokoyama et al., 2010). Mass independent anomalies at the bulk rock scale have been shown for iron meteorites (e.g., Wittig et al., 2013) which should be considered when analysing such meteorites.

The DS deconvolution used in this study is based on the geometric iterative resolution method of Siebert et al. (2001). Measurements were also double checked using an algebraic resolution method used by Millet and Dauphas (2014) and Millet et al. (2016) which yielded identical results. Regardless of the approach, the DS deconvolution consists of resolving the following non-linear equation:

$$R_m = \left[(1-f)R_{standard}(i_x/i_n)^\alpha + fR_{spike}\right] * (i_x/i_n)^\beta$$

where R_m, $R_{standard}$ and R_{spike} are the measured, standard and spike isotope ratios; i_n is the atomic weight of the normalising isotope (^{188}Os); i_x is the atomic weight of one of the three other isotopes used to resolve the equation which in our method are ^{189}Os, ^{190}Os and ^{192}Os; f is the relative proportion of ^{188}Os originating from the spike in the sample–spike mixture; α is the natural and β the processing and instrumental exponential fractionation factors. In this study, the Durham Romil Osmium Standard (DROsS; Luguet et al., 2008; Nowell et al., 2008) has been used as standard. All Os stable isotope compositions are thus reported relative to DROsS, as the per mil deviation (‰) of the $^{190}Os/^{188}Os$ ratios, here after reported as $\delta^{190}Os$:

$$\delta^{190/188}Os_{DROsS} = \left(\frac{\frac{190}{188}Os_{sample}}{\frac{190}{188}Os_{DROsS}} - 1\right) * 1000$$
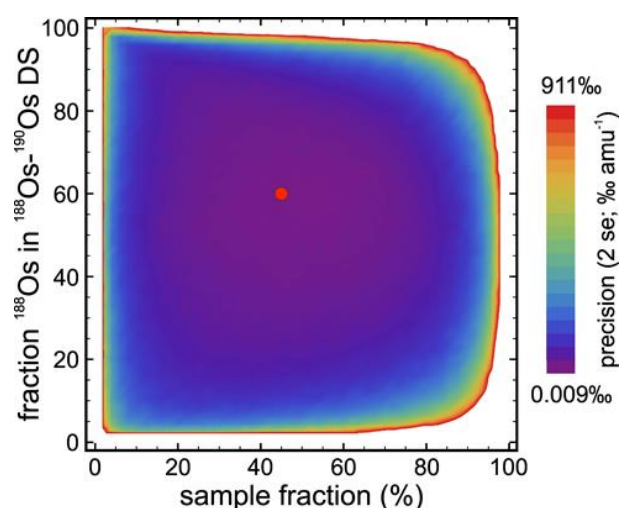
Figure 2-1 Results for an error (2 se) simulation on the stable isotope composition in ‰ amu^{-1} in case of a ^{188}Os-^{190}Os double spike. The red dot indicates that minimal error propagation of ~0.01 ‰ amu^{-1} (2 se) is obtained when using a 60 % ^{188}Os – 40 % ^{190}Os spike that is mixed with a sample in relative proportions of 55 % and 45 %. Note that errors are minimal (<0.02 ‰ amu^{-1}) over a large range of sample-spike mixtures (15 – 81 % sample fraction). The error model is based on the method of Millet and Dauphas (2014) using the following parameters: 6 V; 80 x 8.3 seconds integrations; 10^{11} Ω collectors; T= 290 K.

Radiogenic isotopes ^{186}Os and ^{187}Os are not used in the DS deconvolution. Consequently, the spike proportion, and the geological and analytical fractionation factors resolved within the DS deconvolution can be used to calculate the ^{186}Os/^{188}Os and ^{187}Os/^{188}Os ratios. Osmium concentrations were determined by performing isotope dilution calculations (see addendum).

The analytical uncertainty on double spike measurements is highly dependent on spike composition and sample-spike mixing proportions. To establish the optimal composition and proportions for Os, we have modelled the internal precision of a typical MC-ICP-MS measurement following the model of Millet and Dauphas (2014) which takes into account the errors associated to Johnson noise and counting statistics (see Millet and Dauphas, 2014 for more details). This error model differs from that of Rudge et al. (2009) in that i) errors on the natural fractionation factor (alpha) are calculated on the basis of a constant intensity for the most abundant isotope in the natural Os-DS mixture, rather than calculated based on a constant total Os ion beam and; ii) determination of errors is done through Monte Carlo modelling. In our model, the maximum intensity for the most abundant isotope was set at 6 V. A measurement is assumed to comprise 80 cycles with an integration time of 8.3 seconds per cycle on 10^{11} Ω collectors at T=290 K. The model shows that a minimum internal error, of ~0.01‰ amu^{-1} (2 se), is acquired when using a 0.6:0.4 ^{188}Os – ^{190}Os mixed spike composition and a 0.55:0.45 spike-sample mixture (**Figure 2-1**). This is close to the optimal double spike composition as calculated by Rudge et al. (2009) of 0.66:0.34 ^{188}Os -^{190}Os for a 0.6:0.4 spike-sample mixture. It is important to note that the 2 se error is <0.02‰ amu^{-1} when the sample proportion ranges between 15 % and 81 %. That errors are minimal over a large range of spike-sample mixtures is of great utility when the Os concentration of samples is not well known. A triple spike composition was considered in our calculations but was not found to improve precision.

2.2 PREPARATION and CALIBRATION of ^{188}Os – ^{190}Os DOUBLE SPIKE

Single ^{188}Os and ^{190}Os isotope spikes were purchased as fine-grained metallic powders from Trace Sciences International. In order to ensure purity of the double spike, the metal powders were individually digested using

Carius tubes, followed by extraction and purification as described in section 3.2. Individual spikes were subsequently mixed in calculated optimal proportions and the resulting double spike was diluted with 3 M HCl to desired concentrations.

Calibration of the double spike isotope composition was achieved by measuring a pure standard and pure double spike solution as well as a range of DROsS-DS mixtures. Practically, this involves iterative correction for instrumental mass fractionation of the pure DS measurements to generate a putative true DS composition, with an initial estimate provided by the pure DROsS analysis. This putative true DS composition is then fed into the DS deconvolution and used on all DS-DROsS mixtures, ranging from 0.1:0:9 to 09:0.1 mixing proportions. Calibration is considered satisfactory once most mixtures, especially those around the optimum mixture proportions, display a δ^{190}Os within analytical error of zero. For all these solutions, Carius tubes were used to ensure standard-sample equilibration. Measurements were carried out by MC-ICP-MS with each analysis comprising 220 cycles of 8.39 seconds and were all preceded by on-mass on-peak zero (OPZ) measurement of 20 integrations of 8.39 seconds. The isotope composition of the DS and of reference standard DROsS, as used in the calibration and stable isotope calculations, can be found in **Table 2-1**.

Table 2-1 Osmium isotopic ratios of reference standard DROsS, as determined by Nowell et al. (2008) normalized to ^{189}Os/^{188}Os to correct for mass bias, and of the ^{188}Os-^{190}Os double spike (DS) as used in this study. The quoted error on DROsS represents the 2 sd on 21 analyses, and the error on the DS is the relative 2 se on the analysis used to obtain the DS composition.
Note! – The DS has been recalibrated using the DROsS composition as determined by Luguet et al. (2008), see addendum. This has no significant implication on the stable isotope compositions, but it does on the radiogenic ratios (i.e. ^{186}Os/^{188}Os and ^{187}Os/^{188}Os). Luguet et al. (2008) has normalized to ^{192}Os/^{188}Os to correct for mass bias.

	^{186}Os/^{188}Os	^{187}Os/^{188}Os	^{189}Os/^{188}Os	^{190}Os/^{188}Os	^{192}Os/^{188}Os
Old (as published, Nowell et al., 2008)					
Reference std DROsS (±2 sd)	0.119909 ± 04	0.160916 ± 04	*1.219780*	1.983979 ± 30	3.083580 ± 14
^{188}Os - ^{190}Os spike (±2 se)	0.001372 ± 54	0.001239 ± 58	0.020944 ± 11	0.684512 ± 06	0.036517 ± 14
New (see addendum, Luguet et al., 2008)					
Reference std DROsS (±2 sd)	0.119929 ± 06	0.160924 ± 04	1.219705 ± 15	1.983803 ± 15	*3.083*
^{188}Os - ^{190}Os spike (±2 se)	0.001371 ± 54	0.001240 ± 58	0.020943 ± 11	0.684450 ± 06	0.036510 ± 14

3. MATERIALS AND SAMPLE PROCESSING

3.1 MATERIALS and SAMPLES

Digestion and processing of standards and samples were carried out at Durham University. During the course of this study, we used Romil acids of variable grades (Super Purity Acids and Ultra Purity Acids) with blank levels suitable for the analytical procedure. Nitric acid was further purified by sparging with filtered air. Acid dilutions were performed with ultrapure (18.2 MΩ·cm) water.

Durham Romil Osmium Standard (DROsS; Luguet et al., 2008; Nowell et al., 2008) has been used as a reference standard. This is an international Os isotope reference material supplied by IAGeo Limited that has been widely distributed (e.g., Liu and Pearson, 2014; Chatterjee and Lassiter, 2015) and for which Os isotope ratios have been determined to high precision and accuracy by both MC-ICP-MS (Nowell et al., 2008) and N-TIMS (Luguet et al., 2008). For method testing, we have also measured three in-house pure Os reference solutions, ROMIL, SpecPure, and OsCaR, which were purchased from Romil Ltd, Alfa Aesar, and provided by A. Poirier (OsCaR). As representative rock samples, we used well-characterized and commonly used reference materials: peridotites UB-N (Meisel et al., 2003) and GP-13 (Pearson et al., 2004), and chromitites CHR-Bkg (Potts et al., 1992; Paliulionyte et al., 2006) and CHR-Pt+ (Meisel et al., 2001). Reference material GP-13 is an in-house PGE standard prepared at Durham University which has been widely distributed. The other materials, UB-N, CHR-Bkg and CHR-Pt+, are distributed by CRPG-CRNS, Nancy, France. Furthermore, we included an ordinary H-chondrite, ZAG. These samples were chosen to reflect the range of Os concentrations and sample matrices available for study.

3.2 SAMPLE DIGESTION and CHEMICIAL PURIFICATION of Os

Samples were digested either by Carius tube (CT; Shirey and Walker, 1995; Shen et al., 1996) or high-pressure asher (HPA, Anton Paar; Meisel et al., 2001), with respective maximum of 2.5 g and 2 g powder material per tube. Digestions were performed using inverse aqua regia (1:2; 12 M HCl: 16 M HNO_3) for ≥16 h at temperatures of 230°C in the case of CT and 290-310°C for HPA digestions. The double spike was added to each tube prior to sample digestion. After digestion, the extraction and purification of Os closely followed techniques described by Cohen and Waters (1996) and Birck et al. (1997). Separation of Os from the aqua regia digest solution was achieved by solvent extraction using $CHCl_3$ (Cohen and Waters, 1996). Osmium was then back-extracted from the chloroform solution using concentrated HBr and subsequently purified using the micro-distillation procedure of Roy-Barman (1993) as described by Birck et al. (1997). In the case of measurements by MC-ICP-MS, samples were evaporated and chlorified three times using 300 µL of 8 M HCl before being taken up in 3 M HCl to a total Os concentration of ~0.5 µg mL^{-1}. When performing Os analyses by N-TIMS, samples were dried down after microdistillation to approximately 1-2 µL of sample solution and then loaded onto a Pt ribbon filament. Typical total procedural blanks range between 0.01 and 0.10 pg Os which is similar to previous Os studies carried out at Durham University (e.g., Dale et al., 2009).

4. MASS SPECTROMETRY

Osmium isotope ratios were measured at Durham University on a ThermoFisher Scientific Neptune MC-ICP-MS (Nowell et al., 2008) and a Triton Plus N-TIMS (Creaser et al., 1991; Luguet et al., 2008; Chatterjee and Lassiter, 2015). The use of both MC-ICP-MS and N-TIMS allowed us to exploit the advantages of different ionisation sources and provide a means to assess the relative accuracy of each measurement. The overall introduction and

Table 2-2 Faraday cup configuration used for osmium isotope measurements by static multi-collection on a Thermo Neptune MC-ICP-MS and Thermo Triton Plus N-TIMS at Durham University. Only principal ions measured are listed, see Luguet et al. (2008) for a full list of known polyatomic interferences.

Cup	L4	L3	L2	L1	Ax	H1	H2	H3	H4
MC-ICP-MS									
Analyte isotopes	^{183}W	^{185}Re	^{186}Os	^{187}Os	^{188}Os	^{189}Os	^{190}Os	^{192}Os	^{194}Pt
N-TIMS									
Mass		232	234	235	236	237	238	240	
Seq1		^{184}Os^{16}O$_3^-$	^{186}Os^{16}O$_3^-$	^{187}Os^{16}O$_3^-$	^{188}Os^{16}O$_3^-$	^{189}Os^{16}O$_3^-$	^{190}Os^{16}O$_3^-$	^{192}Os^{16}O$_3^-$	
Mass		236	238	239	240	241	242		
Seq2		^{188}Os^{16}O$_3^-$	^{190}Os^{16}O$_3^-$		^{192}Os^{16}O$_3^-$	^{192}Os^{16}O$_2$^{17}O$^-$	^{192}Os^{16}O$_2$^{18}O$^-$		

ionisation efficiency of MC-ICP-MS is relatively low (~0.08 %; Nowell et al., 2008) which makes it better suited for analysing large samples and calibrating standards. The advantage of the MC-ICP-MS is that Os is measured as Os$^+$ which makes the mass spectrum relatively simple and corrections for isobaric interferences relatively straightforward. By contrast, N-TIMS has a much higher ionisation efficiency for Os (1-5 %; Luguet et al., 2008) which makes it ideal for samples with a low Os abundance or when sample material is limited. However, Os is measured as the tri-oxide ion OsO$_3^-$ which makes the mass spectrum complex and necessitates multiple oxide corrections that add to the overall uncertainty. In both cases, internal errors are presented as the 2 se on δ^{190}Os of each integration, once passed through a 2 se filter to remove outliers.

4.1 MC-ICP-MS

4.1.1 Instrument Set-up and Parameters MC-ICP-MS

The Neptune MC-ICP-MS was set-up for static simultaneous collection of all Os isotopes, apart from the least abundant ^{184}Os. In addition, ^{183}W, ^{185}Re, and ^{194}Pt were collected to monitor and correct for isobaric interference (**Table 2-2**). In this study, interference beam intensities were <0.05 mV for ^{183}W, <0.01 mV for ^{185}Re, and <0.5 mV for ^{194}Pt. Typical instrument operating conditions were similar to those outlined in Nowell et al. (2008). Sample material was introduced in 3 M HCl using an Elemental Scientific Incorporated (ESI) PFA-50 micro-flow nebuliser and Glass Expansion (GE) micro-cyclonic "Cinnabar" spray-chamber. During typical run conditions, the measured sample uptake rate was ca. 80 µL min^{-1} with a sensitivity of ca. 30 V ppm^{-1}. Measurements were carried out in static mode in 1 block of 80 cycles of 8.389 seconds integration time each. Mass calibration was updated by peak-centering on the centre-cup mass ^{188}Os at the start of each session and checked again at the end. Prior to every sample run, baselines were obtained by on-mass on-peak zero (OPZ) measurements for 20 x 8.389 seconds integrations in clean 3 M HCl. Washouts between sample runs used 3 M HCl acid for at least 5 minutes which resulted in the ^{188}Os beam decreasing below 2 mV (~0.03 % of the typical sample signal). Total analysis time, including OPZ and wash-out, was approximately 15 minutes with consumption of 800 µL sample solution, which is equivalent to 400 ng total Os in the case of a 0.5 µg mL^{-1} solution.

4.1.2 Data Reduction MC-ICP-MS

Following analysis, all raw intensity data were exported and re-processed offline on a cycle-by-cycle basis using an in-house Excel spreadsheet. For MC-ICP-MS analyses, corrections were applied in the following order; baseline subtraction using the OPZ measurements, abundance sensitivity (1 ppm; Nowell et al., 2008), isobaric interferences, and DS deconvolution. The abundance sensitivity is assumed to be similar to that determined by Nowell et al. (2008).

4.1.2.1 Effect of beam intensity and on-peak zero

To evaluate the effect of beam size on the accuracy, the main 500 ppb DROsS-DS solution was diluted to various lower concentrated solutions (100 - 5 ppb total Os; **Table 2-3**). This resulted in total Os beam intensities varying between 18 V and 0.1 V, with the corresponding ^{188}Os beam ranging between 6.7 V and 0.005 V. All analyses show Os stable isotope ratios as well as ^{187}Os/^{188}Os within analytical uncertainty of one another (**Figure 2-2**; **Table 2-3**). The ^{186}Os/^{188}Os only shows a significant deviation from the reference value when the total Os beam intensity is 0.14 V, corresponding to solutions with concentrations of ~ 5 ppb total Os which equals the consumption of ~4 ng total Os (i.e., natural plus DS) under standard running conditions.

Table 2-3 Osmium stable isotope compositions ($\delta^{190/188}$Os) of analytical tests on the MC-ICP-MS showing the robustness of our methodology with regards to (i) signal intensity and (ii) matrix effects and interference corrections. The percentages indicate the presence of each named element at x% of the Os abundance, e.g., Si was present at 5 % of the Os abundance. *Lith = Lithophile elements (Si, Al, Mg, Fe, Ca, Ti, Ni, and Cr); **PGE = Platinum Group Elements (Ru, Rh, Pd, Ir, and Pt).

(i) Signal intensity			
Concentration	**$\delta^{190/188}$Os**	**2 se**	**^{Total}Os (V)**
0.10 ppm	0.01	0.01	2.71
0.08 ppm	-0.01	0.01	2.08
0.05 ppm	0.00	0.02	1.31
0.04ppm	-0.01	0.03	1.02
0.03 ppm	0.02	0.03	0.66
0.02 ppm	-0.01	0.04	0.47
0.01 ppm	-0.02	0.05	0.26
0.005 ppm	0.01	0.10	0.14
(ii) Matrix effects and interference corrections			
Doping element	**$\delta^{190/188}$Os**	**2 se**	
Lith* 5%	-0.01	0.02	
PGE** 5%	-0.01	0.01	
Fe, Ni 5%	-0.00	0.02	
Pt 0.01%	0.00	0.02	
Pt 0.1%	0.01	0.02	
Pt 1%	0.01	0.02	
Pt 10%	0.00	0.02	
W 0.01%	0.02	0.02	
W 0.1%	0.00	0.02	
W 1%	0.01	0.02	
W 10%	0.02	0.02	
Re 0.01%	0.01	0.01	
Re 0.1%	0.00	0.01	
Re 1%	0.02	0.01	
Re 10%	0.00	0.02	

Analyses by MC-ICP-MS at low beam intensities critically rely on the absence of memory effects. The on-peak zero (OPZ), used to account for baseline, can introduce an inaccuracy on the stable isotope composition especially when measuring samples with very distinct isotope composition. The importance of the wash-out and sample to sample memory has been discussed in detail by Nowell et al. (2008). They show that when certain precautions are taken (e.g., avoid drying out of the spray chamber between sessions, keep standards and samples in the same chemical form), the effect on the Os isotopic composition is negligible and should not prevent the acquisition of high precision data. Considering that the natural variation in stable isotope compositions is
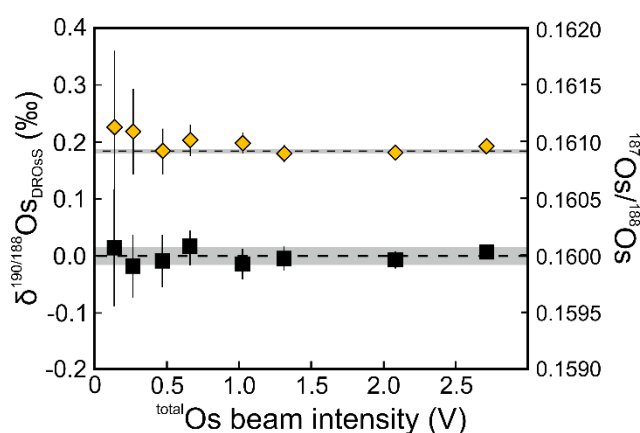
Figure 2-2 Results of double spiked DROsS analyses measured using MC-ICP-MS (closed symbols) at variable beam intensities to assess the effect of beam intensity and the on-peak zero on the accuracy of the $\delta^{190/188}$Os and ^{187}Os/^{188}Os composition. Data show that all measurements display $\delta^{190/188}$Os and ^{187}Os/^{188}Os compositions within analytical uncertainty of the long-term reproducibility as determined for >10 V analyses. The black dotted line indicates the average DROsS value, as obtained from the >10 V analyses, with the ±2 sd represented by the grey band.

expected to be small and that the proportion of sample to spike are well matched, the potential of memory effect on the stable isotope ratios can assumed to be minimal. In this study, the OPZ of the diluted DROsS solutions display signal intensities between 0.04 % and 0.6 % relative to the peak Os signal (^{188}Os) in the main run. The accuracy of the δ^{190}Os values even at low beam intensities suggests that the OPZ has an insignificant effect on the accuracy at levels up to 0.6 %. For DROsS analyses run at total Os beam intensities of >10 V, OPZ analyses are in general <2 mV and <0.04 % of the peak Os signal. The potential of inaccurate δ^{190}Os values as a result of OPZ analyses can, therefore, be neglected. The fact that OPZ correction is less accurate for ^{186}Os/^{188}Os is partly due to the lower intensities of ^{186}Os relative to all other isotopes involved in the double-spike deconvolution (^{188}Os, ^{189}Os, ^{190}Os and ^{192}Os). The ^{186}Os signal of the OPZ analyses at 0.14 V is 4 % of the main run beam. On-peak zero determination is, therefore, critical for obtaining reliable ^{186}Os/^{188}Os simultaneously with δ^{190}Os by MC-ICP-MS.

It should be noted that the higher ionisation efficiency of the N-TIMS allows for small quantities of Os to be measured at higher intensities. For example, while consumption of 4 ng total Os (5 ppb solution) provides a total Os beam intensity of 0.1 V by MC-ICP-MS, we typically obtain a total Os beam intensity of >1 V for a total Os load of ≥5 ng by N-TIMS. Furthermore, **Figure 2-7** shows that the error is significantly increased when the ^{188}Os beam intensity drops below ~1 V (~2.7 V ^{total}Os) which is an important consideration to make when small variations in stable isotope composition are expected. We, therefore, recommend that measurements on less than ~100 ng of total Os be performed by N-TIMS.

4.1.2.2 Matrix effects and interference corrections

Potential atomic isobaric interferences on Os isotopes can arise from incomplete separation of Os from W, Re and Pt. In addition, non-spectral matrix effects can create inaccurate results (Albarède and Beard, 2004). To assess if our method can accurately correct for these interferences, we doped double spiked DROsS with a range of elements that are (i) typically found in silicate rocks (Si, Al, Mg, Fe, Ca, Ti, Ni and Cr), (ii) dominant in iron meteorites (Fe, Ni), (iii) platinum group elements (Ru, Rh, Pd, Ir, and Pt), and (iv) trace elements that have direct isobaric interferences on Os (Pt, W and Re). Test solutions were doped at levels ranging from 0.01-10 % of the total Os concentration. Each element was present in x% of the Os abundance, e.g., Si was present at 5% of the
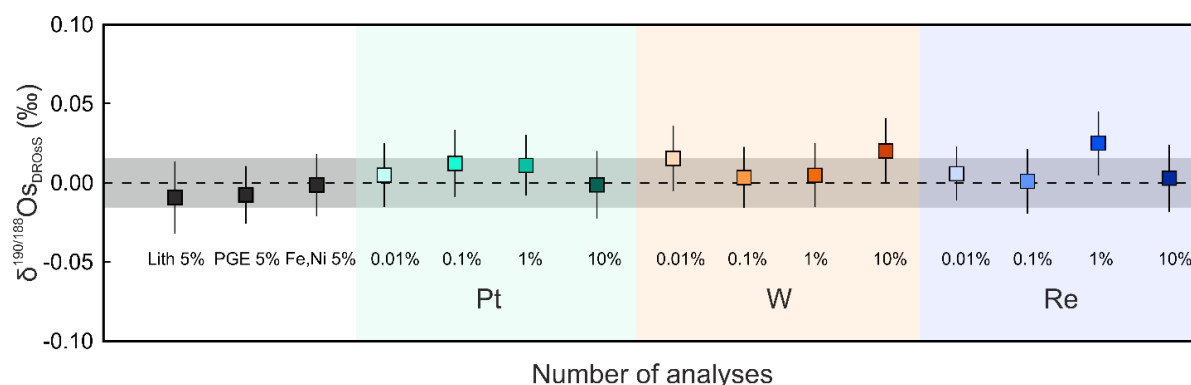
Figure 2-3 Results of doping tests to assess the robustness of the method against residual matrix effects on the MC-ICP-MS. Data show that all measurements display $\delta^{190/188}$Os compositions within analytical uncertainty of undoped DROsS analyses for residual element abundances up to 10 % of the total Os concentration. The percentages indicate the presence of each named element at x% of the Os abundance, e.g. Si was present at 5% of the Os abundance. The black dotted line indicates the average DROsS value with the ±2 sd represented by the grey shaded band as obtained in this study by MC-ICP-MS. Lith = lithophile elements (Si, Al, Mg, Fe, Ca, Ti, Ni, and Cr); PGE = Platinum Group Elements (Ru, Rh, Pd, Ir, and Pt).

Os abundance. All measurements display values within analytical uncertainty of undoped DROsS measurements (**Figure 2-3; Table 2-3**). This illustrates that matrix effects as well as isobaric interferences, even at extreme levels of up to 10 %, can be accurately accounted for. Interference beam intensities monitored for standard solutions and geological sample material processed and analysed in this study are all <0.01 % of the total Os concentration and are, therefore, not expected to have introduced data inaccuracies.

4.2 N-TIMS

4.2.1 Instrument Set-up and Parameters N-TIMS

For N-TIMS analyses, sample material was loaded onto Pt single filaments in concentrated HBr or in 3 M HCl when sample solution was also measured by MC-ICP-MS. After the sample material was dried down on the filament, ~0.5 μL of NaOH-Ba(OH)$_2$ activator was added to enhance ionisation. The amount of Os loaded for this study varied between 2.3 and 45 ng natural Os. Where MC-ICP-MS provides fairly consistent beam intensities for a certain set-up, N-TIMS intensities obtained during measurements are not directly correlated with the amount of Os loaded. This is because it also strongly depends on how the activator and sample material are loaded on the filament. A two-sequence static multi-collection routine was used in order to analyse masses 232 to 242 (**Table 2-2**). Masses 241 and 242 are collected to calculate oxygen isotope compositions (see section 4.2.2). A single analysis consists of 28 blocks, each comprising 10 cycles with 8.389 seconds integration per cycle followed by 3 seconds idle time. Amplifier gain calibrations were performed at the start of each day, even though amplifiers were rotated throughout an analysis to cancel out amplifier gains. Baseline measurements and peak centering, using masses 236 and 240, were carried out prior to every run. The presence of interfering PtO_2^-, ReO_3^-, and WO_3^- were quantified by measuring masses 228, 230-233 by ion counter before and after each Faraday measurement for 4-6 cycles with a total analysis time of 110-160 seconds. During analysis, high purity oxygen

(99.6 % purity, supplied by BOC) was bled into the source chamber with the pressure kept constant at ~2.5 x 10^{-7} mbar.

4.2.2 Data Reduction N-TIMS

Osmium analyses by N-TIMS are performed using the tri-oxide ion (OsO_3^-) and, therefore, corrections for the effects of variable isobaric oxygen isotope interferences of the heavier oxygen isotopes (^{17}O and ^{18}O) are required. For example, correction for $^{188}Os^{16}O_2^{17}O^-$ on $^{189}Os^{16}O_3^-$ at mass 239. In this study, we adopted the method of Luguet et al. (2008) where the O isotope composition is determined in-run for each integration so that any variation throughout an analysis can be accounted for. This is a more accurate approach than using a fixed O isotope composition because the composition has been shown to vary from sample to sample as well as throughout an individual run (e.g., Luguet et al., 2008; Chatterjee and Lassiter, 2015; Nagai and Yokoyama, 2016; Worsham et al., 2016). For comparison, we have also applied the method recommended by Chatterjee and Lassiter (2015) where O isotopic compositions were determined before and after the main run using a separate routine. This routine consisted of the second line as mentioned in **Table 2-2** and data was collected for 10 cycles of 8.389 seconds integrations each. From the 20 cycles, the mean 241/238 and 242/238 values (2 se outlier rejected) were taken as an approximation of the O isotopic composition of the specific run. The collection of masses 241 and 242, which are free from the most abundant Os tri-oxide species ($^{16}O_3$), allows the O isotope compositions to be determined by stripping masses 240, 241 and 242 of minor tri-oxide interferences, such as $^{189}Os^{16}O^{18}O_2^-$ and $^{190}Os^{17}O_3^-$ for mass 240. This will then provide the signal intensity of only $^{192}Os^{16}O_3^-$, $^{192}Os^{16}O_2^{17}O^-$, and $^{192}Os^{16}O_2^{18}O^-$ on respective masses 240, 241, and 242. For this first step of oxygen corrections we used the O_{gas} isotope composition as determined by Luguet et al. (2008). The $^{18}O/^{16}O$ was then calculated from the "stripped" 242/240 ratio and the $^{17}O/^{16}O$ ratio could be determined from the "stripped" 241/240 ratio. However, as discussed in more detail in section 4.2.2.1, in this study $^{17}O/^{16}O$ ratios were inferred using $^{18}O/^{16}O$ ratios. The oxygen correction is described in detail in the Electronic Supplementary Information.

Due to the presence of isobaric Os oxide complexes, additional steps in the data reduction compared to MC-ICP-MS were required. We adopted the following sequence of corrections; abundance sensitivity (0.3 ppm; Luguet et al., 2008), a preliminary oxide isotope composition correction, PtO_2^- and ReO_3^- interference corrections, a second O isotope composition correction, and double spike deconvolution (see section 4.1.2). The first O interference correction is solely used to correct for O isobaric interferences on PtO_2^-. Subsequently, the PtO_2^- interference corrected $^{184}OsO_3^-$ and $^{186}OsO_3^-$ values were used in the second O correction. For isobaric PtO_2^-, WO_3^- and ReO_3^- interference corrections, the ion counter measurement routines (before and after) were utilized, assuming a linear behaviour throughout the main run. Using a linear extrapolation is a simplistic approach but can be justified by the minor variation in beam intensities between the two SEM runs in combination with the minor influence the interference corrections have on the Os isotopic ratios (see section 4.2.2.2). The abundance sensitivity was assumed to be similar to that determined Luguet et al. (2008).

4.2.2.1 Effect of the oxygen isotopic composition

The accuracy of the deconvolved δ^{190}Os value as well as of the radiogenic isotopic ratios is dependent on accurate determinations of O isotopic compositions (i.e., ^{17}O/^{16}O and ^{18}O/^{16}O) that are used for O interference corrections.

The average ^{18}O/^{16}O ratios of individual double spiked DROsS analyses range between 0.002007 and 0.002050, a variation of 21‰, for analyses with a total Os beam intensity of >1 V. This variation is comparable with that reported by previous Os studies by N-TIMS (e.g., Liu et al., 1998 – 30‰; Luguet et al., 2008 – 14‰; Chatterjee and Lassiter, 2015 – 31‰; Chu et al., 2015– 22‰). If the ^{18}O/^{16}O ratio varies by 21‰, and the ^{17}O/^{16}O relationship is changed accordingly along a Terrestrial Fractionation Line (TFL), then the absolute δ^{190}Os value will shift by ±0.11‰. For the ^{187}Os/^{188}Os and ^{186}Os/^{188}Os ratios the resulting absolute shift is about ±20 ppm and ±25 ppm, respectively. It is, therefore, of high importance to determine the specific oxygen isotopic composition of an analysis. When ^{total}Os beam intensities are on average >1 V (>1.3 mV on mass 242), the difference in ^{18}O/^{16}O ratios between the first and last 20 cycles of an individual run ranges, apart from two samples at -12‰, between +5‰ and -7‰, and is on average -1‰. This is similar to the variation observed by Chatterjee and Lassiter (2015). Larger variations are observed for measurements made at lower beam intensities and the variability appears to be more substantial when samples are run over a longer time period (**Figure 2-4**). The latter could be related to fractionation of oxygen sourced from the activator on the filament. If the ^{18}O/^{16}O ratio is changed by ±7‰, the absolute composition of δ^{190}Os shifts by ±0.02‰. The ^{187}Os/^{188}Os and ^{186}Os/^{188}Os ratios are shifted by ±11 ppm and ±26 ppm, respectively. We, therefore, suggest determining the oxygen isotopic composition for each individual cycle, as this is the only way by which small time scale variations throughout the run can be monitored and controlled.
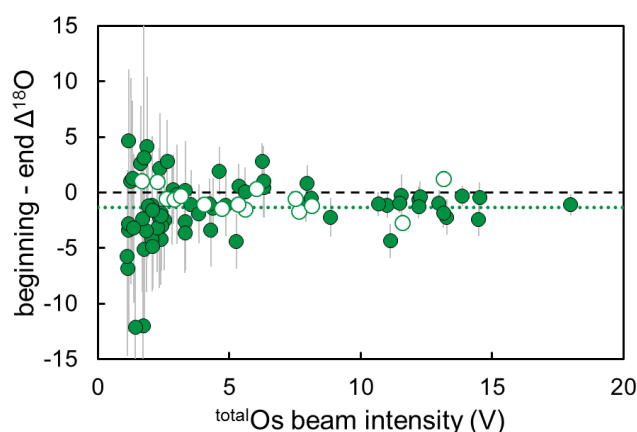
Figure 2-4 The ^{18}O/^{16}O ratios of the first and last 20 cycles of double spiked DROsS analyses (green circles) show an average variability of -1‰ (green dotted line). The variability is shown to increase with decreasing beam intensity and seems to be larger when samples are run twice for 280 cycles. Open symbols represent analyses where the oxygen composition has been measured before and after the main run. Error bars represent 2se.
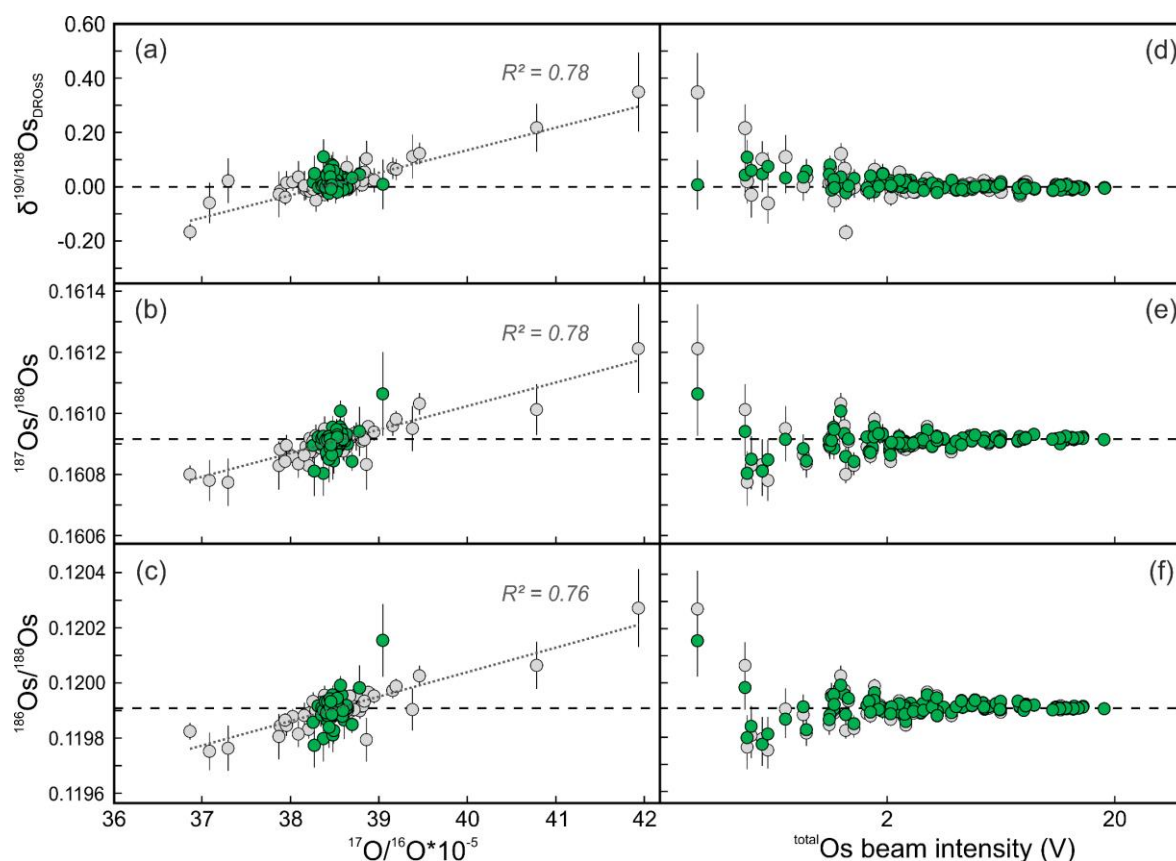
Figure 2-5 Residual correlation for double spiked DROsS analyses by N-TIMS between the measured $^{17}O/^{16}O$ (grey circles) and Os isotopic compositions; (a) $\delta^{190/188}Os$, (b) $^{187}Os/^{188}Os$, and (c) $^{186}Os/^{188}Os$. No residual correlation is observed when the $^{17}O/^{16}O$ is calculated from the measured $^{18}O/^{16}O$ ratio (green circles). The offset from the expected DROsS value is seen to increase with decreasing beam intensities (d-f), with a reduced offset when using calculated $^{17}O/^{16}O$ ratios. With decreasing signal intensity, (d) $\delta^{190/188}Os$ values seem to slightly drift towards heavier values, and (e) $^{187}Os/^{188}Os$ and (f) $^{186}Os/^{188}Os$ towards lower values. The black dashed line represents the expected DROsS value.

Run-specific $^{17}O/^{16}O$ ratios for each individual cycle can either be measured directly, using mass 241, or can be calculated based on the $^{18}O/^{16}O$ ratios. We will first consider the measured $^{17}O/^{16}O$ ratios. For DROsS analyses, the average measured $^{17}O/^{16}O$ ratio was found to display a large variation, of 121‰, with values ranging from 0.000369 to 0.000419. When only considering analyses with total beam intensities of >1 V the $^{17}O/^{16}O$ ratios vary between 0.000369 and 0.000395, 66‰. Analyses with an anomalously high or low $^{17}O/^{16}O$ ratio yield inaccurate $\delta^{190}Os$ values as well as $^{187}Os/^{188}Os$ and $^{186}Os/^{188}Os$ ratios and show a positive correlation with $^{17}O/^{16}O$ (R^2 of 0.78, 0.78 and 0.76 respectively; **Figure 2-5 a-c**). Anomalous values are only obtained for analyses performed at low beam intensities (**Figure 2-5 d-f**). In contrast, the measured $^{18}O/^{16}O$ ratios do not show any co-variation with Os isotopic compositions (R^2=0.28) suggesting that the inaccuracy on the Os isotopic compositions is dominantly introduced by the $^{17}O/^{16}O$ ratio. Mass 241 has been measured at very low beam intensities (<5 mV) that are, in general, 5.2 times lower than for mass 242. The determination of $^{17}O/^{16}O$ is, therefore, more sensitive to inaccuracies introduced by small variations in the instrument baseline occurring during an analysis. Including more and longer baselines with longer integration times during an analysis would enhance the accuracy of the baseline and potentially improve the measurement of the $^{17}O/^{16}O$ ratio. Incorporation of 10^{12} Ω or 10^{13} Ω

resistors to collect mass 241 and 242 would also be advantageous, although these were not explored in this study.

The inaccuracy introduced by the measured $^{17}O/^{16}O$ ratio can be eliminated by calculating the $^{17}O/^{16}O$ from the measured $^{18}O/^{16}O$ ratio. We will refer to this as the "calculated" $^{17}O/^{16}O$ ratio. Recently, a similar approach has been used for N-TIMS isotope measurements of Mo (Worsham et al., 2016), Ru (Bermingham et al., 2016), and W (Trinquier et al., 2016). In this study, we assume that the oxygen isotopic compositions vary as a result of equilibrium mass-dependent isotopic fractionation along a "Terrestrial Fractionation Line" (TFL; Clayton et al., 1973). For natural samples the relationship between $\delta^{17}O$ and $\delta^{18}O$, when considered in logarithmic space, typically varies between 0.524-0.528 (e.g., Barkan and Luz, 2005; Rumble et al., 2007; Ahn et al., 2012). We have taken an average of the published values, 0.526, which translates to an approximately linear slope of 0.0994 x + 0.000183, where x is $^{18}O/^{16}O$, over a $^{18}O/^{16}O$ interval of 0.002007 to 0.002055, the range in $^{18}O/^{16}O$ as observed for analyses in this study. **Figure 2-6** shows that the measured oxygen compositions of double spiked DROsS analyses with a total Os beam intensity of >2 V closely plot along this line. Details of calculation $^{17}O/^{16}O$ from the measured $^{18}O/^{16}O$ are provided in the supplementary information.
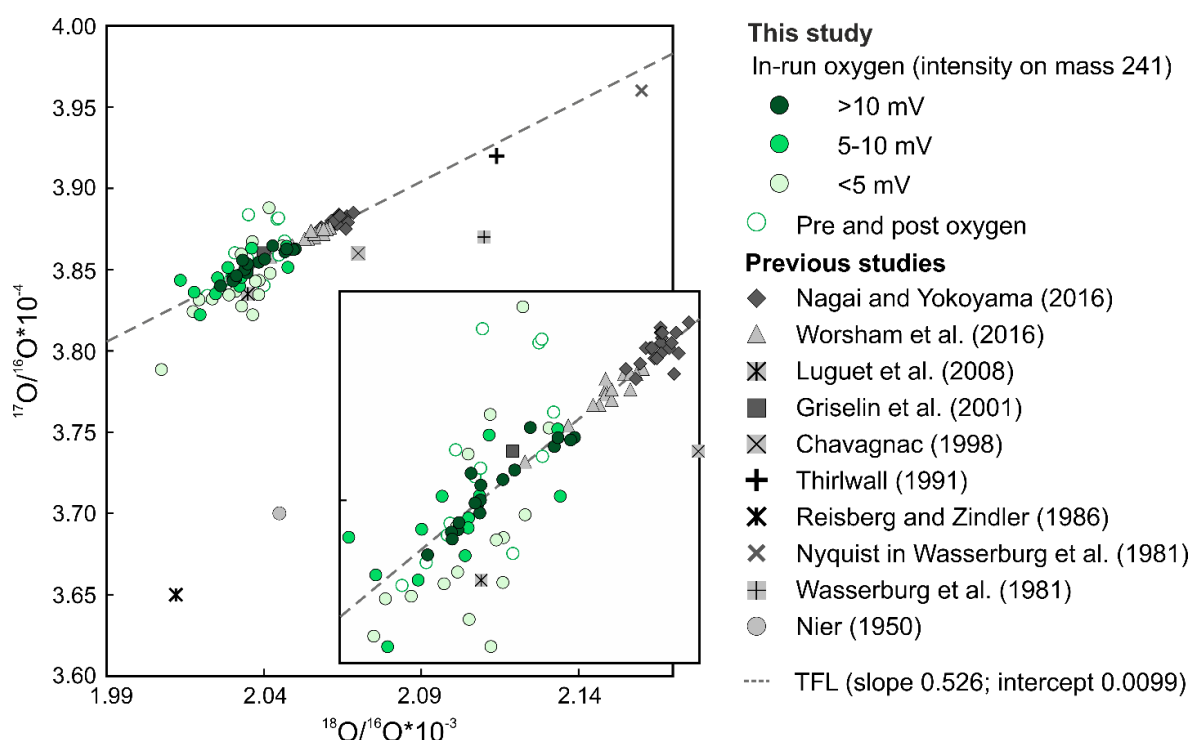
Figure 2-6 Measured $^{18}O/^{16}O$ vs. $^{17}O/^{16}O$ ratios for DROsS analyses run at a total Os beam intensity of >2 V closely follow the Terrestrial Fractionation Line (TFL). Analyses are divided based on the beam intensity on mass 242 (<5 mV; 5-10 mV; >10 mV). The TFL was calculated using a slope of 0.526 which translates to an roughly linear slope of 0.0994 x + 0.000183, where x is $^{18}O/^{16}O$, over a $^{18}O/^{16}O$ interval of 0.002007 to 0.002055, the range in $^{18}O/^{16}O$ obtained in this study. Also shown are oxygen isotope ratios from N-TIMS measurements in previous studies: Nagai and Yokoyama, 2016; Worsham et al., 2016; Luguet et al., 2008; Griselin et al., 2001; Chavagnac, 1998; Thirlwall, 1991; Reisberg and Zindler, 1986; Nyquist in Wasserburg et al., 1981; Nier, 1950.

The resulting calculated $^{17}O/^{16}O$ ratios display a much smaller variation of 20‰ with values ranging between 0.000383 and 0.000390, and is 10‰ when only considering analyses of >1 V. No residual correlation between calculated $^{17}O/^{16}O$ ratios and Os isotopic compositions is observed anymore (Figure 2-5 **a-c**). However, with decreasing beam intensities the $\delta^{190}Os$ values display a preferential drift towards heavier values (up to 0.11‰) instead of showing a normal distribution (Figure 2-5 **d**). The $^{187}Os/^{188}Os$ and $^{186}Os/^{188}Os$, on the other hand, drift preferentially towards lower values although higher values are observed as well (**Figure 2-5 e,f**). When the calculated instead of the measured $^{17}O/^{16}O$ composition is used, the long-term reproducibility of $\delta^{190}Os$ is improved from 0.11‰ to 0.05‰ (2 sd; n = 94), and from 0.06‰ to 0.03‰ for analyses of >1 V (n = 83). For the remainder of this paper, we will only consider analyses with a $^{total}Os$ beam intensity of >1 V, equivalent to, in general, >1.3 mV on mass 242 and >0.35 V on mass 236. The total Os signal intensity obtained for a certain quantity of Os loaded is highly variable, but is typically >1 V for loads of ≥2.3 ng natural Os.

4.2.2.2 Effect of polyatomic interferences

Interference intensities monitored on masses 228, and 230-233 in this study are comparable to those reported by Luguet et al. (2008). Beam intensities on mass 228 (predominantly $^{196}Pt^{16}O_2^-$) ranged from 12,000 – 1,400,000 cps (counts per second) which relates to a potential $^{196}Pt^{18}O_2^-$ interference of 0.05-6 cps on mass 232 (predominantly $^{184}Os^{16}O_3^-$). For mass 230 (mainly $^{198}Pt^{16}O_2^-$) intensities ranged between 4,000-1,050,000 cps which results in respective interferences of 16-4,300 cps and 0.02-4.4 cps on masses 232 ($^{184}Os^{16}O_3^-$) and 234 ($^{186}Os^{16}O_3^-$). The PtO_2^- interference on mass 234 is negligible, whereas the combined PtO_2^- interferences on mass 232 reached a maximum of 4,306 cps. This represents 2.5 % of the typical total signal at mass 232 which can lower the $^{184}Os/^{188}Os$ substantially (~30,000 ppm). In this study, mass 234 was only monitored to correct for polyatomic oxygen interferences on the other Os isotopic ratios. Lowering the $^{184}Os/^{188}Os$ by 30,000 ppm results in a minor shift of -2 ppm on the $^{186}Os/^{188}Os$ and has no noticeable effect on the other Os isotopic ratios. The average difference between the two SEM runs, before and after the main run, was 250,000 cps for mass 228 and 135,000 cps for mass 230. Potential within-run variations of this magnitude have no measurable effect on the isotopic ratios. On mass 231, $^{183}WO_3^-$, we obtained intensities of 6-1,000 cps, which produce insignificant interferences on $^{186}Os^{16}O_3^-$ (Walker et al., 2005; Luguet et al., 2008). Mass 233, $^{185}ReO_3^-$, displayed intensities between 3-460 cps but were generally below 300 cps and on average 73 cps. Translated to $^{187}ReO_3^-$ this means <502 cps or 8 μV that interfered on the $^{187}OsO_3^-$. Typically, this quantity equates to a lowering of the $^{187}Os/^{188}Os$ by <100 ppm and on average 38 ppm, which is close to the 2 se of our measurements (40 ppm) but much smaller than the long-term reproducibility (268 ppm; 2 sd). Between the pre- and post SEM runs, the beam intensities on mass 233 generally varied by 33 cps which equates to a shift of ~18 ppm on the $^{187}Os/^{188}Os$. To summarize, polyatomic interferences from PtO_2^-, WO_3^-, and ReO_3^- monitored in this study had no noticeable effect on the stable Os and $^{186}Os/^{188}Os$ isotopic composition, and were minor for $^{187}Os/^{188}Os$ ratios.

5. RESULTS AND DISCUSSION

Results are presented in **Table 2-4** and **Table 2-5**, and shown in Figures 2.8 to 2.13. All internal errors are quoted as 2 standard error (2 se), whereas short term (i.e., single session) and long-term (i.e., multiple sessions) reproducibilities are given as 2 standard deviations (2 sd).

5.1 INTERNAL PRECISION, EXTERNAL REPRODUCIBILITY, AND ACCURACY

5.1.1 Stable Osmium Isotope Ratios by MC-ICP-MS

The internal precision (2 se; $n \leq 80$ cycles, depending on 2 se outlier rejection) on a single $\delta^{190}Os$ MC-ICP-MS analysis is typically between 0.01-0.02‰ when ^{188}Os beam intensities range between 7-4 V (~18-11 V $^{total}Os$; **Figure 2-7**). The amount of natural Os consumed is ~200 ng. The observed precision is in good agreement with the theoretical error as calculated in section 2.1 (**Figure 2-7**) suggesting that the model considers all the errors that should be accounted for. Small deviations from the calculated error could have arisen from, for example, variation in the spike – sample proportions, or the number of cycles included. The model considers 80 cycles whereas this can be less for MC-ICP-MS if outliers are rejected. This also explains why the error model for N-TIMS displays lower errors for a given intensity, as 280 cycles were considered for N-TIMS analyses.

Repeated analyses of reference standard solution DROsS, obtained during multiple analytical sessions over a time period of ~22 months, show an external reproducibility on $\delta^{190}Os$ of 0.02‰ (2 sd; n = 91; **Figure 2-8**; **Table 2-4**). The short-term reproducibility of a single analytical session when consuming ~200 ng natural Os at total beam intensities of 11-18 V is 0.01-0.03‰ (2 sd; n = 2-10). A similar precision and reproducibility is obtained for in-house Os reference solutions ROMIL, SpecPure and OsCaR (**Figure 2-7** and **Figure 2-9**; **Table 2-4**). As this study is the first to present stable Os isotope compositions, the accuracy cannot be assessed by measurement of pre-calibrated reference materials. Instead we have performed standard-sample bracketing measurements by
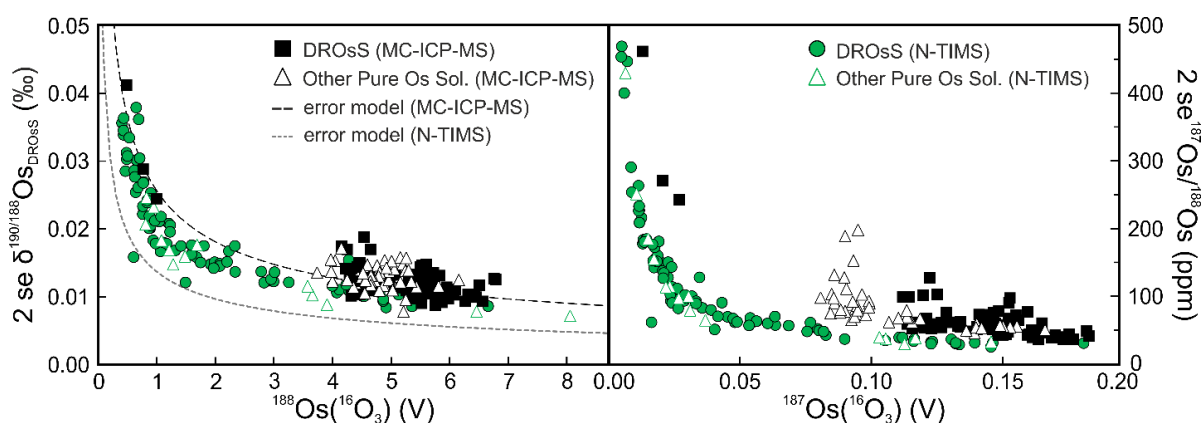
Figure 2-7 The analytical precision (2 se) on (a) $\delta^{190/188}Os$ and (b) $^{187}Os/^{188}Os$ plotted against the average (a) $^{188}OsO_3^-$ and (b) $^{187}OsO_3^-$ beam intensity (V) for analyses of reference material DROsS and other pure Os solutions by MC-ICP-MS or N-TIMS. The dashed (MC-ICP-MS) and dotted (N-TIMS) lines in (a) indicate the modelled error calculated using the method of Millet and Dauphas, 2014 using the following parameters: 80 x 8.3 seconds integrations for MC-ICP-MS and 280 x 8.3 seconds for N-TIMS; $10^{11}\,\Omega$ collectors; T= 290 K. Note that the lower theoretical error for N-TIMS results from the larger amount of cycles incorporated.

MC-ICP-MS using natural (i.e., not spiked) reference solutions. Comparison of this technique with the DS method shows that a similar offset between DROsS and the other Os reference solutions is obtained (**Figure 2-9**; **Table 2-4**) which is in support of the relative accuracy of our method.

5.1.2 Stable Osmium Isotope Ratios by N-TIMS

For a single δ^{190}Os analysis by N-TIMS the internal precision (2 se; n ≤ 280 cycles, depending on 2 se outlier rejection) ranges between 0.01-0.04‰ when ^{188}OsO$_3^-$ beam intensities vary from 6-0.43 V (~18 to 1 V ^{tot}Os beam; **Figure 2-7**). These intensities were obtained for load sizes between 45 and 2.3 ng natural Os. Repeated analyses of double spiked reference solution DROsS, over approximately 22 months, yield an external reproducibility on δ^{190}Os of 0.03‰ (2 sd; *n* = 83; **Figure 2-8**; **Table 2-4**). The majority of these analyses (*n* = 44) comprised a load of 10-20 ng natural Os, 20 analyses had a load of >20 ng, and 19 analyses were performed with less than 10 ng Os. That DROsS yields less precise and less reproducible results for N-TIMS than MC-ICP-MS is, predominantly, a consequence of the lower beam intensities at which the analyses were performed. Analyses of in-house pure Os solutions ROMIL, SpecPure and OsCaR show a similar precision and reproducibility (**Figure 2-7** and **Figure 2-9**; **Table 2-4**). That ROMIL and SpecPure display a similar offset relative to DROsS for N-TIMS as for MC-ICP-MS analyses provides support to the accuracy of our method.
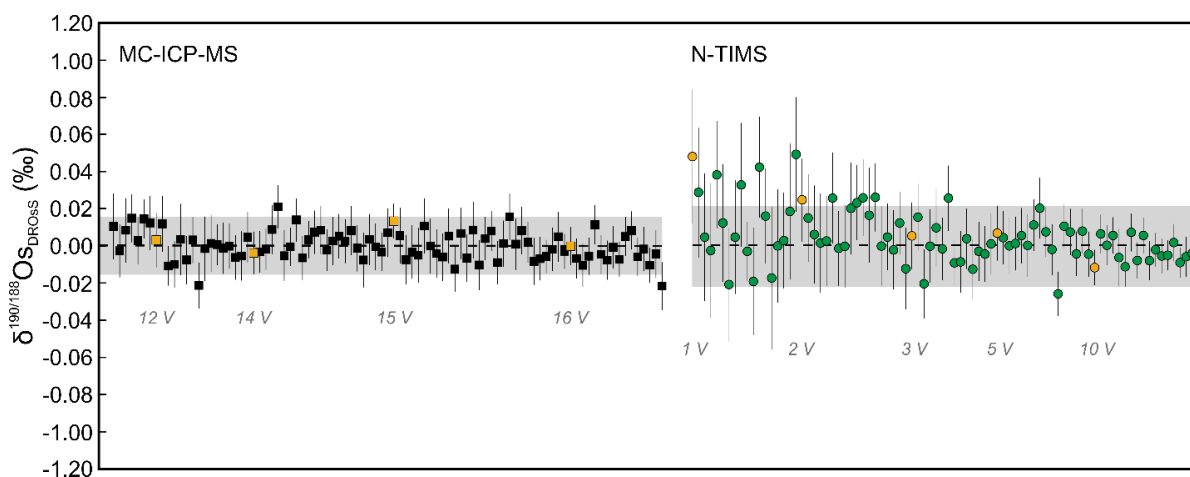
Figure 2-8 Repeated analyses of reference material DROsS on both MC-ICP-MS (squares) and N-TIMS (circles) obtained during multiple analytical sessions over a time period of 22 months. Analyses have been organized on beam intensity, where it should be noted that N-TIMS analyses were obtained at lower beam intensities. Sample sizes were approximately 200 ng natural Os for MC-ICP-MS and ranged between 2.3 and 45 ng natural Os for N-TIMS measurements, with ^{total}Os beam intensities of >4 V for MC-ICP-MS analyses and >1 V for analyses by N-TIMS. Error bars quote the 2 se error on the individual analysis, and the grey band represents the ±2 sd of all analyses. Symbols in yellow correspond to the annotated beam intensity.

5.1.3 Radiogenic Isotope Ratios by MC-ICP-MS

The precision that can be obtained for $^{187}Os/^{188}Os$ and $^{186}Os/^{188}Os$ isotopic ratios is <100 ppm (2 se; n ≤ 280 cycles, depending on 2 se outlier rejection) when ^{187}Os and ^{186}Os average beam intensities are higher than ~0.06 V over the ~11 minutes of the analysis. When average beam intensities of >0.18 V are achieved this improves to ~40 ppm (**Figure 2-7**). This is comparable with the precisions reported by Nowell et al. (2008; <40 ppm at high signal intensities;) and corresponds with the errors predicted by the model described in section 2.1 (30-40 ppm at 0.22 V; **Figure 2-7**). Repeated analyses of double spiked reference standard DROsS yield a reproducibility of 123 and 138 ppm for $^{187}Os/^{188}Os$ and $^{186}Os/^{188}Os$, respectively (2 sd, *n* = 91). This is higher than that reported by Nowell et al. (2008) for DROsS (19 ppm) but is comparable with the long-term reproducibilities reported for reference materials UMd (220 ppm for $^{187}Os/^{188}Os$ and 108 ppm for $^{186}Os/^{188}Os$) and DTM (149 ppm for $^{187}Os/^{188}Os$ and 67 ppm for $^{186}Os/^{188}Os$).

For radiogenic isotopic ratios we can use previous studies to assess the accuracy of our method. In addition, we have compared double spiked data with that from unspiked runs, and used DROsS for un-spiked sample-standard bracketing measurements. We have applied these methods to DROsS as well as to pure Os solutions ROMIL, SpecPure, and OsCaR. Taken together, the various samples encompass a significant range in $^{187}Os/^{188}Os$ isotopic ratios over which to test our analytical methods. **Table 2-4** shows that all values obtained in this study, using the various methods, are within analytical uncertainty with one another as well as with previously published values of un-spiked DROsS measurements (Luguet et al., 2008; Nowell et al., 2008).
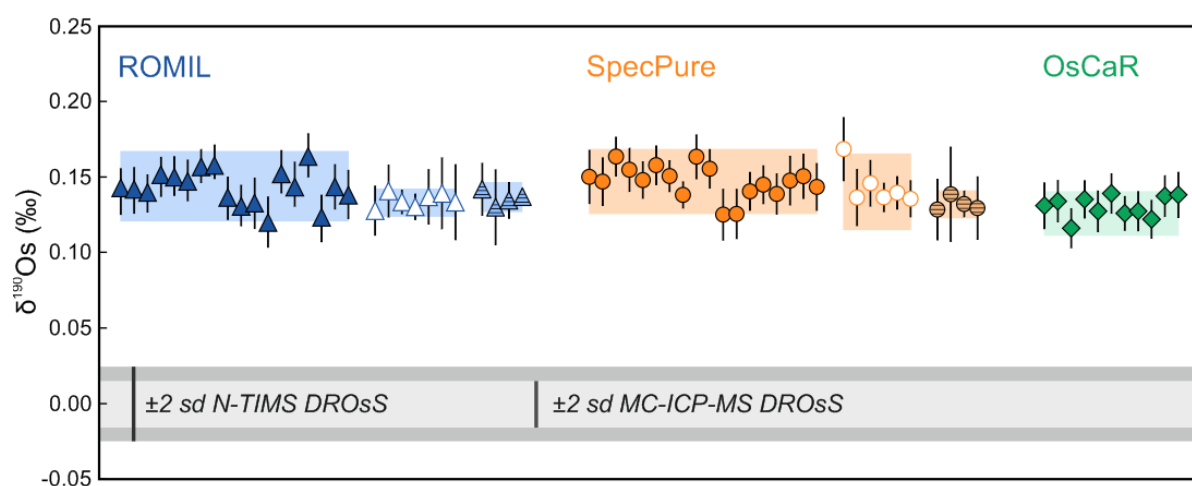
Figure 2-9 The δ$^{190/188}$Os values obtained for repeat analyses of pure Os solutions ROMIL (triangle), SpecPure (circle) and OsCaR (diamond) by both MC-ICP-MS (closed symbols) and N-TIMS (open symbols) obtained during the course of this study. The striped, filled symbols indicate sample-standard bracketing data. All Os solutions show a similar reproducibility as obtained for reference standard DROsS. Values obtained for ROMIL and SpecPure on MC-ICP-MS and N-TIMS show values within analytical uncertainty supporting the accuracy of our method. The grey bands indicate the reproducibility (±2 sd) obtained by MC-ICP-MS and N-TIMS. Error bars represent the 2 se error of an individual analysis.

Table 2-4 Average osmium stable and radiogenic isotope ratios of DROsS, SpecPure, ROMIL and OsCaR obtained in this study using: the double spike (DS) method; sample-standard bracketing by MC-ICP-MS, using non DS solutions and DROsS as the reference bracketing standard; and un-spiked runs by N-TIMS. For comparison, radiogenic isotope compositions of DROsS as obtained by previous studies are included (Nowell et al., 2008; Luguet et al., 2008). Note that the better reproducibility (2 sd) for MC-ICP-MS relative to N-TIMS is, predominantly, related to difference in beam intensities at which analyses have been made (11-18 V vs. 1-18 V total Os beam, respectively). * - Four individual sample-standard bracketing sessions were run, on different days, and include 16 analyses all together. Reported for these analyses are the average and 2 sd of the averages of the four analytical sessions.

Note! – The ^{187}Os/^{188}Os and ^{186}Os/^{188}Os ratios are increased by ~50 and ~167 ppm (or ~8 and 20 ppm absolute), respectively, when using the DROsS values of Luguet et al. (2008). See addendum to this chapter for a revised version of this table.

	n	$\delta^{190/188}$Os	2 sd	^{187}Os/^{188}Os	2 sd	^{186}Os/^{188}Os	2 sd
DROsS							
DS MC-ICP-MS	91	0.00	0.02	0.160916	0.000020	0.119909	0.000017
DS N-TIMS	83	0.00	0.03	0.160916	0.000043	0.119909	0.000043
un-spiked	14	-	-	0.160919	0.000031	-	-
previous study (MC-ICP-MS; Nowell et al., 2008)	21	-	-	0.160924	0.000003	0.119920	0.000002
previous study (N-TIMS; Luguet et al., 2008)	8	-	-	0.160924	0.000004	0.119932	0.000006
ROMIL							
DS MC-ICP-MS	18	0.14	0.02	0.106827	0.000047	0.119806	0.000017
DS N-TIMS	7	0.13	0.01	0.106857	0.000042	0.119803	0.000023
sample-std bracketing MC-ICP-MS	4*	0.14	0.01	0.106861	0.000024	0.119806	0.000007
un-spiked	3	-	-	0.106878	0.000032	-	-
SpecPure							
DS MC-ICP-MS	18	0.15	0.02	0.149162	0.000026	0.119890	0.000019
DS N-TIMS	6	0.14	0.03	0.149161	0.000053	0.119889	0.000031
sample-std bracketing MC-ICP-MS	4*	0.13	0.01	0.149163	0.000012	0.119885	0.000016
un-spiked	3	-	-	0.149180	0.000088	-	-
OsCaR							
DS MC-ICP-MS	11	0.13	0.01	0.128298	0.000022	0.119816	0.000014

Table 2-5 Osmium stable ($\delta^{190/188}$Os) and radiogenic (^{187}Os/^{188}Os and ^{186}Os/^{188}Os) isotope compositions, and Os abundances of geological materials obtained by either MC-ICP-MS or N-TIMS. Samples are digested using carius tubes (CT) or the high-pressure asher (HPA) system. W. mean = weighted mean; * = aliquots of sample material that were combined after digestion and prior to chemical separation of Os. Note! – The ^{187}Os/^{188}Os and ^{186}Os/^{188}Os ratios are increased by ~50 and ~167 ppm (or ~8 and 20 ppm absolute), respectively, when using the DROsS values of Luguet et al. (2008). See addendum to this chapter for a revised version of this table.

				smp weight (g)	^{total}Os (V)	^{188}OsO$_3^-$	^{187}OsO$_3^-$	$\delta^{190/188}$Os	2 se	^{187}Os/^{188}Os	2 se	^{186}Os/^{188}Os	2 se	[Os] ng g^{-1}	2 se
UB-N	1	HPA	N-TIMS	2.51	0.98	0.37	0.008	0.14	0.039	0.126555	0.000040	0.119746	0.000042	4.13	0.002
	2	HPA	N-TIMS	2.51	1.16	0.43	0.009	0.13	0.039	0.126983	0.000039	0.119804	0.000037	4.02	0.002
	3	HPA	N-TIMS	2.49	0.92	0.35	0.007	0.13	0.056	0.127061	0.000047	0.119784	0.000047	3.89	0.003
	4	CT	N-TIMS	2.49	0.82	0.33	0.006	0.11	0.073	0.127073	0.000057	0.119806	0.000061	3.72	0.002
	5*	HPA	N-TIMS	6.03	3.99	1.53	0.030	0.13	0.017	0.127128	0.000011	0.119813	0.000012	3.62	0.001
	6*	HPA	N-TIMS	5.99	3.09	1.19	0.023	0.14	0.015	0.127181	0.000011	0.119815	0.000010	3.55	0.001
w. mean								**0.14**		**0.127126**		**0.119813**		**3.64**	
2 sd								**0.02**		**0.000453**		**0.000053**		**0.46**	
GP-13	1*	HPA	N-TIMS	4.02	4.95	1.87	0.039	0.14	0.015	0.126372	0.000010	0.119825	0.000010	3.87	0.002
	2*	HPA	N-TIMS	4.05	4.67	1.76	0.036	0.15	0.016	0.126426	0.000009	0.119804	0.000009	3.82	0.002
w. mean								**0.15**		**0.126401**		**0.119813**		**3.84**	
2 sd								**0.01**		**0.000077**		**0.000030**		**0.07**	
CHR-Bkg	1	HPA	N-TIMS	0.93	4.68	1.75	0.037	0.14	0.016	0.126667	0.000010	0.119813	0.000010	27.96	0.01
	2	HPA	N-TIMS	0.92	2.74	1.03	0.022	0.14	0.021	0.127671	0.000016	0.119819	0.000016	27.48	0.01
	3	CT	N-TIMS	0.55	1.21	0.46	0.009	0.12	0.033	0.127340	0.000034	0.119827	0.000035	26.32	0.01
	4a	HPA	MC-ICP-MS	2.06	3.42	1.29	0.026	0.13	0.034	0.127210	0.000040	0.119856	0.000047	24.72	0.001
	4b	HPA	N-TIMS	""	6.02	2.30	0.046	0.12	0.014	0.127503	0.000008	0.119798	0.000009	24.72	0.001
	5	HPA	N-TIMS	0.92	9.64	3.80	0.070	0.12	0.011	0.128170	0.000006	0.119822	0.000006	23.11	0.01
	6	CT	N-TIMS	0.58	1.81	0.71	0.013	0.13	0.027	0.127929	0.000025	0.119809	0.000025	22.97	0.01
	7	HPA	N-TIMS	0.92	9.50	3.79	0.067	0.11	0.011	0.127830	0.000006	0.119815	0.000007	21.95	0.01
w. mean								**0.12**		**0.127803**		**0.119818**		**24.73**	
2 sd								**0.02**		**0.000945**		**0.000034**		**4.39**	

Table 2-5 continued

			smp weight (g)	^{total}Os (V)	^{188}OsO$_3^-$	^{187}OsO$_3^-$	$\delta^{190/188}$Os	2 se	^{187}Os/^{188}Os	2 se	^{186}Os/^{188}Os	2 se	[Os] ng g^{-1}	2 se
CHR-Pt+	1a	HPA	MC-ICP-MS	0.23	15.54	5.62	0.129	0.18	0.022	0.128992	0.000011	0.119819	0.000009	2121	6
	1b	HPA	N-TIMS	""	15.35	5.59	0.129	0.20	0.008	0.129278	0.000004	0.119823	0.000005	2121	4
	2a	HPA	MC-ICP-MS	0.25	25.05	9.41	0.195	0.15	0.009	0.129012	0.000006	0.119794	0.000004	1805	6
	2b	HPA	N-TIMS	""	6.60	2.49	0.052	0.18	0.012	0.129260	0.000008	0.119833	0.000008	1805	6
	3	CT	MC-ICP-MS	0.25	23.15	8.76	0.178	0.15	0.005	0.129029	0.000004	0.119796	0.000003	1785	4
	4	CT	MC-ICP-MS	0.25	12.02	4.54	0.092	0.13	0.011	0.128993	0.000012	0.119744	0.000009	1747	6
w. mean								**0.16**		**0.129033**		**0.119804**		**1879**	
2 sd								**0.05**		**0.000273**		**0.000064**		**349**	
ZAG	1a	HPA	MC-ICP-MS	0.24	6.73	2.51	0.049	0.13	0.02	0.129518	0.000018	0.119780	0.000025	929	6
	1b	HPA	N-TIMS	""	3.28	1.26	0.025	0.11	0.01	0.129759	0.000007	0.119815	0.000007	929	4
	2	HPA	MC-ICP-MS	0.25	8.94	3.28	0.067	0.13	0.01	0.126549	0.000011	0.119818	0.000012	926	6
	3	HPA	MC-ICP-MS	0.25	9.16	3.38	0.068	0.13	0.02	0.128046	0.000014	0.119779	0.000013	905	6
	4	HPA	MC-ICP-MS	0.25	8.63	3.18	0.064	0.13	0.01	0.128557	0.000012	0.119801	0.000014	904	6
	5	HPA	MC-ICP-MS	0.50	5.78	2.15	0.042	0.13	0.02	0.129214	0.000028	0.119789	0.000021	892	3
	6	HPA	MC-ICP-MS	0.50	12.05	4.47	0.088	0.11	0.01	0.128650	0.000011	0.119790	0.000010	887	3
	7	HPA	MC-ICP-MS	0.25	8.73	3.24	0.064	0.13	0.02	0.128382	0.000013	0.119819	0.000013	884	6
	8	HPA	MC-ICP-MS	0.25	9.03	3.40	0.065	0.14	0.02	0.128303	0.000014	0.119787	0.000013	861	6
	9	CT	N-TIMS	0.08	5.05	1.90	0.040	0.12	0.02	0.128699	0.000015	0.119830	0.000015	839	17
w. mean								**0.12**		**0.128407**		**0.119804**		**896**	
2 sd								**0.02**		**0.001791**		**0.000036**		**59**	

5.1.4 Radiogenic Isotope Ratios by N-TIMS

For N-TIMS analyses the internal precision on both $^{187}Os/^{188}Os$ and $^{186}Os/^{188}Os$ is <100 ppm (2 se; n ≤ 280 cycles, depending on 2 se outlier rejection) for analyses with average $^{187}OsO_3^-$ and $^{186}OsO_3^-$ beam intensities >0.03 V over the 280 cycles of analysis, and improves to <40 ppm at high signal intensities (>0.18 V; **Figure 2-7**). This is slightly greater than the precisions reported by Luguet et al. (2008; <30 ppm at >0.08 V). Repeated analyses of reference standard DROsS yield a reproducibility of 268 ppm and 361 ppm for $^{187}Os/^{188}Os$ and $^{186}Os/^{188}Os$ ratios, respectively (2 sd, n = 83) for loads varying between 2.3 and 45 ng natural Os. This is significantly higher than the values reported by Luguet et al. (2008; 26 and 48 ppm, respectively). Where Luguet et al. (2008) have only included analyses with $^{187}OsO_3^-$ and $^{186}OsO_3^-$ beam intensities of 80 mV or above we have taken analyses with intensities down to 20 mV into account. When excluding the analyses with beam intensities <80 mV on $^{187}OsO_3^-$ and $^{186}OsO_3^-$ we obtain a long-term reproducibility of 90 and 89 ppm, respectively (2 sd; n = 22). These slightly higher analytical uncertainties are related to error propagation inherent in double-spike deconvolution. That errors are higher than predicted by the model is, predominantly, because the error on the oxygen composition was not incorporated in the model whereas it has been propagated for the actual analyses.

To assess the accuracy, we have compared radiogenic values obtained by our DS method with those determined for unspiked runs and with previous studies (**Table 2-4**). All values are within analytical uncertainty of one another which demonstrates that our method is able to obtain accurate $^{187}Os/^{188}Os$ and $^{186}Os/^{188}Os$ isotopic ratios by N-TIMS. This provides a valuable quality control on the DS calculations and allows the acquisition of both the stable and radiogenic isotope composition within a single analytical run.

5.2. GEOLOGICAL MATERIALS

During the course of this study, we have measured four international geological reference materials. The selected materials cover a range of matrices; (1) UB-N (Meisel et al., 2003), a serpentinised and fertile lherzolite from the Voges in France; (2) GP-13 (Pearson and Woodland, 2000; Pearson et al., 2004), a fertile lherzolite from the Beni Bousera massif in Morocco; (3) CHR-Bkg (Potts et al., 1992; Paliulionyte et al., 2006) and (4) CHR-Pt+ (Potts et al., 1992; Bédard and Barnes, 2004), which are both chromitites from the Shetland ophiolite in Scotland, UK. Furthermore, we have analysed the ordinary H-chondrite Zag. Although this is not an international reference material, sufficient sample material was available to perform several replicate analyses allowing the exploration of another type of sample matrix. Stable and radiogenic Os isotope compositions, together with Os abundances, are given in **Table 2-5** and shown in Fig. 10-13.

5.2.1 Radiogenic Osmium Isotope Compositions for Geological Materials

We have shown that double spiked DROsS analyses display $^{187}Os/^{188}Os$ and $^{186}Os/^{188}Os$ ratios consistent with previous published studies, and that ROMIL and SpecPure yield similar values for various methods (i.e., non-DS, DS, standard sample bracketing). This means that although the main aim of this method is to obtain high precision stable isotope data it also has the potential to provide radiogenic isotopic ratios within the same analyses. This is particularly beneficial when dealing with limited amounts of available sample material that only allows a single analysis. Furthermore, it significantly reduces processing and measurement time.

Apart from three UB-N analyses, all data is obtained at average $^{187}OsO_3^-$ and $^{186}OsO_3^-$ beam intensities of ≥ 0.01 V for N-TIMS ($^{total}Os \geq 1$ V) analyses and ^{187}Os and $^{186}Os \geq 0.03$ V for MC-ICP-MS

Figure 2-10 The $^{187}Os/^{188}Os$ isotope ratios of geological materials UB-N, GP-13, CHR-Bkg, CHR-Pt+ and Zag analysed by MC-ICP-MS (closed symbols) or N-TIMS (open symbols) display values consistent with previous studies (grey bars). Literature data for maximum and minimum values: UB-N (Meisel et al., 2003; Harvey et al., 2011); GP-13 (Puchtel et al., 2007; Marchesi et al., 2014); CHR-Bkg – (Meisel et al., 2003); CHR-Pt+ - no previous published data; Zag (Meisel et al., 1996; Walker et al., 2002).

($^{total}Os \geq 1$ V). The influence of the $^{17}O/^{16}O$ composition and OPZ on the accuracy of the isotopic compositions is shown to be negligible at these intensities. Geological materials analysed in this study display $^{187}Os/^{188}Os$ values that are consistent with the range of values obtained by previous studies (**Figure 2-10** and **Figure 2-13**). However, a significant degree of irreproducibility (up to 7,400 ppm) can be observed which will be discussed in section 5.2.3. The variability observed for $^{186}Os/^{188}Os$ ratios is much smaller, 251-537 ppm, and comparable with the

Figure 2-11 The $^{186}Os/^{188}Os$ ratios of geological materials UB-N, GP-13, CHR-Bkg, CHR-Pt+ and Zag analysed by MC-ICP-MS (closed symbols) or N-TIMS (open symbols). In case the DROsS values of Nowell et al. (2008) are used, most samples plot below the upper mantle value of 0.119837±5 (2 sd; Ireland et al., 2011). CT = Carius tube digestions, all other sample aliquots are processed using the high-pressure asher system. * = an analysis for which digestions were combined prior to chemical Os extraction. Error bars indicate the 2 se on the individual analysis. Note! - see the addendum for a revised version of this figure.

long-term reproducibility obtained for N-TIMS DROsS analyses (361 ppm). Assessment of the accuracy of our $^{186}Os/^{188}Os$ values by direct comparison with previously published values for these samples is not possible as they have not been measured for $^{186}Os/^{188}Os$ before. The $^{186}Os/^{188}Os$ ratios of all samples range from 0.119746 ± 42 to 0.119856 ± 47, which is in close approximation of the upper mantle value (0.119837±5; Ireland et al., 2011) but consistently lower when using the DROsS values of Nowell et al. (2008; **Figure 2-11**). In the addendum, this inconsistency is further discussed and it is shown that the discrepancy with literature data can be resolved when using the DROsS data as provided by Luguet et al. (2008) instead of those by Nowell et al. (2008). See the addendum for a revised version of Figure 2-11.

5.2.2 Stable Osmium Isotope Compositions for Geological Materials

The internal precision and external reproducibility on $\delta^{190}Os$ are similar to that obtained for pure Os isotope solutions. One exception is the reproducibility reported by CHR-Pt+. This will be discussed in more detail in section 5.2.3. Similar to Os standard solutions, replicate analyses of chondrite ZAG show similar values for MC-ICP-MS and N-TIMS analyses, providing further support for the accuracy of our method on a real sample matrix.

All reference materials are derived from Earth's mantle. The materials show no resolvable variation at the 95 % c.i. level and provide an average $\delta^{190}Os$ value of 0.13 ± 0.03‰ (2 sd; n = 4). The geological reference material CHR-Bkg displays the lightest composition of $\delta^{190}Os$ = 0.12 ± 0.02‰ (2 sd; n = 7) and chromitite CHR-Pt+ the heaviest at 0.16 ± 0.05 (2 sd; n = 4). Ordinary chondrite Zag yields a $\delta^{190}Os$ value of +0.12 ± 0.02‰ (2 sd; n = 9) which is indistinguishable, within uncertainty, from the mantle derived samples.

Interestingly, DROsS is the only material that displays a different, isotopically lighter, composition relative to the other materials measured in this study. This offset could (a) be a product of the chemical extraction of Os from the source material, or (b) reflect the original composition of the material from which the Os was sourced.
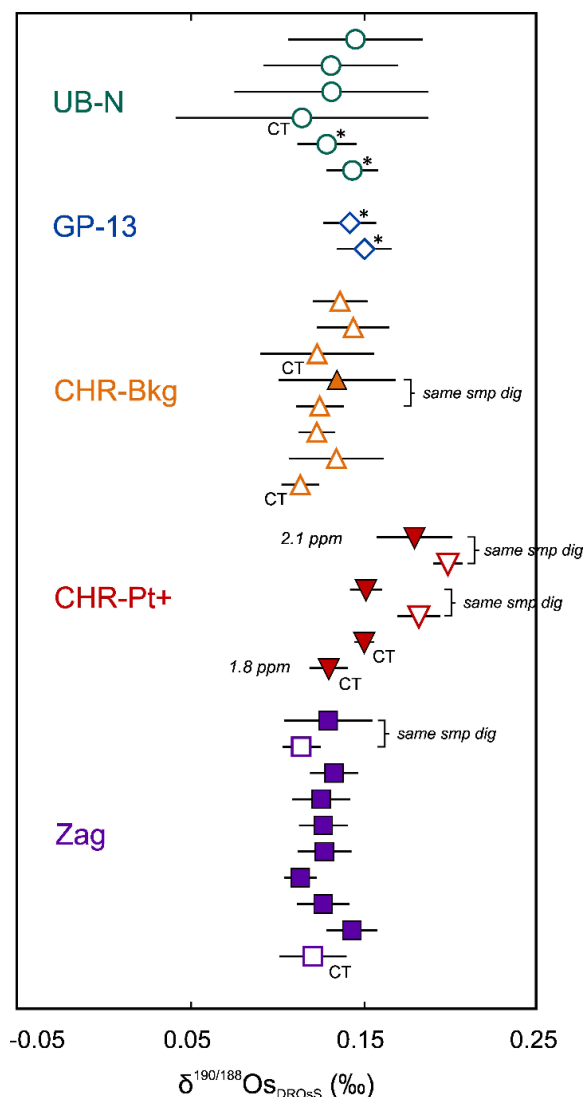
Figure 2-12 Osmium stable isotope compositions ($\delta^{190/188}Os$) of geological materials UB-N, GP-13, CHR-Bkg, CHR-Pt+ and Zag, analysed by either MC-ICP-MS (closed symbols) or N-TIMS (open symbols). Symbols are ordered from high to low Os concentration, revealing a broad correlation with $\delta^{190/188}Os$ for CHR-Pt+. Apart from Zag, which is an ordinary chondrite, all samples are reference materials sourced by the Earth's mantle. Symbols and annotations as in Fig. 11.

5.2.3 Effect of Sample Digestion

In mantle rocks, osmium is concentrated in refractory accessory phases that are heterogeneously distributed throughout the rock (the "nugget" effect). This has led to difficulties in repeating results when considering Os abundances and ^{187}Os/^{188}Os ratios. Over the past two decades, various digestion methods have been assessed in order to resolve this problem (e.g., Meisel et al., 2001; Reisberg and Meisel, 2002; Meisel et al., 2003; Ishikawa et al., 2014). Acid attack digestions using sealed glass Carius tubes (CT; Shirey and Walker, 1995; Shen et al., 1996) and the high-pressure asher system (HPA; Meisel et al., 2001) are most frequently used. This is because they are considered to be most efficient in attacking the highly resistant phases that are likely to contain appreciable Os (such as Cr-spinel and platinum-group minerals). In this study, we have applied both techniques to various geological materials. A limitation of both techniques is the maximum amount of sample material that can be digested effectively (≤2 g). In the case of geological samples with low Os abundances (e.g., most mantle material like UB-N, and nearly all crustal material) more than 2 g of material is needed to obtain high precision data. To circumvent this problem, we have digested several sample aliquots of UB-N and GP-13, and combined them prior to solvent extraction. As for the individual processed samples, each aliquot was spiked before digestion. As the proportion of spike is one of the unknowns calculated during the resolution of the DS equation system, it should be noted that reaching a 100 % yield across all aliquots during sample processing is not required to generate accurate isotope ratios and concentration determinations, providing that spike-sample equilibration occurs before loss of any Os during sample processing.

Apart from CHR-Pt+, replicate digestion of individual samples shows no detectable stable isotope variation and no systematic difference between CT or HPA digestions. For the combined aliquots of UB-N, relative to the single digestions, we do not observe any variation for stable Os isotopes either (**Figure 2-12**; **Table 2-5**). The two analyses of combined GP-13 aliquots show consistent stable isotope compositions as well. By contrast, statistically resolvable variations in ^{187}Os/^{188}Os ratio and Os abundance were observed in all the samples tested. In the case of UB-N and CHR-Bkg, ^{187}Os/^{188}Os is positively correlated with 1/[Os] (**Figure 2-13**). This co-variation was observed previously, in a more extensive study of UB-N, by Meisel et al. (2003). The CHR-Bkg analyses reported within that study display a more limited variation and no significant co-variation between Os
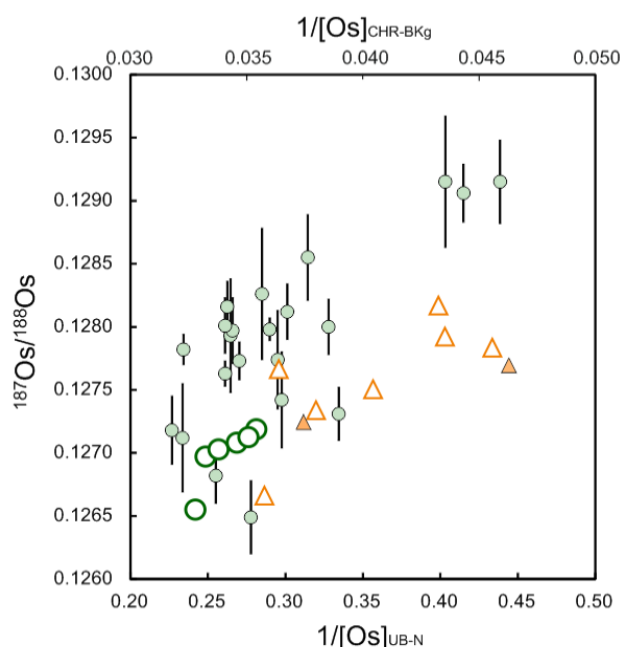
Figure 2-13 Correlation between ^{187}Os/^{188}Os ratios and 1/[Os] for reference materials UB-N (circles) and CHR-Bkg (triangles), as obtained for independently processed sample aliquots in this study (open symbols). Included are data as obtained by Meisel et al., 2003 (filled symbols).

abundance and radiogenic isotopic composition was discussed. If we incorporate the CHR-Bkg data of Meisel et al. (2003) they fall within the trend obtained in this study. The observed variation in radiogenic isotopes can be explained by incomplete digestion and/or sample heterogeneity. In both cases this indicates that within the digested material different phases, or phases of different generations, possess distinct radiogenic isotopic composition. The absence of stable Os isotope variation, for these particular aliquots, implies that there is no significant difference in stable isotope composition of the phases in these samples. As such, the type of digestion technique, or the combination of individual digestions, appears to have no influence on the stable isotope composition for these particular samples.

For CHR-Pt+ we observe a larger range in stable Os isotope compositions (δ^{190}Os = +0.13 − +0.20‰), which is reflected in the relatively poor reproducibility (0.05‰). The stable isotope data appear to co-vary with Os abundance, with the heavier values corresponding to higher Os abundance of about 21% (1747 relative to 2121 ppb; Table 2-5 Osmium stable ($\delta^{190/188}$Os) and radiogenic (^{187}Os/^{188}Os and ^{186}Os/^{188}Os) isotope compositions, and Os abundances of geological materials obtained by either MC-ICP-MS or N-TIMS. Samples are digested using carius tubes (CT) or the high-pressure asher (HPA) system. W. mean = weighted mean; * = aliquots of sample material that were combined after digestion and prior to chemical separation of Os.**Table 2-5**). As discussed before, variance in isotopic composition correlating with Os abundance may indicate that phases within the whole rock contain different stable isotopic signatures. Our preliminary data suggests that phases within chromitite CHR-Pt+ possess different stable Os isotopic compositions. Previous studies that focused on the origin of chromitites derived from the Cliff deposit in the Shetland Ophiolite concluded that initial PGE concentrations were caused by magmatic processes followed by a hydrothermal overprint which locally remobilized and re-concentrated the PGE (Lord et al., 1994). This secondary process might be the source of Os stable isotope fractionation, but further investigation is required.

6. CONCLUSIONS

We have developed a method for high-precision measurement of stable Os isotope compositions by both plasma source (MC-ICP-MS) and thermal ionisation mass spectrometry (N-TIMS). The method utilizes a ^{188}Os-^{190}Os double spike that is added to the sample prior to digestion with a spike-sample proportion of 0.55:0.45. We show that the technique is robust when dealing with matrix effects and interference corrections on MC-ICP-MS, even for levels up to 10 % of the total Os concentration, and that the memory effect for MC-ICP-MS analyses is negligible. Analyses performed by N-TIMS show that the oxygen isotopic composition exerts a major control on the accuracy of the isotopic ratios. It is suggested that the oxygen isotopic composition is obtained for every specific run, by measuring the ^{18}O/^{16}O for each individual cycle, and calculating the ^{17}O/^{16}O ratio from the ^{18}O/^{16}O ratio, especially when the total Os signal intensity drops below 2 V.

The internal precision (2 se) on the δ^{190}Os measurement (permil difference of the ^{190}Os/^{188}Os ratio relative to reference standard DROsS) of a single analysis is 0.01-0.02‰ for MC-ICP-MS (~200 ng natural Os; *n* = 80 cycles) and 0.01-0.03‰ for N-TIMS (2.3-45 ng natural Os; *n* = 280 cycles). The long-term reproducibility of

reference material DROsS is 0.02‰ (2 sd; n = 91) and 0.03‰ (2 sd; n = 83) for MC-ICP-MS and N-TIMS, respectively.

The method is shown to be capable of obtaining Os stable isotope compositions of terrestrial and extra-terrestrial materials with a high precision and reproducibility. The first data obtained for geological materials are all within analytical uncertainty of one another, despite the measurement of samples reflecting a range of source regions, chemical compositions, geological history, and radiogenic isotope ratios. Minor variations between different digestions of chromitite CHR-Pt+ hints at Os stable isotope fractionation as a result of Os remobilization due to hydrothermal alteration. Overall, our preliminary δ^{190}Os value for the Earth's upper mantle is +0.13 ± 0.03‰ (2 sd; n = 4), which is indistinguishable from a value of +0.12 ± 0.02‰ (2 sd; n = 9) obtained for the ordinary H-chondrite Zag.

ACKNOWLEDGEMENTS

APPENDIX to CHAPTER 2

2.A-1 Calculating $^{17}O/^{16}O$ Based on Measured $^{18}O/^{16}O$

An important step in the N-TIMS data reduction, is the correction for oxygen interferences. In this study, we have applied a two-step correction, where in step one a starting oxygen composition is used in order to determine the "true" oxygen isotope composition of the particular measurement. For the first step we have used the compositions as determined by Luguet et al. (2008):

$$^{17}O/^{16}O_{Luguet} = R_1 = 0.00038582 \tag{1}$$

$$^{18}O/^{16}O_{Luguet} = R_2 = 0.00203486 \tag{2}$$

The intensities obtained on a certain mass (I_x in V) were corrected for the effects of variable isobaric oxygen isotope interferences of the heavier oxygen isotopes (^{17}O and ^{18}O) following:

$$O_1 = 3*R_1 \tag{3}$$

$$O_2 = 3*R_1^2 + 3*R_2 \tag{4}$$

$$O_3 = R_1^3 + 6*R_1*R_2 \tag{5}$$

$$O_4 = 3*R_1^2*R_2 + 3*R_2^2 \tag{6}$$

$$O_5 = 3*R_1*R_2^2 \tag{7}$$

$$O_6 = R_2^3 \tag{8}$$

Where O_i represent the difference in mass (i in amu) between the analyte mass of interest and the lightest mass that could generate a potential oxide interference. For example, the ions collected on mass 234 (I_{234}) are predominantly representing $^{186}Os^{16}O_3^-$ (I^{186}) ions but also reflect oxygen complexes originating from ^{184}Os ($^{184}Os^{16}O^{17}O_2^-$ and $^{184}Os^{16}O_2^{18}O^-$). In this case, the mass difference is 2 amu and thus $O_i = O_2$. Using equations 3-8, the intensities of $^jOs^{16}O_3^-$ ions (I^j) can be determined as follows:

$$I^{184} = I_{232} \tag{9}$$

$$I^{186} = I_{234} - (I_{232}*O_2) \tag{10}$$

$$I^{187} = I_{235} - (I_{232}*O_3) - (I_{234}*O_1) \tag{11}$$

$$I^{188} = I_{236} - (I_{232}*O_4) - (I_{234}*O_2) - (I_{235}*O_1) \tag{12}$$

$$I^{189} = I_{237} - (I_{232}*O_5) - (I_{234}*O_3) - (I_{235}*O_2) - (I_{236}*O_1) \tag{13}$$

$$I^{190} = I_{238} - (I_{232}*O_6) - (I_{234}*O_4) - (I_{235}*O_3) - (I_{236}*O_2) - (I_{237}*O_1) \tag{14}$$

$$I^{192} = I_{240} - (I_{234}*O_6) - (I_{235}*O_5) - (I_{236}*O_4) - (I_{237}*O_3) - (I_{238}*O_2) \tag{15}$$

By obtaining the intensities on the various $^jOs^{16}O_3^-$ ions, masses 241 ($^{192}Os^{16}O_2^{17}O^- = I^{192}17$) and 242 ($^{192}Os^{16}O_2^{18}O^- = I^{192}18$) can be stripped from minor tri-oxide interferences as well, following:

$$I^{192}17 = I_{241} - (I_{235}*O_6) - (I_{236}*O_5) - (I_{237}*O_4) - (I_{238}*O_3) \tag{16}$$

$$I^{192}18 = I_{242} - (I_{236}*O_6) - (I_{237}*O_5) - (I_{238}*O_4) \tag{17}$$

Subsequently, these intensities were used to determine the "true" oxygen isotope compositions ($^{17}O/^{16}O$ and $^{18}O/^{16}O$) of the individual cycle:

$$^{17}O/^{16}O_{true} = R'_1 = (I^{192}17 / I^{192}) / 3 \tag{18}$$

$$^{18}O/^{16}O_{true} = R'_2 = (I^{192}18 / I^{192}) / 3 \tag{19}$$

These oxygen compositions were then used to perform the "stripping" again (equations 3-15), now with the "true" oxygen composition. This means that R_1 and R_2 in equations 3-8 are replaced by R'_1 and R'_2.

In this study, we observed that the $^{17}O/^{16}O$ composition imposes a significant inaccuracy on the stable Os isotope composition when total Os signal intensities dropped below 1 V. Therefore, instead of accomplishing equations (16) and (18), the $^{17}O/^{16}O$ composition was based on the "true or measured" $^{18}O/^{16}O$ composition as determined in equation (19). In order to calculate the $^{17}O/^{16}O$ from the measured $^{18}O/^{16}O$ the relationship between the stable oxygen isotopes needs to be considered. In this study, we assume that the oxygen isotopic compositions vary as a result of equilibrium mass-dependent isotopic fractionation. The relationship among the three stable oxygen isotopes is exponential and can be written as:

$$\delta^{17}O + 1 = \left(\delta^{18}O + 1\right)^{\lambda} \tag{20}$$

, where λ defines the slope of the line. By taking a logarithm, equation (20) can be linearized (Miller, 2002):

$$10^3 * ln\left(\delta^{17}O/10^3 + 1\right) = \lambda * \left(10^3 * ln\left(\delta^{18}O/10^3 + 1\right)\right) \tag{21}$$

To calculate the $^{17}O/^{16}O$ composition, equation (21) can be re-written:

$$\delta^{17}O = e^{\lambda*\left(ln\left(\left(\delta^{18}O/10^3\right)+1\right)\right)} * 10^3 \tag{22}$$

with,

$$^{17}O/^{16}O_{true} = \left(\delta^{17}O/10^3 + 1\right) * {^{17}O/^{16}O_{VSMOW}} \tag{23}$$

, where λ is 0.526, as we assume that the fractionation occurs along the "Terrestrial Fractionation Line" (TFL; Clayton et al., 1973) for which the average literature values is 0.526 (e.g., Barkan and Luz, 2005; Rumble et al., 2007; Ahn et al., 2012). The $\delta^{17}O$ and $\delta^{18}O$ use the VSMOW (Vienna Standard Mean Ocean Water) as reference values. Generally, the $^{18}O/^{16}O$ ratio of VSMOW is accepted to be 0.0020052 (Baertschi, 1976) whereas there is more debate about the $^{17}O/^{16}O$ ratio, with values ranging between 0.000380 (Li et al., 1988) and 0.000384 (Lorin, 1992). Using data of this study we obtain an intercept with zero at a value of 0.000382 which is within the range previously observed and, therefore, used in this study (Fig. S.1). To determine this intercept we used analyses that were obtained at a beam intensity of >2 mV on mass 241. If these analyses are plotted in 10^3 ln(1+$\delta^{17}O/10^3$) vs. 10^3 ln(1+ $\delta^{18}O/10^3$) space, following the approach of Miller (2002), a regression coefficient (λ) of 0.488±0.072 (95 c.i.) is obtained (Fig. S.1). Isoplot 4 was used to calculate the slope as well as the error on the slope. When the selected analyses are considered in $^{17}O/^{16}O$ vs. $^{18}O/^{16}O$ space an approximate linear relationship with a slope of 0.092 ± 0.014 (95 c.i.) and an intercept of 0.000197 ± 0.000027 (95 c.i.) is obtained. This is within error of the values obtained when assuming a slope of 0.526 over the $^{18}O/^{16}O$ interval of 0.002007 to 0.002055 (the range in $^{18}O/^{16}O$ observed in this study); 0.0994 x + 0.000183, where x is $^{18}O/^{16}O$.
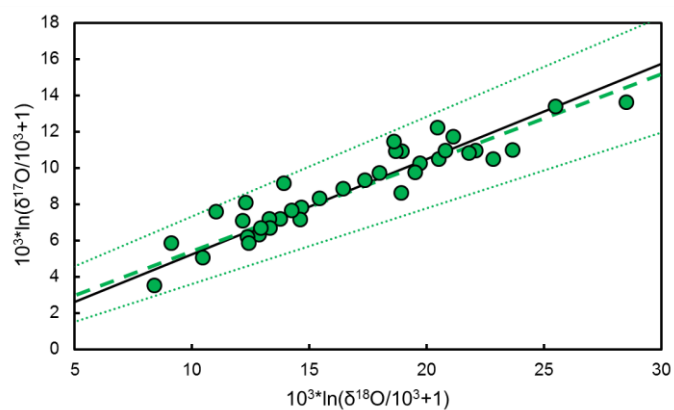
Figure S.1 Measured $^{17}O/^{16}O$ and $^{18}O/^{16}O$ compositions of analyses with a beam intensity of >2 mV on mass 241 plotted as delta values in logarithmic form. The regression line (dashed line) is within error (dotted lines) of the terrestrial fractionation line with a slope of 0.526 (solid line).

ADDENDUM to CHAPTER 2

During the course of this study the observation was made that ^{186}Os/^{188}Os isotope ratio data, as obtained by the DS method developed as part of the thesis, was offset to consistently lower values compared to literature data. In this appendix we discuss the reason for this discrepancy. First, we provide a more detailed background as to how the radiogenic isotope ratios (^{186}Os/^{188}Os and ^{187}Os/^{188}Os) are obtained.

I-1 Radiogenic formula

The formulas used to obtain ^{186}Os/^{188}Os ratios are outlined below. The same principle is used for calculating ^{187}Os/^{188}Os isotope ratios.

$$^{186}Os/^{188}Os_{sample} = {}^{186}Os/^{188}Os_{DROsS} + rad186$$

Where "DROsS" is the reference standard and "rad186" is the radiogenic component of the sample, which is calculated as follows:

$$rad186 = \frac{\left(\left({}^{186}Os/^{188}Os_{raw} * \left(\frac{At.M.186}{At.M.188}\right)^{\beta}\right) - \left(f * {}^{186}Os/^{188}Os_{DS}\right)\right)}{\left((1-f) * \left(\frac{At.M.186}{At.M.188}\right)^{\alpha}\right)} - {}^{186}Os/^{188}Os_{DROsS}$$

Where "α" is the natural and "β" the processing and instrumental exponential fractionation factors, respectively, "f" is the relative proportion of ^{188}Os originating from the spike in the sample–spike mixture, At. M. stands for Atomic Mass and "DS" for Double Spike. This formula is based on the double spike formula:

$$\frac{^{186}Os}{^{188}Os_{measured}} = \left(f * {}^{186}Os/^{188}Os_{DS} + (1-f) * \left({}^{186}Os/^{188}Os_{DROsS} + rad186\right) * \left(\frac{At.M.186}{At.M.188}\right)^{\alpha}\right)$$
$$* \left(\frac{At.M.186}{At.M.188}\right)^{\beta}$$

The relative proportion of ^{188}Os originating from the spike in the sample–spike mixture, f, is calculated following:

$$f = \frac{\left({}^{189}Os/^{188}Os_{raw} * \left(\frac{At.M.189}{At.M.188}\right)^{\beta} - {}^{189}Os/^{188}Os_{DROsS} * \left(\frac{At.M.189}{At.M.188}\right)^{\alpha}\right)}{\left({}^{189}Os/^{188}Os_{DS} - {}^{189}Os/^{188}Os_{DROsS} * \left(\frac{At.M.189}{At.M.188}\right)^{\alpha}\right)}$$

Using this approach, the radiogenic values are corrected for mass-dependent stable isotope fractionation. The $^{186}Os/^{188}Os$ ratios in this study should, therefore, provide the same values as obtained when performing conventional Os isotope analyses – i.e. for an unspiked Os isotope measurement where the radiogenic ratio is corrected for mass bias by internal normalization.

Figure 2-14 of Chapter 2 shows that the $^{186}Os/^{188}Os$ data of mantle reference material is consistently lower than the upper mantle value reported by Ireland et al. (2011), obtained using conventional methods (the "unspiked" approach). Below, we discuss that this is related to the isotope composition that was used for the reference material.

I-2 DROsS reference standard composition

The DROsS composition of Nowell et al. (2008; Table I-1) is taken as the reference standard for the Os DS method here. This standard was chosen as it's composition has been determined by MC-ICP-MS and the DS was calibrated using the same instrumentation. Nowell et al. (2008) report that the reference materials analyzed in that study show extremely good agreement between MC-ICP-MS and N-TIMS (Luguet et al., 2008) for the $^{190}Os/^{188}Os$, $^{189}Os/^{188}Os$ and $^{187}Os/^{188}Os$ ratios, but consistently lower values for the $^{186}Os/^{188}Os$ and $^{184}Os/^{188}Os$ ratios obtained by MC-ICP-MS. The magnitude of the offset for $^{186}Os/^{188}Os$ ratios was found to be 167 ppm when compared to the values obtained by Luguet et al. (2008; Table I-1), although the reason for this discrepancy was not apparent (Nowell et al., 2008).

When using the $^{186}Os/^{188}Os$ as determined by Luguet et al. (2008) this results in an increase of ~167 ppm which resolves the discrepancy observed for the geological reference materials (See Figure I-1a and I-1b). Where most $^{186}Os/^{188}Os$ values were initially lower than the PUM value, they now scatter around the primitive upper mantle value.

The double spike has been re-calibrated using the isotope composition for DROsS as reported by Luguet et al. (2008). The new DS composition is given in Table I-2. Data reported in Chapter 2, i.e., Table 2-4 and Table 2-5, has been revised and can be found in Table I-3 and Table I-4. Using the values of Luguet et al. (2008) as reference standard has no significant implication on the stable isotope composition, whereas it does significantly changes the $^{186}Os/^{188}Os$ and $^{187}Os/^{188}Os$ ratios. In the remainder of this thesis, the DROsS value of Luguet et al. (2008) has been used as reference standard composition, in combination with the re-calibration spike composition.

Tabel I-1 Osmium isotope composition for DROsS as determined by Nowell et al. (2008) and Luguet et al. (2008). Data was obtained either by MC-ICP-MS (P) or N-TIMS (T). Note that the ratios given differ from those reported in Table 2-4 due to a difference in the normalizing isotope pair. See Luguet et al. (2008) and Nowell et al. (2008) for more detail.

	$^{186}Os/^{188}Os$	$^{187}Os/^{188}Os$	$^{189}Os/^{188}Os$	$^{190}Os/^{188}Os$	$^{192}Os/^{188}Os$
Nowell et al. (P)	0.119909 ± 04	0.160916 ± 04	*1.219780*	1.983979 ± 30	3.083580 ± 14
Luguet et al. (T)	0.119929 ± 06	0.160924 ± 04	1.219705 ± 15	1.983803 ± 15	*3.083*

The values in italic are the normalizing isotopic pairs.

Table I-2 Double spike composition. "Old" is using DROsS composition as reported by Nowell et al. (2008) and "New" using that as reported by Luguet et al. (2008).

DS composition						
	$^{184}Os/^{188}Os$	$^{186}Os/^{188}Os$	$^{187}Os/^{188}Os$	$^{189}Os/^{188}Os$	$^{190}Os/^{188}Os$	$^{192}Os/^{188}Os$
old	0.000030	0.001372	0.001239	0.020944	0.684512	0.036517
new	0.000030	0.001371	0.001240	0.020943	0.684450	0.036510

Figure I - 1a Original Figure 2-11 (see Chapter 2 for caption).
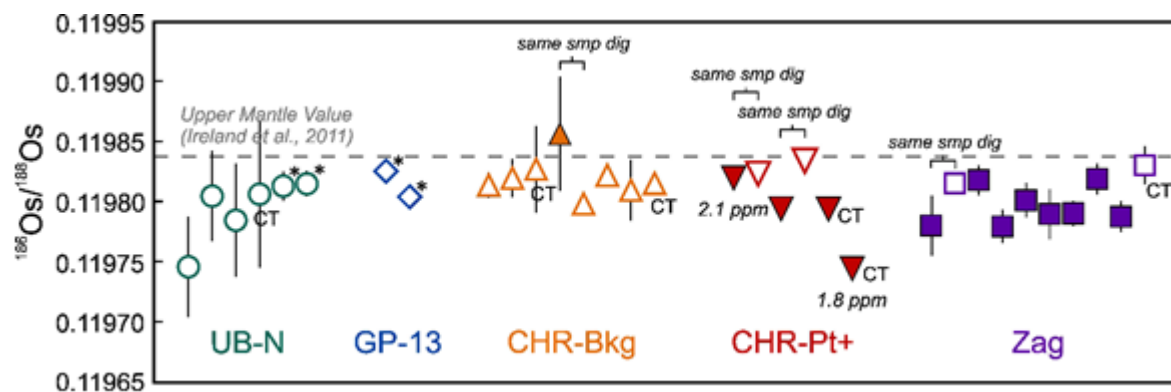
Figure I – 1b Revised Figure 2-11. Data was obtained using the DROsS isotope composition of Luguet et al. (2008). Where in the original figure the $^{186}Os/^{188}Os$ ratios plot consistently lower (see figure above) compared to the upper mantle value, the data below are, in general, within analytical uncertainty of the upper mantle value.
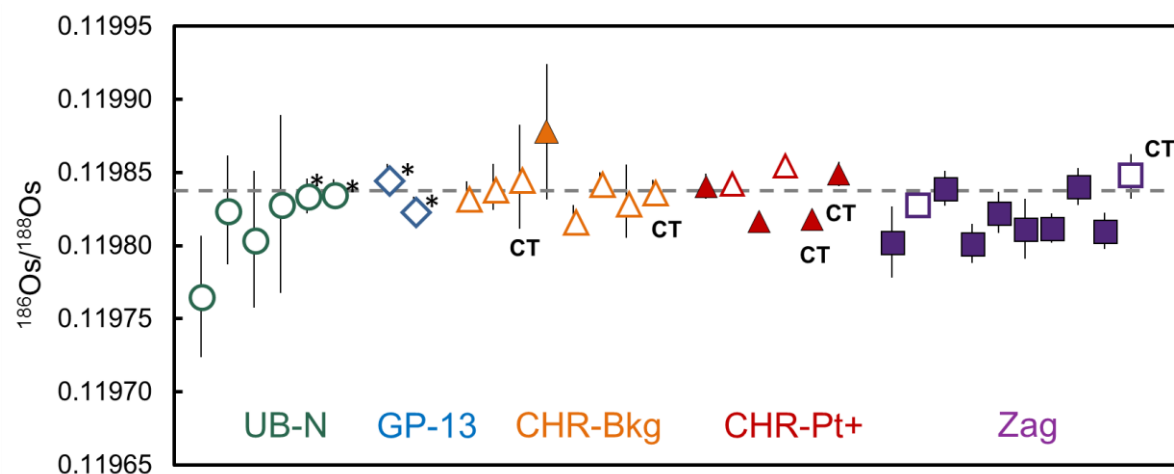
Table I-3 Revised data presented in Table 2-4 of Chapter 2.

	n	$\delta^{190/188}Os$	2 sd	$^{187}Os/^{188}Os$	2 sd	$^{186}Os/^{188}Os$	2 sd
DROsS							
DS MC-ICP-MS	91	0.00	0.02	0.160924	0.000020	0.119929	0.000017
DS N-TIMS	83	0.00	0.03	0.160924	0.000043	0.119929	0.000043
un-spiked	14	-	-	0.160919	0.000031	-	-
previous study (MC-ICP-MS; Nowell et al., 2008)	21	-	-	0.160916	0.000003	0.119909	0.000002
previous study (N-TIMS; Luguet et al., 2008)	8	-	-	0.160924	0.000004	0.119929	0.000006
ROMIL							
DS MC-ICP-MS	18	0.14	0.02	0.106837	0.000018	0.119826	0.000016
DS N-TIMS	7	0.13	0.01	0.106844	0.000033	0.119823	0.000023
sample-std bracketing MC-ICP-MS	4*	0.14	0.01	0.106861	0.000024	0.119806	0.000007
un-spiked	3	-	-	0.106878	0.000032	-	-
SpecPure							
DS MC-ICP-MS	18	0.15	0.02	0.149171	0.000026	0.119908	0.000018
DS N-TIMS	6	0.14	0.03	0.149164	0.000049	0.119907	0.000031
sample-std bracketing MC-ICP-MS	4*	0.13	0.01	0.149163	0.000012	0.119885	0.000016
un-spiked	3	-	-	0.149180	0.000088	-	-
OsCaR							
DS MC-ICP-MS	11	0.13	0.01	0.128304	0.000019	0.119837	0.000015

Table I-4 Revised data presented in Table 2-5 of Chapter 2.

				smp weight (g)	totalOs (V)	$^{188}OsO_3^-$	$^{187}OsO_3^-$	$\delta^{190/188}Os$	2 se	$^{187}Os/^{188}Os$	2 se	$^{186}Os/^{188}Os$	2 se	[Os] ng g^{-1}	2 se
UB-N	1	HPA	N-TIMS	2.51	0.98	0.37	0.008	0.14	0.04	0.126569	0.000040	0.119765	0.000042	4.13	0.002
	2	HPA	N-TIMS	2.51	1.16	0.43	0.009	0.13	0.04	0.126995	0.000039	0.119824	0.000037	4.02	0.002
	3	HPA	N-TIMS	2.49	0.92	0.35	0.007	0.13	0.06	0.127059	0.000047	0.119804	0.000047	3.89	0.003
	4	CT	N-TIMS	2.49	0.82	0.33	0.006	0.11	0.07	0.127059	0.000057	0.119828	0.000061	3.72	0.002
	5*	HPA	N-TIMS	6.03	3.99	1.53	0.030	0.13	0.02	0.127105	0.000011	0.119834	0.000012	3.62	0.001
	6*	HPA	N-TIMS	5.99	3.09	1.19	0.023	0.14	0.01	0.127178	0.000011	0.119835	0.000010	3.55	0.001
w. mean								**0.14**		**0.127116**		**0.119834**		**3.64**	
2 sd								**0.02**		**0.000434**		**0.000054**		**0.46**	
GP-13	1*	HPA	N-TIMS	4.02	4.95	1.87	0.039	0.14	0.02	0.126362	0.000010	0.119846	0.000010	3.87	0.002
	2*	HPA	N-TIMS	4.05	4.67	1.76	0.036	0.15	0.02	0.126436	0.000009	0.119825	0.000009	3.82	0.002
w. mean								**0.15**		**0.126402**		**0.119834**		**3.84**	
2 sd								**0.01**		**0.000104**		**0.000030**		**0.07**	
CHR-Bkg	1	HPA	N-TIMS	0.93	4.68	1.75	0.037	0.14	0.02	0.126663	0.000010	0.119834	0.000010	27.96	0.01
	2	HPA	N-TIMS	0.92	2.74	1.03	0.022	0.14	0.02	0.127678	0.000016	0.119840	0.000016	27.48	0.01
	3	CT	N-TIMS	0.55	1.21	0.46	0.009	0.12	0.03	0.127311	0.000034	0.119847	0.000036	26.32	0.01
	4a	HPA	MC-ICP-MS	2.06	3.42	1.29	0.026	0.13	0.03	0.127489	0.000039	0.119878	0.000046	24.72	0.001
	4b	HPA	N-TIMS	""	6.02	2.30	0.046	0.12	0.01	0.127490	0.000008	0.119818	0.000009	24.72	0.001
	5	HPA	N-TIMS	0.92	9.64	3.80	0.070	0.12	0.01	0.128171	0.000006	0.119844	0.000006	23.12	0.01
	6	CT	N-TIMS	0.58	1.81	0.71	0.013	0.13	0.03	0.127923	0.000025	0.119830	0.000025	22.97	0.01
	7	HPA	N-TIMS	0.92	9.50	3.79	0.067	0.11	0.01	0.127843	0.000006	0.119838	0.000007	21.95	0.01
w. mean								**0.12**		**0.127759**		**0.119840**		**24.73**	
2 sd								**0.02**		**0.000918**		**0.000035**		**4.39**	

Table I-4 continued

			smp weight (g)	totalOs (V)	$^{188}OsO_3^-$	$^{187}OsO_3^-$	$\delta^{190/188}Os$	2 se	$^{187}Os/^{188}Os$	2 se	$^{186}Os/^{188}Os$	2 se	[Os] ng g^{-1}	2 se
CHR-Pt+	1a	HPA	MC-ICP-MS	0.23	15.54	5.62	0.129	0.18	0.02	0.129256	0.000011	0.119840	0.000009	2121	6
	1b	HPA	N-TIMS	""	15.35	5.59	0.129	0.20	0.01	0.129267	0.000004	0.119842	0.000005	2121	4
	2a	HPA	MC-ICP-MS	0.25	25.05	9.41	0.195	0.15	0.01	0.129260	0.000006	0.119816	0.000004	1805	6
	2b	HPA	N-TIMS	""	6.60	2.49	0.052	0.18	0.01	0.129270	0.000008	0.119854	0.000008	1805	6
	3	CT	MC-ICP-MS	0.25	23.15	8.76	0.178	0.15	0.01	0.129170	0.000005	0.119818	0.000003	1785	4
	4	CT	MC-ICP-MS	0.25	12.02	4.54	0.092	0.13	0.01	0.129251	0.000012	0.119849	0.000009	1747	6
w. mean								0.16		0.129264		0.119826		1879	
2 sd								0.05		0.000075		0.000032		349	
ZAG	1a	HPA	MC-ICP-MS	0.24	6.73	2.51	0.049	0.13	0.02	0.129778	0.000018	0.119803	0.000024	929	6
	1b	HPA	N-TIMS	""	3.28	1.26	0.025	0.11	0.01	0.129760	0.000007	0.119827	0.000007	929	4
	2	HPA	MC-ICP-MS	0.25	8.94	3.28	0.067	0.13	0.01	0.126811	0.000011	0.119839	0.000012	926	6
	3	HPA	MC-ICP-MS	0.25	9.16	3.38	0.068	0.13	0.02	0.128296	0.000014	0.119801	0.000013	905	6
	4	HPA	MC-ICP-MS	0.25	8.63	3.18	0.064	0.13	0.01	0.128807	0.000012	0.119823	0.000014	904	6
	5	HPA	MC-ICP-MS	0.50	5.78	2.15	0.042	0.13	0.02	0.129479	0.000028	0.119812	0.000020	892	3
	6	HPA	MC-ICP-MS	0.50	12.05	4.47	0.088	0.11	0.01	0.128920	0.000011	0.119812	0.000010	887	3
	7	HPA	MC-ICP-MS	0.25	8.73	3.24	0.064	0.13	0.02	0.128633	0.000013	0.119840	0.000013	884	6
	8	HPA	MC-ICP-MS	0.25	9.03	3.40	0.065	0.14	0.02	0.128554	0.000014	0.119810	0.000012	861	6
	9	CT	N-TIMS	0.08	5.05	1.90	0.040	0.12	0.02	0.128698	0.000015	0.119847	0.000015	839	17
w. mean								0.12		0.128615		0.119823		896	
2 sd								0.02		0.001720		0.000033		59	

REFERENCES

Ahn, I., Lee, J. I., Kusakabe, M., and Choi, B.-G., 2012, Oxygen isotope measurements of terrestrial silicates using a CO_2-laser BrF_5 fluorination technique and the slope of terrestrial fractionation line: Geosciences Journal, v. 16, no. 1, p. 7-16.

Albarède, F., and Beard, B., 2004, Analytical methods for non-traditional isotopes: Reviews in Mineralogy and Geochemistry, v. 55, no. 1, p. 113-152.

Baertschi, P., 1976, Absolute ^{18}O content of standard mean ocean water: Earth and Planetary Science Letters, v. 31, no. 3, p. 341-344.

Barkan, E., and Luz, B., 2005, High precision measurements of $^{17}O/^{16}O$ and $^{18}O/^{16}O$ ratios in H2O: Rapid Communications in Mass Spectrometry, v. 19, no. 24, p. 3737-3742.

Bédard, L. P., and Barnes, S.-J., 2004, Improved Platinum-Group Element Extraction by NiS Fire Assay from Chromitite Ore Samples Using a Flux Containing Sodium Metaphosphate: Geostandards and Geoanalytical Research, v. 28, no. 2, p. 311-316.

Bermingham, K. R., Walker, R. J., and Worsham, E. A., 2016, Refinement of high precision Ru isotope analysis using negative thermal ionization mass spectrometry: International Journal of Mass Spectrometry, v. 403, p. 15-26.

Birck, J. L., Barman, M. R., and Capmas, F., 1997, Re-Os Isotopic Measurements at the Femtomole Level in Natural Samples: Geostandards Newsletter, v. 21, no. 1, p. 19-27.

Brandon, A. D., Creaser, R. A., Shirey, S. B., and Carlson, R. W., 1996, Osmium recycling in subduction zones: Science, v. 272, no. 5263, p. 861-863.

Brandon, A. D., Humayun, M., Puchtel, I. S., Leya, I., and Zolensky, M., 2005, Osmium isotope evidence for an s-Process carrier in primitive chondrites: Science, v. 309, no. 5738, p. 1233-1236.

Brandon, A. D., Walker, R. J., Morgan, J. W., Norman, M. D., and Prichard, H. M., 1998, Coupled ^{186}Os and 187Os evidence for core-mantle interaction: Science, v. 280, no. 5369, p. 1570-1573.

Brennecka, G. A., Borg, L. E., Hutcheon, I. D., Sharp, M. A., and Anbar, A. D., 2010, Natural variations in uranium isotope ratios of uranium ore concentrates: Understanding the $^{238}U/^{235}U$ fractionation mechanism: Earth and Planetary Science Letters, v. 291, no. 1–4, p. 228-233.

Burton, K. W., 2006, Global weathering variations inferred from marine radiogenic isotope records: Journal of Geochemical Exploration, v. 88, no. 1, p. 262-265.

Carlson, R. W., 2005, Application of the Pt–Re–Os isotopic systems to mantle geochemistry and geochronology: Lithos, v. 82, no. 3, p. 249-272.

Chatterjee, R., and Lassiter, J. C., 2015, High precision Os isotopic measurement using N-TIMS: Quantification of various sources of error in $^{186}Os/^{188}Os$ measurements: Chemical Geology, v. 396, no. 0, p. 112-123.

Chavagnac, V., 1998, Behaviour of the Sm-Nd isotopie system during metamorphism: Examples from the HT-LP metamorphic terrane of the Limpopo Belt,

South Africa and the UHP metamorphic terrane of Dabieshan, Central China: Université Rennes 1.

Chu, Z.-Y., Li, C.-F., Chen, Z., Xu, J.-J., Di, Y.-K., and Guo, J.-H., 2015, High precision measurement of $^{186}Os/^{188}Os$ and $^{187}Os/^{188}Os$: isobaric oxide corrections with in-run measured oxygen isotope ratios: Analytical chemistry.

Clayton, R. N., Grossman, L., and Mayeda, T. K., 1973, A component of primitive nuclear composition in carbonaceous meteorites: Science, v. 182, no. 4111, p. 485-488.

Cohen, A. S., and Waters, F. G., 1996, Separation of osmium from geological materials by solvent extraction for analysis by thermal ionisation mass spectrometry: Analytica Chimica Acta, v. 332, no. 2, p. 269-275.

Creaser, R. A., Papanastassiou, D. A., and Wasserburg, G. J., 1991, Negative thermal ion mass spectrometry of osmium, rhenium and iridium: Geochimica et Cosmochimica Acta, v. 55, no. 1, p. 397-401.

Creech, J. B., Baker, J. A., Handler, M. R., and Bizzarro, M., 2014, Platinum stable isotope analysis of geological standard reference materials by double-spike MC-ICPMS: Chemical Geology, v. 363, no. 0, p. 293-300.

Creech, J. B., Baker, J. A., Handler, M. R., Schiller, M., and Bizzarro, M., 2013, Platinum stable isotope ratio measurements by double-spike multiple collector ICPMS: Journal of Analytical Atomic Spectrometry, v. 28, no. 6, p. 853-865.

Dale, C. W., Burton, K. W., Pearson, D. G., Gannoun, A., Alard, O., Argles, T. W., and Parkinson, I. J., 2009, Highly siderophile element behaviour accompanying subduction of oceanic crust: Whole rock and mineral-scale insights from a high-pressure terrain: Geochimica et Cosmochimica Acta, v. 73, no. 5, p. 1394-1416.

Dale, C. W., Gannoun, A., Burton, K. W., Argles, T. W., and Parkinson, I. J., 2007, Rhenium–osmium isotope and elemental behaviour during subduction of oceanic crust and the implications for mantle recycling: Earth and Planetary Science Letters, v. 253, no. 1, p. 211-225.

Dodson, M. H., 1963, A theorethical study of the use of international standards for precise isotopic analysis by the surface ionisation technique: Part I - General first-order algebraic solutions: Journal of Scientific Instruments, v. 40, p. 289-295.

Galer, S. J. G., 1999, Optimal double and triple spiking for high precision lead isotopic measurement: Chemical Geology, v. 157, no. 3, p. 255-274.

Griselin, M., Van Belle, J., Pomies, C., Vroon, P., Van Soest, M., and Davies, G., 2001, An improved chromatographic separation technique of Nd with application to NdO^+ isotope analysis: Chemical Geology, v. 172, no. 3, p. 347-359.

Harvey, J., Dale, C. W., Gannoun, A., and Burton, K. W., 2011, Osmium mass balance in peridotite and the effects of mantle-derived sulphides on basalt petrogenesis: Geochimica et Cosmochimica Acta, v. 75, no. 19, p. 5574-5596.

Ireland, T. J., Walker, R. J., and Brandon, A. D., 2011, ^{186}Os–^{187}Os systematics of Hawaiian picrites revisited: New insights into Os isotopic variations in ocean island basalts: Geochimica et Cosmochimica Acta, v. 75, no. 16, p. 4456-4475.

Ishikawa, A., Senda, R., Suzuki, K., Dale, C. W., and Meisel, T., 2014, Re-evaluating digestion methods for highly siderophile element and ^{187}Os isotope analysis: Evidence from geological reference materials: Chemical Geology, v. 384, p. 27-46.

Li, W. J., Ni, B. L., Jin, D. Q., and Zhang, Q. G., 1988, Measurement of the absolute abundance of O-17 in V-SMOW: Kexue Tongbao, v. 33, no. 19, p. 1610-1613.

Liu, J., and Pearson, D. G., 2014, Rapid, precise and accurate Os isotope ratio measurements of nanogram to sub-nanogram amounts using multiple Faraday collectors and amplifiers equipped with 10^{12} Ω resistors by N-TIMS: Chemical Geology, v. 363, p. 301-311.

Liu, Y., Huang, M., Masuda, A., and Inoue, M., 1998, High-precision determination of osmium and rhenium isotope ratios by in situ oxygen isotope ratio correction using negative thermal ionization mass spectrometry: International Journal of Mass Spectrometry and Ion Processes, v. 173, no. 3, p. 163-175.

Lord, R. A., Prichard, H. M., and Neary, C. R., 1994, Magmatic platinum-group element concentrations and hydrothermal upgrading in Shetland ophiolite complex: Transactions - Institution of Mining & Metallurgy, Section B.

Lorin, J. C., 1992, Oxygen-isotope analysis on the Cameˊ ca® ims-300: Chemical Geology: Isotope Geoscience section, v. 101, no. 1-2, p. 193-195.

Luguet, A., Nowell, G. M., and Pearson, D. G., 2008, $^{184}Os/^{188}Os$ and $^{186}Os/^{188}Os$ measurements by Negative Thermal Ionisation Mass Spectrometry (N-TIMS): Effects of interfering element and mass fractionation corrections on data accuracy and precision: Chemical Geology, v. 248, no. 3, p. 342-362.

Marchesi, C., Dale, C. W., Garrido, C. J., Pearson, D. G., Bosch, D., Bodinier, J.-L., Gervilla, F., and Hidas, K., 2014, Fractionation of highly siderophile elements in refertilized mantle: Implications for the Os isotope composition of basalts: Earth and Planetary Science Letters, v. 400, p. 33-44.

Meibom, A., Sleep, N. H., Chamberlain, C. P., Coleman, R. G., Frei, R., Hren, M. T., and Wooden, J. L., 2002, Re–Os isotopic evidence for long-lived heterogeneity and equilibration processes in the Earth's upper mantle: Nature, v. 419, no. 6908, p. 705-708.

Meisel, T., Moser, J., Fellner, N., Wegscheider, W., and Schoenberg, R., 2001, Simplified method for the determination of Ru, Pd, Re, Os, Ir and Pt in chromitites and other geological materials by isotope dilution ICP-MS and acid digestion: Analyst, v. 126, no. 3, p. 322-328.

Meisel, T., Reisberg, L., Moser, J., Carignan, J., Melcher, F., and Brügmann, G., 2003, Re–Os systematics of UB-N, a serpentinized peridotite reference material: Chemical geology, v. 201, no. 1, p. 161-179.

Meisel, T., Walker, R. J., and Morgan, J. W., 1996, The osmium isotopic composition of the Earth's primitive upper mantle: Nature, v. 383, no. 6600, p. 517-520.

Miller, M. F., 2002, Isotopic fractionation and the quantification of ^{17}O anomalies in the oxygen three-isotope system: an appraisal and geochemical significance: Geochimica et Cosmochimica Acta, v. 66, no. 11, p. 1881-1889.

Millet, M.-A., Baker, J. A., and Payne, C. E., 2012, Ultra-precise stable Fe isotope measurements by high resolution multiple-collector inductively coupled plasma mass spectrometry with a ^{57}Fe–^{58}Fe double spike: Chemical Geology, v. 304, p. 18-25.

Millet, M.-A., and Dauphas, N., 2014, Ultra-precise titanium stable isotope measurements by double-spike high resolution MC-ICP-MS: Journal of Analytical Atomic Spectrometry, v. 29, no. 8, p. 1444-1458.

Millet, M.-A., Dauphas, N., Greber, N. D., Burton, K. W., Dale, C. W., Debret, B., Macpherson, C. G., Nowell, G. M., and Williams, H. M., 2016, Titanium stable isotope investigation of magmatic processes on the Earth and Moon: Earth and Planetary Science Letters, v. 449, p. 197-205.

Nagai, Y., and Yokoyama, T., 2016, Molybdenum isotopic analysis by negative thermal ionization mass spectrometry (N-TIMS): effects on oxygen isotopic composition: Journal of Analytical Atomic Spectrometry, v. 31, no. 4, p. 948-960.

Nielsen, S. G., Rehkämper, M., and Halliday, A. N., 2006a, Large thallium isotopic variations in iron meteorites and evidence for lead-205 in the early solar system: Geochimica et Cosmochimica Acta, v. 70, no. 10, p. 2643-2657.

Nielsen, S. G., Rehkamper, M., Norman, M. D., Halliday, A. N., and Harrison, D., 2006b, Thallium isotopic evidence for ferromanganese sediments in the mantle source of Hawaiian basalts: Nature, v. 439, no. 7074, p. 314-317.

Nier, A. O., 1950, A redetermination of the relative abundances of the isotopes of carbon, nitrogen, oxygen, argon, and potassium: Physical Review, v. 77, no. 6, p. 789.

Nowell, G. M., Luguet, A., Pearson, D. G., and Horstwood, M. A., 2008, Precise and accurate $^{186}Os/^{188}Os$ and $^{187}Os/^{188}Os$ measurements by multi-collector plasma ionisation mass spectrometry (MC-ICP-MS). Part 1, solution analyses: Chemical Geology, v. 248, no. 3-4, p. 363-393.

Paliulionyte, V., Meisel, T., Ramminger, P., and Kettisch, P., 2006, High Pressure Asher Digestion and an Isotope Dilution-ICP-MS Method for the Determination of Platinum-Group Element Concentrations in Chromitite Reference Materials CHR-Bkg, GAN Pt-1 and HHH: Geostandards and Geoanalytical Research, v. 30, no. 2, p. 87-96.

Pearson, D. G., Irvine, G. J., Ionov, D. A., Boyd, F. R., and Dreibus, G. E., 2004, Re–Os isotope systematics and platinum group element fractionation during mantle melt extraction: a study of massif and xenolith peridotite suites: Chemical Geology, v. 208, no. 1, p. 29-59.

Pearson, D. G., Parman, S. W., and Nowell, G. M., 2007, A link between large mantle melting events and continent growth seen in osmium isotopes: Nature, v. 449, no. 7159, p. 202-205.

Pearson, D. G., and Woodland, S. J., 2000, Solvent extraction/anion exchange separation and determination of PGEs (Os, Ir, Pt, Pd, Ru) and Re–Os isotopes in geological samples by isotope dilution ICP-MS: Chemical Geology, v. 165, no. 1–2, p. 87-107.

Pegram, W. J., Krishnaswami, S., Ravizza, G. E., and Turekian, K. K., 1992, The record of sea water 187Os/186Os variation through the Cenozoic: Earth and Planetary Science Letters, v. 113, no. 4, p. 569-576.

Peucker-Ehrenbrink, B., and Ravizza, G., 2000, The marine osmium isotope record: Terra Nova, v. 12, no. 5, p. 205-219.

Potts, P. J., Gowing, C. J. B., and Govindaraju, K., 1992, Preparation, homogeneity evaluation and cooperative study of two new chromitite reference samples CHR-Pt+ and CHR-BKg: Geostandards Newsletter, v. 16, no. 1, p. 81-108.

Puchtel, I. S., Humayun, M., and Walker, R. J., 2007, Os–Pb–Nd isotope and highly siderophile and lithophile trace element systematics of komatiitic rocks from the Volotsk suite, SE Baltic Shield: Precambrian Research, v. 158, no. 1–2, p. 119-137.

Rehkämper, M., Frank, M., Hein, J. R., Porcelli, D., Halliday, A., Ingri, J., and Liebetrau, V., 2002, Thallium isotope variations in seawater and hydrogenetic, diagenetic, and hydrothermal ferromanganese deposits: Earth and Planetary Science Letters, v. 197, no. 1, p. 65-81.

Reisberg, L., and Meisel, T., 2002, The Re-Os Isotopic System: A Review of Analytical Techniques: Geostandards Newsletter, v. 26, no. 3, p. 249-267.

Reisberg, L., and Zindler, A., 1986, Extreme isotopic variations in the upper mantle: evidence from Ronda: Earth and Planetary Science Letters, v. 81, no. 1, p. 29-45.

Roy-Barman, M., 1993, Mesure du rapport 187Os-186Os dans les basaltes et les péridotites: contribution à la systématique 187Re-187Os dans le manteau [Thesis: Université de Paris VII.

Rudge, J. F., Reynolds, B. C., and Bourdon, B., 2009, The double spike toolbox: Chemical Geology, v. 265, no. 3–4, p. 420-431.

Rumble, D., Miller, M. F., Franchi, I. A., and Greenwood, R. C., 2007, Oxygen three-isotope fractionation lines in terrestrial silicate minerals: An inter-laboratory comparison of hydrothermal quartz and eclogitic garnet: Geochimica et Cosmochimica Acta, v. 71, no. 14, p. 3592-3600.

Shen, J. J., Papanastassiou, D. A., and Wasserburg, G. J., 1996, Precise Re-Os determinations and systematics of iron meteorites: Geochimica et Cosmochimica Acta, v. 60, no. 15, p. 2887-2900.

Shirey, S. B., and Walker, R. J., 1995, Carius tube digestion for low-blank rhenium-osmium analysis: Analytical Chemistry, v. 67, no. 13, p. 2136-2141.

-, 1998, The Re-Os isotope system in cosmochemistry and high-temperature geochemistry: Annual Review of Earth and Planetary Sciences, v. 26, no. 1, p. 423-500.

Siebert, C., Nägler, T. F., and Kramers, J. D., 2001, Determination of molybdenum isotope fractionation by double-spike multicollector inductively coupled plasma mass spectrometry: Geochemistry, Geophysics, Geosystems, v. 2, no. 7, p. 1032.

Snow, J. E., and Reisberg, L., 1995, Os isotopic systematics of the MORB mantle: results from altered abyssal peridotites: Earth and Planetary Science Letters, v. 133, no. 3, p. 411-421.

Stein, H. J., Sundblad, K., Markey, R. J., Morgan, J. W., and Motuza, G., 1998, Re-Os ages for Archean molybdenite and pyrite, Kuittila-Kivisuo, Finland and Proterozoic molybdenite, Kabeliai, Lithuania: testing the chronometer in a metamorphic and metasomatic setting: Mineralium Deposita, v. 33, no. 4, p. 329-345.

Stirling, C. H., Andersen, M. B., Potter, E.-K., and Halliday, A. N., 2007, Low-temperature isotopic fractionation of uranium: Earth and Planetary Science Letters, v. 264, no. 1–2, p. 208-225.

Thirlwall, M., 1991, High-precision multicollector isotopic analysis of low levels of Nd as oxide: Chemical Geology, v. 94, no. 1, p. 13-22.

Trinquier, A., Touboul, M., and Walker, R. J., 2016, High-Precision Tungsten Isotopic Analysis by Multicollection Negative Thermal Ionization Mass Spectrometry Based on Simultaneous Measurement of W and 18O/16O Isotope Ratios for Accurate Fractionation Correction: Analytical chemistry, v. 88, no. 3, p. 1542-1546.

Walker, R. J., 2009, Highly siderophile elements in the Earth, Moon and Mars: Update and implications for planetary accretion and differentiation: Chemie der Erde-Geochemistry, v. 69, no. 2, p. 101-125.

Walker, R. J., Brandon, A. D., Bird, J. M., Piccoli, P. M., McDonough, W. F., and Ash, R. D., 2005, 187Os–186Os systematics of Os–Ir–Ru alloy grains from southwestern Oregon: Earth and Planetary Science Letters, v. 230, no. 1–2, p. 211-226.

Walker, R. J., Horan, M. F., Morgan, J. W., Becker, H., Grossman, J. N., and Rubin, A. E., 2002, Comparative 187Re-187Os systematics of chondrites: Implications regarding early solar system processes: Geochimica et Cosmochimica Acta, v. 66, no. 23, p. 4187-4201.

Wasserburg, G., Jacobsen, S., DePaolo, D., McCulloch, M., and Wen, T., 1981, Precise determination of SmNd ratios, Sm and Nd isotopic abundances in standard solutions: Geochimica et Cosmochimica Acta, v. 45, no. 12, p. 2311-2323.

Wittig, N., Humayun, M., Brandon, A. D., Huang, S., and Leya, I., 2013, Coupled W–Os–Pt isotope systematics in IVB iron meteorites: In situ neutron dosimetry for W isotope chronology: Earth and Planetary Science Letters, v. 361, p. 152-161.

Worsham, E. A., Walker, R. J., and Bermingham, K. R., 2016, High-precision molybdenum isotope analysis by negative thermal ionization mass spectrometry: International Journal of Mass Spectrometry, v. 407, p. 51-61.

Yokoyama, T., Alexander, C. M. D., and Walker, R. J., 2010, Osmium isotope anomalies in chondrites: results for acid residues and related leachates: Earth and Planetary Science Letters, v. 291, no. 1, p. 48-59.

Yokoyama, T., Rai, V. K., Alexander, C. M. D., Lewis, R. S., Carlson, R. W., Shirey, S. B., Thiemens, M. H., and Walker, R. J., 2007, Osmium isotope evidence for uniform distribution of s-and r-process components in the early solar system: Earth and Planetary Science Letters, v. 259, no. 3, p. 567-580.

– CHAPTER 3 –

The Osmium Stable Isotope Composition

of Chondrites and Earth's Mantle

Implications for Planetary Formation and Differentiation

ABSTRACT

Two key reservoirs for understanding Earth's formation, differentiation and subsequent evolution are chondritic meteorites (chondrites) and the Earth's mantle. Chondrites are thought to represent Earth's building blocks and as such can be used as a proxy of bulk Earth, as long as processes acting in the solar nebula and during accretion have not substantially altered the composition. The mantle represents the predominant part of the silicate portion after core segregation. Constraining the signature of the Earth's mantle is, therefore, important for understanding, for example, processes associated with core formation or to constrain the extent of late accreted material after core formation, i.e., efficient metal-silicate segregation, had ceased. In this chapter, the stable osmium isotope composition of chondrites and a suite of terrestrial mantle rocks is constrained. The aim is to better understand what has controlled the highly siderophile element (HSE) abundance of the Earth's mantle. Establishing this will allow for a better understanding of processes associated with planetary differentiation and core formation, specifically those related to the Earth's formation. The stable osmium isotope composition ($\delta^{190/188}$Os) of 34 bulk chondrite samples, representing different parts of the solar nebula and variable metamorphic grades, is shown to be homogeneous with an average value of 0.12±0.05‰ (2 sd; n = 37). These data illustrate that the processes that have acted on chondrite parent bodies have not resulted in significant mass-dependent fractionation and that, as a whole, the inner region of the solar nebula possesses a homogeneous stable Os composition. Subsequently, the stable isotope compositions of terrestrial mantle samples are discussed, including the reference materials presented in Chapter 2, an extensive set of mantle xenoliths representing present-day sub-continental lithosphere, and two samples of Archean age. The mantle xenoliths are shown to display resolvable variations in $\delta^{190/188}$Os. To understand this variability, various processes that are known to have affected the chemical composition are evaluated. Inter-mineral fractionation seems to be the most likely explanation, potentially resulting from supergene weathering whereby oxidized material preferentially incorporates heavier isotopes which is subsequently removed. However, a mineral-scale study would be required to discriminate between the various hypotheses. Finally, the average mantle compositions of the post-Archean and Archean samples from the various localities are compared with chondrites and the implications for the late-veneer hypothesis and hence the HSE abundance of the Earth's mantle are discussed. All averaged terrestrial compositions are within analytical uncertainty of chondrites. This implies that if the Earth's silicate portion contained a heavier isotope composition as a result of core formation, then this was readily overprinted by late accreted material with a broadly chondritic bulk composition. Furthermore, our preliminary results for Archean samples argue for efficient mixing of Os derived from late accreted material into the mantle, as these also yield chondritic Os stable isotope compositions. This study shows that stable Os isotopes provide a useful and interesting tool for future studies, i.e., application of the novel system to a more extensive set of Archean samples and an inter-mineral scale study, with sulphides and alloys as the most interesting phases. This will provide a better understanding of the extent and timing of mixing in of late accreted material. Inter-mineral scale studies will provide better insights into the behaviour of Os in the mantle, which in turn will lead to an increased knowledge of mantle processes.

CONTENT CHAPTER 3

1. INTRODUCTION

Over recent decades, the abundance of highly siderophile elements (HSE; Re, Os, Ir, Ru, Pt, Rh, Pd and Au) in the Earth's mantle has been a topic of much debate. Metal-silicate equilibrium experiments show that during differentiation of planetary bodies, HSE are quantitatively extracted into the metal-rich core (e.g., Jones and Drake, 1986; Borisov and Palme, 1995; O'Neill et al., 1995; Borisov and Palme, 1997; Righter, 2003). The abundance of HSE in Earth's mantle is, however, significantly higher than predicted from experiments performed at low pressures (see recent review of Day et al., 2016). Furthermore, metal-silicate segregation is shown to fractionate HSE whereas the HSE in fertile mantle peridotites display, predominantly, chondritic relative proportions. This, in combination with the chondritic ^{187}Os/^{188}Os and ^{186}Os/^{188}Os ratios of the Earth's upper mantle – which indicates broadly chondritic Re/Os ratios over Earth's history (e.g., Walker et al., 1997; Brandon et al., 1998; Brandon et al., 2000; Meisel et al., 2001b; Brandon et al., 2006; Lorand et al., 2008) – are key observations that have led to the hypothesis of a late accretion of predominantly chondrite-like materials (the so-called "late veneer"; e.g., Kimura et al., 1974; Chou, 1978; Morgan, 1985; Morgan et al., 2001). This hypothesis is also consistent with, for example, the detection of small enrichments in ^{182}W in early Archean terrestrial rocks (e.g., Willbold et al., 2011) and the tungsten isotope signature of the Moon (Kruijer et al., 2015) as a result of these reservoirs being poor in late accreted material. Late accreted material refers to matter that was added after core segregation and is thought to have re-enriched the Earth's mantle in highly siderophile elements. In recent years, metal-silicate partition coefficients have been constrained at higher pressures and temperatures to reconstruct conditions that are relevant to metal-silicate equilibration in a deep magma ocean (e.g., Cottrell and Walker, 2006; Righter et al., 2008; Mann et al., 2012). For some siderophile elements (e.g., Ni, Co, W, Au, Pt, Pd) these studies have suggested that their mantle abundance might be explained by metal-silicate equilibration and thus without the need of a "late veneer". Brenan and McDonough (2009) and Mann et al. (2012) show that this is not the case for all HSE (**Figure 3-1**). They propose a hybrid model and conclude that a "late veneer" of chondrite-like material is still required. The contribution of meteoritic material to the HSE abundance of Earth's mantle remains poorly constrained, as is the timing and degree of admixing of late accreted material.

Figure 3-1 Metal-silicate partition coefficients for Os, Ir, and Au as a function of inverse absolute temperature. Data are obtained by performing solubility experiments at conditions relevant to metal-silicate equilibration in a deep magma ocean. It can be observed that equilibrium partitioning during core formation could explain the observed concentration of gold in the mantle, but not that of osmium and iridium. Figure adjusted from Brenan and McDonough (2009).
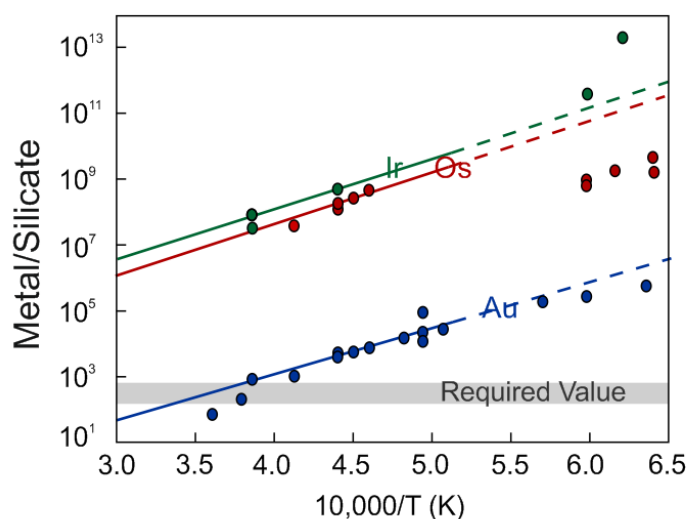
Stable isotope fractionation is expected to occur as a result of metal-silicate differentiation (Shahar et al., 2009; Shahar et al., 2011; Hin et al., 2013). Consequently, stable isotope systematics have been used as a new tool to explore planetary differentiation (e.g., Armytage et al., 2011; Burkhardt et al., 2014; Bonnand et al., 2016; Creech et al., 2017). Hin et al. (2013) show that for the moderately siderophile element Mo, substantial metal-silicate isotope fractionation takes place up to ~3000°C. This is supported by findings of Burkhardt et al. (2014) who observed that the silicate portions of differentiated planetary bodies display heavier signatures compared to chondrites and iron meteorites. Recently, Creech et al. (2017) report that the same principle holds for Pt isotopes where primitive achondrites yield a heavier isotope signature as a consequence of core formation. Furthermore, they observe that the Pt stable isotope signature of Earth's post-Archean mantle is similar to chondrites, supporting the "late veneer" hypothesis. Archean mantle samples, on the other hand, display relatively heavier isotope compositions. The non-chondritic composition is interpreted to reflect the mantle signature after core formation due to incomplete mixing with late accreted material.

Osmium is one of the HSE and is highly refractory. This property makes Os less susceptible to condensation or evaporation processes in the solar nebula. As such, it has been a key element in constraining the mechanisms that control the HSE abundances of the Earth's mantle. Osmium has not only provided fundamental arguments in support of the late veneer hypothesis (e.g., Meisel et al., 2001b; Brandon et al., 2006), but has also been used to determine the nature of late accreted materials (Morgan, 1985; Meisel et al., 1996; Meisel et al., 2001b). Most of this knowledge is obtained by use of the radiogenic isotope systems, Re-Os and Pt-Os. Utilizing these systems can be complicated due to various secondary processes that obscure the original signature, such as melt removal and melt-rock reactions (e.g., Büchl et al., 2002; Lorand et al., 2009; Luguet et al., 2015). It is hypothesised that Os stable isotopes can be fractionated differentially during these processes such that they can be used as a potential powerful complementary tool to unravel these processes. Another important difference is that stable isotope fractionation is not, necessarily, directly affected by time whereas decay systems are. Regarding the high partition coefficient of Os between metal and silicate (D=~10^7 for Earth conditions at 2,773K; Brenan et al., 2005), and considering that Os will hold different oxidation states in these different reservoirs, the fractionation of stable Os isotopes during metal-silicate differentiation could be substantial.

In this chapter, we present the first Os stable isotope compositions, by application of the new method as described in Chapter 2, of an extensive set of chondrites (n = 37) covering a range of oxidation states and petrological types. These data will help constrain the initial degree of stable Os isotope variability present in the solar system and allow an assessment of whether stable Os isotopes can be used to address questions related to planetary differentiation. In addition, a first estimate of the Os stable isotope composition of Earth's early Archean and modern-day mantle has been obtained by the measurement of (a) four reference materials (RM) representing peridotite and chromititic mantle materials, (b) ten peridotite xenoliths from Kilbourne Hole (KH) in New Mexico, USA, and (c) two Archaean Isua Greenstone Belt samples. The Os stable isotope data for chondrites and the Earth's upper mantle are then used to constrain processes that may have affected the Os

isotope and HSE budget of the Earth during early differentiation and subsequent evolution of the Earth's upper mantle.

2. SAMPLES

2.1 CHONDRITES

Chondrites formed early in the history of the solar system and are thought to represent some of the most primitive solar system material. The chemical and isotope compositions of chondrites provide a wealth of information regarding early Solar System processes. Furthermore, they have the capacity to provide a record of the degree of homogeneity of the solar nebula and of processes pertaining to the early stages of planet formation and accretion. Chondrites are divided into different classes (i.e., enstatite, ordinary, carbonaceous) each of which are subdivided into different groups (**Figure 3-2**; Weisberg et al., 2006). This classification is based on their mineralogical and petrographic characteristics, and their chemical compositions (Weisberg et al., 2006). The different classes are thought to represent different parts of the inner solar nebula and to have experienced various oxidation states (Clayton, 1993). In order to obtain a representative average of the bulk composition of the solar nebula we have examined chondrites from different groups, covering variable petrological types. Examined in this study are 23 ordinary chondrites (H, L, LL; defined in **Figure 3-2** caption), 5 enstatite chondrites (EH, EL), and 9 carbonaceous chondrites (CV, CM, CI, CK, CO), representing thermal metamorphic grades of 3 up to 6. The petrological type expresses the degree of metasomatism (type 3-6) or aqueous alteration (type 1 and 2) experienced. These and other secondary processes are known to have affected the original chemical composition of chondrites (Huss et al., 2006; Archer et al., 2014; McAdam et al., 2015). By sampling a variety of samples, the effect of these processes on the stable Os isotope composition can be assessed. Carbonaceous chondrites are shown to hold components with nucleosynthetic anomalies (Brandon et al., 2005; Yokoyama et al., 2007; Reisberg et al., 2009; Yokoyama et al., 2010). The effect that this imposes on the stable Os isotope compositions is considered in section 6.1.
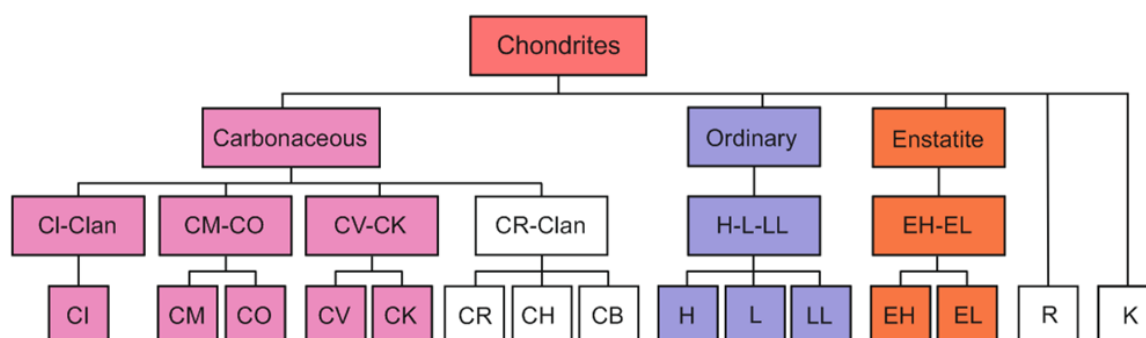
Figure 3-2 Chondrite classification. In colour are the various sections that samples were measured for. Figure after Weisberg et al. (2006). C – carbonaceous; CI - Ivuna-like; CM - Mighei-like; CO - Ornans-like; CV - Vigarano-like; CK - Karoonda- like; CR - Renazzo-like; CB - Bencubbin-like; and CH - high Fe, ALH 85085-like; E – enstatite; H – high iron; L – low iron; LL – low iron, low metal; R - Rumurutti-like; K - Kakangari-like.

2.2 MANTLE SAMPLES

Samples of the Earth's mantle were selected based on availability and extent of characterization. Considered for discussion in this Chapter are four international geological reference materials, which are the same as reported in Chapter 2. All reference materials are of orogenic origin: (i) UB-N, a serpentinised garnet and spinel-bearing peridotite from the Vosges, France (Meisel et al., 2003b); (ii) GP-13, a fertile lherzolite from the Beni Bousera massif in Morocco (Pearson and Woodland, 2000b; Pearson et al., 2004); (iii) CHR-Bkg and (iv) CHR-Pt+, both chromitites from the Shetland ophiolite in Scotland, UK (Potts et al., 1992; Meisel et al., 2001a; Bédard and Barnes, 2004; Paliulionyte et al., 2006). Not all of these samples are fertile mantle samples and as such will not provide the stable Os isotope composition of the Earth's primitive upper mantle. Nevertheless, they provide an idea of the range in compositions that can be observed in mantle material. In addition, ten

mantle xenolith samples from Kilbourne Hole were examined (see section 2.2.1). They were selected so as to be representative of a wide range of melt extraction conditions to allow for the assessment of melt depletion on the Os stable isotope composition (**Figure 3-3**). Furthermore, two ultramafic rocks from the Itsaq Gneiss Complex were analysed. These were sampled from enclaves, located in an orthogneiss terrain adjacent to the Isua Supracrustal Belt in Southwest Greenland (Nutman and Friend, 2009). Samples from this locality were examined because they are dated at 3.7-3.8 Ga (Nutman and Friend, 2009) and as such could provide us with an estimate of the stable Os isotope composition of the early Archean mantle. The Isua samples analysed in this study, SM/GR/00/12 and SM/GR/00/24, have been previously examined for ^{182}W, HSE, and radiogenic Os ratios by Dale et al. (2017).
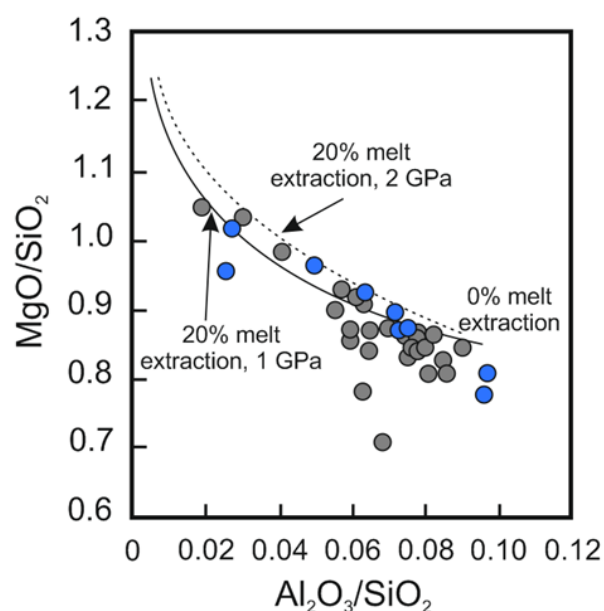
Figure 3-3 MgO/SiO$_2$ vs. Al$_2$O$_3$/SiO$_2$ diagram displaying the range of melt depletion as experienced by Kilbourne Hole xenoliths. In blue are the samples selected for this study. Melt extraction curves are after Herzberg (2004). Figure adjusted from Harvey et al. (2012).

2.2.1 Geological Background – Kilbourne Hole

Tectonically emplaced ("orogenic") peridotites often experience various processes on their way towards the surface, such as metamorphism or infiltration of external fluids, while abyssal peridotites are often heavily serpentinised through interaction with seawater. Peridotite xenoliths, on the other hand, are brought rapidly to the surface by volcanism. Interaction with the host lava can potentially change the geochemical signature but where this is shown to be minimal they provide an insight into the geochemistry of the Earth's mantle.

They form a perfect candidate to examine primary processes occurring in the mantle, such as melt depletion, refertilization, melt-rock interaction, and metasomatism. However, deciphering these various processes can be complicated, particularly when the sub-continental lithospheric mantle (SCLM) has experienced a multi-stage history with the potential of overprinting original chemical signatures (e.g., Bodinier and Godard, 2003; Le Roux et al., 2007).

Kilbourne Hole (KH) is a mantle xenolith locality situated in the Potrillo Volcanic Field, New Mexico, USA, that has been extensively studied (Carter, 1965; Reid and Woods, 1978; Irving, 1979; Irving, 1980; Bussod and Irving, 1981; Bussod, 1983; Dromgoole and Pasteris, 1987; Burton et al., 1999; Kil and Wendlandt, 2004; Harvey et al., 2011; Harvey et al., 2012; Harvey et al., 2015). Eruption of the host lava took place only 80-141 Ka suggesting that the xenoliths are representative of the present-day SCLM underlying the south-western USA (Hoffer, 1976; Dromgoole and Pasteris, 1987; Bussod and Williams, 1991; Thompson et al., 2005). Xenoliths are Cr-diopside spinel lherzolites and spinel harzburgites derived from the upper-mantle through to deep crustal levels (e.g., Perkins and Anthony, 2011). The geological setting, petrology, and petrography of Kilbourne Hole xenoliths imply, at first sight, a simple history, with variable degrees of melt depletion and minimal metasomatic processes influencing the geochemical composition. It, therefore, provides an ideal location for studying the impact of melt depletion on elemental systems. However, although no discrete metasomatic phases have been detected for KH xenoliths by any previous studies, their geochemistry and textural evidence indicate that they have experienced a complex multi-event metasomatic history (e.g., Schiano and Clocchiatti, 1994; Kil and Wendlandt, 2004; Harvey et al., 2011; 2012; 2015). There are broadly two types of metasomatism that can be distinguished. An early episode of peridotite-melt interaction that can be identified by (a) anomalous low olivine modal abundances, (b) high-bulk rock SiO_2, and (c) secondary clinopyroxene. This type of metasomatism lacks any macro-scale textural evidence which implies that the protoliths of the affected xenoliths were retained at mantle P-T conditions sufficiently long to allow textural re-equilibration. In contrast, there is textural evidence for the second type of metasomatism, which suggests that this occurred closer to the time of entrainment in the host basalt, with little time for textural re-equilibration. Textural evidence is preserved as a "spongy" reaction texture around clinopyroxene grains which is, in most cases, accompanied by interstitial high-SiO_2 glass veins or glass pockets. Elevated bulk-rock $(La/Yb)_N$ values were also given as indication of this type of metasomatism. Some evidence for metasomatism has not been linked to a specific type, for example, the non-systematic decoupling of Sr and Nd isotopes or the inconsistent fractionation of high-field strength elements (HFSE) between clinopyroxene and bulk-rock. Taken together, it is evident that KH xenoliths have witnessed multiple, temporally distinct, metasomatic events. The number, extent, and timing of metasomatic episodes remain, however, unconstrained.

Due to the chalcophile and siderophile behaviour of Os it is, together with the other HSE (PGE, Re, Au, Ag) and chalcogenides (Se and Te), dominantly hosted in Cu-Fe-Ni sulphide phases (Lorand and Luguet, 2016 and references therein). In the KH xenoliths, three sulphide groups have been distinguished based on their Fe:Ni:Cu ratio (**Figure 3-4a**): (1) low [Cu] and low Fe:Ni ratio; (2) low [Cu] and high Fe:Ni ratio; and (3) higher [Cu] and low [Ni]. The first two groups are broadly equivalent to pentlandite-rich and pentlandite-poor
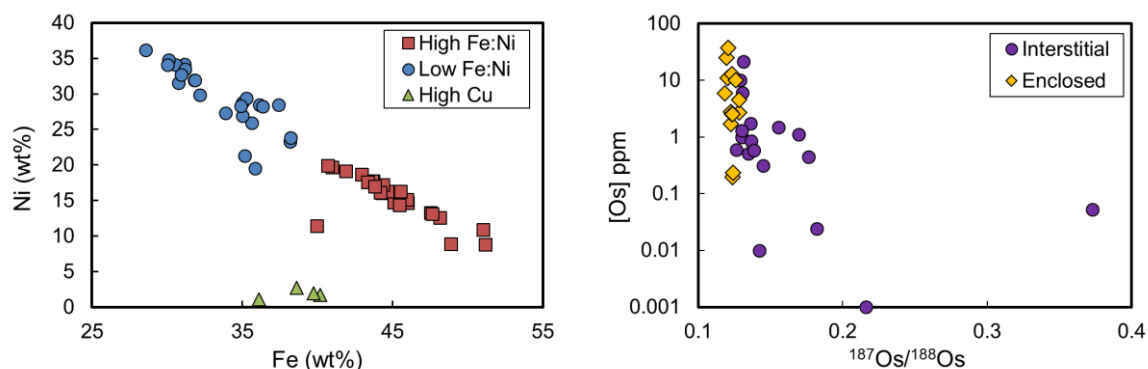
Figure 3-4 (a) Major element abundances (Fe vs Ni in wt.%) of sulphide grains in peridotite xenoliths from Kilbourne Hole, New Mexico, USA. The different symbols represent distinct groups, based on their Fe:Ni and Cu ratio, with the triangles high in Cu content and the circles and squares low. **(b)** $^{187}Os/^{188}Os$ and [Os] of individual sulphide grains from Kilbourne Hole peridotite xenoliths. Note that only interstitial grains display high $^{187}Os/^{188}Os$ ratios associated with low Os abundances. Figure adjusted after and data from Harvey et al. (2011; 2012).

monosulphide solid solution (mss), whereas the third group is an analogue to chalcopyrite-rich sulphides. In terms of Re-Os systematics and morphology, two discrete populations were observed (**Figure 3-4b**); (1) enclosed sulphides, which are rounded in shape, typically contain high [Os], low [Re], and unradiogenic, sub-chondritic $^{187}Os/^{188}Os$; and (2) interstitial sulphides, which are irregular in shape, possess lower [Os], higher [Re], and a wider range of $^{187}Os/^{188}Os$ with typically supra-chondritic values. The latter population is thought to represent metasomatic sulphide. Most sulphides contain evidence of supergene weathering, where part of the mineral has been replaced by amorphous Fe-oxyhydroxide (Harvey et al., 2015). Platinum group minerals have, thus far, not been observed in KH xenoliths (Dromgoole and Pasteris, 1987; Burton et al., 1999; Harvey et al., 2011).

3. METHODS

3.1 SAMPLE PREPARATION

Chondrite samples were provided by the Field Museum of Chicago as pieces of ≤1 g and were, subsequently, processed at Durham University. They were crushed to powder using an agate mortar that was cleaned between each sample by grinding of pure quartz sand and rinsing with ethanol and MilliQ water. The geological reference materials were either available as in-house standard (GP-13) or provided in powder form by CRPG-CRNS (UB-N, CHR-Bkg, CHR-Pt+). Samples from Kilbourne Hole were provided by Jason Harvey which were used in previous studies (Harvey et al., 2011; 2012; 2015). Methods used in these studies, to acquire sample powders, included cutting of the samples and repeated rinsing in ultra-pure water to remove traces of host basalt, surface alteration and contamination. After the samples were dried, they were powdered in an agate mortar. Aliquots were taken from Isua powder samples that were available in-house, and were crushed in a similar way to the KH samples.

3.2 CHEMICAL PROCESSING

Sample powders were digested by high pressure asher (HPA, Anton Paar; Meisel et al., 2001a) at 290-310°C for ≥16 h using inverse aqua regia (1:2; 12 M HCl: 16 M HNO$_3$). A ^{188}Os-^{190}Os double spike was added before digestion in order to correct for mass-dependent fractionation as a result of sample processing and analysis. The amount of material digested in a single HPA tube ranged between 0.1 – 2.5 g, and the total amount of sample material processed through chemistry, in some cases after combining individual digestions, ranged from 0.1 up to 12 g. Multiple HPA digestions were combined for samples with a low Os abundance to ensure high precision data. The digestions were combined prior to the chemical extraction. Once digested, samples were processed in the clean-lab, closely following techniques described by Cohen and Waters (1996) and Birck et al. (1997). Osmium was removed from the aqua regia digest solution by solvent extraction using chloroform, then back extracted into concentrated HBr, and finally purified by micro-distillation (Roy-Barman and Allègre, 1995).

3.3 MASS SPECTROMETRY and DATA REDUCTION

Osmium isotope measurements were carried out using a Thermo Scientific Neptune multi-collector inductively coupled plasma mass spectrometer (MC-ICP-MS) and a Thermo Scientific Triton Plus thermal ionisation mass spectrometer operation in negative mode (N-TIMS) both at Durham University. Instrument parameters were similar to those reported in Chapter 2.

For MC-ICP-MS analyses, samples were introduced in 3 M HCl with a typical sample uptake rate of ca. 80 µL min^{-1} and instrument sensitivity of ~30 V ppm^{-1} total Os. Each sample analysis comprised 1 block of 80 x 8.389 sec integrations and was preceded by measuring on-peak zero (OPZ) for 20 x 8.389 sec integrations using clean 3 M HCl to correct for background. Between sample and OPZ measurements, the washouts were carried out in 3 M HCl for 5 min or until all beam signal intensities were dropped below 2 mV. Total sample analysis time, excluding the washout, corresponds to ~14 min. If sufficient sample solution was available, samples were run twice. Isobaric interferences on ^{183}W were <0.01 mV, <0.02 mV on ^{185}Re, and <0.03 mV for ^{194}Pt, which imposes a negligible effect on the Os isotope ratios.

For N-TIMS analyses, samples were loaded on a Pt-ribbon in combination with a NaOH-Ba(OH)$_2$ activator. Osmium isotope ratios were obtained using a two-sequence static multi-collection routine comprised of 28 blocks of 10 x 8.389 sec integrations and a 3 sec idle time. Method development was still ongoing while measuring, which is why for some samples the oxygen composition was collected only prior and after the main sequence and for other samples it was collected within the run. The different procedures are described in detail in Chapter 2. For all samples the ^{17}O/^{16}O was calculated based on the ^{18}O/^{16}O. Prior to and after each analysis isobaric interferences of PtO$_2^-$, ReO$_3^-$, and WO$_3^-$ were assessed by a 4 cycle ion counter run. Baseline and gain calibration were performed at least at the start of each analysis day and peak centering before the start of every sample run. Total sample analysis time corresponded to ~96 minutes (excluding

sample heating and focussing). In this study, interference beam intensities range from 3,400 – 1,300,000 cps on mass 228 ($\sim^{196}Pt^{16}O_2^-$), between 2,600 and 950,000 cps on mass 230 ($\sim^{198}Pt^{16}O_2^-$), and from 1-540 cps ($\sim^{183}WO_3^-$) and 19-275 ($\sim^{185}ReO_3^-$) on mass 231 and 233, respectively. The maximum values are all lower than those reported in Chapter 2 for which it has been concluded that the effect is minimal on the stable Os isotope composition.

The ^{188}Os-^{190}Os double spike, added prior to digestion, has been used to correct for mass fractionation and was introduced by sample processing and mass spectrometry analysis. A detailed description of the design and calibration of the DS as well as mass spectrometry and off-line data treatment protocols is given in Chapter 2. All Os stable isotope data in this paper are reported as $\delta^{190}Os$ values which is the per mil deviation (‰) in the measured $^{190}Os/^{188}Os$ ratio of the sample relative to international pure Os reference standard DROsS, as given by Luguet et al. (2008). Osmium concentrations were determined by performing isotope dilution calculations on double-spiked samples.

3.4 DATA QUALITY

During the course of this study, the reference standard DROsS has been included in every digestion cycle and measured as an unknown to provide a means of assessing the accuracy of the digestion and chemical separation procedures. Furthermore, pure Os reference solutions, i.e., SpecPure, ROMIL and OsCar, have been repeatedly analysed. These data have been discussed in detail in Chapter 2. To summarize, the data show that reproducibility on the $\delta^{190}Os$ of 0.02‰ (2sd; n = 91) can be obtained for MC-ICP-MS and 0.02‰ (2sd; n = 61) by N-TIMS. Also shown is that the offset between DROsS relative to ROMIL and SpecPure is consistent when comparing the MC-ICP-MS and N-TIMS analyses, confirming the accuracy of the method. As an additional check on accuracy, a number of samples were run by both MC-ICP-MS and N-TIMS. This will be discussed in the results section. Typical total procedure blanks range between 0.01 and 0.10 pg Os which is similar to previous Os studies carried out at Durham University (Dale et al., 2007; Dale et al., 2009).

4. RESULTS

Osmium abundance, stable ($\delta^{190/188}Os_{DROsS}$), and radiogenic isotope ($^{186}Os/^{188}Os$ and $^{187}Os/^{188}Os$) compositions are given in **Table 3-1** and shown in Figures 3-5 to 3-14. We present the first $^{187}Os/^{188}Os$ radiogenic data for 17 out of the 34 chondrites and for 25 chondrites the first $^{186}Os/^{188}Os$ data. The internal precision on each single $\delta^{190}Os$ analysis is, in general, less than 0.03‰ (2 se). Replicate digestions and analysis of ordinary H-chondrite ZAG show good internal reproducibility with a 2 sd of 0.02‰ (n= 9). Several samples that have been analysed by both MC-ICP-MS and N-TIMS show consistent values between the two techniques attesting to the accuracy of the methods (**Table 3-1**, **Table 3-2,** and **Figure 3-5**) For these analyses, where multiple measurements are acquired from the same sample digestion, the weighted average and 95% c.i. is given. Isoplot was used to calculate these values.

Table 3-1 Osmium stable ($\delta^{190/188}$Os) and radiogenic (^{187}Os/^{188}Os and ^{186}Os/^{188}Os) isotope compositions, and Os abundances of carbonaceous (C), ordinary (O), and enstatite (E) chondrites obtained by either MC-ICP-MS or N-TIMS. W. mean = weighted mean, obtained using isoplot. * indicates that multiple analyses of the same solution were made. For samples with more than one analysis, Isoplot was used to obtain a weighted mean, with a 95% c.i. as error.

Sample		*n*	MC-ICP-MS/N-TIMS	$\delta^{190/188}$Os	2 se	^{187}Os/^{188}Os	2 se	^{186}Os/^{188}Os	2 se	[Os] ppb	2 se
Carbonaceous Chondrites											
Allende*	CV	2	N-TIMS	0.13	0.01	0.126398	4	0.119835	85	720	5
Karoonda	CK	1	N-TIMS	0.15	0.01	0.118311	7	0.119837	7	825	7
Mighei	CM	1	MC-ICP-MS	0.14	0.01	0.126912	11	0.119758	6	574	6
Murchison	CM	1	N-TIMS	0.19	0.01	0.127050	7	0.119819	7	610	7
Murray	CM	1	N-TIMS	0.15	0.01	0.126561	6	0.119819	7	578	8
Ningqiang	C3-ung	1	MC-ICP-MS	0.12	0.01	0.126306	9	0.119784	5	711	6
Orgeuil*	CI	2	N-TIMS	0.15	0.01	0.126312	6	0.119794	6	462	5
Ornans*	CO	3	N-TIMS	0.10	0.01	0.126660	4	0.119895	19	760	4
Vigarano	CV	1	MC-ICP-MS	0.14	0.01	0.126778	8	0.119802	4	865	6
W. mean C; 95% c.i.		9		0.13	0.02	0.126574	193	0.119799	19	683	100
2sd					0.05		4818		74		0
Ordinary Chondrites											
H											
Allegan 1	H5	1	MC-ICP-MS	0.12	0.01	0.128596	22	0.119821	15	875	3
Allegan 2		1	MC-ICP-MS	0.13	0.02	0.129460	28	0.119832	23	882	3
Allegan average*				0.12	0.01	0.128935	5360	0.119824	13	878	44
Dhajala	H3.8	1	MC-ICP-MS	0.14	0.01	0.129441	9	0.119827	8	972	7
Forest City	H5	1	MC-ICP-MS	0.11	0.01	0.129247	10	0.119834	7	886	7
Forest Vale	H4	1	MC-ICP-MS	0.14	0.01	0.129610	9	0.119832	8	918	7
Ochansk	H4	1	MC-ICP-MS	0.14	0.02	0.129200	8	0.119829	8	975	7
Richardton	H5	1	MC-ICP-MS	0.12	0.02	0.128820	41	0.119801	24	974	4

Trenzano	H3/4	1	MC-ICP-MS	0.13	0.03	0.128666	38	0.119827	30	634	4
Weston	H4	1	MC-ICP-MS	0.09	0.01	0.128425	10	0.119836	7	873	7
		1	N-TIMS	0.09	0.01	0.128424	7	0.119837	8	873	7
Weston average*				0.09	0.01	0.128424	6	0.119837	5	873	5
Zag*	H3-6	10	Both	0.13	0.01	0.129262	463	0.119825	10	896	16
W. mean H; 95% c.i.		9		0.13	0.01	0.129010	389	0.119831	3	913	39
2sd					0.04		917		19		161
L											
Bjurbole	L/LL4	1	MC-ICP-MS	0.10	0.02	0.128978	15	0.119804	12	404	7
Farmington	L5	1	MC-ICP-MS	0.10	0.02	0.135632	11	0.119841	9	602	8
		1	N-TIMS	0.10	0.01	0.135606	7	0.119842	7	602	8
Farmington average*				0.10	0.01	0.135613	146	0.119841	5	602	5
Fisher	L6	1	MC-ICP-MS	0.11	0.04	0.129964	55	0.119807	47	579	4
Harleton	L6	1	MC-ICP-MS	0.11	0.02	0.128155	11	0.119827	10	516	7
Homestead	L5/6	1	MC-ICP-MS	0.12	0.02	0.129490	44	0.119883	30	550	4
Kendleton	L4	1	MC-ICP-MS	0.14	0.02	0.129165	11	0.119832	10	602	7
L'Aigle	L6	1	MC-ICP-MS	0.10	0.02	0.129968	15	0.119839	23	578	4
Long Island	L6	1	MC-ICP-MS	0.14	0.02	0.128215	45	0.119834	30	542	4
Mauerkirchen	L6	1	MC-ICP-MS	0.09	0.02	0.128810	41	0.119806	28	513	4
Waconda	L6	1	MC-ICP-MS	0.12	0.04	0.144975	47	0.119845	45	514	4
W. mean L; 95% c.i.		10		0.11	0.01	0.128964	559	0.119833	10	550	26
2sd					0.04		9501		40		114
LL											
Dhurmsala	LL6	1	MC-ICP-MS	0.11	0.02	0.130868	18	0.119841	27	503	4
Holbrook	L/LL6	1	MC-ICP-MS	0.16	0.03	0.126836	24	0.119841	30	616	4
Jelica	LL6	1	MC-ICP-MS	0.16	0.02	0.127777	15	0.119837	12	383	7
		1	N-TIMS	0.14	0.02	0.127790	16	0.119846	15	383	7

Jelica average*				0.15	0.02	0.127783	11	0.119840	9	383	5
Olivenza	LL5	1	MC-ICP-MS	0.15	0.02	0.126524	15	0.119855	12	396	7
W. mean LL; 95% c.i.		4		0.15	0.03	0.127917	2693	0.119845	7	498	163
2sd					0.04		3081		13		193
W. mean O; **95% c.i.**		**23**		**0.12**	**0.03**	**0.128980**	**317**	**0.119833**	**14**	**660**	**511**
2sd					**0.04**		**1236**		**15**		**453**
Enstatite Chondrites											
EH											
ABEE	EH4	1	MC-ICP-MS	0.11	0.02	0.125708	19	0.119807	13	512	13
Indarch	EH4	1	N-TIMS	0.13	0.01	0.128245	9	0.119838	9	608	12
St Mark's	EH5	1	MC-ICP-MS	0.13	0.02	0.128040	14	0.119821	11	588	12
W. mean EH; 95% c.i.		3		0.12	0.01	0.127851	2596	0.119826	38	572	122
2sd					0.04		2234		28		83
EL											
Happy Canyon	EL6/7	1	MC-ICP-MS	0.11	0.01	0.127775	12	0.119812	9	576	7
Khairpur	EL6	1	MC-ICP-MS	0.10	0.02	0.128905	10	0.119824	9	851	9
		1	N-TIMS	0.09	0.01	0.128917	6	0.119843	6	851	9
Khairpur average*				0.09	0.01	0.128914	70	0.119837	114	851	7
W. mean EL; 95% c.i.		2		0.10	0.01	0.127909	2433	0.119812	9	720	1745
2sd					0.02		1611		36		389
W. mean E; 95% c.i.		**5**		**0.11**	**0.15**	**0.127828**	**1775**	**0.119813**	**8**	**573**	**122**
2sd					**0.03**		**61**		**20**		**208**
W. mean; 95% c.i.		**3**		**0.12**	**0.01**	**0.127242**	**3227**	**0.119821**	**41**	**680**	**87**
2sd		**37**			**0.05**		**2407**		**34**		**116**

Table 3-2 Osmium stable ($\delta^{190/188}$Os) and radiogenic (^{187}Os/^{188}Os and ^{186}Os/^{188}Os) isotope compositions, and Os abundances of Kilbourne Hole (KH) mantle xenoliths, Archean mantle rocks derived from the Itsaq Gneiss Complex, and geological reference materials for the terrestrial mantle. All samples were analysed by N-TIMS. W. mean = weighted mean, with the error as the 95% c.i., obtained using Isoplot. °- indicates values that were not considered for the overall average value for KH.

Sample	n	sample weight (g)	$\delta^{190/188}$Os	2 se	^{187}Os/^{188}Os	2 se	^{186}Os/^{188}Os	2 se	[Os] ppb	2 se	total Os beam (V)
Kilbourne Hole Peridotite Xenoliths											
KH03-2		8.00	0.18	0.01	0.120897	7	0.119837	9	1.60	0.78	6.6
KH03-3		8.56	0.18	0.02	0.131727	18	0.119856	17	1.02	0.71	2.7
KH03-6		9.93	0.13	0.02	0.126804	12	0.119811	12	1.46	0.44	2.7
KH03-10a°		6.01	0.20	0.04	0.125172	39	0.119816	42	3.30	1.05	1.0
KH03-10b		4.77	0.13	0.01	0.125074	8	0.119841	8	3.28	1.30	8.0
KH03-15		7.98	0.16	0.02	0.121456	9	0.119834	9	2.03	0.77	5.0
KH03-16a		5.87	0.19	0.03	0.116226	30	0.119827	30	3.74	1.10	1.2
KH03-16b		4.01	-0.06	0.02	0.116212	17	0.119829	16	3.14	1.52	2.9
KH03-18a°		6.02	0.12	0.02	0.126522	15	0.119826	15	2.47	1.03	2.8
KH03-18b°		6.01	0.16	0.01	0.126523	9	0.119818	10	2.46	1.03	5.9
w. mean		-	0.15	0.23	0.126523	8	0.119820	8	2.46	0.06	-
KH03-21		8.03	0.10	0.02	0.132282	10	0.119841	10	1.85	0.78	4.5
KH03-25a°		8.00	0.03	0.01	0.119182	7	0.119839	8	1.82	0.77	6.2
KH03-25b°		6.79	0.03	0.01	0.119572	8	0.119828	8	1.84	0.91	6.2
w. mean		-	0.03	0.01	0.119377	418	0.119834	6	1.83	0.12	-
KH03-27		9.94	0.07	0.01	0.119332	7	0.119826	7	1.52	0.44	5.6
w. mean all	11	**-**	**0.11**	**0.04**	**0.123071**	**3090**	**0.119834**	**5**	**1.75**	**0.44**	**-**
Archean Mantle Rocks											
SM/GR/00/12		8.00	0.14	0.02	0.109874	19	0.119811	24	1.27	0.8	0.8
SM/GR/00/24		4.00	0.14	0.02	0.167322	16	0.119873	18	2.36	1.5	1.3
Geological Reference Materials											
UB-N	6	-	0.14	0.02	0.127116	434	0.119834	54	3.64	0.46	-
GP-13	2	-	0.14	0.01	0.126402	104	0.119834	30	3.84	0.07	-
CHR-Bkg	7	-	0.12	0.02	0.127759	918	0.119840	45	24.73	4.39	-
CHR-Pt+	4	-	0.16	0.05	0.129264	75	0.119826	32	1898	350	-

4.1 CHONDRITES

4.1.1 Data Reliability

Chondrites were measured by either MC-ICP-MS or N-TIMS at total Os beam intensities of >1.9 V and >2.5 V, respectively. As discussed in Chapter 2, at these high beam intensities for N-TIMS the oxygen composition does not impose a significant inaccuracy on the stable isotope composition. Total Os beam intensities obtained for OPZ by MC-ICP-MS are <4 mV and <0.1% relative to beams in the main run, which is negligible. As mentioned in the method section, the isobaric interferences were insignificant and did not introduce any significant inaccuracy on δ^{190}Os.

A number of powder aliquots of Zag (ordinary H-chondrite) have been processed and analysed to assess the reproducibility of the method for a chondritic matrix. The reproducibility (2 sd) on δ^{190}Os is 0.02‰ (n = 9; **Figure 3-5a**), which is comparable with the reproducibility as obtained for DROsS (2 sd = 0.02‰). During the course of this study, 8 samples were measured first by MC-ICP-MS and subsequently by N-TIMS. These samples display a range of δ^{190}Os values (0.09 - 0.16‰) and concentrations (383 – 918 ppb). Apart from one analysis, they are within analytical uncertainty of one another, and all deviations between the two measurements fall within the reproducibility as obtained for ZAG (**Figure 3-5b**). This all provides support for the accuracy and reproducibility of the method.

4.1.2 Osmium Stable Isotope Data

Chondrite bulk samples possess δ^{190}Os values ranging from 0.09 ‰ to 0.19‰ (**Figure 3-6**). Ordinary chondrites cover a range from 0.09 ‰ to 0.16‰, with the H-chondrite Weston displaying the lightest value (0.09‰) and Holbrook (LL) the heaviest (0.16‰). Average weighted values for the individual sub-groups, H, L, and LL, yield values that are within analytical uncertainty of each other, 0.13 ±0.04 (n=9), 0.11 ±0.04 (n=10), and 0.15 ±0.04, (n=4), respectively. Enstatite chondrites show a slightly smaller range, from 0.09 to 0.13‰ (n=5), although fewer samples have been measured. The weighted average is 0.10 ±0.02 (2sd; n=2) for EL-type and 0.12 ±0.04 (2sd; n=3) for EH chondrites. Carbonaceous chondrites cover the largest range with values from 0.10 to 0.19‰
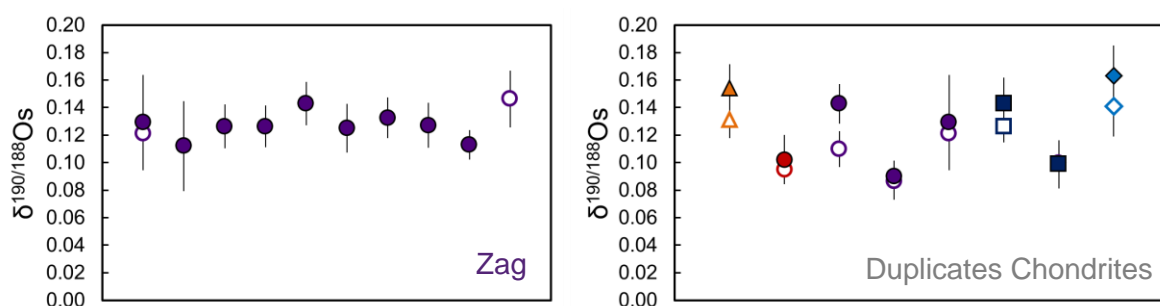
Figure 3-5 (a) Individual digestions of Zag showing reproducibility (2 sd) on $\delta^{190/188}$Os of 0.02‰ (n = 9). **(b)** Comparison of measurement by MC-ICP-MS (closed symbol) and N-TIMS (open symbols) using the same sample solution of various chondrites. Apart from one sample, all data is within analytical uncertainty. Error bars represent the ±2se on the individual analysis.

(*n*=9). The CM chondrite sample Murray records the heaviest Os stable isotope composition (0.19‰) obtained for a bulk chondrite sample. Weighted average values for ordinary, 0.12±0.03‰ (2sd; *n*=23), enstatite, 0.11±0.03‰ (2sd; *n*=5), and carbonaceous chondrites, 0.13±0.05‰ (2sd; *n*=9) show no resolvable differences. The weighted average δ^{190}Os value for all chondrites is 0.12±0.05‰ (2sd; *n*=37).

4.1.3 Osmium Concentrations and Radiogenic Isotope Data

Concentrations of osmium range from 383 ng/g, for ordinary LL-chondrite Jelica, to 975 ng/g, for ordinary H-chondrite Ochansk, which compares well with previous isotope dilution (ID) ICP-MS data (Walker et al., 2002; Horan et al., 2003; Fischer-Gödde et al., 2010; **Figure 3-7a**). In accordance with literature data, the Os contents of ordinary chondrites decrease with decreasing metal abundance from H>L>LL. As observed in these previous studies and observed for replicate analysis of Zag and Allegan aliquots, the absolute concentration and Os isotope values can vary substantially. Mineral-scale studies (e.g., Horan et al., 2003; Fischer-Gödde et al., 2010) show that this is because of petrologic heterogeneity which is enhanced when analysing small quantities of sample material, as is the case for this study.

The ^{187}Os/^{188}Os ratios for chondrites analysed in this study range between 0.11831 and 0.14498, which is in excellent agreement with previously published values (**Figure 3-7b**). Similar to previous studies, we observe a lower averaged ^{187}Os/^{188}Os ratio for carbonaceous chondrites (0.12657 ±19, excluding Karoonda) than for ordinary (0.12898 ±32) and enstatite (0.12752 ±178) chondrites. The very low value obtained for Karoonda (0.11831 ±1; CK) is in agreement with literature data (Walker et al., 2002; Fischer-Gödde et al., 2010) and has been related to a low Re/Os ratio set in the early history of the meteorite. In this study, we obtain the most radiogenic ^{187}Os/^{188}Os value measured so far for chondrites, of 0.14498 ±5 for Waconda (L). The previous highest reported value was 0.13282 for an L chondrite (Fischer-Gödde et al., 2010).
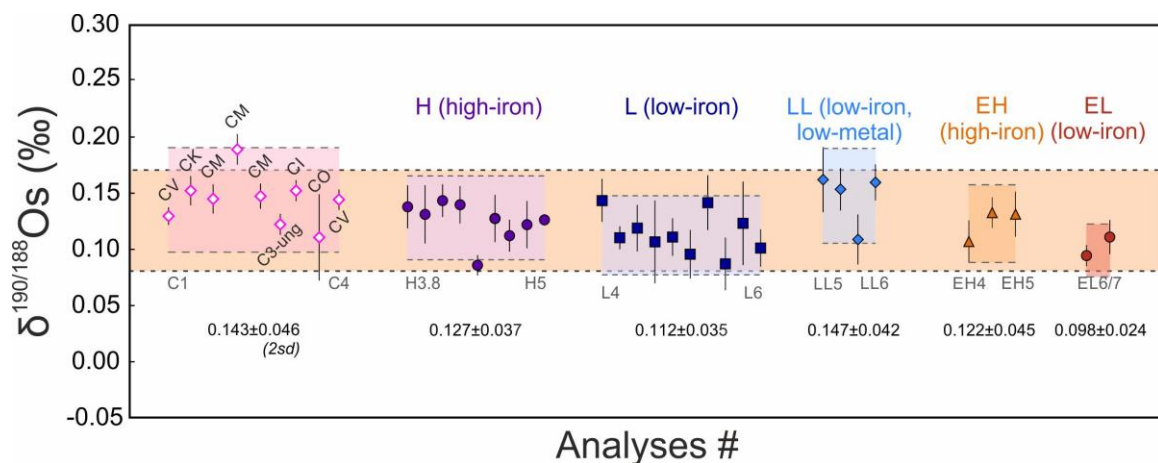
Figure 3-6 Osmium stable isotope ($\delta^{190/188}$Os) results of bulk rock chondrite samples for different classes (C - carbonaceous, ordinary, E - enstatite). Each data point represents an individual chondrite sample. Within the groups, data are ordered from low to high petrographic grade (1-6/7). The shaded areas represent the ±2 sd relative to the weighted average of the subgroups. The weighted errors are provided in Table 3-1 and were obtained by using Isoplot.
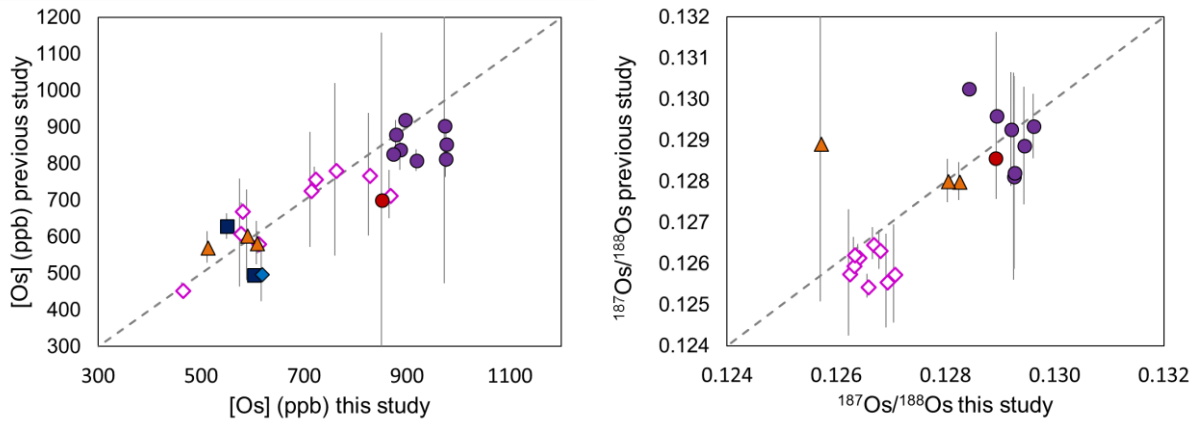
Figure 3-7 Comparison of **(a)** [Os] concentrations (ppb) and **(b)** $^{187}Os/^{188}Os$ of this study with that of literature data. Data is in good agreement, plotting along a 1:1 correlation line. The variability in the literature data is presented by a ±2sd error bar. Literature data from Morgan and Lovering (1967); Meisel et al. (1996); Rubin et al. (1988); Shen et al. (1998); Chen et al., 1998); Walker et al. (2002); Horan et al. (2003); Brandon et al. (2005); Brandon et al. (2006); Fischer-Gödde et al. (2010); van Acken et al. (2011). Symbols as in Figure 3-6.
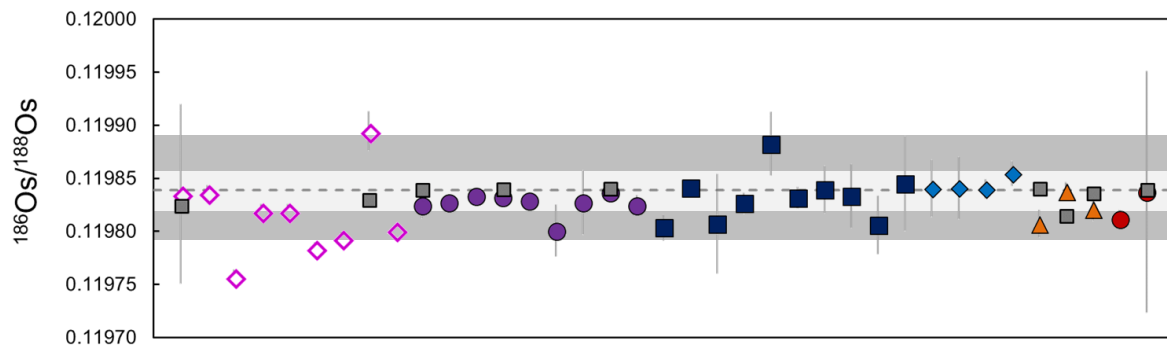
Figure 3-8 The $^{186}Os/^{188}Os$ isotope ratios obtained in this study for chondrites. Symbols as in Figure 3-6, with the grey squares representing literature data obtained from Walker et al. (1997; 2012), Brandon et al. (2006), van Acken et al. (2011). The dashed line indicates the primitive upper mantle (PUM) value from Day et al. (2016). The light grey bar indicates the ±2se on this value. The dark grey bar represents the range in $^{186}Os/^{188}Os$ data as observed for chondrites by Walker et al. (1997; 2012), Brandon et al. (2006), van Acken et al. (2011). Apart from one carbonaceous chondrites, all chondrites plot within this range. Error bars represent the ±2se on the individual measurement.

The present-day $^{186}Os/^{188}Os$ ratios of chondrites analysed in this study ranges from 0.119758 to 0.119895, with a weighted average of 0.119821 ±34 (2 sd, *n*=37). The lowest value is displayed by Mighei (CM) and the highest by Ornans (CO). The variability observed for C-chondrites is more substantial than for O- and E-chondrites. As is observed for $^{187}Os/^{188}Os$ ratios, carbonaceous chondrites display a lower average value, of 0.119799 ±74 (2 sd, n=9), compared to that of ordinary and enstatite chondrites, 0.119833 ±15 (2 sd, *n*=23) and 0.119813 ±20 (2 sd, *n*=5), respectively. If we compare O- and E-chondrites, the average $^{186}Os/^{188}Os$ values increase from EL<EH<H<L<LL (**Table 3-1**) and show a positive correlation with the average Pt/Os ratios of the various groups (Tagle and Berlin, 2008). In this study, $^{190}Pt/^{188}Os$ ratios were not established which means that initial $^{186}Os/^{188}Os$ ratios could not be determined. However, previous studies show that Pt/Os ratios for

chondrites range between 1.71 and 2.09 (Brandon et al., 2006), which results in a maximum difference in ^{186}Os/^{188}Os radiogenic ingrowth of ~20 ppm. The observed difference in ^{186}Os/^{188}Os for O- and E- chondrites is substantially larger than this, by a factor of 10, and hence the effect of radiogenic ingrowth cannot fully account for the observed variability. This heterogeneity might result from incomplete digestion of nucleosynthetic carrier phases, which are shown to be most substantial for ^{186}Os as this is predominantly produced by s-process nucleosynthesis (98.9%; Beer et al., 1997). Previous studies have concluded that refractory pre-solar grains, most likely SiC, retain pre-solar s-process Os (Brandon et al., 2005; Yokoyama et al., 2007; van Acken et al., 2011). That no anomalies have been reported in high metamorphic grade chondrites, supports the idea that refractory phases are the host for ^{186}Os. This is because chondrite metamorphism has been shown to destroy pre-solar graphite and SiC (Huss et al., 2006). The variability in ^{186}Os/^{188}Os is, therefore, expected to decrease with increasing metamorphic grade. This is, however, not what we observe. Instead the largest variability is observed for grade 6 chondrites, which suggests that nucleosynthetic anomalies cannot account for the isotope variation. The most likely explanation for this variability is analytical and relates to OPZ corrections. Since the natural abundance of ^{186}Os, and hence the beam intensity, is very low compared to those isotopes used for stable isotope determination (i.e., ^{188}Os, ^{189}Os, ^{190}Os, ^{192}Os), the effect of the OPZ is more substantial. As it was not our main aim to obtain ^{186}Os/^{188}Os ratios, the potential of a memory effect on ^{186}Os has not been properly taken into account for MC-ICP-MS. It should be noted that this was only noticeable for the ^{186}Os/^{188}Os composition of some samples and not for any other isotope ratios. That carbonaceous chondrites show a large variability, of 1183 ppm, might be because they were analysed by N-TIMS instead of MC-ICP-MS as for the other chondrites. In Chapter 2, it is discussed that the accuracy of N-TIMS analyses at low signal intensities (<1 V total Os) is highly dependent on the oxygen correction. However, all carbonaceous chondrite samples were analysed at total Os beam intensities of >1.9 V. It can, therefore, be assumed that the oxygen correction has not imposed an inaccuracy on the isotope ratios. Instead, the observed variation most likely results from the presence of carriers of nucleosynthetic anomalies. It is in this group, that the largest anomalies have been reported. That this variability is not reflected in δ^{190}Os is consistent with the minimal effect of nucleosynthetic anomalies on the other Os isotopes.

Literature data for ^{186}Os/^{188}Os ratios is limited, but for the few samples for which it is available the data is, in general, in agreement with each other (**Figure 3-8**). The other samples, apart from one carbonaceous chondrite, plot within the range of ^{186}Os/^{188}Os values as obtained for chondrites by Walker et al. (1997; 2012), Brandon et al. (2006) and van Acken et al. (2011).

4.2 GEOLOGICAL REFERENCE MATERIALS

The four standard reference materials have been discussed in detail in Chapter 2. To summarize, they show Os stable isotope compositions within analytical uncertainty of each other (**Figure 3-7**). Orogenic peridotites UB-N and GP-13 yield weighted averages of 0.14 ±0.02‰ (n=6) and 0.14 ±0.01‰ (n=2). The chromitite standards display values of 0.12 ±0.02‰ (n=7; CHR-Bkq) and 0.16 ±0.05‰ (n=4; CHR-Pt+). CHR-Pt+ displays a slightly larger range in δ^{190}Os and shows a positive correlation with Os abundance. This could indicate that individual phases hold distinct stable isotope signatures. All values are within analytical uncertainty of the bulk composition as determined for chondrites.
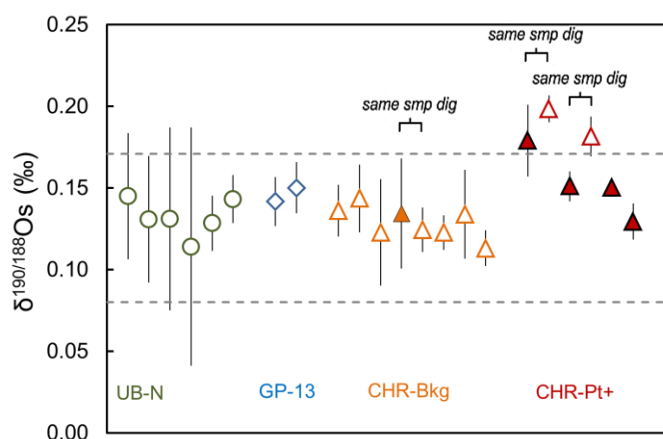
Figure 3-7 Osmium stable isotope compositions ($\delta^{190/188}$Os) of geological materials UB-N, GP-13, CHR-Bkg, CHR-Pt+ and Zag analysed by MC-ICP-MS (closed symbols) or N-TIMS (open symbols). Symbols are ordered from high to low Os concentration. All samples are reference materials sourced from the Earth's mantle, and plot on average within the chondritic range (dashed lines indicate the ±2sd on the average chondrite value). Error bars represent the 2se on the individual measurement.

4.3 KILBOURNE HOLE

4.3.1 Data Quality

All data for Kilbourne Hole samples was obtained by N-TIMS at total Os beam intensities of > 1 V (**Figure 3-9a**). Consequently, as discussed in Chapter 2, any inaccuracy on δ^{190}Os resulting from the oxygen correction can considered to be negligible. To support this conclusion, **Figure 3-9b** shows that the difference in δ^{190}Os when using the calculated or measured ^{17}O/^{16}O is <±0.03‰. This is, with the exception of one sample, smaller than the within-run analytical uncertainty (2 se), and for all samples within the external reproducibility as obtained by repeated analyses of reference material DROsS (0.02‰; 2 sd).
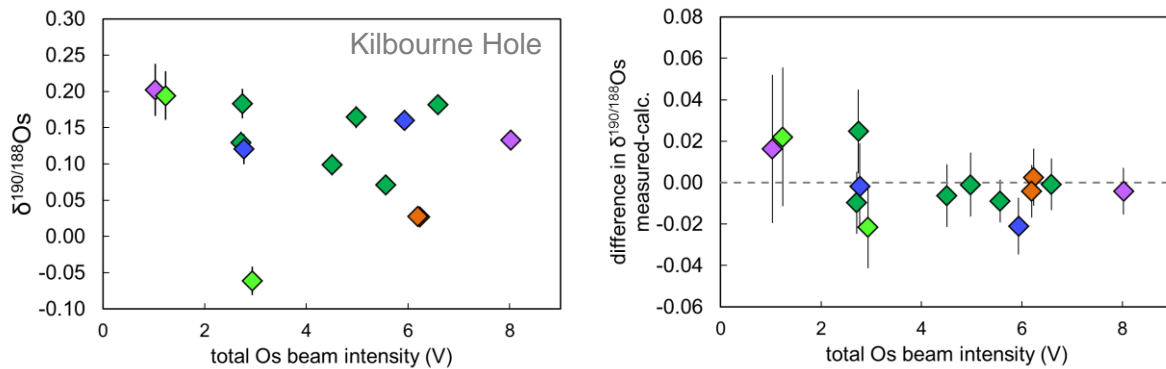
Figure 3-9 (a) The stable isotope composition ($\delta^{190/188}Os$) of Kilbourne Hole peridotites displayed against the total Os beam intensities at which they were analysed by N-TIMS. All samples are analysed at beam intensities (>1V) for which the oxygen correction has been shown in Chapter 2 to have a negligible effect on $\delta^{190/188}Os$. **(b)** The difference in $\delta^{190/188}Os$ using a measured within-run $^{17}O/^{16}O$ and using a $^{17}O/^{16}O$ calculated based on $^{18}O/^{16}O$. Note that the difference is, apart for one sample, smaller than the analytical uncertainty (2se, error bars) on the individual analyses. Symbols that are not dark green indicates sample that have been duplicated, see Figure 3-11.

For four KH samples, two aliquots from the same batch of sample powder were separately processed and measured. Variation in $\delta^{190}Os$ between aliquots ranges from 0.00‰ for KH03-25 to 0.25‰ for KH03-16 (**Figure 3-8a**). Sample KH03-10 shows a difference of 0.07‰ and KH03-18 of 0.04‰. Apart from KH03-16 these replicates are all within typical reproducibility of the method. No processing or analytical anomaly can be detected for the KH03-16 aliquots, suggesting that the difference in $\delta^{190}Os$ results from stable Os mass-dependent isotope fractionation. Although no evidence was found that indicates sample contamination, this cannot be excluded. Interestingly, KH03-16 also displays a substantial difference in Os concentration (19%), whereas this is not the case for the other duplicates (≤1%; **Figure 3-8b**). The difference in concentration could result from a nugget effect since only 4 g was digested for KH03-16b relative to 6 g for KH03-16a. The smaller aliquot of 4 g (KH03-16b) yields a lower Os concentration and a lighter $\delta^{190}Os$ value. A potential source of fractionation will be given in the discussion. For further discussion of data in geological context (section 5), an average will be taken for KH03-18, -25, and the analysis obtained at 8V for KH03-10(b). For KH03-16, both values will be considered.
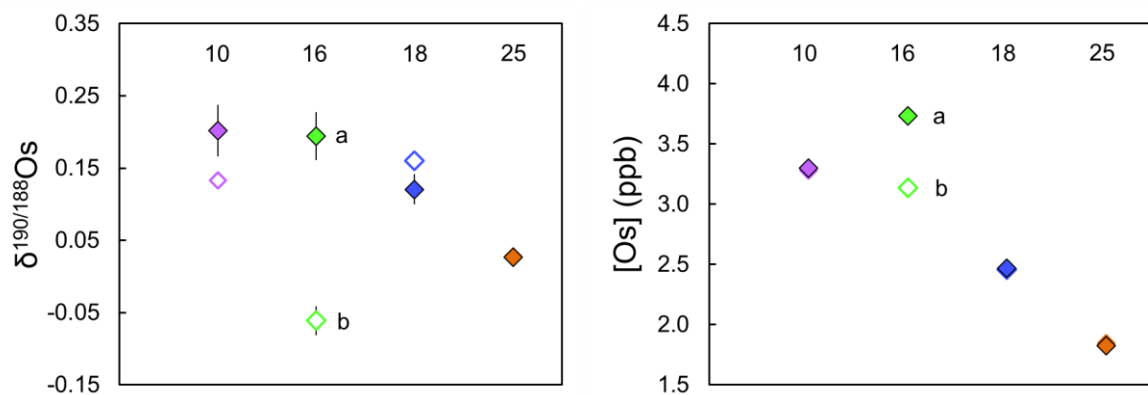
Figure 3-8 For four samples (KH03-10, 16, 18, 25) of Kilbourne Hole peridotites, powder aliquots of the same batch were taken. Comparison of the **(a)** $\delta^{190/188}Os$ and **(b)** Os concentration shows that KH03-16 displays a substantial difference. Note that this is the case for both $\delta^{190/188}Os$ and [Os].

4.3.2 Comparison with literature data

Harvey et al. (2011) determined the $^{187}Os/^{188}Os$ composition and Os abundance of the same sample powders as used in this study, providing a framework to assess the reliability of our method. Before comparison it should be noted that, apart from the fundamental difference in mass fractionation correction (DS versus non-DS), a few important factors differ between the studies that might have resulted in data variability. First of all, the digestion technique; Harvey et al. (2011) digested samples by Carius Tubes (CT), whereas we used the High Pressure Asher (HPA) system. The HPA applies a pressure of 100 bar which, consequently, allows higher temperatures to be attained (300°C vs. 230°C by Harvey et al., 2011). Under these more extreme conditions, digestion is considered by some to be more efficient in dissolving resistant phases (Meisel et al., 2003a). However, Ishikawa et al. (2014) have recently shown that CT can be as effective as HPA digestions when a longer digestion time is applied. Considering that Harvey et al. (2011) digested samples over a time period of 7 days, the difference in digestion efficiency can be assumed to be minimal. Secondly, the amount of sample material used varies. HPA and CT digestions are limited to the amount of sample material that can be digested in a single tube (<2 g). In order to assure high precision for our data, we combined a number of 2 g digestions so that a total amount of >10 ng natural Os was obtained. The total amount of sample material digested and combined ranged between 4 g and 10 g, compared to ~2 g by Harvey et al. (2011). Various studies have shown that the measurement of Os in mantle rocks is sensitive to sample heterogeneity because >95% of the Os is hosted in volumetrically
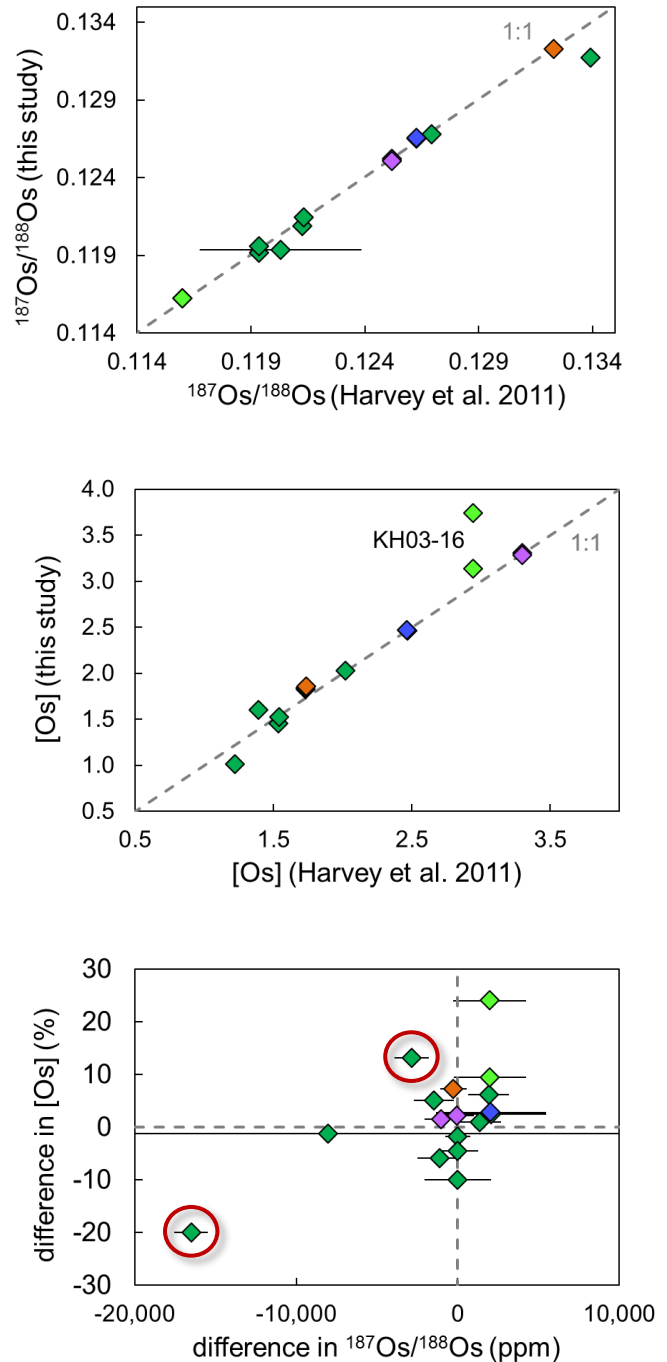
Figure 3-10 Comparison of **(a)** $^{187}Os/^{188}Os$ and **(b)** [Os] data of this study with literature data of Harvey et al. (2011) shows that values are in good agreement with each other. **(c)** The absolute difference in $^{187}Os/^{188}Os$ (ppm) and [Os] (%) between the two studies is, in general, smaller than the analytical uncertainty on the analyses of Harvey et al. (2011). The red circles indicate two samples for which the difference is larger than the analytical uncertainty. Symbols as in Figure 3-10 and 3-11.

insignificant sulphides, resulting in the so-called "nugget effect" (Pearson and Woodland, 2000a). The potential for a nugget effect is larger for small amounts of material and thus more likely to be reflected in the data of Harvey et al. (2011). Individual sulphide analyses have shown that KH xenoliths contain various sulphide populations that yield different Os concentrations as well as radiogenic isotope compositions. Consequently, the nugget effect will not only result in sampling different quantities of sulphides but also in variable representation of those sulphide populations which will influence the reproducibility of the data. Finally, the way by which data was acquired differs. Harvey et al. (2011) collected individual masses by peak jumping on a secondary electron multiplier, whereas we used faraday cups for simultaneous collection of the isotopes. This does not necessarily affect the data accuracy but has a major effect on the precision of the individual analysis. Where the relative 2 se on $^{187}Os/^{188}Os$ is ≤308 ppm for our study, with an average of 113, this is ≤29,590 ppm for Harvey et al. (2011), with an average of 3345 ppm. In either case, the precision is much smaller than the isotope variation between different samples.

Nevertheless, comparison of the data shows that the $^{187}Os/^{188}Os$ ratios are in excellent agreement with that of the non-DS method (**Figure 3-10a**). Variations are, in general, <3,000 ppm which is smaller than the analytical uncertainty on the measurements made by Harvey et al. (2011). The Os abundance data, apart from KH03-16, are also in good agreement (**Figure 3-10b**). Differences range from -20 to +24%, on average +2.3%, with the absolute offset ranging between -0.20 ppb to +0.90 ppb. For samples where the $^{187}Os/^{188}Os$ difference exceeds the analytical uncertainty, a correspondingly large difference in [Os] is observed (**Figure 3-10c**, indicated by red circles). This suggests that the large difference is likely to be due to sample heterogeneity whereby differing proportions of the different sulphide populations were sampled. Furthermore, duplicate measurements made in this and the previous study show a variation up to 4200 ppm in $^{187}Os/^{188}Os$, suggesting that the samples do indeed have a heterogeneous composition. That the variation appears to be unrelated to the type of data acquisition supports the reliability of the DS technique. Sample heterogeneity has implications for direct comparison of the Os isotope data of this study with the elemental data of Harvey et al. (2011; 2012; 2015). For elements that are controlled by the dominant phases, such as major elements and most trace elements, this is unlikely to have any impact. It should, however, be taken into consideration when comparing elements that are also controlled by minor accessory phases, such as S, Se, Te, Au and other HSE (i.e., Ir, Ru, Rh, Pt, Pd, Re).

4.3.3 Osmium Stable Isotope Data

The stable Os isotope compositions ($\delta^{190/188}Os$) of 10 Kilbourne Hole samples analysed in this study vary between -0.06‰ and 0.18‰, and between 0.03‰ and 0.18‰ if aliquots of KH03-16 are not taken into account (**Figure 3-11**). The analytical uncertainty (2 se) on an individual analysis, apart from KH03-16a (0.03‰), is <0.02‰ and on average 0.01‰. The weighted average is 0.11 ±0.04‰ (95% c.i.; n = 11) and 0.11 ±0.04‰ if KH03-16 is excluded (95% c.i.; n = 9), with normal averages of 0.11 ±0.05‰ and 0.12 ±0.03‰ (2 se), respectively. This is not resolvable from the average chondrite value of 0.12 ±0.01‰ (95% c.i.; n = 37) and is
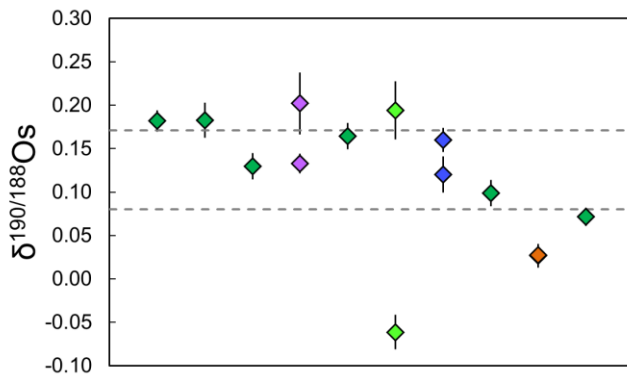
Figure 3-11 The stable Os isotope composition ($\delta^{190/188}$Os) of 10 different peridotite xenolith samples from Kilbourne Hole. Dashed lines indicate the ±2 sd on the weighted average chondrite value. Symbols as in Figure 3-10 and 3-11.

similar to the average value obtained for the reference materials that sample the Earth's mantle, 0.13 ±0.02‰ (95% c.i.; n = 4). The Kilbourne Hole data do, however, display more variability than chondrites and the reference materials, and show differences between KH samples that are resolvable, suggesting that Os stable isotope fractionation may have occurred.

4.3.4 ^{186}Os/^{188}Os Radiogenic Data

Apart from collecting ^{187}Os/^{188}Os and Os abundance data, which could be compared with the study of Harvey et al. (2010), see section 4.3.2, ^{186}Os/^{188}Os data was obtained. This study is the first to report ^{186}Os/^{188}Os data for Kilbourne Hole xenoliths. The ^{186}Os/^{188}Os ratios range from 0.119811 to 0.119856. The weighted mean of 0.119834 ±23 (2 sd, n = 11) is in good agreement with estimates of the primitive upper mantle (PUM) (e.g., 0.119838 ±2, 2 sd – Chatterjee and Lassiter, 2016; 0.119839 ±3, 2 sd – Day et al., 2016; **Figure 3-12**) and present-day H chondrite value (0.119840 ±2, 2 se; Brandon et al., 2006).
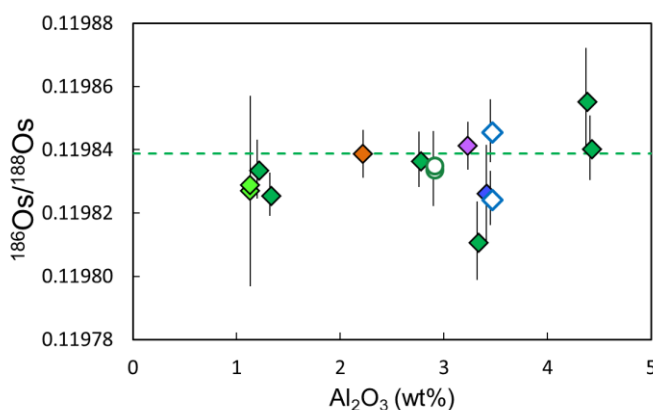
Figure 3-12 The Al_2O_3 (wt.%), as a proxy of melt depletion, versus ^{186}Os/^{188}Os for Kilbourne Hole samples. All ^{186}Os/^{188}Os ratios are within analytical uncertainty of the primitive upper mantle (PUM) value (dashed line) as determined by Day et al. (2016; 0.119839±3). Symbols for Kilbourne Hole as in Figure 3-10 and 3-11.

4.4 ARCHEAN ROCKS

Archean ultramafic rocks from southwest Greenland possess a δ^{190}Os of 0.14‰. Concentration data, 1.27 and 2.36 ppb Os, are consistent with those reported by Dale et al. (2017). The ^{187}Os/^{188}Os ratio displayed by SM12 corresponds well with that reported by Dale et al. (2017), whereas a significant different value was obtained for sample SM24 (0.167322 compared to 0.11878 as reported by Dale et al., 2017). Other samples from the same region haver reported ratios as high as 0.37064. This makes a nugget effect, possibly related to a metasomatic overprint, a likely explanation for the observed difference in ^{187}Os/^{188}Os for SM24. The ^{186}Os/^{188}Os ratios are 0.119811 ±24 and 0.119873 ±18.

5. DISCUSSION

5.1 The EFFECT of MASS-INDEPENDENT ISOTOPE VARIATIONS

A pitfall of the double-spike method is that it can give inaccurate values if any of the isotopes involved in the data reduction process are affected by an abundance anomaly, such as nucleosynthetic anomalies or cosmogenic isotope effects. Carbonaceous (C) chondrites have been shown to possess Os nucleosynthetic anomalies for individual components but at the bulk meteoritic scale they appear to be homogeneous (Brandon et al., 2006; Yokoyama et al., 2007; Yokoyama et al., 2010). Although bulk samples were examined in this study, it cannot be guaranteed that complete digestion of the most refractory phases took place (e.g., nano-diamonds or silicon carbides). Previous studies have shown that both CT and HPA acid digestion can result in incomplete digestion of these phases. It is in these pre-solar grains that isotope anomalies are identified. The potential effect that nucleosynthetic anomalies might impose on the mass-dependent isotope variation has been modelled. When the largest anomaly is considered (Brandon et al. 2006), the resulting shift in δ^{190}Os is smaller than our analytical uncertainty. Nucleosynthetic anomalies are, therefore, considered to have a negligible effect on δ^{190}Os values of C-chondrites. This is supported by the absence of any resolvable variation in δ^{190}Os. Creech et al. (2017) observe a larger variability in Pt stable isotopes for C-chondrites and suggest that this might be due to the presence of nucleosynthetic anomalies. This is not observed for Os stable isotopes. It should, however, be noted that it would be best to obtain unspiked and spiked data from aliquots of a single sample solution in order to apply an accurate correction.

5.2 OSMIUM STABLE ISOTOPE BEHAVIOUR in the SOLAR NEBULA

The stable Os isotope compositions of chondrites, representing different classes (EC, OC, CC) and petrological types (3-6), show no detectable variation, indicating that processes acting on the parent bodies do not result in mass-dependent Os isotope fractionation, or at least none that is resolvable using current techniques. Furthermore, the different classes (EC, OC, CC) are thought to have experienced various oxidation states, thus suggesting that redox effects on the Os stable isotope system are subtle or absent. Finally, the lack of

detectable stable isotope variation with petrological type indicates that no significant fractionation occurred as a result of thermal metamorphism on the chondrite parent bodies. This is consistent with the observation that absolute concentrations of HSE are not controlled by thermal metamorphism in the parent bodies (Fischer-Gödde et al., 2010) and thus that no large scale redistribution of Os occurred during metamorphism.

Chondrites are argued to show open system behaviour, long after original formation, for the Re-Os system (Becker et al., 2001; Walker et al., 2002). Substantial low T secondary processes have, for example, been suggested to explain the low $^{187}Os/^{188}Os$ ratio observed for CK4 chondrite Karoonda (Walker et al., 2002; Fischer-Gödde et al., 2010). That Karoonda shows a similar $\delta^{190/188}Os$ to the other chondrites suggests that this has not impacted the stable Os isotopes.

Most carbonaceous groups contain high-temperature components (chondrules, calcium-aluminium-rich inclusions and metal grains) with their abundance increasing from CI to CK, CM, CV and CO chondrites (Brearley and Jones, 1998). Luck et al. (2005) observed that refractory material in C-chondrites contains isotopically light Zn and explain this by a reaction of refractory material with a gas phase that is enriched in lighter Zn isotopes. No co-variation with $\delta^{190}Os$ and increasing refractory material has been observed. This suggests that these components do not host a preferential heavy or light Os isotope composition and thus that no fractionation occurred during their formation. Regarding the highly refractory behaviour of Os (1812 K - 50% Tc; Lodders, 2003) compared to the much more volatile Zn (723 K; Lodders, 2003), this is not unexpected.

Enstatite chondrites display a lighter Si isotope signature compared to O- and C- chondrites (Armytage et al., 2011; Fitoussi and Bourdon, 2012; Savage and Moynier, 2013) and possibly for Cr (Bonnand et al., 2016). This observation has important implications for reconstructing the building blocks of proto-Earth. No such observation has been made for Os, which is consistent with other more refractory elements such as Pt (Creech et al., 2007) or Ni (Moynier et al., 2007).

Mass-dependent isotope fractionation in carbonaceous chondrites has been detected for the siderophile element Mo, with CM and CK chondrites displaying heavier values (Burkhardt et al., 2014). This variation has been attributed to fractionation in the solar nebula. The most likely mechanisms causing this fractionation being (i) heterogeneous distribution of fractionated metal phases (ii) evaporative losses. If the latter would be the case, the very refractory behaviour of Os might explain why we do not observe any variation for Os. It could also be that Os has been fractionated, but that the effect is smaller due to the higher mass and, consequently, can not be resolved with the current analytical precision.

To summarize, the various processes that chondrite parent bodies have encountered since their formation have not resulted in any resolvable stable Os isotope fractionation. This is consistent with observations for other siderophile and highly siderophile stable isotope systematics, i.e., Ru - Hopp et al. (2016), and Pt - Creech et al. (2017). Absence of any resolvable variation limits the use of the stable Os system to investigate processes in the solar nebula. It does, however, provide us with a perfect framework for examining the late veneer hypothesis.

5.3 OSMIUM STABLE ISOTOPE BEHAVIOUR during MANTLE PROCESSES

5.3.1 Kilbourne Hole

Kilbourne Hole xenoliths show a larger range in δ^{190}Os, 0.25‰, compared to 0.10‰ for chondrites and 0.09‰ observed for the terrestrial reference materials. This variation is also larger than the external reproducibility obtained for geological materials, ±0.05‰. This implies that the variability could be caused by geological processes that occur during the formation and/or emplacement of these xenoliths. The range in δ^{190}Os could reflect a heterogeneous source or be caused by processes acting in the mantle that have overprinted the original signature. To explore the latter hypothesis, the following sections evaluate various processes that are argued to have been experienced by Kilbourne Hole xenoliths (Harvey et al., 2011; 2012; 2015).

Melt extraction   The dominant process that has acted upon KH xenoliths is melt depletion which is expected to result in depletion of, amongst other elements, Yb. Ytterbium is thought to not have been significantly influenced by metasomatism and as such can provide a relative estimate of the amount of melt depletion (**Figure 3-13a**). No co-variation between Yb, or other indices of melt depletion, and δ^{190}Os are observed which implies that the variability in δ^{190}Os is not simply a result of melt extraction (**Figure 3-14a**). It does, however, seem that the scatter in data is more substantial at higher degrees of melting. Osmium is highly compatible during mantle melting. This behaviour is, however, dependent on the stability of the phases in which it is hosted, which in turn are mainly controlled by the S content. As partial melting proceeds, S becomes exhausted and mono sulphide solutions (mss) decompose to refractory PGE-rich phases (platinum-group minerals (PGM); i.e., alloys and laurite; Lorand and Luguet, 2016 and references therein). In this case, fractionation might occur as a consequence of the different bonding environments of these phases. Although PGM have not been observed in KH samples, a few samples possess an extremely low S content, a high Os content, high (Os/Ir)$_{PUM}$, and have experienced high degrees of partial melting. This suggests that PGE-rich alloys might have been stabilised as a result of complete exhaustion of base-metal sulphides (BMS) with prolonged melt extraction. The absence of visible PGM might be due to their inclusion in opaque Cr-spinels, which is supported by the less radiogenic composition observed for spinel (Burton et al., 1999), or because they are embedded, as micro- or nano-inclusions, in sulphides as observed elsewhere (Griffin et al., 2002).

Metasomatism   Apart from melt depletion, the KH samples have experienced various metasomatic events. Relative to the residual mantle, metasomatic melts and fluids possess low Os concentrations which makes the xenoliths and Os isotope system fairly robust to metasomatic overprinting. However, as with melt depletion, the actual impact will be controlled by the stability of the phases Os is hosted in. Depending on the S-saturation of the percolating reagents, sulphides and PGM can be scavenged and/or precipitated. An initial S-undersaturated silicate metasomatic melt, into which sulphides dissolve and are removed, may, upon ascent, become S-saturated and precipitate BMS. Most susceptible to percolating metasomatic fluids are the interstitial sulphides. The PGM, on the other hand, are refractory, dense and less likely to be affected. The presence of interstitial sulphides as well as that of CO_2- and S-saturated silicate-rich melt inclusions suggests that BMS in KH xenoliths have indeed been affected by metasomatism. Furthermore, the sub-parallel offset of

HSE (**Figure 3-15b**) might be explained by removal of BMS. A potential source of mass-dependent isotope fractionation is (partial) breakdown of sulphides when interacting with the percolating reagents. Subsequently, if metasomatic sulphides contain a different δ^{190}Os compared to residual sulphides, their mobilization and/or precipitation could result in isotope variability.

Although other trace elements are controlled by different phases than Os, the (La/Yb)$_{PUM}$ ratio can provide an estimate of the extent of metasomatism (**Figure 3-13a**). Furthermore, the relative offset of HSE might be used as a proxy, with iridium being most resistant to melt depletion and alteration (**Figure 3-13b**). To use Ir as a proxy, the assumption is made that the protolith was homogeneous and contained a PUM starting composition. No systematic co-variation between δ^{190}Os and extent of metasomatism can be observed (**Figure 3-14b,c**), which suggests that metasomatism is not systematically controlling the variation in δ^{190}Os. However, KH xenoliths have experienced a multi-history of metasomatic events, including refertilization. This makes it difficult to establish the systematic effects of a singular episode of metasomatism and, thus, the significance of the interpretations that can be deduced from **Figure 3-14** is unclear. However, what is evident from previous work is that samples KH03-03, -15 and -16 have been affected most extensively by metasomatic events. This suggests that their slightly supra-chondritic δ^{190}Os composition might result from metasomatism, but that this process did not modify La/Yb in a systematic manner.

Sub-solidus exsolution Upon cooling, sulphides tend to exsolve to low-temperature assemblages (e.g., pyrrhotite, pentlandite, chalcopyrite). Pentlandite is the dominant phase observed in KH xenoliths, showing a large range of compositions (**Figure 3-4** and **Figure 3-15a**). The amount of any given PGE that can be hosted in this phase is dependent on the relative proportions of Ni, Fe, and Cu. Sulphides with a higher Ni content have more octahedral sites in which Os is commonly hosted (e.g., Cabri, 1992). Using the data of Harvey et al. (2011) it can be observed that the sulphides with a high Ni content have a lower S content, and thus are expected to display a high Os/S ratio (**Figure 3-15a**). Considering that lighter isotopes, in general, are preferentially incorporated into phases with a higher coordination, sulphides with a high Os/S ratio are likely to possess a lighter isotope signature. A broadly negative correlation between Os/S and δ^{190}Os can be observed, suggesting that subsolidus exsolution results in stable Os isotope fractionation (**Figure 3-15b**). That sample KH03-15 falls outside the trend might be explained by the fact that Os is most likely hosted in this sample by PGM rather than sulphides. However, if subsolidus exsolution caused the observed variation, this would imply that the bulk rock Os budget was altered or that exsolution happened at a significantly large scale that massive sample heterogeneity resulted. Selective removal of exsolved phases would be one mechanism by which to change
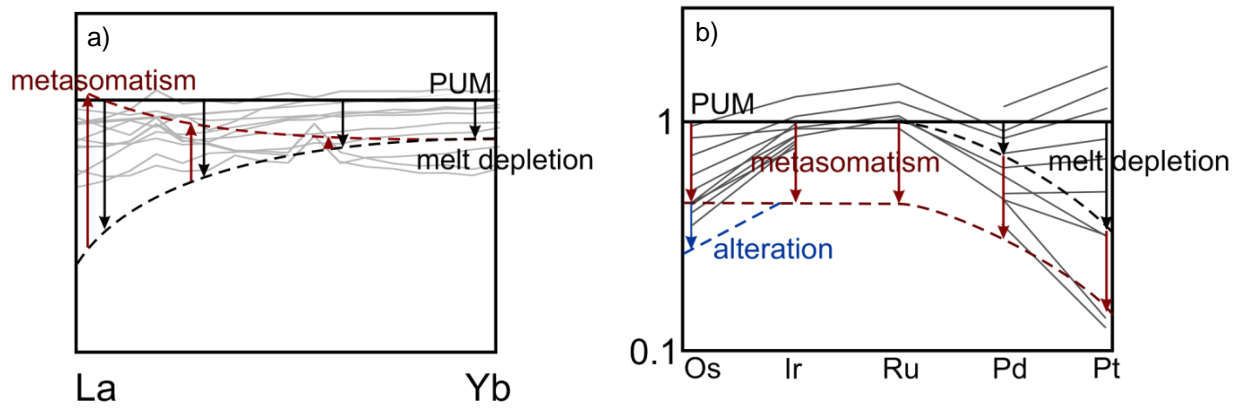
Figure 3-13 Illustration adjusted from Harvey et al. (2015) showing the effect that melt depletion (black dotted line and arrows), followed by metasomatism (red) and finally alteration (blue) have had on Kilbourne Hole mantle xenoliths. This effect is shown for **(a)** REE and **(b)** PGE patterns. Values are normalized against primitive upper mantle values determined by Palme and O'Neill (2003) for REE and Becker et al. (2006) for PGE.
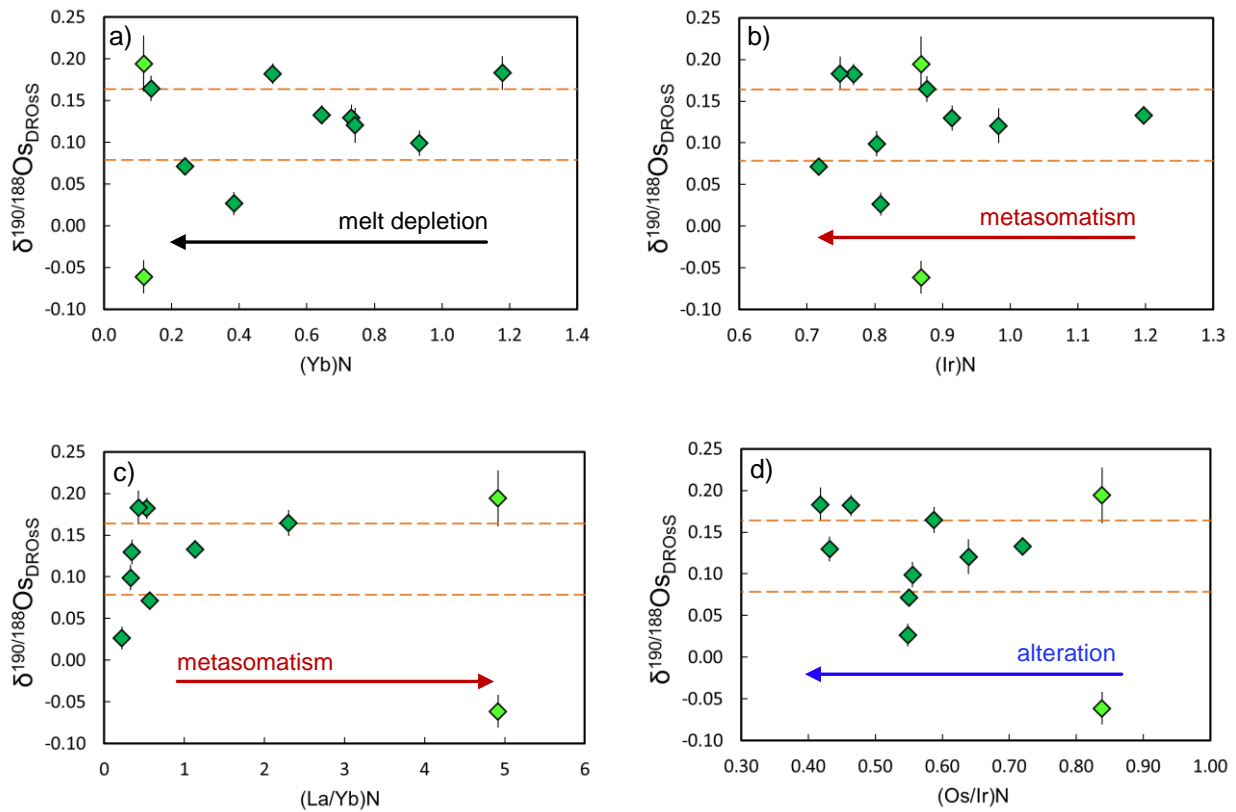
Figure 3-14 These figures reflect the various approaches that are illustrated in Figure 3-16 to quantify the effect of **(a)** melt depletion by Yb$_N$, **(b, c)** metasomatism by Ir$_N$ and (La/Yb)$_N$, and **(d)** alteration using Os/Ir$_N$ as a proxy. No systematic co-variation between δ^{190}Os and any of the proxies is observed. Trace element and PGE data were taken from Harvey et al. (2011), and Harvey et al. (2012), and values were normalised against primitive upper mantle (underscore "N") values determined by Palme and O'Neill (2003) for La and Yb and Becker et al. (2006) for Os and Ir. Arrows points towards and increasing degree of a certain process.
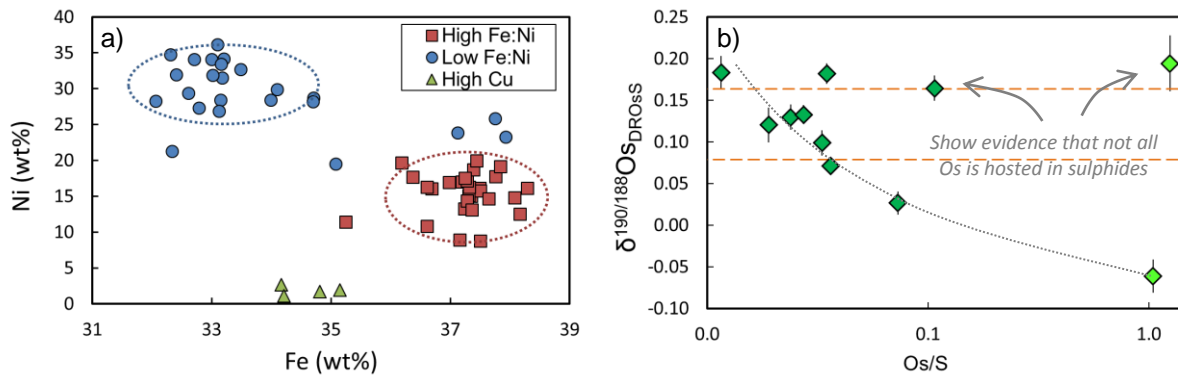
Figure 3-15 (a) Major element composition of sulphides obtained by Harvey et al. (2011) showing that pentlandite separates out in two distinct groups; high Ni – low S, and low Ni – high S. **(b)** The stable isotope composition shows a broadly negative correlation with increasing Os/S content. The relative position of the two pentlandite groups correspond with the hypothesis of fractionation between the distinct phases. That some samples plot outside the trend might be explained by a different principal Os host phase.

the Os budget of the whole rock. However, no clear evidence has been found to support this hypothesis.

Supergene weathering Once Kilbourne Hole xenoliths were exposed at the surface, they would have been affected by another type of percolating fluid; ground- or meteoric waters. During supergene weathering, sulphides are partially oxidized to sulphate and Os to OsO_4, with subsequent removal of both species. Regarding the higher oxidation state of the removed substance, the expectation is that heavier isotopes are removed in case of equilibrium fractionation, leaving the altered sulphide with a lighter isotope composition. This hypothesis fits with the observation that the isotopically lighter aliquot of KH03-16 yields a lower concentration, suggesting that isotopically heavy Os could have been removed during alteration. It must be noted that the geochemical signature of KH03-16 suggests that Os is hosted in PGM which might not have been affected by supergene weathering in a similar way. Most BMS in Kilbourne Hole xenoliths have experienced alteration. The extent of this alteration is, however, poorly quantified. **Figure 3-13b** and **Figure 3-16a** illustrate different approaches that have been used to quantify the extent of alteration. One approach is to look at the relative difference between Os and Ir, as Ir is thought to be more resistant to alteration, whereas Os is more readily mobilized (**Figure 3-13b**). Fractionation of Os from Ir might have occurred as a result of mss subsolidus exsolution, during scavenging of BMS during metasomatism. If this has been the case, the difference in Os and Ir abundance does not only reflect secondary alteration. Another approach is to look at the relationship between Al_2O_3 and S. Here the offset from the general melt depletion trend is considered to be an indication of alteration (**Figure 3-16a**). Overall, none of these proxies reveals a systematic co-variation with $\delta^{190}Os$ and the relative relationship of the samples differs for each proxy (**Figure 3-14d** and **Figure 3-16a**). That the different proxies yield different results most likely reflects the complex history that the KH xenoliths have experienced, which is further complicated by the fact that different phases and populations of sulphides (i.e., enclosed and interstitial) will react differently during alteration.

To summarize, various processes witnessed by Kilbourne Hole xenoliths could have resulted in stable Os isotope fractionation. Most of those considered here, however, can only be fully assessed with the aid of a mineral scale study. With regard to the current analytical constraints, such work is not feasible, in particular,
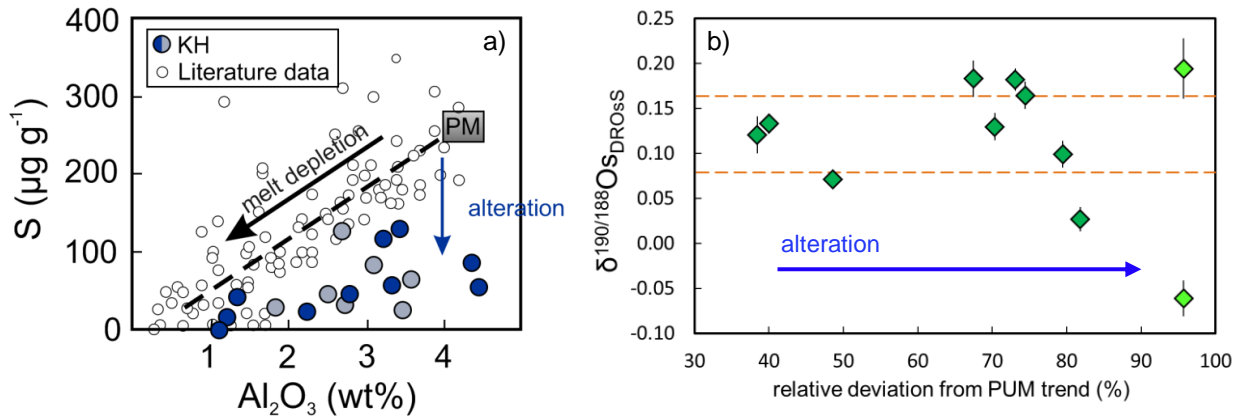
Figure 3-16 (a) Progressive melt depletion will result in a negative correlation between S and Al_2O_3. Alteration will result in a drop of S, causing the Kilbourne Hole (KH) samples to plot below the melt depletion trend. PM indicates the primitive upper mantle value. Figure adjusted from Harvey et al. (2015), literature data from Lorand et al. (2010, 2012), Alard et al. (2011), König et al. (2012, 2014), Wang et al. (2013), and Le Roux et al. (2007). **(b)** The relative deviation of KH samples from the PM trend was calculated (in %) and plotted against $\delta^{190/188}Os$. No clear co-variation with increasing degree of alteration is observed.

because of the need for relatively large quantities of Os. It should also be noted that the variability could simply reflect the poorer reproducibility for mantle samples by N-TIMS measurement. For now, an average of the KH xenoliths will be considered in any further discussion.

5.3.2 Archean Rocks

One of the main uncertainties regarding the 3.7-3.8 Ga samples from the Itsaq Gneiss Complex is whether they represent ancient fragments of mantle or whether they are ultramafic cumulate rocks (see Dale et al., 2017). Their field relations, occurring as numerous enclaves or pods in the ~3.8 Ga orthogneiss terrain to the south of Isua, does not permit this to be distinguished. Ultramafics in the Isua supracrustal belt itself have been interpreted to be cumulate in origin (Szilas et al., 2015), but it has been suggested that the ultramafics analysed here may be mantle samples (Friend et al., 2002; Rollinson, 2007). This remains a matter of debate. In either case, the existence of fresh olivine precludes significant regional metamorphism during their history and also indicates a lack of pervasive aqueous alteration which would otherwise have produced serpentine minerals at the expense of olivine. In this case, it is not expected that their Os stable isotope composition will have been affected by these factors. Potentially more cryptic effects, such as metasomatism, have not been fully investigated, nor has the presence or distribution of sulphides.

The relative HSE abundances of the Isua samples (Dale et al., 2017) are broadly similar to the estimate for the primitive mantle (Becker et al., 2006), with somewhat elevated Ru/Ir and Pd/Ir ratios compared to chondrites, but with HSE abundances between 35 and 70% of the PM estimate. This is possibly consistent with their derivation as mantle fragments from an early Archaean mantle which had only received 50-60% of the full late veneer complement. In this case, their HSE patterns would suggest that they represent fertile mantle that has not undergone significant melt depletion, or mantle that has been re-enriched by melt percolation after

melt depletion. Currently, our understanding of the petrography of these rocks is not sufficiently developed to distinguish between these two possibilities. Primitive mantle-like HSE abundances also does not preclude a cumulate origin, although most cumulates have strongly fractionated HSE proportions (Day et al., 2008; O'Driscoll et al., 2009; Szilas et al., 2015).

What is notable about the Isua samples is that they possess Os stable isotope values that fall within the modern mantle range, despite a two-fold difference in Os concentration. This suggests either that this is the predominant composition of the Archaean mantle or that the stable isotope composition has been pervasively overprinted. The lack of evidence for such large-scale mobility of HSE (both petrographically and in the systematic HSE patterns) largely precludes this latter possibility. If a cumulate origin is assumed, then whether their Os stable isotope composition reflects their mantle source depends on whether any significant fractionation occurred during partial melting. The evidence derived from Kilbourne Hole samples is that such fractionation during melting is unlikely. In this case, it is likely that, regardless of the exact origin of the Isua samples, their Os stable isotope composition reflects that of the mantle in the region at 3.7-3.8 Ga – possibly a mantle lacking in a portion of Earth's late veneer.

5.4 IMPLICATIONS "LATE VENEER" HYPOTHESIS

Chondrites show no resolvable Os stable isotope variation, rendering this isotope system of little use for investigating processes that have acted upon chondrites within the solar nebula. The homogeneous composition does, however, provide a framework by which to compare Earth's mantle with Earth-like building blocks (i.e., chondrites) in order to test the late veneer hypothesis. To recall, the expectation is that Earth's present-day mantle possesses a similar signature to that of chondrites. Here, the assumption is made that, with time, the accreted material has been effectively homogenized throughout the mantle.

With the current analytical precision, the average composition of the Kilbourne Hole xenoliths and the four reference materials show no resolvable difference relative to chondrites. This result is consistent with recent studies of mass-dependent isotope variation for other HSE elements (Pt -Creech et al., 2017; Ru – personal communication) and non-HSE elements (e.g., K – Humayun and Clayton, 1995, Wang and Jacobsen, 2016; Li – Magna et al., 2006; Seitz et al., 2007; Fe – Schoenberg and von Blanckenburg, 2006). These observations either imply that no (significant) isotope fractionation took place during metal-silicate segregation or that the signature of core formation was overprinted by a subsequent process, in particular, the addition of late accreted material preserving a chondrite-like composition. These hypotheses are not mutually exclusive, as stable isotope fractionation could have been absent during core formation followed by significant incorporation of late accreted material with a chondritic signature. Metal-silicate isotope partitioning experiments could be conducted to examine stable Os isotope fractionation during core formation. These experiments are, however, challenging because of the volatile behaviour of Os and low Os abundances in the silicate fraction. Another approach would be to examine rocks from the early history of the Earth. Maier et al. (2009) show that PGE abundances of early Archean komatiites (3.5–3.2 Ga) display lower values compared to

late-Archean and post-Archean komatiites. This has been interpreted to reflect progressive mixing of late accreted material into the mantle. If we assume, based on data obtained for the Mo isotope system, that core segregation resulted in a heavier isotope composition in the mantle and that late accreted material possesses a chondritic isotope composition, then terrestrial Archean rocks, representing melting of Earth's earliest mantle, could potentially preserve a record of the trend from supra-chondritic to chondritic values. A recent study by Creech et al. (2017) indicates that Archean terrestrial rocks do indeed display non-chondritic, heavy Pt stable isotope compositions. This has been interpreted to result from metal-silicate stable isotope fractionation that occurred during core formation which has been preserved because late accreted material was not completely homogeneously mixed. In contrast, the two Isua samples analysed in this study display stable Os isotope compositions that are not significantly different from chondrites. Creech et al. (2017) have modelled the effect of mixing meteoritic material into a HSE depleted mantle and show that the initial concentration of the pre-late-veneer mantle controls how readily the isotope composition is overprinted. If the Os concentration was substantially lower than for Pt, this might explain why no heavier δ^{190}Os compositions were observed. Experimental studies indeed show that the metal-silicate partitioning of Pt is lower than Os by an order of 2-3 (Brenan and McDonough, 2009; Mann et al., 2012). Another possibility is that the original signature was overprinted by supergene weathering processes, similar to that potentially experienced by Kilbourne Hole xenoliths. Considering that Isua samples have been exposed at the surface for a considerable time, sulphides may have broken down creating a potential source of fractionation. A more detailed study of Archean rocks is required. Here, it is important to monitor the degree of secondary processes, such as metamorphism and alteration, potentially occurring during and after being transported from the mantle to the surface.

6. CONCLUSIONS

Chondrites display a homogeneous stable Os isotope composition, which implies that processes acting upon them after their accretion have not resulted in significant Os isotope fractionation. All Earth's mantle samples studied here display an average composition that is similar to that of chondrites. This supports the hypothesis that the HSE abundance of the Earth's mantle results from meteoritic material that was added to the mantle after core formation, although it cannot be excluded that metal-silicate segregation did not result in significant stable Os isotope fractionation. The average composition of Kilbourne Hole samples is chondritic, however, the overall variability observed suggests that inter-mineral stable Os isotope fractionation has occurred. That Archean rocks from the Isua supracrustal sequence display chondritic compositions suggesting either that the stable Os isotope composition was more readily overprinted than observed for Pt in similar rock types, or that processes that acted in the mantle, as argued for Kilbourne Hole xenoliths, have obscured the "true" overall primitive mantle signature.

ACKNOWLEDGEMENTS

REFERENCES

Archer, G., Ash, R., Bullock, E., and Walker, R., 2014, Highly siderophile elements and ^{187}Re–^{187}Os isotopic systematics of the Allende meteorite: Evidence for primary nebular processes and late-stage alteration: Geochimica et Cosmochimica Acta, v. 131, p. 402-414.

Armytage, R., Georg, R., Savage, P., Williams, H., and Halliday, A., 2011, Silicon isotopes in meteorites and planetary core formation: Geochimica et Cosmochimica Acta, v. 75, no. 13, p. 3662-3676.

Becker, H., Horan, M., Walker, R., Gao, S., Lorand, J.-P., and Rudnick, R., 2006, Highly siderophile element composition of the Earth's primitive upper mantle: constraints from new data on peridotite massifs and xenoliths: Geochimica et Cosmochimica Acta, v. 70, no. 17, p. 4528-4550.

Becker, H., Morgan, J. W., Walker, R. J., MacPherson, G. J., and Grossman, J. N., 2001, Rhenium-osmium systematics of calcium-aluminium-rich inclusions in carbonaceous chondrites: Geochimica et Cosmochimica Acta, v. 65, no. 19, p. 3379-3390.

Bédard, L. P., and Barnes, S.-J., 2004, Improved Platinum-Group Element Extraction by NiS Fire Assay from Chromitite Ore Samples Using a Flux Containing Sodium Metaphosphate: Geostandards and Geoanalytical Research, v. 28, no. 2, p. 311-316.

Beer, H., Corvi, F., and Mutti, P., 1997, Neutron capture of the bottleneck isotopes 138Ba and 208Pb, s-process studies, and the r-process abundance distribution: The Astrophysical Journal, v. 474, no. 2, p. 843.

Birck, J. L., Barman, M. R., and Capmas, F., 1997, Re-Os Isotopic Measurements at the Femtomole Level in Natural Samples: Geostandards Newsletter, v. 21, no. 1, p. 19-27.

Bodinier, J.-L., and Godard, M., 2003, Orogenic, ophiolitic, and abyssal peridotites: Treatise on geochemistry, v. 2, p. 568.

Bonnand, P., Williams, H., Parkinson, I., Wood, B., and Halliday, A., 2016, Stable chromium isotopic composition of meteorites and metal–silicate experiments: Implications for fractionation during core formation: Earth and Planetary Science Letters, v. 435, p. 14-21.

Borisov, A., and Palme, H., 1995, The solubility of iridium in silicate melts: new data from experiments with Ir 10 Pt 90 alloys: Geochimica et Cosmochimica Acta, v. 59, no. 3, p. 481-485.

-, 1997, Experimental determination of the solubility of platinum in silicate melts: Geochimica et Cosmochimica Acta, v. 61, no. 20, p. 4349-4357.

Brandon, A. D., Humayun, M., Puchtel, I. S., Leya, I., and Zolensky, M., 2005, Osmium Isotope Evidence for an s-Process Carrier in Primitive Chondrites: Science, v. 309, no. 5738, p. 1233-1236.

Brandon, A. D., Snow, J. E., Walker, R. J., Morgan, J. W., and Mock, T. D., 2000, 190 Pt–^{186}Os and ^{187} Re–^{187}Os systematics of abyssal peridotites: Earth and Planetary Science Letters, v. 177, no. 3, p. 319-335.

Brandon, A. D., Walker, R. J., Morgan, J. W., Norman, M. D., and Prichard, H. M., 1998, Coupled ^{186}Os and ^{187}Os evidence for core-mantle interaction: Science, v. 280, no. 5369, p. 1570-1573.

Brandon, A. D., Walker, R. J., and Puchtel, I. S., 2006, Platinum–osmium isotope evolution of the Earth's mantle: Constraints from chondrites and Os-rich alloys: Geochimica et Cosmochimica Acta, v. 70, no. 8, p. 2093-2103.

Brearley, A. J., and Jones, R. H., 1998, Chondritic meteorites: Reviews in mineralogy and geochemistry, v. 36, no. 1, p. 3.1-3.398.

Brenan, J. M., and McDonough, W. F., 2009, Core formation and metal-silicate fractionation of osmium and iridium from gold: Nature Geosci, v. 2, no. 11, p. 798-801.

Brenan, J. M., McDonough, W. F., and Ash, R., 2005, An experimental study of the solubility and partitioning of iridium, osmium and gold between olivine and silicate melt: Earth and Planetary Science Letters, v. 237, no. 3, p. 855-872.

Büchl, A., Brügmann, G., Batanova, V. G., Münker, C., and Hofmann, A. W., 2002, Melt percolation monitored by Os isotopes and HSE abundances: a case study from the mantle section of the Troodos Ophiolite: Earth and Planetary Science Letters, v. 204, no. 3, p. 385-402.

Burkhardt, C., Hin, R. C., Kleine, T., and Bourdon, B., 2014, Evidence for Mo isotope fractionation in the solar nebula and during planetary differentiation: Earth and Planetary Science Letters, v. 391, no. 0, p. 201-211.

Burton, K. W., Schiano, P., Birck, J.-L., and Allègre, C. J., 1999, Osmium isotope disequilibrium between mantle minerals in a spinel-lherzolite: Earth and Planetary Science Letters, v. 172, no. 3, p. 311-322.

Bussod, G., and Irving, A., Thermal and rheologic history of the upper mantle beneath the Southern Rio Grande Rift: evidence from Kilbourne Hole xenoliths, *in* Proceedings Processes of Planetary Rifting1981, Volume 457, p. 145.

Bussod, G. Y., and Williams, D. R., 1991, Thermal and kinematic model of the southern Rio Grande rift: inferences from crustal and mantle xenoliths from Kilbourne Hole, New Mexico: Tectonophysics, v. 197, no. 2, p. 373-389.

Bussod, G. Y. A., 1983, Thermal and kinematic history of mantle xenoliths from Kilbourne Hole, New Mexico: Los Alamos National Lab., NM (USA).

Cabri, L. J., 1992, The distribution of trace precious metals in minerals and mineral products: Mineralogical magazine, v. 56, no. 3, p. 289-308.

Carter, J. L., 1965, The origin of olivine bombs and related inclusions in basalts.

Chatterjee, R., and Lassiter, J. C., 2016, $^{186}Os/^{188}Os$ variations in upper mantle peridotites: Constraints on the Pt/Os ratio of primitive upper mantle, and implications for late veneer accretion and mantle mixing timescales: Chemical Geology, v. 442, p. 11-22.

Chen, J. H., Papanastassiou, D. A., and Wasserburg, G. J., 1998, Re-Os systematics in chondrites and the fractionation of the platinum group elements in the early solar system: Geochimica et Cosmochimica Acta, v. 62, no. 19–20, p. 3379-3392.

Chou, C.-L., Fractionation of siderophile elements in the Earth's upper mantle, *in* Proceedings Lunar and Planetary Science Conference Proceedings1978, Volume 9, p. 219-230.

Clayton, R. N., 1993, Oxygen isotopes in meteorites: Annual Review of Earth and Planetary Sciences, v. 21, no. 1, p. 115-149.

Coggon, J. A., Luguet, A., Nowell, G. M., and Appel, P. W., 2013, Hadean mantle melting recorded by southwest Greenland chromitite ^{186}Os signatures: Nature Geoscience, v. 6, no. 10, p. 871-874.

Cohen, A. S., and Waters, F. G., 1996, Separation of osmium from geological materials by solvent extraction for analysis by thermal ionisation mass spectrometry: Analytica Chimica Acta, v. 332, no. 2, p. 269-275.

Cottrell, E., and Walker, D., 2006, Constraints on core formation from Pt partitioning in mafic silicate liquids at high temperatures: Geochimica et Cosmochimica Acta, v. 70, no. 6, p. 1565-1580.

Creech, J., Baker, J., Handler, M., Lorand, J., Storey, M., Wainwright, A., Luguet, A., Moynier, F., and Bizzaro, M., 2017, Late accretion history of the terrestrial planets inferred from platinum stable isotopes.

Dale, C. W., Burton, K. W., Pearson, D. G., Gannoun, A., Alard, O., Argles, T. W., and Parkinson, I. J., 2009, Highly siderophile element behaviour accompanying subduction of oceanic crust: Whole rock and mineral-scale insights from a high-pressure terrain: Geochimica et Cosmochimica Acta, v. 73, no. 5, p. 1394-1416.

Dale, C. W., Gannoun, A., Burton, K. W., Argles, T. W., and Parkinson, I. J., 2007, Rhenium–osmium isotope and elemental behaviour during subduction of oceanic crust and the implications for mantle recycling: Earth and Planetary Science Letters, v. 253, no. 1, p. 211-225.

Dale, C. W., Kruijer, T. S., and Burton, K. W., 2017, Highly siderophile element and ^{182}W evidence for a partial late veneer in the source of 3.8 Ga rocks from Isua, Greenland: Earth and Planetary Science Letters, v. 458, p. 394-404.

Day, J. M., Brandon, A. D., and Walker, R. J., 2016, Highly siderophile elements in Earth, Mars, the Moon, and asteroids: Reviews in Mineralogy and Geochemistry, v. 81, no. 1, p. 161-238.

Day, J. M., Pearson, D. G., and Hulbert, L. J., 2008, Rhenium–osmium isotope and platinum-group element constraints on the origin and evolution of the 1· 27 Ga Muskox layered intrusion: Journal of Petrology, v. 49, no. 7, p. 1255-1295.

Dromgoole, E. L., and Pasteris, J. D., 1987, Interpretation of the sulfide assemblages in a suite of xenoliths from Kilbourne Hole, New Mexico: Geological Society of America Special Papers, v. 215, p. 25-46.

Fischer-Gödde, M., Becker, H., and Wombacher, F., 2010, Rhodium, gold and other highly siderophile element abundances in chondritic meteorites: Geochimica et Cosmochimica Acta, v. 74, no. 1, p. 356-379.

Fitoussi, C., and Bourdon, B., 2012, Silicon isotope evidence against an enstatite chondrite Earth: Science, v. 335, no. 6075, p. 1477-1480.

Friend, C., Bennett, V., and Nutman, A., 2002, Abyssal peridotites> 3,800 Ma from southern West Greenland: field relationships, petrography, geochronology, whole-rock and mineral chemistry of dunite and harzburgite inclusions in the Itsaq Gneiss Complex: Contributions to Mineralogy and Petrology, v. 143, no. 1, p. 71-92.

Griffin, W., Spetsius, Z., Pearson, N., and O'Reilly, S. Y., 2002, In situ Re-Os analysis of sulfide inclusions in kimberlitic olivine: New constraints on depletion events in the Siberian lithospheric mantle: Geochemistry, Geophysics, Geosystems, v. 3, no. 11, p. 1-25.

Harvey, J., Dale, C., Gannoun, A., and Burton, K., Rhenium-osmium heterogeneity of enriched mantle basalts explained by composition and behaviour of mantle-derived sulfides, *in* Proceedings AGU Fall Meeting Abstracts2010, Volume 1, p. 2292.

Harvey, J., Dale, C. W., Gannoun, A., and Burton, K. W., 2011, Osmium mass balance in peridotite and the effects of mantle-derived sulphides on basalt petrogenesis: Geochimica et Cosmochimica Acta, v. 75, no. 19, p. 5574-5596.

Harvey, J., König, S., and Luguet, A., 2015, The effects of melt depletion and metasomatism on highly siderophile and strongly chalcophile elements: S–Se–Te–Re–PGE systematics of peridotite xenoliths from Kilbourne Hole, New Mexico: Geochimica et Cosmochimica Acta, v. 166, p. 210-233.

Harvey, J., Yoshikawa, M., Hammond, S. J., and Burton, K. W., 2012, Deciphering the Trace Element Characteristics in Kilbourne Hole Peridotite Xenoliths: Melt–Rock Interaction and Metasomatism

beneath the Rio Grande Rift, SW USA: Journal of Petrology, v. 53, no. 8, p. 1709-1742.

Herzberg, C., 2004, Geodynamic information in peridotite petrology: Journal of Petrology, v. 45, no. 12, p. 2507-2530.

Hin, R. C., Burkhardt, C., Schmidt, M. W., Bourdon, B., and Kleine, T., 2013, Experimental evidence for Mo isotope fractionation between metal and silicate liquids: Earth and Planetary Science Letters, v. 379, p. 38-48.

Hoffer, J. M., 1976, The Potrillo basalt field, south-central New Mexico: Cenozoic Volcanism in Southwestern New Mexico, v. 5, p. 89-92.

Hopp, T., Fischer-Gödde, M., and Kleine, T., Ruthenium Isotope Fractionation During Planetesimal Core Crystallization, in Proceedings Lunar and Planetary Science Conference2016, Volume 47, p. 1231.

Horan, M., Walker, R., Morgan, J., Grossman, J., and Rubin, A., 2003, Highly siderophile elements in chondrites: Chemical Geology, v. 196, no. 1, p. 27-42.

Humayun, M., and Clayton, R. N., 1995, Potassium isotope cosmochemistry: Genetic implications of volatile element depletion: Geochimica et Cosmochimica Acta, v. 59, no. 10, p. 2131-2148.

Huss, G. R., Rubin, A. E., and Grossman, J. N., 2006, Thermal metamorphism in chondrites: Meteorites and the early solar system II, p. 567-586.

Irving, A., 1979, Kilbourne Hole spinel lherzolites: samples of multiply depleted, enriched and deformed mantle: EOS Transactions, American Geophysical Union, v. 60, p. 418.

Irving, A. J., 1980, Petrology and geochemistry of composite ultramafic xenoliths in alkalic basalts and implications for magmatic processes within the mantle: American Journal of Science, v. 280, no. 2, p. 389-426.

Ishikawa, A., Senda, R., Suzuki, K., Dale, C. W., and Meisel, T., 2014, Re-evaluating digestion methods for highly siderophile element and [187]Os isotope analysis: Evidence from geological reference materials: Chemical Geology, v. 384, p. 27-46.

Jones, J. H., and Drake, M. J., 1986, Geochemical constraints on core formation in the Earth.

Kil, Y., and Wendlandt, R., 2004, Pressure and temperature evolution of upper mantle under the Rio Grande Rift: Contributions to Mineralogy and Petrology, v. 148, no. 3, p. 265-280.

Kimura, K., Lewis, R. S., and Anders, E., 1974, Distribution of gold and rhenium between nickel-iron and silicate melts: implications for the abundance of siderophile elements on the Earth and Moon: Geochimica et Cosmochimica Acta, v. 38, no. 5, p. 683-701.

Kruijer, T. S., Kleine, T., Fischer-Godde, M., and Sprung, P., 2015, Lunar tungsten isotopic evidence for the late veneer: Nature, v. advance online publication.

Le Roux, V., Bodinier, J.-L., Tommasi, A., Alard, O., Dautria, J.-M., Vauchez, A., and Riches, A., 2007, The Lherz spinel lherzolite: refertilized rather than pristine mantle: Earth and Planetary Science Letters, v. 259, no. 3, p. 599-612.

Lodders, K., 2003, Solar system abundances and condensation temperatures of the elements: The Astrophysical Journal, v. 591, no. 2, p. 1220.

Lorand, J.-P., and Luguet, A., 2016, Chalcophile and siderophile elements in mantle rocks: Trace elements controlled by trace minerals: Reviews in Mineralogy and Geochemistry, v. 81, no. 1, p. 441-488.

Lorand, J.-P., Luguet, A., and Alard, O., 2008, Platinum-group elements: a new set of key tracers for the Earth's interior: Elements, v. 4, no. 4, p. 247-252.

Lorand, J. P., Alard, O., and Godard, M., 2009, Platinum-group element signature of the primitive mantle rejuvenated by melt-rock reactions: evidence from Sumail peridotites (Oman Ophiolite): Terra Nova, v. 21, no. 1, p. 35-40.

Luck, J.-M., Othman, D. B., and Albarède, F., 2005, Zn and Cu isotopic variations in chondrites and iron meteorites: Early solar nebula reservoirs and parent-body processes: Geochimica et Cosmochimica Acta, v. 69, no. 22, p. 5351-5363.

Luguet, A., Behrens, M., Pearson, D. G., König, S., and Herwartz, D., 2015, Significance of the whole rock Re–Os ages in cryptically and modally metasomatised cratonic peridotites: Constraints from HSE–Se–Te systematics: Geochimica et Cosmochimica Acta, v. 164, p. 441-463.

Magna, T., Wiechert, U., and Halliday, A. N., 2006, New constraints on the lithium isotope compositions of the Moon and terrestrial planets: Earth and Planetary Science Letters, v. 243, no. 3, p. 336-353.

Maier, W. D., Barnes, S. J., Campbell, I. H., Fiorentini, M. L., Peltonen, P., Barnes, S.-J., and Smithies, R. H., 2009, Progressive mixing of meteoritic veneer into the early Earth/'s deep mantle: Nature, v. 460, no. 7255, p. 620-623.

Mann, U., Frost, D. J., Rubie, D. C., Becker, H., and Audétat, A., 2012, Partitioning of Ru, Rh, Pd, Re, Ir and Pt between liquid metal and silicate at high pressures and high temperatures - Implications for the origin of highly siderophile element concentrations in the Earth's mantle: Geochimica et Cosmochimica Acta, v. 84, p. 593-613.

McAdam, M. M., Sunshine, J. M., Howard, K. T., and McCoy, T. M., 2015, Aqueous alteration on asteroids: Linking the mineralogy and spectroscopy of CM and CI chondrites: Icarus, v. 245, p. 320-332.

Meisel, T., Fellner, N., and Moser, J., 2003a, A simple procedure for the determination of platinum group elements and rhenium (Ru, Rh, Pd, Re, Os, Ir and Pt) using ID-ICP-MS with an inexpensive on-line matrix separation in geological and environmental materials: Journal of Analytical Atomic Spectrometry, v. 18, no. 7, p. 720-726.

Meisel, T., Moser, J., Fellner, N., Wegscheider, W., and Schoenberg, R., 2001a, Simplified method for the determination of Ru, Pd, Re, Os, Ir and Pt in chromitites and other geological materials by isotope dilution ICP-MS and acid digestion: Analyst, v. 126, no. 3, p. 322-328.

Meisel, T., Reisberg, L., Moser, J., Carignan, J., Melcher, F., and Brügmann, G., 2003b, Re–Os systematics of UB-N, a serpentinized peridotite reference material: Chemical geology, v. 201, no. 1, p. 161-179.

Meisel, T., Walker, R. J., Irving, A. J., and Lorand, J.-P., 2001b, Osmium isotopic compositions of mantle

xenoliths: a global perspective: Geochimica et Cosmochimica Acta, v. 65, no. 8, p. 1311-1323.

Meisel, T., Walker, R. J., and Morgan, J. W., 1996, The osmium isotopic composition of the Earth's primitive upper mantle: Nature, v. 383, no. 6600, p. 517-520.

Morgan, J., Walker, R., Brandon, A., and Horan, M., 2001, Siderophile elements in Earth's upper mantle and lunar breccias: data synthesis suggests manifestations of the same late influx: Meteoritics & Planetary Science, v. 36, no. 9, p. 1257-1275.

Morgan, J. W., 1985, Osmium isotope constraints on Earth's late accretionary history: Nature, v. 317, no. 6039, p. 703-705.

Morgan, J. W., and Lovering, J. F., 1967, Rhenium and osmium abundances in chondritic meteorites: Geochimica et Cosmochimica Acta, v. 31, no. 10, p. 1893-1909.

Nutman, A. P., and Friend, C. R., 2009, New 1: 20,000 scale geological maps, synthesis and history of investigation of the Isua supracrustal belt and adjacent orthogneisses, southern West Greenland: a glimpse of Eoarchaean crust formation and orogeny: Precambrian Research, v. 172, no. 3, p. 189-211.

O'Driscoll, B., Day, J. M., Daly, J. S., Walker, R. J., and McDonough, W. F., 2009, Rhenium–osmium isotopes and platinum-group elements in the Rum Layered Suite, Scotland: Implications for Cr-spinel seam formation and the composition of the Iceland mantle anomaly: Earth and Planetary Science Letters, v. 286, no. 1, p. 41-51.

O'Neill, H. S. C., Dingwell, D., Borisov, A., Spettel, B., and Palme, H., 1995, Experimental petrochemistry of some highly siderophile elements at high temperatures, and some implications for core formation and the mantle's early history: Chemical Geology, v. 120, no. 3, p. 255-273.

Paliulionyte, V., Meisel, T., Ramminger, P., and Kettisch, P., 2006, High Pressure Asher Digestion and an Isotope Dilution-ICP-MS Method for the Determination of Platinum-Group Element Concentrations in Chromitite Reference Materials CHR-Bkg, GAN Pt-1 and HHH: Geostandards and Geoanalytical Research, v. 30, no. 2, p. 87-96.

Palme, H., and O'Neill, H. S. C., 2003, Cosmochemical estimates of mantle composition: Treatise on geochemistry, v. 2, p. 568.

Pearson, D., and Woodland, S., 2000a, Solvent extraction/anion exchange separation and determination of PGEs (Os, Ir, Pt, Pd, Ru) and Re–Os isotopes in geological samples by isotope dilution ICP-MS: Chemical Geology, v. 165, no. 1, p. 87-107.

Pearson, D. G., Irvine, G. J., Ionov, D. A., Boyd, F. R., and Dreibus, G. E., 2004, Re–Os isotope systematics and platinum group element fractionation during mantle melt extraction: a study of massif and xenolith peridotite suites: Chemical Geology, v. 208, no. 1, p. 29-59.

Pearson, D. G., and Woodland, S. J., 2000b, Solvent extraction/anion exchange separation and determination of PGEs (Os, Ir, Pt, Pd, Ru) and Re–Os isotopes in geological samples by isotope dilution ICP-MS: Chemical Geology, v. 165, no. 1–2, p. 87-107.

Perkins, D., and Anthony, E. Y., 2011, The evolution of spinel lherzolite xenoliths and the nature of the mantle at Kilbourne Hole, New Mexico: Contributions to Mineralogy and Petrology, v. 162, no. 6, p. 1139-1157.

Potts, P. J., Gowing, C. J. B., and Govindaraju, K., 1992, PREPARATION, HOMOGENEITY EVALUATION AND COOPERATIVE STUDY OF TWO NEW CHROMITITE REFERENCE SAMPLES CHR-PT+ AND CHR-BKG: Geostandards Newsletter, v. 16, no. 1, p. 81-108.

Reid, J. B., and Woods, G. A., 1978, Oceanic mantle beneath the southern Rio Grande rift: Earth and Planetary Science Letters, v. 41, no. 3, p. 303-316.

Reisberg, L., Dauphas, N., Luguet, A., Pearson, D., Gallino, R., and Zimmermann, C., 2009, Nucleosynthetic osmium isotope anomalies in acid leachates of the Murchison meteorite: Earth and Planetary Science Letters, v. 277, no. 3, p. 334-344.

Righter, K., 2003, Metal-Silicate Partitioning of Siderophile Elements and Core Formation in the Early Earth*: Annual Review of Earth and Planetary Sciences, v. 31, no. 1, p. 135-174.

Righter, K., Humayun, M., and Danielson, L., 2008, Partitioning of palladium at high pressures and temperatures during core formation: Nature Geoscience, v. 1, no. 5, p. 321-323.

Rollinson, H., 2007, Recognising early Archaean mantle: a reappraisal: Contributions to Mineralogy and Petrology, v. 154, no. 3, p. 241-252.

Roy-Barman, M., and Allègre, C. J., 1995, $^{187}Os/^{186}Os$ in oceanic island basalts: tracing oceanic crust recycling in the mantle: Earth and Planetary Science Letters, v. 129, no. 1, p. 145-161.

Rubin, A. E., Wang, D., Kallemeyn, G. W., and Wasson, J. T., 1988, The Ningqiang meteorite: Classification and petrology of an anomalous CV chondrite: Meteoritics, v. 23, no. 1, p. 13-23.

Savage, P. S., and Moynier, F., 2013, Silicon isotopic variation in enstatite meteorites: Clues to their origin and Earth-forming material: Earth and Planetary Science Letters, v. 361, p. 487-496.Schiano, P., and Clocchiatti, R., 1994, Worldwide occurrence of silica-rich melts in sub-continental and sub-oceanic mantle minerals: Nature, v. 368, no. 6472, p. 621-624.

Schoenberg, R., and von Blanckenburg, F., 2006, Modes of planetary-scale Fe isotope fractionation: Earth and Planetary Science Letters, v. 252, no. 3, p. 342-359.

Seitz, H.-M., Brey, G. P., Zipfel, J., Ott, U., Weyer, S., Durali, S., and Weinbruch, S., 2007, Lithium isotope composition of ordinary and carbonaceous chondrites, and differentiated planetary bodies: bulk solar system and solar reservoirs: Earth and Planetary Science Letters, v. 260, no. 3, p. 582-596.

Shahar, A., Hillgren, V. J., Young, E. D., Fei, Y., Macris, C. A., and Deng, L., 2011, High-temperature Si isotope fractionation between iron metal and silicate: Geochimica et Cosmochimica Acta, v. 75, no. 23, p. 7688-7697.

Shahar, A., Ziegler, K., Young, E. D., Ricolleau, A., Schauble, E. A., and Fei, Y., 2009, Experimentally determined Si isotope fractionation between silicate and Fe metal and implications for Earth's core

formation: Earth and Planetary Science Letters, v. 288, no. 1, p. 228-234.

Shen, J., Papanastassiou, D., and Wasserburg, G., 1998, Re-Os systematics in pallasite and mesosiderite metal: Geochimica et cosmochimica acta, v. 62, no. 15, p. 2715-2723.

Szilas, K., Kelemen, P. B., and Rosing, M. T., 2015, The petrogenesis of ultramafic rocks in the> 3.7 Ga Isua supracrustal belt, southern West Greenland: Geochemical evidence for two distinct magmatic cumulate trends: Gondwana research, v. 28, no. 2, p. 565-580.

Tagle, R., and Berlin, J., 2008, A database of chondrite analyses including platinum group elements, Ni, Co, Au, and Cr: Implications for the identification of chondritic projectiles: Meteoritics & Planetary Science, v. 43, no. 3, p. 541-559.

Thompson, R., Ottley, C., Smith, P., Pearson, D., Dickin, A., Morrison, M., Leat, P., and Gibson, S., 2005, Source of the Quaternary alkalic basalts, picrites and basanites of the Potrillo Volcanic Field, New Mexico, USA: lithosphere or convecting mantle?: Journal of Petrology, v. 46, no. 8, p. 1603-1643.

van Acken, D., Brandon, A. D., and Humayun, M., 2011, High-precision osmium isotopes in enstatite and Rumuruti chondrites: Geochimica et Cosmochimica Acta, v. 75, no. 14, p. 4020-4036.

Walker, R. J., Horan, M. F., Morgan, J. W., Becker, H., Grossman, J. N., and Rubin, A. E., 2002, Comparative

[187]Re-[187]Os systematics of chondrites: Implications regarding early solar system processes: Geochimica et Cosmochimica Acta, v. 66, no. 23, p. 4187-4201.

Walker, R. J., Morgan, J. W., Beary, E. S., Smoliar, M. I., Czamanske, G. K., and Horan, M. F., 1997, Applications of the [190]Pt/[186]Os isotope system to geochemistry and cosmochemistry: Geochimica et Cosmochimica Acta, v. 61, no. 22, p. 4799-4807.

Wang, K., and Jacobsen, S. B., 2016, Potassium isotopic evidence for a high-energy giant impact origin of the Moon: Nature, v. 538, no. 7626, p. 487-490.

Weisberg, M. K., McCoy, T. J., and Krot, A. N., 2006, Systematics and evaluation of meteorite classification: Meteorites and the early solar system II, v. 19.

Willbold, M., Elliott, T., and Moorbath, S., 2011, The tungsten isotopic composition of the Earth/'s mantle before the terminal bombardment: Nature, v. 477, no. 7363, p. 195-198.

Yokoyama, T., Alexander, C. M. D., and Walker, R. J., 2010, Osmium isotope anomalies in chondrites: results for acid residues and related leachates: Earth and Planetary Science Letters, v. 291, no. 1, p. 48-59.

Yokoyama, T., Rai, V. K., Alexander, C. M. D., Lewis, R. S., Carlson, R. W., Shirey, S. B., Thiemens, M. H., and Walker, R. J., 2007, Osmium isotope evidence for uniform distribution of s-and r-process components in the early solar system: Earth and Planetary Science Letters, v. 259, no. 3, p. 567-580.

– CHAPTER 4 –

The Osmium Stable Isotope Compositions

of Magmatic Iron Meteorites

Implications for Planetary Core Evolution

ABSTRACT

Iron meteorites provide us with information on planetary differentiation, core formation and core solidification. This chapter reports the first measurements of the stable osmium (Os) isotope composition of four major magmatic iron meteorite groups; the IIAB (n=5), IIIAB (n=5), IVA (n=2), and IVB (n=3). The different magmatic iron groups are thought to be derived from distinct parent bodies, yielding elemental trends that are broadly consistent with fractional crystallization. However, more complex models are needed to explain the scatter within the trends, involving processes such as late segregation or melt trapping. The extent of these parallel or secondary processes remains poorly constrained. The aim of this project is to better constrain the formation history of the different iron meteorite groups and, ultimately, the planetary cores of their parent body.

The metal fractions of iron meteorites show the largest variation in $\delta^{190/188}Os_{DROsS}$ yet reported in geological materials, with values ranging from +0.05 to +0.49‰. The stable Os isotope compositions of IIAB irons are in general heavier ($\delta^{190/188}Os$ = 0.21-0.49‰), compared to the IIIAB ($\delta^{190/188}Os$ = 0.05-0.38‰), IVA ($\delta^{190/188}Os$ = 0.15-0.20‰), and IVB groups ($\delta^{190/188}Os$ = 0.08-0.13‰). Irons of the IIAB and IIIAB show significant deviations from the chondritic range, with the IIIAB irons showing both supra- and sub-chondritic values. Mass-independent isotope anomalies cannot account for the observed variations which indicates that mass-dependent stable Os isotope fractionation has taken place.

The IIAB and IIIAB groups preserve resolvable isotope compositions within group, indicating that metal-silicate segregation was not the dominant process controlling fractionation. The observation that individual groups do not show a systematic relation between $\delta^{190/188}Os$ and Os concentration indicates that fractional crystallization alone cannot explain the observed variation either. Simple mass balance calculations show that the partitioning of Os into non-metal phases is too low to be a significant source of mass-dependent Os isotope fractionation. Instead, it is clear that certain IIAB and IIIAB irons require a more complex history than simple fractional crystallization of a metallic liquid, which is in accord with previous studies. By constructing fractional crystallization models combined with mixing models it is shown that some IIAB irons require mixing in of either late segregated material or of an evolved melt with an early crystallized solid. This shows that the IIAB iron meteorite group witnessed a more complex history then generally thought. For the IIIAB irons it becomes clear that mixing of an early crystallized solid with a more evolved liquid needs to have occurred. Furthermore, the stable Os isotope fractionation factors estimated from these models are negatively correlated with initial S contents. This suggests that sulphur (S) plays a role in controlling the degree of isotope fractionation, potentially providing a new tool by which to determine the initial S content of the parent body.

CONTENT CHAPTER 4

1. INTRODUCTION

Iron meteorites are believed to sample the metallic cores of planetary bodies and provide us with the closest analogue to materials that comprise Earth's core. As such, they have been extensively studied to understand the processes associated with planetary differentiation and core evolution. Iron meteorites can be divided in two groups, "magmatic" and "non-magmatic" iron meteorites. In this study, magmatic iron meteorites are examined, which exhibit elemental trends that are generally consistent with fractional crystallization of a central metallic core of an asteroid-sized parent body (e.g., Wasson, 1967; Scott, 1972; Scott and Wasson, 1975). A closer look at the elemental trends reveals that simple fractional crystallisation models are not able to explain the observed scatter, suggesting that other processes must have occurred. More complex models have been suggested that include processes as melt trapping (**Figure 4-1**; e.g., Wasson, 1999; Wasson et al., 2007), liquid immiscibility (e.g., Ulff-Møller, 1998; Chabot and Drake, 2000; Corgne et al., 2008), or mixing (e.g., Esbensen et al., 1982; Haack and Scott, 1993; Chabot and

Figure 4-1 Elemental trend of log[Ir] vs log[Au] for IIAB iron meteorites, after Wasson et al. (2007). The solid lines indicate the estimated solid trend (blue) and liquid trend (red) in case of simple fractional crystallization. The green diamonds represent sample compositions. Wasson et al. (2007) explain their offset from the fractional crystallization trend by trapping of various amounts of melt. The amount can be estimated by the crosses, 5% between each cross, at 0%, 30%, 43% and 49% of crystallization.

Drake, 1999; Cook et al., 2004). The extent of these processes is, however, still a subject of much debate.

Different bonding environments and oxidation states of metal liquid, metal solid, and non-metal phases, as well as the occurrence of sub-solidus diffusion provide ideal circumstances for mass-dependent isotope fractionation. With the development of new methods for detecting stable isotope variation, these systems have provided a new means by which to examine processes associated with core solidification (e.g., Poitrasson et al., 2005; Weyer et al., 2005; Williams et al., 2006; Cook et al., 2007; Williams and Archer, 2011; Bridgestock et al., 2014). Deciphering the nature and extent of fractionation can, however, be complex when a number of processes are in play (e.g., Chernonozhkin et al., 2016). The possibility of both kinetic and equilibrium fractionation, with the potential of counteracting fractionation, may further complicate the story (e.g., Williams and Archer, 2011). While isotope variability may be linked to specific processes, the dependency of isotope fractionation on factors such as temperature also allows us to place quantitative constraints on these parameters. Another objective in examining the Os stable isotope systematics of iron meteorites is to assess genetic links between these and other meteorite groups, such as chondrites or achondrites.

Highly siderophile elements (HSE), including Os, are of particular interest for deciphering core formation and solidification processes due to the affinity of these elements for metallic iron. During core

crystallization, the partitioning of HSE into the solid core relative to the residual molten liquid, is strongly controlled by the elemental composition of the evolving liquid, particularly the S and phosphorous (P) contents (e.g., Jana and Walker, 1997; Fleet et al., 1999; Chabot et al., 2003; Chabot and Jones, 2003; Chabot and Haack, 2006; Corgne et al., 2008). Osmium becomes increasingly compatible with progressive crystallization due to the increase of S and P concentrations in the residual liquid. The partitioning behaviour of Re and Pt is slightly different, resulting in fractionation of Os from Re and Pt during fractional crystallization (Pernicka and Wasson, 1987; Morgan et al., 1992). Consequently, the Re-Os and Pt-Os decay systems provide key information for reconstructing the timing of core crystallisation (e.g., Herr et al., 1961; Hirt et al., 1963; Luck et al., 1980; Morgan et al., 1995; Walker et al., 1997; Cook et al., 2004). Isochrons for the magmatic iron groups examined in this study, i.e., IIAB, IIIAB, IVA and IVB, indicate that the Os isotope system remained closed after their formation (IIAB and IIIAB - Cook et al., 2004; IVA – McCoy et al., 2011; IVB - Walker et al., 2008). Any variation in stable Os isotope composition should, therefore, result from core formation and crystallization, and should not have been modified by secondary processes operating in the solar nebula. Another useful characteristic of Os is that, due to its strong partitioning into solid metal relative to liquid metal, late crystallizing liquids are likely to be, relatively, very low in Os. This makes Os a sensitive tracer for detecting processes that occur in parallel with fractional crystallization, such as mixing or late segregation (e.g., Cook et al., 2004). Furthermore, non-metal phases exhibit substantially lower abundances of Os relative to metal phases (Shen et al., 1996), and thus their formation will only have a very limited effect on the Os isotope systematics in the metal.

A potential complication that arises when considering stable Os isotopic variation is the presence of mass-independent isotopic Os anomalies in iron meteorites (Huang and Humayun, 2008; Walker, 2012; Wittig et al., 2013). These anomalies result from cosmic ray irradiation with neutron capture on ^{189}Os leading to the production of ^{190}Os. This process has the potential to obscure the signature created by mass-dependent fractionation processes and requires consideration. However, in contrast to W, Ru, and Mo, nucleosynthetic anomalies have not been detected for Os isotopes in iron meteorites (Wittig et al., 2013), therefore, this process is unlikely to have a major effect.

This study reports, for the first time, the stable Os isotope composition of iron meteorites (n=15) from four of the largest magmatic groups: IIAB, IIIAB, IVA and IVB. Each group is thought to represent a distinct parent body, where division is based on variations in their major and trace element concentrations (e.g., Haack and McCoy, 2003). Samples were selected to cover a wide range of chemical compositions, which allows us to explore the effect of fractional crystallization on the stable Os isotope signature. The application of this data to simple fractional crystallization-mixing models is then undertaken to re-examine previously proposed crystallization models for iron meteorites.

2. SAMPLE DESCRIPTION

2.1 GENERAL BACKGROUND

Iron meteorites are predominantly composed of Fe-Ni alloys (**Figure 4-2a**), with kamacite and taenite being the main phases. Taenite forms at high temperatures with the exsolution of kamacite from, and at the expense of, taenite during cooling of the parent body (e.g., Yang et al., 1996). The interlocking of these two mineral phases is known as the "Widmanstätten pattern" (**Figure 4-2a**). This textural pattern has been used to classify iron meteorites into (a) hexahedrites (>2 mm), (b) octahedrites (0.05 – 2 mm), (c) ataxites (<0.05 mm) (Buchwald, 1975). Several parameters, such as Ni and P contents, and the cooling rate, control the texture and relative proportions of the Fe-Ni alloys that are formed (e.g., Dean and Goldstein, 1986; Yang et al., 1996). The growth of kamacite from taenite is diffusion limited. It has been shown to result in compositional gradients and stable isotope fractionation which have been used to constrain cooling rates (e.g., Wood, 1964; Rasmussen et al., 1988; Weyer et al., 2005; Yang and Goldstein, 2006; Cook et al., 2007; Dauphas, 2007). The presence of other phases in iron meteorites is, predominantly, dependent on the abundance of minor elements in the parent body, including Co, P, S, C. Most common are troilite (FeS) and schreibersite ($[Fe,Ni]_3P$; **Figure 4-2b**), which are thought to reflect the presence of residual, trapped melt (e.g., Wasson, 1999). Recent reviews on iron meteorites are provided by Chabot and Haack (2006), McCoy et al. (2006), Goldstein et al. (2009b), and Benedix et al. (2014).

2.2 IIAB

Group IIAB iron meteorites are the second largest magmatic iron group (~103 members). They contain the lowest Ni concentration (5.3 – 6.6 wt. % Ni) of any iron meteorite group and display a very large range in Ir (**Figure 4-3**; Wasson et al., 2007). Elemental trends are generally consistent with simple fractional crystallization, but are thought to be better explained in combination with equilibrium melt trapping (Wasson et al., 2007). The metal phase consists predominantly of kamacite, with structures ranging from hexahedrite to the coarsest octahedrites. The low Ni content, combined with the absence of phosphates and occurrence of graphite (Buchwald, 1975; 1984), indicates that IIAB iron meteorites were formed from highly reduced material. Of the examined iron groups, estimates of the initial non-metal content are the highest (~17 wt. % S; Chabot and Drake, 2000). At such high levels, it has been shown that liquid immiscibility of a P-rich and a S-rich

Figure 4-2 (a) Iron meteorite hand specimen showing a Widmanstätten pattern. Source: Toby Smith. **(b)** Iron meteorite Santa Luzia (IIIAB) including troilite (elongated nodules) and schreibersite (skeletal inclusions). Source: Wasson et al. (2007).

liquid takes place (Ulff-Møller, 1998; Chabot and Drake, 2000), although conclusive evidence has yet been found to support this hypothesis. Application of the Re-Os and Pt-Os decay systems have put the time of crystallization at 4530 ± 50 Ma and 4323 ± 80 Ma, respectively (Cook et al., 2004). The discrepancy between the two decay systems has been attributed to the uncertainty in the decay constant for ^{190}Pt. Cooling rates are low (0.8-10°C Myr^{-1}; Randich and Goldstein, 1978), although Goldstein et al. (2009a) suggested that these cooling rates should be re-investigated on the basis of significant variations in the quality of the available data.

For this study, I have analysed 5 IIAB irons: Coahuila, Gressk, Mount Joy, Navajo, and North Chile. Sikhote-Alin was also digested and chemically processed, but the signal intensity obtained was not sufficient to yield any meaningful data. Samples represent different parts of the Ni-Ir elemental trend with concentrations ranging between 55 and 60 mg/g for Ni, and between 24 and 16,100 ppb Ir (**Figure 4-3**).

2.3 IIIAB

With over 200 members, the IIIAB irons compose the largest group. All IIIAB irons are classified as medium octahedrites with Ni abundances ranging between ~7.1 and 10.5 wt.% (e.g., Scott and Wasson, 1975; Cook et al., 2004). They contain the highest abundance of phosphates which suggests that the parent body was formed from relatively oxidized material (Olsen and Fredriksson, 1966; Kracher et al., 1977; Olsen et al., 1999). The initial bulk S content has been estimated at 12 wt. % (Chabot and Drake, 2000). The crystallization history is more complex than reported for IIAB irons. This is reflected in large compositional variations, especially for iron meteorites that are associated with the Cape York fall (e.g., Esbensen et al., 1982). The observed variation has
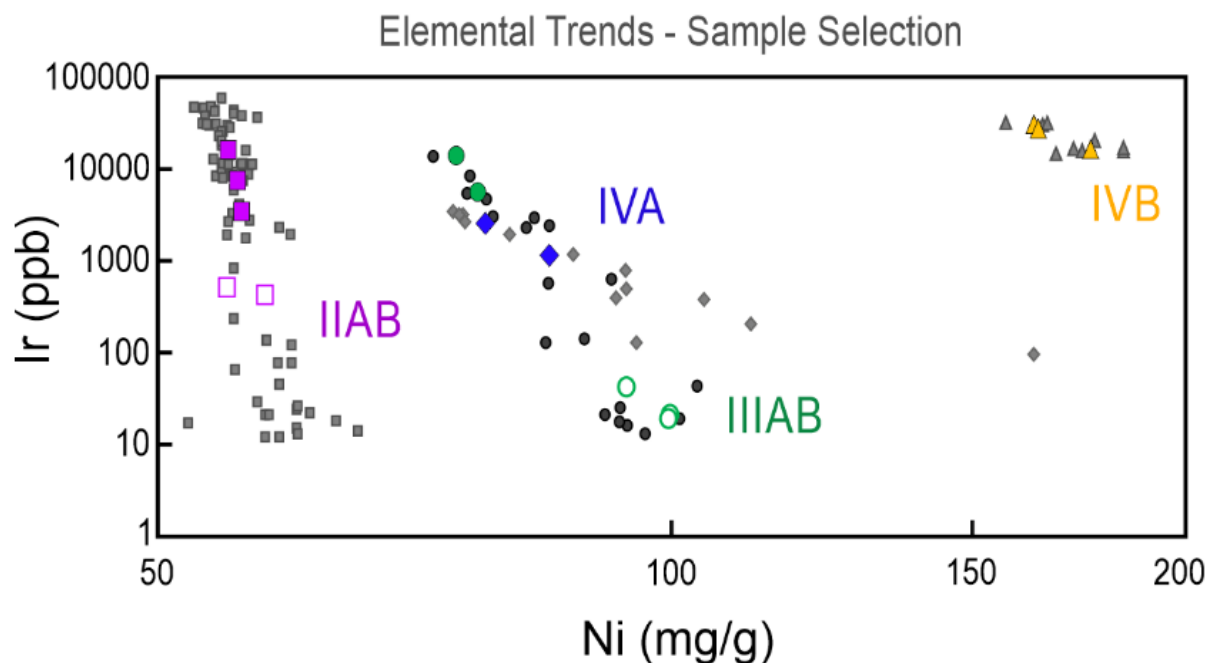
Figure 4-3 Logarithmic plots of Ir vs Ni plot for IIAB, IIIAB, IVA, IVB iron meteorites. Indicated in colour are the samples analysed in this study. Data is obtained from Wasson et al. (2007) – IIAB; Wasson (1999) – IIIAB; McCoy et al. (2011) – IVA; Walker et al. (2008) – IVB.

been attributed to mixing (Esbensen et al., 1982; Haack and Scott, 1993; Chabot and Drake, 1999; Cook et al., 2004) or equilibrium melt trapping (Wasson, 1999). Metallographic cooling rates are variable and range from 56 to 338°C Myr^{-1} (Yang and Goldstein, 2006). Most recent Re-Os and Pt-Os isotope data show that the isotopic system has been closed after its formation and constrain an age of 4517 ± 32 Ma and 4325 ± 26 Ma, respectively (Cook et al., 2004). This is unresolvable from ages determined for the IIAB group.

For this study, 5 IIIAB iron meteorites were investigated; Bear Creek, Cape York, Costilla Peak, Chupaderos, and Grant. Samples were selected to represent different stages of crystallization, with Ni and Ir concentrations of 75 - 100 mg/g and 19 - 14,000 ppb, respectively (**Figure 4-3**).

2.4 IVA

The IVA irons are a group of ~70 fine octahedrites, the third largest group, with nickel concentrations varying from ~7.5 to 12.4 wt.% (Buchwald, 1975; Wasson and Richardson, 2001). They are characterised by low volatile concentrations at moderate Ni contents. Estimates of the initial S content of the parent body are highly variable with values ranging from 0.5 to 9 wt.% S (Chabot and Drake, 2000; Wasson and Richardson, 2001; McCoy et al., 2011). Various models have been proposed to explain the chemical history but there are substantial difficulties in accounting for all the observed elemental trends (e.g., Wasson and Richardson, 2001). Another complicated feature of the IVA group is the large variation in cooling rate (100–6600°K Myr^{-1}; Rasmussen et al., 1995; Yang et al., 2008). In general, this has been explained by an impact event at high temperatures (e.g., Haack et al., 1996; Yang et al., 2008; McCoy et al., 2011). High precision Re-Os isotopic data reported by McCoy et al. (2011) show an age of 4540 ± 17 Ma that has led to the conclusion that the HSE systematics remained a closed system after core formation.

For this study, 2 IVA iron meteorites have been examined; Gibeon and Muonionalusta. They contain Ni concentrations of 78 and 85 ng/g, and Ir concentrations of 2,560 and 1,146 ppb, respectively (**Figure 4-3**).

2.5 IVB

The IVB group consists, currently, of only 12 members with high Ni contents of ~16-18 wt.%. They are structurally classified as ataxites meaning there is no intergrowth of taenite and kamacite (Scott, 1972; Campbell and Humayun, 2005). Relative to the IVA irons they are even more depleted in volatiles, including S (0 - 2 wt.%; e.g., Willis and Goldstein, 1982; Chabot and Drake, 2000; Chabot, 2004; Walker et al., 2008), and possess high contents of refractory elements (e.g., Scott, 1972; Rasmussen et al., 1984; Smoliar et al., 1996; Walker et al., 2008). This observation led some researchers to conclude that these irons originated from non-chondritic material with fractionation caused by a high temperature condensation processes (e.g., Kelly and Larimer, 1977; Campbell and Humayun, 2005; Walker et al., 2008). The elemental variation within the IVB group is consistent with simple fractional crystallization models (e.g., Walker et al., 2008). Projected initial sub-chondritic Re/Os and Pt/Os ratios do, however, remain unexplained. Metallographic cooling rates were highly

variable ranging between 475 and 5000°K Myr^{-1} with a corresponding parent body core radius of 70 ± 15 km (Yang et al., 2010). The Re-Os systematics provide a crystallization age of 4579 ± 34 Ma and indicate closed system behaviour since crystallization (Smoliar et al., 1996; Walker et al., 2008).

In this study, 3 IVB iron meteorites were examined; Hoba, Tlacotepec, and Weaver Mountains. Tlacotepec and Hoba ([Ni] = 163 and 164 mg/g; [Ir] = 30,800 and 27,600 ppb; respectively) are thought to represent earlier crystalized metals relative to Weaver Mountains ([Ni] = 176 mg/g; [Ir] = 16,500 ppb; **Figure 4-3**).

3. METHODS

3.1 SAMPLE PREPARATION and CHEMICAL PROCESSING

Iron meteorites were provided by the Field Museum of Chicago as slices or fragments of 0.5 – 1.4 gram in weight. Fragments of Gibeon and Muonionalusta also taken from the personal collection of Kevin Burton. Samples were cut to the desired quantity using a dremel corundite .025" blade, using a separate blade for each sample to avoid cross-contamination. Subsequently, all edges were manually cleaned by polishing with silicon carbide and then leached at room temperature for ~30 min in 0.5 M HCl to remove any residual surface contamination. After leaching, samples were rinsed three times with MQ water, three times with ethanol, and finally dried in air at room temperature.

Fe-Ni metal from iron meteorites can be digested with addition of HCl and HNO_3. There is, therefore, no need for use of the HPA asher, and the Carius tube technique was used instead (Shirey and Walker, 1995). Tubes of 30 mL or 45 mL in size were used, with the addition of 6 mL conc. HNO_3 and 3 mL conc. HCl. Dissolution and equilibration between spike and sample was achieved at 220°C over a 64- to 88 h period. The amount of sample material digested weighed between 0.06 gram and 0.89 gram. The quantity of double spike added, was determined based on literature Os concentration data. Apart from one sample, IIIAB iron Henbury which turned out to be significantly underspiked (83 % sample material instead of the desired 45 %), all other sample analyses showed a sample proportion between 44 % and 64 %. This is well within the range that is shown to provide reliable stable Os isotope data (15 % - 81 %; Ch.2 – section 2.1), with expected errors of <0.02‰ amu^{-1} when signal intensities for the most abundant isotope are >6 V at ideal MC-ICP-MS conditions.

After sample digestion, the Os was recovered following the same procedure as for chondrites and terrestrial mantle samples, which is described in detail in Ch.2 – section 3. In short, from the reverse aqua regia solution, the Os was extracted via solvent extraction using CCl_4 (Cohen and Waters, 1996), back-extracted into HBr (Cohen and Waters, 1996; Birck et al., 1997), and finally purified via micro-distillation (Roy-Barman, 1993). After micro-distillation, the Os fraction was either transferred into an HCl solution for analysis by MC-ICP-MS or dried down to a sample solution of ~1 µL prior to loading on a Pt-filament for N-TIMS analysis.

3.2 MASS SPECTROMETRY

Osmium isotope analyses of the iron meteorites highly concentrated in Os were conducted using a Neptune MC-ICP-MS whereas samples with an Os concentration of <200 ng total Os were analysed on a Triton Plus N-TIMS. All analyses were performed at Durham University following the procedure as described in Chapter 2 of this thesis.

Analyses by MC-ICP-MS yielded total beam intensity, in general, between 8 V and 30 V with a ^{188}Os signal of 3 V and 10 V, respectively. Two analyses fall outside this range with a ^{total}Os beam of 3 V and 83 V. Apart from the analyses at 3 V, all masses of the OPZ measurements displayed signal intensities of less than 0.03 % (<0.001 mV) relative to the peak Os signal in the main run (^{188}Os). Interference beam intensities for W, Re and Pt have been monitored and are all below 0.003% of the ^{total}Os concentration. Such levels of memory effect and isobaric interferences have been shown to impart an insignificant effect on the Os isotopic ratios (Ch2 - section 4.1.2.1 and 4.1.2.2).

Analyses by N-TIMS yielded a total Os beam intensities between 0.3 V and 3.4 V, with a corresponding mean ^{188}OsO$_3^-$ beam of 0.1 V and 1.2 V, respectively. The signals obtained on mass 234 (predominantly ^{186}OsO$_3^-$) and mass 235 (predominantly ^{187}OsO$_3^-$) varied between 2 mV and 30 mV. For the oxygen correction, the ^{18}O/^{16}O ratios are determined within run, for each individual cycle, and the ^{17}O/^{16}O was inferred from the measured ^{18}O/^{16}O. The ^{18}O/^{16}O ratio varied between 0.002008 and 0.002076, with corresponding ^{17}O/^{16}O isotope compositions of 0.000383 and 0.000389. This is close to the range that is observed for repeated analyses of DROsS with a total Os beam signal of >1 V. Although care must be taken for analyses obtained at <1 V, the oxygen compositions suggest that little inaccuracy was introduced as a result of the oxygen composition. Poly-atomic interferences were collected prior to and after the main run. Intensities ranged between 1,272 cps and 540,525 cps on mass 228, mass 230 recorded 586 cps to 154,728 cps, on mass 231 between 5 cps and 224 cps were collected, and mass 233 yielded levels between 6 cps and 53 cps. These intensities are all within the range reported for the reference standard DROsS (Ch2 – section 4.2.2.2) for which it was concluded that they have no measurable effect on the stable Os or ^{186}Os/^{188}Os isotope compositions. The maximal potential interference on ^{187}OsO$_3^-$ was 143 cps or 2.3 µV, which can also be considered negligible.

To monitor the quality of the chemical procedure and mass spectrometry measurements, DROsS standards were incorporated in the various different batches of digestion and were processed and measured simultaneously with the samples. Furthermore, a stock DROsS solution was included within every loading sequence. All DROsS analyses display values within uncertainty of one another and yield a long-term reproducibility of 0.02‰ on δ^{190}Os for MC-ICP-MS and 0.02‰ by N-TIMS (**Figure 4-6**). This corresponds with findings reported in Chapter 2.

Table 4-1 Osmium isotope and concentration results for IIAB, IIIAB, IVA and IVB iron meteorites.

Sample Name	Instrument		Sample Weight (g)	$\delta^{190/188}$Os (‰)	2 se	^{187}Os/^{188}Os	2 se	^{186}Os/^{188}Os	2 se	[Os] ng g^{-1}	2 se
IIAB											
Coahuila	MC-ICP-MS	h	0.170	0.39	0.01	0.141672	0.000007	0.119769	0.000005	10303	9
Gressk*	MC-ICP-MS	h	0.225	0.49	0.01	0.153126	0.000113	0.119859	0.000119	3459	5
Mount Joy	N-TIMS	og	0.085	0.42	0.04	0.156727	0.000041	0.120423	0.000043	130	80
replicate	N-TIMS		0.111	0.37	0.03	0.156824	0.000021	0.120461	0.000021	151	62
Navajo*	N-TIMS	og	0.204	0.21	0.04	0.157004	0.000051	0.120286	0.000056	182	30
replicate*	N-TIMS		0.099	0.21	0.02	0.156963	0.000017	0.120364	0.000018	186	52
North Chile	MC-ICP-MS	h	0.380	0.39	0.02	0.169492	0.000010	0.119928	0.000011	1047	4
IIIAB											
Bear Creek	N-TIMS	om	0.852	0.05	0.05	0.135974	0.000066	0.120881	0.000066	12	7
Cape York*	MC-ICP-MS	om	0.372	0.38	0.01	0.135113	0.000005	0.119810	0.000004	4380	3
Chupaderos	N-TIMS	om	0.892	0.13	0.09	0.140027	0.000113	0.120519	0.000105	13	7
Costilla Peak*	MC-ICP-MS	om	0.137	0.05	0.01	0.124473	0.000005	0.119761	0.000004	18354	421
Grant*	N-TIMS	om	0.726	0.08	0.04	0.139555	0.000049	0.120519	0.000048	25	6
IVA											
Gibeon 1#	MC-ICP-MS	om	0.309	0.15	0.02	0.132215	0.000024	0.119996	0.000032	2657	5
Gibeon 2#a*	MC-ICP-MS		0.378	0.19	0.01	0.132170	0.000006	0.119799	0.000003	2820	3
Gibeon 2#b	N-TIMS		" "	0.20	0.02	0.132162	0.000013	0.119816	0.000017	2820	4
average 2#*	both		-	0.19	0.01	0.132169	0.000005	0.119799	0.000037	2820	2
Muonionalusta	MC-ICP-MS	of	0.125	0.18	0.01	0.135440	0.000010	0.119814	0.000006	1603	9
IVB											
Hoba	MC-ICP-MS	a	0.062	0.09	0.01	0.121992	0.000006	0.119763	0.000005	44364	28
Tlacotepec*	MC-ICP-MS	a	0.082	0.13	0.01	0.120942	0.000005	0.119811	0.000210	47600	800
Weaver Mountains	MC-ICP-MS	a	0.061	0.08	0.02	0.126032	0.000006	0.119814	0.000006	18867	27

h – hexahedrites (>2mm), og - coarse octahedrites (1.2 – 2 mm), om - medium octahedrites (0.5 – 1.2 mm), of - fine octahedrites (0.05 – 0.5 mm), a –ataxites (<0.05 mm) (Buchwald (1975). * - indicates sample solution that were measured twice. For these samples the weighted average and ±95% c.i. are provided, which were obtained using Isoplot.

4. RESULTS

Osmium stable isotope compositions along with radiogenic isotopic and concentration data for 5 IIAB, 5 IIIAB, 2 IVA, and 3 IVB magmatic iron meteorites are presented in **Error! Reference source not found.** and shown in **Figure 4-6** and **Figure 4-6**. Corresponding uncertainties are expressed as 2 standard errors (2 se) on the individual analyses or, in cases where the same sample solution was measured twice, it represents the 95% c.i. on the weighted average of the measurements, which was obtained using Isoplot. Appendix 4-A reports all the data that has been used for comparison of this study with previous studies.

Osmium concentrations for the IIAB, IIIAB, IVA, and IVB groups are highly variable, ranging from 130 ppb to 10,303 ppb, from 12 ppb to 18,364 ppb, from 1,603 ppb to 2,820 ppb, and from 18,867 ppb to 47,600 ppb, respectively. The data obtained are in good agreement with literature data (**Figure 4-6c**; e.g., Morgan et al., 1995; Smoliar et al., 1996; Cook et al., 2004). With the exception of Chupaderos (13%) and Muonionalusta
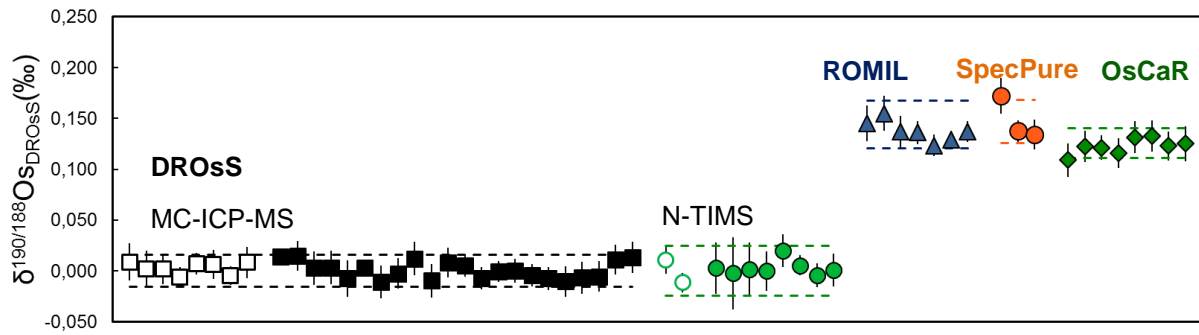
Figure 4-6 Stable isotope compositions of reference standard DROsS, and reference solutions ROMIL, SpecPure, and OsCaR run during the course of this study. Of note, these analyses are different from those reported in Chapter 2. All values are consistent with the reproducibility of these materials as reported in Chapter 2, which is shown here by the dashed lines. Open symbols represent external processed materials and closed symbols data obtained by analysis of a stock solution. Error bars represent the ±2 se on an individual analysis.
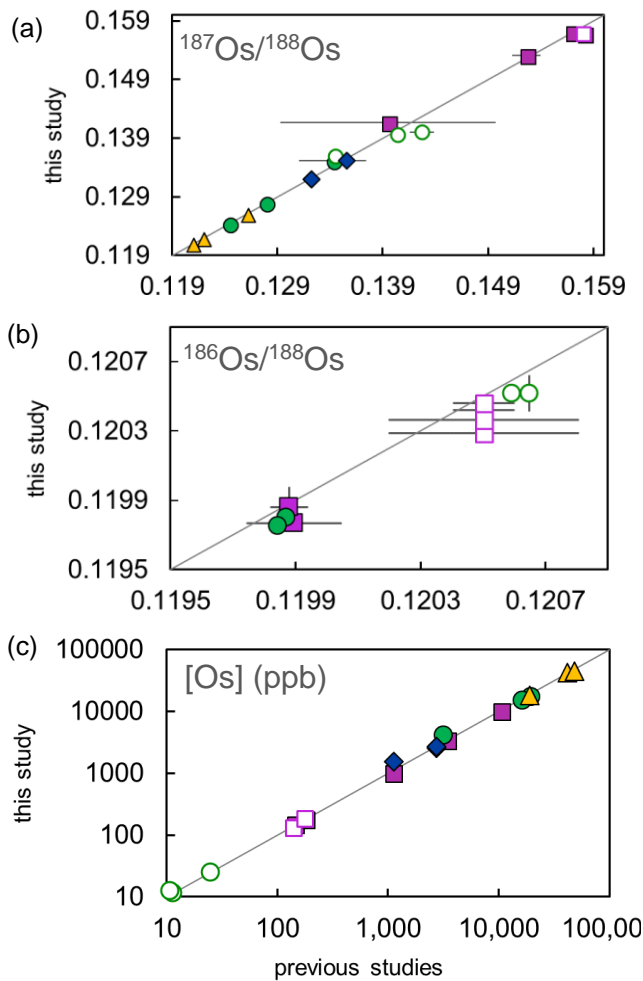
Figure 4-6 Comparison of the (a, b) radiogenic isotope ratios and (c) concentration of this study with previous studies. The dotted line is the regression line through the data points, and the solid line is a 1:1 line. Error bars represent the ±2 se for data of this study and the ±2 sd on the average of published data. Literature sources can be found in Appendix 4-A. Symbols as in Figure 4-5.
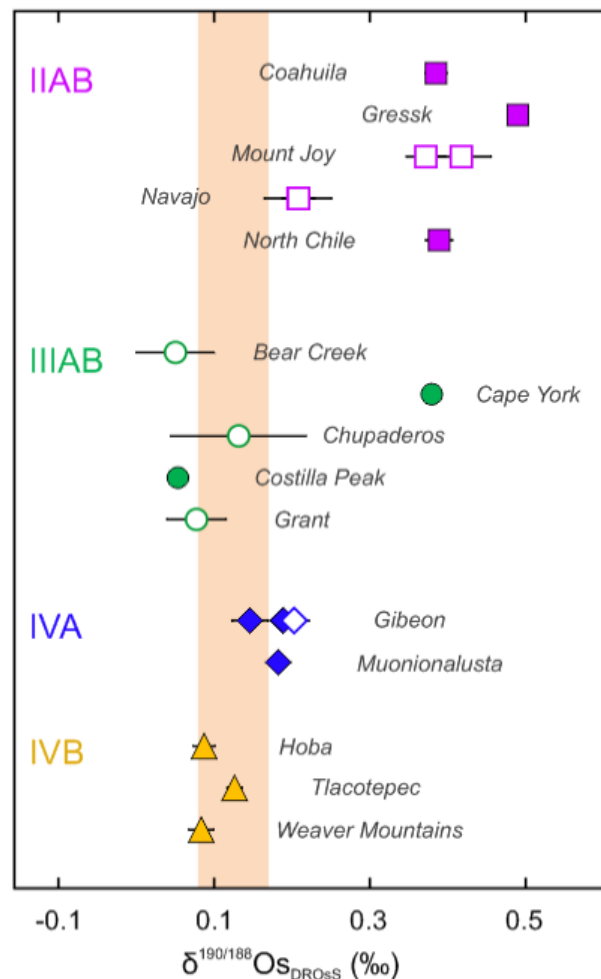
Figure 4-6 Osmium stable isotope data for the metal fraction of IIAB, IIIAB, IVA, and IVB iron meteorites. Error bars represent the ±2 se on the individual analysis or, in case the same sample solution was measured twice, it represents the ±95% c.i. on the weighted mean. The orange band indicates the average $\delta^{190}Os$ ±2 sd of chondrites as determined in Chapter 3. Open symbols indicate analyses by MC-ICP-MS and represent early crystallized solids. Closed symbols were measured by N-TIMS, because of their lower Os concentration, and represent late crystallized melts.

(32%), deviations from published values are <6% (Appendix 4-A). Duplicate analyses of Mount Joy, Navajo, and Gibeon display variations of 16%, 2%, and 6%, respectively. The larger variations most likely reflect sample heterogeneity related to either different Os contents in the kamacite and taenite (Mullane et al., 2004) or related to the relative positioning of the metal from a non-metal inclusion (Papanastassiou et al., 1996).

The analysed iron meteorites display $^{187}Os/^{188}Os$ isotope compositions, ranging from 0.12094 to 0.16949, that are in excellent agreement with previously published values (**Figure 4-6a**; e.g., Morgan et al., 1995; Smoliar et al., 1996; Chen et al., 2002; Cook et al., 2004). Differences are typically <0.4%, with the exception of -1.6% shown by Chupaderos (IIIAB) which is most likely related to the higher concentration. The $^{186}Os/^{188}Os$ ratios yield values from 0.119763 to 0.120881. Two previous studies have reported $^{186}Os/^{188}Os$ isotope ratios for iron meteorites (Walker et al., 1997; Cook et al., 2004). Comparison of our data with these studies shows that values are, in general, in good agreement with one another (**Figure 4-6b**).

The stable Os isotope compositions ($\delta^{190/188}Os_{DROsS}$, in the text referred to as $\delta^{190}Os$) of metal fractions from IIAB, IIIAB, IVA and IVB irons range from +0.05‰ (Bear Creek - IIIAB) to +0.49‰ (Gressk - IIAB). Thus far, this is the largest stable isotope variation observed for Os. Metal fractions separated from IIIAB irons display the largest variation, of 0.35‰, within a specific group. Four samples yield sub- and near chondritic values, +0.05-0.13‰, whereas one sample, Cape York, yields a heavier isotope signature of 0.38‰. All irons from group IIAB show supra-chondritic values, between 0.21‰ and 0.49‰. Only two IVA iron meteorites were analysed which define an isotopic composition of 0.15-0.19‰ and 0.18‰. The three IVB irons examined here are all within analytical uncertainty of the chondritic range, 0.08-0.13‰. As only 2 and 3 samples of the IVB and IVA groups were analysed, the within group variation is yet to be examined. No systematic correlation between $\delta^{190}Os$ and Os concentration or radiogenic isotope signature was observed.

For two samples, Mount Joy and Navajo (IIAB irons), two aliquots were taken from the same hand specimen. The $\delta^{190}Os$ of the duplicates differ by 0.05‰ and 0.00‰, respectively, which for both is within the analytical uncertainty on the analyses. Gibeon (IVA) was also sampled twice, although cuts were taken from different hand specimens (i.e., pieces from different collections). The aliquots show a resolvable difference in $\delta^{190}Os$ of 0.04‰.

5. DISCUSSION

5.1 EFFECT of MASS-INDEPENDENT ISOTOPIC SIGNATURE

The presence of mass-independent Os isotopic anomalies has the potential to introduce an inaccuracy into the stable isotope compositions. This is because the double spike technique assumes that the isotopic difference between sample and standard is purely mass-dependent. Osmium isotopes are shown to be affected by galactic cosmic ray (GCR) irradiation whereas, contrary to Ru, Mo and W, nucleosynthetic anomalies have not been detected (e.g. Walker, 2012; Wittig et al., 2013). For this study, the potential effect of GCR spallation on the mass-dependent signature of Os has been examined by using the data of Wittig et al. (2013). The cosmogenic isotopic anomalies determined for various samples were implemented using a pure reference

standard composition. Subsequently, these compositions were put through a DS calculation revealing the change in isotope composition. Results are displayed in **Figure 4-7** and show that the presence of cosmogenic anomalies causes the δ^{190}Os to be shifted to lower values. The largest anomaly yet observed for iron meteorites is Tlacotepec, which has a negative anomaly in ε^{189}Os of -0.6ε and complementary ε^{190}Os of $+0.4\varepsilon$ (Wittig et al., 2013). This sample would require a correction on δ^{190}Os of $+0.04$‰. This is only slightly greater than the general analytical uncertainty

Figure 4-7 The effect of mass-independent Os isotopic variations (ε^{190}Os) on the stable osmium isotope composition ($\delta^{190/188}$Os). The largest anomaly observed, 0.4ε (Wittig et al., 2013), results in a $\delta^{190/188}$Os that is 0.04 ‰ lower than is actually the case.

($\sim$0.02‰), showing that the presence of mass-independent anomalies imparts a limited effect on mass-dependent stable isotope compositions. In this study, no mass-independent anomaly data has been obtained for the sample materials analysed, and considering that the effect is minimal, no correction has been applied to the reported δ^{190}Os data. An important conclusion to draw from the modelled effect is that it cannot explain the 0.44‰ variation that is observed amongst iron meteorites. Consequently, the variation in δ^{190}Os must have been caused by a mass-dependent fractionation process or processes.

5.2 SOURCE of MASS-DEPENDENT ISOTOPE FRACTIONATION

5.2.1 Metal-Silicate Segregation

The first major differentiation process that a planetary core experiences is during its formation when metal segregates from silicate. Experimental studies have shown that this process can result in stable isotope fractionation (e.g., Shahar et al., 2009; 2011; Hin et al., 2013; Hin et al., 2014). The extent of fractionation decreases as a function of temperature, roughly in proportion to $1/T^2$ (Bigeleisen and Mayer, 1947; Urey, 1947). If core formation was associated with metal-silicate equilibration in a deep magma ocean (e.g., Wood et al., 2006), high pressure and temperature conditions would have prevailed. Under these conditions, stable isotope fractionation is in general limited. Even though the expected variation is small, geochemical analyses of natural rocks have provided evidence for the moderately siderophile element molybdenum (Mo). The silicate portion of planetary bodies, i.e., eucrites, angrites, and shergottites, display heavier isotopic compositions in line with experimental data (Burkhardt et al., 2014). Considering the strong partitioning of Mo into the core, it was considered that it was unlikely to be able to detect a signature of metal-silicate segregation in core material (Hin et al., 2013; Burkhardt et al., 2014). As the metal-silicate partition coefficient for Os is even higher than that of Mo (D=$\sim$10^7 for Earth conditions at 2,773K; Brenan et al., 2005) it follows that the bulk δ^{190}Os composition of planetary cores will display the same composition as bulk chondrites. To illustrate this concept,

the experimental metal silicate Mo stable isotope fractionation factor obtained by Hin et al. (2013) was scaled for Os (**Figure 4-8**). Note that, because of a lack of experimental data for Os, this calculation assumes that the force constants of the bonds in the metal and silicate melts for Os are the same as for Mo. The figure clearly shows that the δ^{190}Os composition of the core cannot be resolved from the chondritic range when partition coefficients are > 2, even if segregation takes place at 1000°C. That metal-silicate differentiation is unlikely to explain the observed variation is also apparent from the observation that the stable isotope composition of IIAB and IIIAB iron

Figure 4-8 The bulk core $\delta^{190/188}$Os vs. metal-silicate partition coefficient (D_{Os}). The hypothetical stable isotope composition of the core at different temperature scenarios, represented by the dashed (1000°C) and dotted (1600°C) lines, is shown to be within analytical uncertainty of the chondritic average if D>2 (orange band – average ± 2 sd). The lines are based on the experimental metal silicate Mo stable isotope fractionation factor as determined by Hin et al. (2013).

meteorites display heavier δ^{190}Os values relative to the chondritic value, as well as showing variation within the group. The possibility cannot be excluded, however, that a signature of metal-silicate segregation has been overprinted by a subsequent event, such as fractional crystallization or inter-mineral sub-solidus diffusion.

If the bulk stable Os isotope composition of a planetary core is indistinguishable from that of chondrites (δ^{190}Os = 0.12 ± 0.05; 2sd), any deviation from this value must be generated by one or several processes occurring during crystallization of the core, assuming that the system was closed after its formation. In the following sections, various processes that are associated with the evolution of iron meteorites are assessed for their potential to cause Os stable isotope variations.

5.2.2 Solid Metal – Liquid Metal Partitioning (Simple Fractional Crystallization)

The main process taking place after core formation is fractional crystallization of the metallic melt. This process is shown to be the dominant control on elemental behaviour and might be an important mechanism of mass-dependent isotope fractionation. Fractionation may result from a kinetic effect during crystallization where lighter isotopes, because of their lower mass, are preferentially incorporated into solids relative to the residual liquid. A difference in bonding environment between the solid and liquid metal phase could be a potential driving force of equilibrium isotopic fractionation. Alfe and Gillan (1998) simulated the formation of a liquid iron- sulphur alloy under Earth's core conditions. They show that the covalent Fe-S bond is considerably stronger than the metallic bonding between Fe atoms, and that the coordination number for Fe-S (~2.8) is
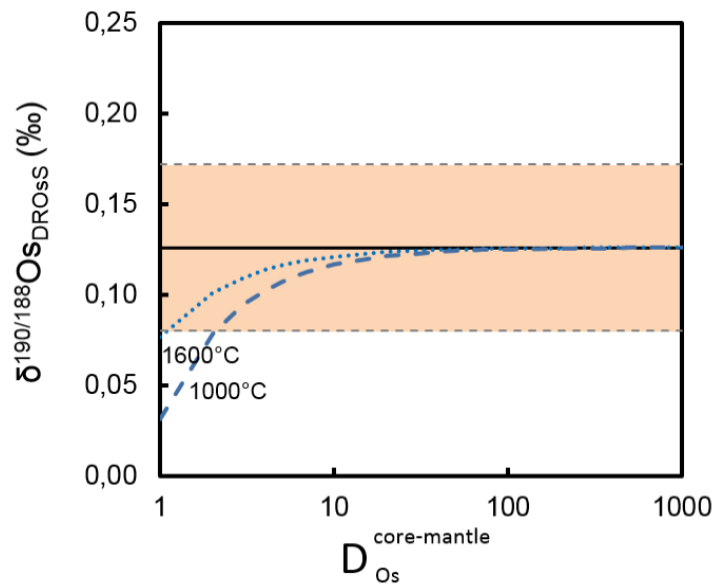
Figure 4-9 The $\delta^{190/188}$Os vs. [Os] (ppb) of (a) IIAB and (b) IIIAB iron meteorites, show no co-variation with Os concentration. The dashed arrow represents a hypothetical trend in case fractional crystallization controls the stable Os isotope composition. Symbols as in Figure 4-5.

lower than that for Fe-Fe (~10.8). The similarity in electronic configuration allows Os to be substituted for Fe (Pepperhoff and Acet, 2001). Osmium is indeed shown to be incorporated into the metallic phase within iron meteorites and to hold a coordination of 11.5 within the metal whereas the bonding of Os-S yields a coordination of 5.6 (Sakakibara et al., 2005). This has important implications when considering stable isotope fractionation as the general behaviour of heavier isotopes is to prefer stronger chemical bonds and a lower coordinated system (Schauble, 2004; Young et al., 2015). Considering that S is highly incompatible with respect to solid metal and thus resides in the liquid, the expectation is that the solidifying metal will preferentially incorporate lighter isotopes leaving the remaining metallic liquid with a heavier isotope composition. With progressive crystallization the melt will evolve to heavier isotopic compositions as is illustrated in **Figure 4-9**.

Recently, it was found that the Ru stable isotope compositions of IIAB, IIIAB, IVB groups are offset from chondrites and correlated with Ru content, with the late-crystallized irons showing a heavy Ru isotopic composition (Hopp et al., 2016). This has been explained by stable isotope fractionation during crystallization of the metallic melt consistent with the prediction outlined above. The Fe and W isotope systematics in IIIAB irons also display isotopic variation in line with fractional crystallization, although no co-variation between $\delta^{57/54}$Fe and Ir was found for IIAB irons and only limited data is available for W (Chernonozhkin et al., 2016 and Fukami et al., 2010, respectively). Ruthenium also displays a non-chondritic stable isotope compositions for IVA and IID iron meteorites, but no correlation with Ru content is observed. This has been related to a more complex formation history (Hopp et al., *pers. comm.*).

Considering that the Os abundance is dominantly controlled by crystallization of the metallic melt, with the Os concentration decreasing with progressive crystallization (e.g., Wasson, 1999), a correlation between Os content and stable isotope composition is expected. However, for the IIAB and IIIAB iron meteorites it is evident that δ^{190}Os is decoupled from the concentration data, with late crystallized samples showing chondritic values (**Figure 4-9**). There is also no correlation between δ^{190}Os and the more classic indices of metal crystallization, such as Ir/Au and Ga/Ge. This implies that metal crystallization alone cannot account

for the range in δ^{190}Os and thus that other mechanisms must have affected the isotopic composition. This observation is in line with previous studies where more complex models involving mixing or late segregation have been proposed (e.g., Cook et al., 2004). Before mixing models will be discussed, two other processes that have been shown to result in mass-dependent isotope fractionation within iron meteorites will be considered, that is, formation of non-metal phases and subsolidus exsolution of kamacite from taenite.

5.2.3 Formation of Non-Metal Phases

Previous studies have shown that non-metal phases in iron meteorites (e.g., troilite, schreibersite, chromite) hold different isotopic signatures relative to the coexisting metal (e.g., Weyer et al., 2005; Williams et al., 2006; Williams and Archer, 2011; Bridgestock et al., 2014). The isotopic fractionation has been related to equilibrium and/or kinetic isotope fractionation during exsolution from the melt or to sub-solidus diffusion. For example, isotope fractionation as a result of troilite formation has been proposed to explain the stable Fe isotope systematics in iron meteorites with troilites yielding an isotopically lighter δ^{56}Fe than the coexisting metal phases (Williams et al., 2006).

Osmium is known to partition into troilite and schreibersite (Shen et al., 1996; van Acken et al., 2012). Distribution coefficients, determined by examining IAB and IIIAB irons, for Os in metal relative to sulphide range between 1300 and 1600 (Papanastassiou et al., 1996; Shen et al., 1996). Partition coefficients of Os between metal and schreibersite are lower, varying from 29 to 44 (Papanastassiou et al., 1996; Shen et al., 1996). Simple mass balance calculations (equation 1) can be used to predict whether equilibrium fractionation related to the formation of troilite and/or schreibersite is likely to have played a significant role. Here the following equation was used:

$$\delta^{\frac{190}{188}}Os_b = f_m^{Os} \cdot \delta^{\frac{190}{188}}Os_m + f_t^{Os} \cdot \delta^{\frac{190}{188}}Os_t + f_s^{Os} \cdot \delta^{\frac{190}{188}}Os_s \tag{1}$$

Where $\delta^{190/188}$Os$_{b,m,t,s}$ represent the respective stable isotope compositions of the bulk core (b), metal (m), troilite (t) and schreibersite (s), f_m^{Os} are the corresponding proportions of Os in the various phases, and the sum of the relative proportions equals 1. The stable isotope composition of the bulk was set at 0.12‰ as determined for chondrites, and for the metal a value of 0.38‰ was chosen as determined for several of the IIAB and IIIAB irons. The relative proportions (*f*) of Os in each phase can be calculated using the following equations:

The Os content (C^{Os}) of the system can be expressed as:

$$C_{bulk}^{Os} = X_m \cdot C_m^{Os} + X_t \cdot C_t^{Os} + X_s \cdot C_s^{Os} \tag{2}$$

Where X_m, X_t, and X_s are the respective proportions of metal, troilite, and schreibersite. Consequently, the proportion of Os in each phase (i.e., $f_m^{Os}, f_t^{Os}, f_s^{Os}$) can be expressed as:

$$f_m^{Os} = \frac{X_m \cdot C_m^{Os}}{X_m \cdot C_m^{Os} + X_t \cdot C_t^{Os} + X_s \cdot C_s^{Os}} \tag{3}$$

$$f_t^{Os} = \frac{X_s \cdot c_s^{Os}}{X_m \cdot c_m^{Os} + X_t \cdot c_t^{Os} + X_s \cdot c_s^{Os}}$$

(4)

$$f_s^{Os} = \frac{X_t \cdot c_t^{Os}}{X_m \cdot c_m^{Os} + X_t \cdot c_t^{Os} + X_s \cdot c_s^{Os}}$$

(5)

Figure 4-10 shows predictions of $\delta^{190/188}$Os for troilite and schreibersite considering abundances varying between 0-10%, using the partitioning of Os between metal and troilite (~1500) and between metal and schreibersite (~35) taken from Shen et al. (1996). Estimated Os stable isotope compositions range from -56022‰ at 1% troilite and 0% schreibersite, to a $\delta^{190/188}$Os$_{t,s}$ of -2.4‰ and 101‰, respectively, in case 10% troilite and 10% schreibersite are formed. Assuming equilibrium fractionation this requires very high fractionation factors that are not realistic for the investigated high-temperature system.

Subsolidus diffusion is another mechanism by which to fractionate isotopes. This is due to differences in diffusion rate, with the lighter isotopes diffusing faster than the heavier isotopes (e.g., Richter et al., 2003; Roskosz et al., 2006; Dauphas, 2007; Richter et al., 2009; Watson et al., 2016). Osmium contents in metal adjacent to schreibersite show concentration gradients, with enrichment of Os in the surrounding metal of up to 39% (Papanastassiou et al., 1996). This has been attributed to the exclusion of Os from the schreibersite during sub-solidus diffusion (Papanastassiou et al., 1995; 1996; Shen et al., 1996; Birck and Allegre, 1998). The corresponding Re-Os isochron data display younger ages which indicates that this must have been a long-term process, extending to rather low temperatures (Papanastassiou et al., 1996). The signature of sub-solidus diffusion would only be reflected in the metal if it was sampled in close proximity of schreibersite. Since small pieces were provided to us, the distance involved for the non-metal phases is unknown. However, if Os is excluded from the schreibersite, kinetic isotope fractionation would result in an enrichment of lighter isotopes which contrasts with the heavier isotopic signatures observed.

The formation of non-metal phases could have overprinted a signature resulting from metal fractional crystallization. Considering that previous studies have shown that troilite tends to possess an isotopically light signature (e.g., Williams et al., 2006), the expectation would be that the isotope composition of the corresponding metal would be driven to higher values on top of the isotope fractionation resulting from metal crystallization. That the IIAB and IIIAB iron groups display lower isotopic values for the samples that are expected to form in a later stage of crystallization compared to a heavier isotope composition displayed by early crystallized solids suggests the formation of non-metal phases does not play a role in the observed fractionation.
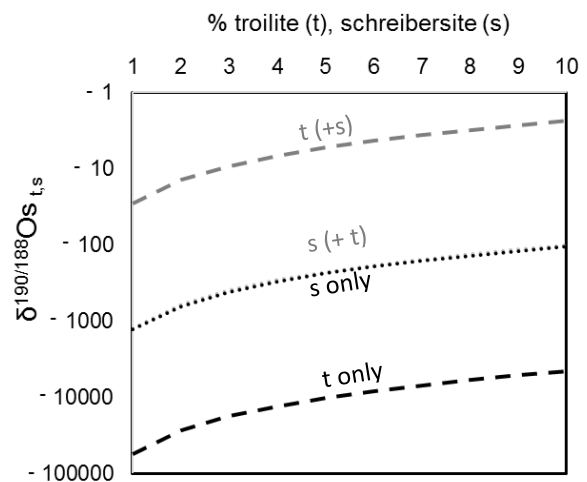

Figure 4-10 Modelled effect of Os stable isotope fractionation resulting from the formation of 1-10% of troilite (t) and schreibersite (s). Lines indicate $\delta^{190/188}$Os in troilite and schreibersite in case fractionation takes place from formation of (1) only troilite, (2) only schreibersite, (3) both troilite and schreibersite.

To summarize, the low partitioning of Os in non-metal phases and the low relative abundance of these phases compared to metal make it unlikely that they play a significant role in the recorded Os stable isotope fractionation in early formed iron meteorites. However, to properly constrain the effect of the formation of non-metal phases on the Os stable isotope composition, a mineral scale study should be undertaken. Measuring Os stable isotopes in non-metal phases will be technically challenging because of the low Os abundances in these phases. Another topic of further study, is the measurement of Os stable isotope compositions in metal adjacent to non-metal phases, along a traverse. This would reveal the potential for fractionation during sub-solidus diffusion. During these studies it would be good to focus on multi-element analyses for direct comparison of data and thus to control the sampling heterogeneity.

5.2.4 Exsolution of Kamacite from Taenite

A number of studies have shown that stable isotope fractionation takes place as a result of kamacite exsolution from taenite during subsolidus cooling (Weyer et al., 2005; Cook et al., 2007; Dauphas, 2007; Watson et al., 2016). Kamacite possesses a 12-fold coordination whereas taenite has an 8-fold coordination. The difference in coordination between kamacite and taenite creates the potential for equilibrium isotope fractionation at the interface between the phases. Heavier isotopes are known to prefer phases with a lower coordination. Consequently, taenite would be expected to possess a lighter isotope signature relative to kamacite. Kinetic fractionation during sub-solidus diffusion is another potential source of fractionation. It is known that Os is mobilized and redistributed as a result of sub-solidus diffusion, with preferentially incorporation of Os in taenite over kamacite ($D_{taenite/kamacite}$= ~1.2; Mullane et al., 2004). When diffusion is not fast enough to maintain equilibrium as cooling proceeds, compositional zoning is developed. The observation that taenite-kamacite profiles display a slight M-shaped profile for Os implies that equilibrium was not achieved (Hsu et al., 2000).

The signature of isotope fractionation between taenite and kamacite will only be observed when one phase has been preferentially sampled over the other. Some of the low-Ni IIAB iron meteorites are comprised completely of kamacite, i.e., hexahedrites (e.g., Coahuila and Gressk), and the high-Ni IVB iron meteorites are composed of only taenite, i.e., ataxites (e.g., Hoba and Tlacotepec). Given that only one phase is present, for these samples, this precludes exsolution as a source of fractionation. Other samples display very fine exsolution textures (e.g., Muonionalusta), which makes heterogeneous sampling unlikely. Samples comprising only one metal phase, either kamacite or taenite, and samples with fine exsolution textures still display an offset in δ^{190}Os relative to chondrites, as well as yielding variability between the samples. This indicates that kamacite-taenite dissolution cannot be the main source of fractionation. Even though it cannot be the dominant source of stable isotope fractionation, the effect should be considered for octahedrites, samples where both kamacite and taenite form visible banding. For these type of iron meteorites, heterogeneous sampling is more likely and might explain some of the observed variation. Duplicates of Mount Joy, a coarse octahedrites with a bandwidth of ~10 mm (Buchwald, 1975), differ by 21 ppb in their Os concentration. Considering that Os is not equally distributed between taenite and kamacite, this implies that the quantity of taenite and kamacite sampled varied, with the higher concentration representing relatively more taenite. The analysis yielding a higher

concentration (151 ppb) displays a lower stable Os isotope composition ($\delta^{190/188}$Os is 0.37 relative to 0.42), in line with the expectation that taenite preferentially incorporates the lighter isotopes. It should, however, be noted that the stable isotope compositions are within analytical uncertainty of each other, indicating that the extent of isotope fractionation between kamacite and taenite is minimal. A more detailed study is required to quantify the degree of fractionation resulting from kamacite exsolution, whereby controlled spatial sampling should be accomplished and a multi-element approach is recommended.

5.3 FRACTIONAL CRYSTALLIZATION and MIXING MODELS

5.3.1 Fractional Crystallization Models

To assess how much of the isotopic variation could be attributed to fractional crystallization, simple fractional crystallization models were constructed. The models assume equilibrium fractionation in small discrete steps, which allows for an assessment of changing the partition coefficient as crystallization proceeds. The following formula was used:

$$R_l = \frac{C(Os_l)_i \cdot (R_l)_i}{f_s \cdot C(Os_s) \cdot \alpha_{s-l} + (1-fs) \cdot C(Os_l)} \tag{6}$$

Where $C(Os_l)_i$ and $(R_l)_i$ represent the Os concentration and isotope ratio of the liquid in the preceding step. In equation (6), f_s defines the mass fraction of solid metal crystallized, which was set at an initial value of 1/10,000, α_{s-l} refers to the isotope fractionation factor, and $C(Os_s)$ and $C(Os_l)$ represent the Os concentration of solid and liquid, respectively. The isotope composition of the coexisting solid, Rs, can be obtained by:

$$R_s = R_l \cdot \alpha_{s-l} \tag{7}$$

The concentration in the liquid was determined by:

$$C(Os_l) = \frac{C(Os_l)_i}{D_{Os} \cdot Xs + (1-Xs)} \tag{8}$$

from which the concentration of the coexisting liquid can be calculated following:

$$C(Os_s) = D(Os) \cdot C(Os_l) \tag{9}$$

In equations 8 and 9, D(Os) represents the solid metal/liquid metal distribution coefficient of Os. The partition coefficient is strongly dependent on the S content, where D(Os) is shown to increase significantly with increasing S content (e.g., Chabot and Jones, 2003; Chabot, 2004; Chabot et al., 2011). Due to the low solubility of S in the solid metal, the concentration of S is enriched in the remaining liquid metal and D(Os) is changed accordingly. To account for this in the models, a parameterization method was used (Jones and Malvin, 1990; Chabot and Jones, 2003; Chabot et al., 2017). This method uses empirical parameterization values derived from experimental elemental partitioning data, and expresses D(Os) following:

$$\frac{1}{D(Os)} = \frac{\left(\frac{1-2 \cdot XS}{1-XS}\right)^{\beta}}{D(Os)_0} \tag{10}$$

where XS is the mole fraction of S in the preceding step, $D(Os)_0$ defines the partitioning of Os in the endmember, light element-free system, and β is the slope of the fit to the experimental data. Both $D(Os)_0$ and β are constants that have been derived from Chabot et al. (2017). The effect of P and C on $D(Os)$ was considered to be insignificant (Chabot and Drake, 2000).

By performing the calculations two model curves were obtained; one displaying the evolution of the liquid and one of the solid with progressive fractional crystallization (red and blue line, respectively, in **Figure 4-11**). In the case where the metal represents a solid crystallized from a liquid with which it was in equilibrium, either as direct precipitate or from a trapped melt, it will have a composition that plots along the "solid trend". The coexisting liquid plots along the "liquid trend". A mixture of equilibrium solid and liquid plots between the two trends. Any values plotting outside of this field, restricted by the solid and liquid trends, require additional process(es), such as non-equilibrium mixing or late segregation (section 5.3.3). Of note, these processes can also result in samples plotting in between the solid and liquid trends.
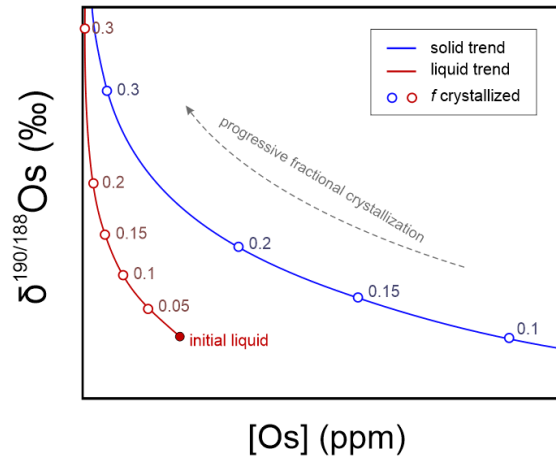
Figure 4-11 Example model, showing hypothetical trends for the evolution of $\delta^{190/188}Os$ and Os content in solid metal (blue line) and liquid metal (red line) as fractional crystallization proceeds. The fraction (0-1) crystallized (*f*) is annotated.

5.3.2 Input Parameters

The first calculation step in each model requires a knowledge of the liquid composition of the parental melt. All input parameters, used in the various models that are presented in this study, are provided in Appendix 4-B. Needed are [1] the initial S content, [2] the initial Os isotope composition, and [3] the initial Os concentration. For these: [1] The initial S content of the parent body is taken from Chabot (2004). Since for the IIAB and IIIAB substantially different initial concentrations have been suggested (e.g., Wasson, 1999), models have also been constructed to evaluate the effect of variable S content. [2] Regarding the high partition of Os between metal and silicate ($D=\sim10^7$ for Earth conditions at 2,773K; Brenan et al., 2005) the initial Os isotope compositions is assumed to be chondritic ($\delta^{190/188}Os = 0.12‰$ – Chapter 3 of this thesis). [3] Previous studies, where fractional crystallization models have been constructed to account for the elemental variation of Os, provide constraints on the initial Os concentration. These studies have used different methods to determine $D(Os)$. To ensure consistency with the approach taken here, fractional crystallization models to account for the variation in Re and Os concentrations were reassessed using the parameterization of Chabot et al. (2017). The initial Os concentrations that were obtained from these models were subsequently used as an input parameter for modelling the evolution of the stable Os isotope composition.

One variable for which no previous constraints have been made, is the Os isotopic fractionation factor, "α". The models are, therefore, fitted by trial-and-error. Hereby, the assumption is made that one or more of the analysed samples plot along the solid track, with no samples plotting to the right of the solid curve. This concept is illustrated in **Figure 4-11**. The idealized models presented here are, therefore, not unique. Nevertheless, from best-fit models, an estimate of the fractionation factor was obtained.

5.3.3 Mixing Models

To account for samples that do not plot along the solid trend of simple fractional crystallization, the following mixing models are evaluated; (1) equilibrium mixing, (2) non-equilibrium mixing, (3) late segregation. Process 1 reflects melt trapping (e.g., Wasson, 1999; Wasson et al., 2007) or mechanical mixing (e.g., Esbensen et al., 1982). The second process involves the mixing of an evolved melt with an early formed solid (e.g., Haack and Scott, 1993), and the last process considers the mixing of primitive melt with evolved melt (e.g., Pernicka and Wasson, 1987; Chabot and Drake, 1999). The latter two models are able to explain values that plot to the left of the liquid evolution line. The two-component mixing models follow:

$$C(Os)_M = f \cdot C(Os)_A + (1-f) \cdot C(Os)_B \qquad (11)$$

where $C(Os)_{M,A,B}$ are the concentrations of Os in the resulting mixture of component A and B, and f is the fraction of component A that has been mixed with component B. The isotope composition of the mixture, $\delta(Os)_M$, is determined by:

$$\delta(Os)_M = \frac{f \cdot C(Os)_A \cdot \delta(Os)_A + (1-f) \cdot C(Os)_B \cdot \delta(Os)_B}{f \cdot C(Os)_A + (1-f) \cdot C(Os)_B} \qquad (12)$$

where $\delta(Os)_{A,B}$ are the isotope composition of component A and B. Using the fractional crystallization models, constraints can then be placed on the input parameters.

5.3.4 IIAB

It is, in general, accepted that the IIAB parent body contained a substantial amount of S. The exact quantity is, however, debated. Wasson et al. (2007) determined an initial S content of ca. 6 wt.% which contrasts with other studies consistently yielding results in line with ~17 wt.% S (e.g., Jones and Drake, 1983; Chabot and Jones, 2003; Chabot, 2004; Cook et al., 2004). The large difference may result from the different methods used to estimate the abundance of S. For this study, models to explain the range in Re and Os concentrations were reassessed using an initial S content of 6 wt.% and the parametrization method (Chabot et al., 2017). When considering 6 wt.% S as input parameter, the range in Re and Os concentrations could only be accounted for if the initial Os content was set at >21 ppm and supra-chondritic Re/Os ratio were adopted. This is inconsistent
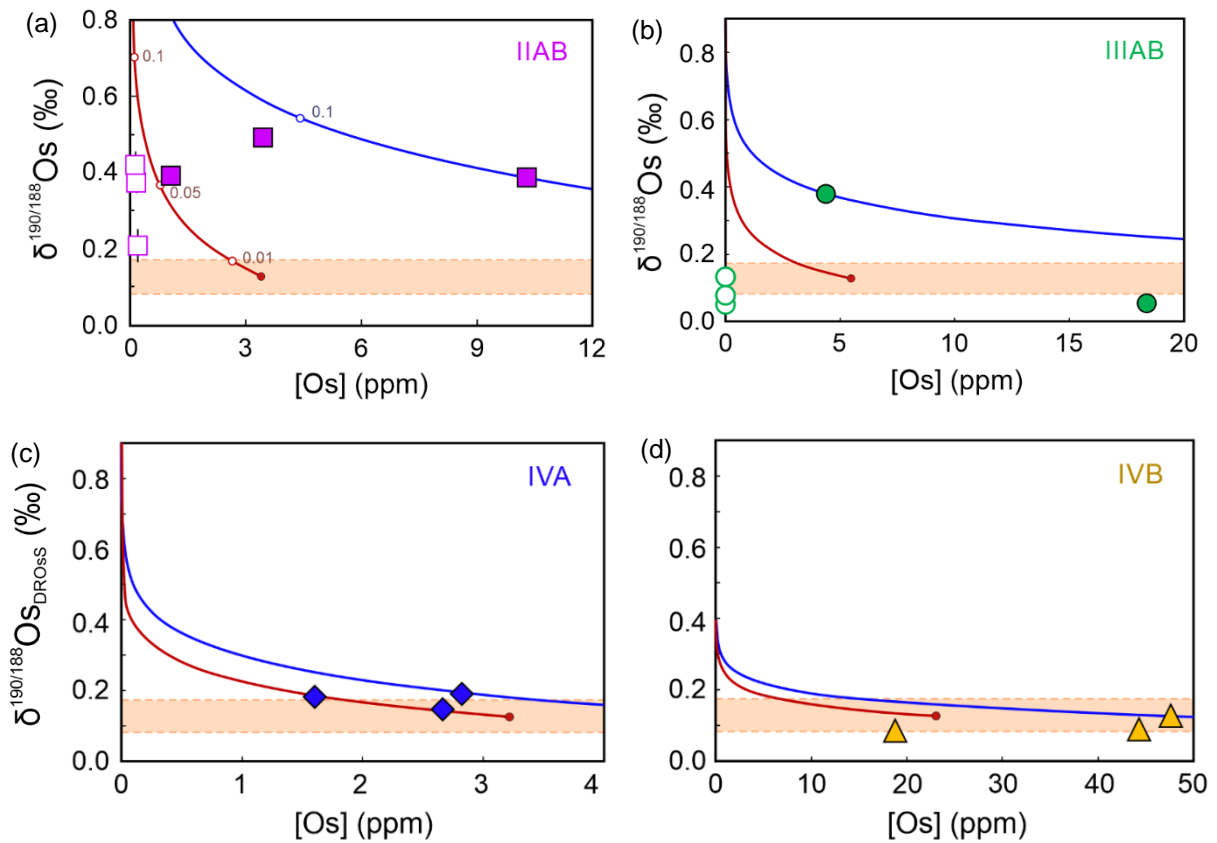
Figure 4-13 The stable Os isotope composition versus Os concentration of **(a)** IIAB, **(b)** IIIAB, **(c)** IVA, and **(d)** IVB magmatic iron meteorites, compared to idealized fractional crystallization models constructed for this study. Symbols as in Figure 4-5, whereby it should be noted that closed and open symbols represent early and late crystallized melts, respectively. The lines represent the trajectories of metallic liquid (red) and solid (blue) with progressive fractional crystallization. The initial liquid composition is indicated by the red dot. Parameters used to construct the models are provided in Appendix 4-B.
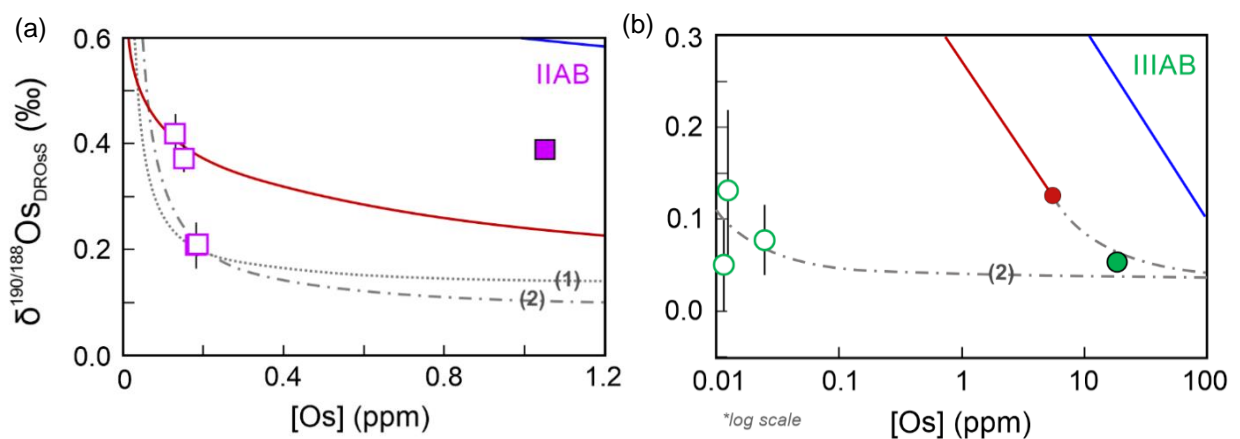
Figure 4-12 A close up of Figure 4-12a,b, focussing on the samples that do not plot in between the liquid and solid trajectories of the **(a)** IIAB and **(b)** IIIAB iron meteorite groups, indicating that disequilibrium mixing should have been in place. (a) Mixing lines show that IIAB iron meteorite Navajo can be explained by either (1) mixing in of late segregated metallic liquid or (2) mixing of early crystallized melt with more evolved liquid. (b) Sub-chondritic values displayed by IIIAB irons can only be explained by mixing of early crystallized melt with more evolved liquid. Note the log scale in (b).

with predictions made for the parent body. Consequently, the model discussed below uses an estimate of 17 wt. % S in the IIAB parent body.

Figure 4-13 shows that the minimal fractionation factor is 0.999842 ($\Delta^{190/188}Os_{\text{liq metal-sol metal}}$ = -0.16‰) in order for Coahuila to be crystallized from a metallic liquid. The assumption that Coahuila plots along the solid track is supported by models constructed for the Re-Os elemental system where Coahuila is shown to plot along the solid track as well (Appendix 4-B). The other samples, plot either in between the solid and liquid trends (Gressk and North Chille), or to the left of the liquid trend (Mount Joy and North Chile). Gressk and North Chile could be explained by equilibrium mixing of liquid and solid, whereas Mount Joy and North Chile require either non-equilibrium mixing or late-segregation. **Figure 4-12a** shows that both mixing of a late segregated liquid, and mixing of an early crystallized melt with a more evolved liquid can explain the isotope composition of these samples. This contrast with the study of Wasson et al. (2007), who concluded that all elemental variations can be explained by trapping of melt. It does, however, confirm the conclusion of Morgan et al. (1995) who argue that the Re-Os systematics indicate a gradual addition of late segregated metallic liquid. The discrepancy with the study of Wasson et al. (2007) might be related to the different approaches used. It should also be noted that they did not discuss the Os elemental systems whereas this is, due to its high partitioning, a sensitive tracer of mixing processes.

5.3.5 IIIAB

The best-fit model for the IIIAB irons, shows that all the low-Os samples (12-25 ppb) plot to the left of the liquid trend (i.e., Bear Creek, Chupaderos, and Grant). Furthermore, the model is unable to fit Costilla Peak through the solid trend. That some samples plot to the left of the solid trend indicates that they require a process additional to simple fractional crystallization of a metal liquid. Costilla Peak, as well as some of the low Os concentration samples, display sub-chondritic values. This implies that their composition cannot be explained by late segregation of a chondritic melt. Instead early crystallized melt with a sub-chondritic isotope composition needs to mixed with a more evolved melt to explain these values (**Figure 4-12b**). Another option would be that the IIAB irons initially possessed a non-chondritic liquid metal composition. However, no previous evidence has been found to suggest this.

5.3.6 IVA and IVB

Only a couple of samples were analysed from the IVA and IVB iron meteorite groups, which makes it difficult to deduce any systematic behaviour for these groups. It is, however, evident that their isotopic composition is not offset from chondrites as much as is observed for the IIAB and IIIAB irons (**Figure 4-13c,d**). The potential low abundance of S in the IVA group (0.5-9 %; Chabot and Drake, 2000; Wasson and Richardson, 2001; McCoy et al., 2011), and essential lack in IVB irons (0-2 wt.%; Chabot and Drake, 2000; Walker et al., 2008), might explain

the absence of any significant stable Os isotopic fractionation in these groups. This support the suggestion that the degree of fractionation is controlled by the S content.

Models constructed to explain the Ru mass-dependent stable isotope systematics, suggest that the IVB group possessed a heavier initial Ru isotopic composition relative to ordinary chondrites and to IIAB, IIIAB, and IVA magmatic iron groups. (Hopp et al., *personal comm.*). For Os, there is no evidence that the initial composition of the IVB irons was non-chondritic. This might be related to the insensitivity of Os to the process that caused the non-chondritic signature for Ru. Walker et al. (2008) report a multi-stage history for the IVB irons, including high temperature volatilization and condensation in the solar nebula which has resulted in fractionation of refractory siderophile elements. This process is most likely the source of Ru isotopic fractionation. It is evident from CI normalized HSE patterns that Os is the least depleted of the HSE during this process (Campbell and Humayun, 2005; Walker et al., 2008), related to its relatively higher condensation temperature. That minimal loss of Os has occurred is consistent with a chondritic isotopic signature.

5.4 CONTROL of S CONTENT on DEGREE of FRACTIONATION

Sulphur is relatively insoluble in metal, consequently, it is heterogeneously distributed in troilite nodules. Sulphur can, therefore, not be directly measured in the metal, which makes it difficult to quantify its abundance in planetary bodies. One way by which the S content has been determined is by estimating the amount of trapped sulphides (e.g., Esbensen et al., 1982; Wasson, 1999; Wasson et al., 2007). Another approach used, is to quantify the dependency of other elements on the amount of S present, through experiments, and to combine these data with models to infer the initial S content (e.g., Jones and Drake, 1983; Haack and Scott, 1993; Chabot, 2004). The use of these two different methods has led to substantially different values. For example, Wasson (1999) and Chabot (2004) derive S contents for the IIAB iron group that differ by an order of 6. Constraining the abundance more precisely is of substantial importance since it controls the physical chemistry of the solidifying metallic melt and thus determines the distribution of other elements. Furthermore, it controls liquidus temperature, which has important constraints on the cooling history of the parent body. Another, independent way by which to determine the initial S content would, therefore, be very useful.

The fractionation factors that have been deduced from the models here show a negative correlation with the initial S content of the various
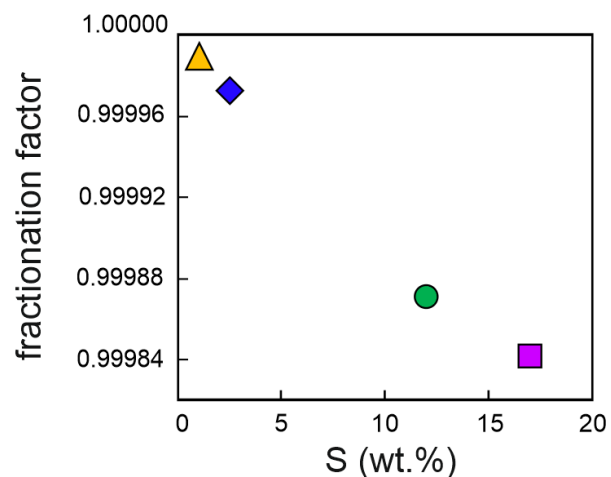
Figure 4-14 Negative correlation between S content and fractionation factor, deduced from models constructed in this study. The co-variation between these two parameters suggests that the degree of fractionation is controlled by the abundance of S.

parent bodies investigated (**Figure 4-14**). This suggests that S plays a role in controlling the degree of fractionation, which would be in support of isotope fractionation resulting from a difference in Fe-S and Fe-Fe bonding. It could also be related to the control of S on the liquidus temperature of metal, with the variation in temperature controlling the extent of fractionation. That the degree of fractionation shows a correlation with the initial S content suggests that Os stable isotopes could provide a new tool by which to constrain the abundance of S. An experimental study also could help to quantify the relationship between S content and isotope fractionation, and would aid in our knowledge of the source of Os stable isotope fractionation.

6. CONCLUSIONS

Osmium mass-dependent isotope systematics reveal significant variations within the IIAB and IIIAB magmatic iron meteorite groups that are resolvable from chondrites. Irons from the IVA and IVB groups yield limited variation, although it should be noted that only a few samples were analysed. The signature displayed by the IIAB and IIIAB irons can be explained by fractional crystallization of a metallic liquid, most likely equilibrium fractionation due to a difference between Fe-Fe and Fe-S bonding of the metallic solid and liquid, respectively. The degree of isotope fractionation appears to be dependent on the S content, potentially providing a new tool by which to determine the initial S content. It would be of interest to perform an experimental study to investigate this relationship in more detail. The IIAB and IIIAB irons both show clear evidence of a more complex history, where the signature of simple fractional crystallization of a metallic liquid has been overprinted by parallel processes including disequilibrium mixing. Sub-chondritic values observed for IIIAB irons are indicative of mixing of early crystallized melt with a more evolved liquid. Altogether, this study has shown that Os stable isotopes potentially provide a powerful tool to better constrain the formation history of iron meteorites.

ACKNOWLEDGEMENTS

SUPPLEMENTARY INFORMATION

Appendix 4-A Compilation of literature data

Table A4-1 Literature data of [Os] (ppb), $^{187}Os/^{188}Os$, and $^{186}Os/^{188}Os$ compositions, used for comparison with data obtained in this study (Figure 4-6).

	This study		Previous studies										corresponding reference
		2se	average	2 sd	*all values incorporated*								*corresponding reference*
IIAB													
Os (ppb)													
Coahuila	10303	0.01	10349	1101	11600	10440	10440	10222	10200	10138	9480	10310	10310	1; 3; 3; 4; 5; 7; 8; 10; 10
Gressk	3459	0.00	3388	3	3389	3386	3388							4; 4; 5
Mount Joy	130	0.08	141	6	143	145	138	137	143	141				2; 5; 7; 7; 10; 10
	151	0.06												
Navajo	182	0.03	178	6	177	174	181	179						5; 7; 10; 10
	186	0.05												
North Chille	1047	0.00	1088	90	1140	1057	1068							1; 2; 2
$^{187}Os/^{188}Os$													
Coahuila	0.141672	0.000007	0.139500	0.010227	0.141320	0.141300	0.141467	0.127907	0.141625	0.141340	0.141540			3; 3; 4; 4; 7; 10; 10
Gressk	0.153126	0.000113	0.152659	0.001339	0.152185	0.153132								4; 4
Mount Joy	0.156727	0.000041	0.158105	0.000732	0.157788	0.158452	0.158390	0.157790						7; 7; 10; 10
	0.156824	0.000021												
Navajo	0.157004	0.000051	0.157004	0.000221	0.157131	0.156950	0.156930							7; 10; 10
	0.156963	0.000017												
North Chille	0.169492	0.000010	-											
$^{186}Os/^{188}Os$													
Coahuila	0.119769	0.000005	0.119896	0.000153	0.119950	0.119842								5; 7
Gressk	0.119859	0.000119	0.119880	0.000060	*	0.119880								5

																Ref
Mount Joy	0.120423	0.000043	0.120503	0.000099		0.120560	0.120479	0.120470								5; 7; 7
	0.120461	0.000021														
Navajo	0.120286	0.000056	0.120503	0.000304		0.120610	0.120395									5; 7
	0.120364	0.000018														
North Chille	0.119928	0.000011	-													

IIIAB

Os (ppb)

																Ref
Bear Creek	12	7	11.4			11.4										6
Cape York	4380	3	3082	2224		2411	4366	2469								3; 7; 8
Chupaderos	4380	3	10.8	0.3		10.9	10.6									6; 7
Costilla Peak	13	7	19121	1084		19600	19580	18629	18675							1; 2; 4; 7
Grant	18354	421	24.9	3.6		27.0	24.0	23.8								1; 6; 7

^{187}Os/^{188}Os

									Ref
Bear Creek	0.135974	0.000066	0.134500	0.000200	*	0.134500			6
Cape York	0.135113	0.000005	0.134247	0.003186		0.133120	0.135373		3; 7
Chupaderos	0.140027	0.000113	0.142710	0.001161		0.143120	0.142299		6; 7
Costilla Peak	0.124473	0.000005	0.124440	0.000086		0.124409	0.124470		4; 7
Grant	0.139555	0.000049	0.140405	0.000636		0.140180	0.140630		6; 7

^{186}Os/^{188}Os

							Ref
Bear Creek	0.120881	0.000066	-				
Cape York	0.119810	0.000004	0.119866	0.000006	*	0.119866	7
Chupaderos	0.120519	0.000105	0.120649	0.000025	*	0.120649	7
Costilla Peak	0.119761	0.000004	0.119839	0.000008	*	0.119839	7
Grant	0.120519	0.000048	0.120592	0.000014	*	0.120592	7

IVA

Os (ppb)

																Ref
Gibeon	2657	5	2647	466		2418	2406	2774	2676	2675	2418	2406	3094	2810	2797	4; 6; 6; 6; 12; 12; 3; 3; 8
Muonionalusta	1603	9	1091			1091										12

	^{187}Os/^{188}Os												
Gibeon	0.132215	0.000024	0.132123	0.000224		0.132240	0.132000	0.132020	0.132150	0.132180	0.132235	0.132260	4; 6; 6; 6; 6; 12; 12
Muonionalusta	0.132170	0.000006	0.135460	0.000068	*	0.135460							12
IVB													
	Os (ppb)												
Hoba	44364	28	40348	2134		40900	41010	40800	39391	41900	39206	39229	3; 3; 3; 4; 9; 11; 11
Tlacotepec	47600	800	46733	5314		47920	47007	47030	46891	50600	46742	46676 41000	3; 4; 4; 9; 11; 11; 13
Weaver Mountains	18867	27	18383	267		18497	18469	18203	18361				4; 4; 11; 11
	^{187}Os/^{188}Os												
Hoba	0.121992	0.000006	0.121896	0.000063		0.121890	0.121920	0.121860	0.121947	0.121880	0.121880		3; 3; 3; 4; 11; 11
Tlacotepec	0.120942	0.000005	0.120955	0.000088		0.120890	0.120944	0.121027	0.120950	0.120960	0.120960		3; 4; 4; 11; 11; 11
Weaver Mountains	0.126032	0.000006	0.126089	0.000026		0.126097	0.126097	0.126070	0.126090				4; 4; 11; 11

Corresponding references: 1 – Pernicka and Wasson, 1987; 2 – Horan et al., 1992; 3 – Shen et al., 1996; 4 – Smoliar et al., 1996; 5 – Walker et al., 1997; 6 – Chen et al., 2002; 7 – Cook et al. 2004; 8 – Pataev and Jacobsen, 2004; 9 – Campbell and Humayun, 2005 – 10 – Morgan et al., 2005; 11 – Walker et al., 2008; 12 - McCoy et al., 2011; 13 – Hirata and Nesbitt, 1997.

* - indicates that the error on the individual analysis is taken.

Appendix 4-B Fractional crystallization models

Below, the parameters used to construct fractional crystallization models are provided.

General Parameters

Parameters	All groups
$\delta^{190/188}Os_{initial}$	0.12
$\beta_{S\,(Os)}$	-5.34
$\beta_{S\,(Re)}$	-5.04
$D(Os)_0$	1.71
$D(Re)_0$	1.49

Group Specific Parameters

Parameters	IIAB	IIIAB	IVA	IVB
$[S]_{initial}$ (wt.%)	17	12	2.5	1
$[Os]_{initial}$ (µg/g)	3.40	4.1	6.2	23.4
$[Re]_{initial}$ (µg/g)	0.305	0.335	0.508	1.74
Obtained from best-fit models:				
Fract. factor, α	0.999842	0.999871	0.999973	0.99999
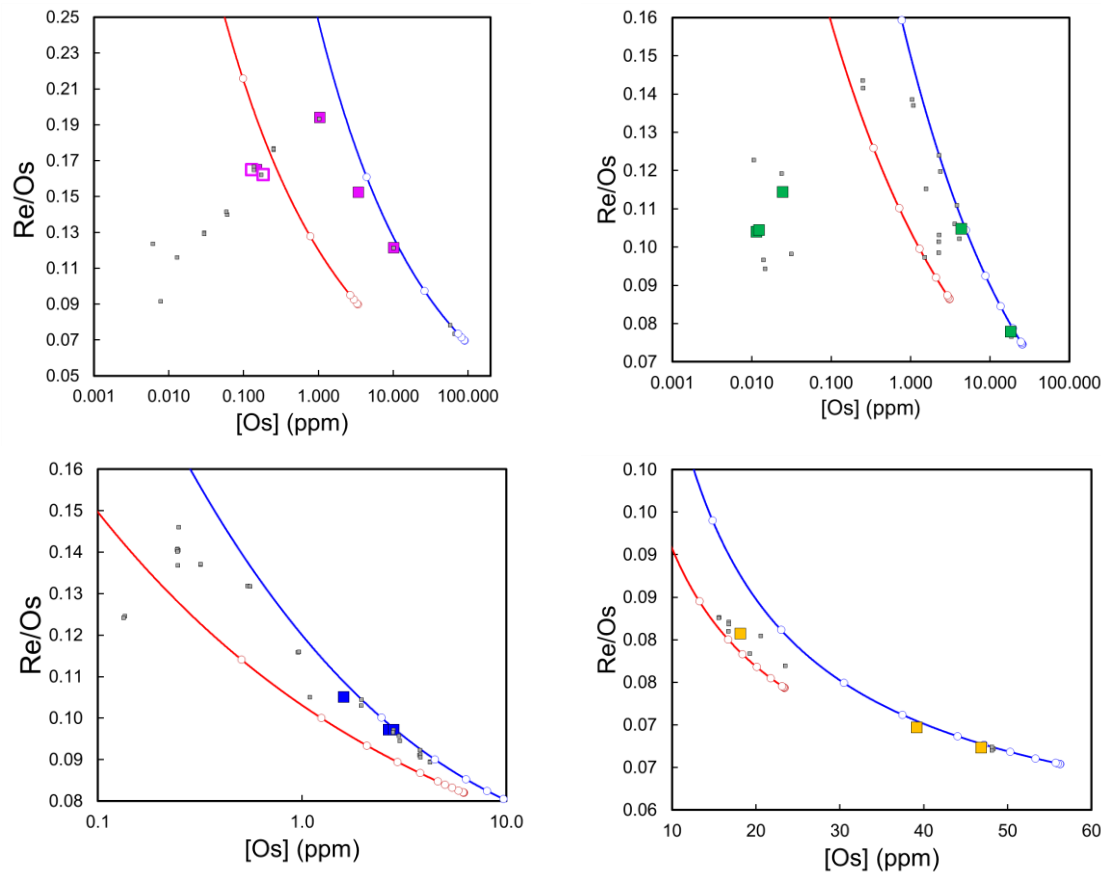
REFERENCES

Alfe, D., and Gillan, M. J., 1998, First-principles simulations of liquid Fe-S under Earth's core conditions: Physical Review B, v. 58, no. 13, p. 8248.

Benedix, G. K., Haack, H., and McCoy, T., 2014, Iron and stony-iron meteorites: Meteorites and Cosmochemical Processes, p. 267-285.

Bigeleisen, J., and Mayer, M. G., 1947, Calculation of equilibrium constants for isotopic exchange reactions: The Journal of Chemical Physics, v. 15, no. 5, p. 261-267.

Birck, J. L., and Allegre, C. J., 1998, Rhenium-187—osmium-187 in iron meteorites and the strange origin of the Kodaïkanal meteorite: Meteoritics & Planetary Science, v. 33, no. 4, p. 647-653.

Birck, J. L., Barman, M. R., and Capmas, F., 1997, Re-Os Isotopic Measurements at the Femtomole Level in Natural Samples: Geostandards Newsletter, v. 21, no. 1, p. 19-27.

Brenan, J. M., McDonough, W. F., and Ash, R., 2005, An experimental study of the solubility and partitioning of iridium, osmium and gold between olivine and silicate melt: Earth and Planetary Science Letters, v. 237, no. 3, p. 855-872.

Bridgestock, L., Williams, H., Rehkämper, M., Larner, F., Giscard, M., Hammond, S., Coles, B., Andreasen, R., Wood, B., and Theis, K., 2014, Unlocking the zinc isotope systematics of iron meteorites: Earth and Planetary Science Letters, v. 400, p. 153-164.

Buchwald, V. F., 1975, Handbook of iron meteorites.

Buchwald, V. F., 1984, Phosphate minerals in meteorites and lunar rocks, Phosphate minerals, Springer, p. 199-214.

Burkhardt, C., Hin, R. C., Kleine, T., and Bourdon, B., 2014, Evidence for Mo isotope fractionation in the solar nebula and during planetary differentiation: Earth and Planetary Science Letters, v. 391, no. 0, p. 201-211.

Campbell, A. J., and Humayun, M., 2005, Compositions of group IVB iron meteorites and their parent melt: Geochimica et Cosmochimica Acta, v. 69, no. 19, p. 4733-4744.

Chabot, N., and Haack, H., 2006, Evolution of asteroidal cores: IIC, v. 7, p. 1.0.

Chabot, N. L., 2004, Sulfur contents of the parental metallic cores of magmatic iron meteorites: Geochimica et Cosmochimica Acta, v. 68, no. 17, p. 3607-3618.

Chabot, N. L., Campbell, A. J., Jones, J. H., Humayun, M., and Agee, C. B., 2003, An experimental test of Henry's Law in solid metal-liquid metal systems with implications for iron meteorites: Meteoritics & Planetary Science, v. 38, no. 2, p. 181-196.

Chabot, N. L., and Drake, M. J., 1999, Crystallization of magmatic iron meteorites: the role of mixing in the molten core: Meteoritics & Planetary Science, v. 34, no. 2, p. 235-246.

-, 2000, Crystallization of magmatic iron meteorites: The effects of phosphorus and liquid immiscibility: Meteoritics & Planetary Science, v. 35, no. 4, p. 807-816.

Chabot, N. L., and Jones, J. H., 2003, The parameterization of solid metal-liquid metal partitioning of siderophile elements: Meteoritics & Planetary Science, v. 38, no. 10, p. 1425-1436.

Chabot, N. L., McDonough, W. F., Jones, J. H., Saslow, S. A., Ash, R. D., Draper, D. S., and Agee, C. B., 2011, Partitioning behavior at 9 GPa in the Fe–S system and implications for planetary evolution: Earth and Planetary Science Letters, v. 305, no. 3–4, p. 425-434.

Chabot, N. L., Wollack, E. A., McDonough, W. F., Ash, R. D., and Saslow, S. A., 2017, Experimental determination of partitioning in the Fe-Ni system for applications to modeling meteoritic metals: Meteoritics & Planetary Science, v. 52, no. 6, p. 1133-1145.

Chen, J., Papanastassiou, D., and Wasserburg, G., 2002, Re-Os and Pd-Ag systematics in Group IIIAB irons and in pallasites: Geochimica et cosmochimica acta, v. 66, no. 21, p. 3793-3810.

Chernonozhkin, S. M., Goderis, S., Costas-Rodríguez, M., Claeys, P., and Vanhaecke, F., 2016, Effect of parent body evolution on equilibrium and kinetic isotope fractionation: a combined Ni and Fe isotope study of iron and stony-iron meteorites: Geochimica et Cosmochimica Acta, v. 186, p. 168-188.

Cohen, A. S., and Waters, F. G., 1996, Separation of osmium from geological materials by solvent extraction for analysis by thermal ionisation mass spectrometry: Analytica Chimica Acta, v. 332, no. 2, p. 269-275.

Cook, D. L., Wadhwa, M., Clayton, R. N., Dauphas, N., Janney, P. E., and Davis, A. M., 2007, Mass-dependent fractionation of nickel isotopes in meteoritic metal: Meteoritics & Planetary Science, v. 42, no. 12, p. 2067-2077.

Cook, D. L., Walker, R. J., Horan, M. F., Wasson, J. T., and Morgan, J. W., 2004, Pt-Re-Os systematics of group IIAB and IIIAB iron meteorites 1: Geochimica et Cosmochimica Acta, v. 68, no. 6, p. 1413-1431.

Corgne, A., Wood, B. J., and Fei, Y., 2008, C- and S-rich molten alloy immiscibility and core formation of planetesimals: Geochimica et Cosmochimica Acta, v. 72, no. 9, p. 2409-2416.

Dauphas, N., 2007, Diffusion-driven kinetic isotope effect of Fe and Ni during formation of the Widmanstätten pattern: Meteoritics & Planetary Science, v. 42, no. 9, p. 1597-1613.

Dean, D. C., and Goldstein, J., 1986, Determination of the interdiffusion coefficients in the Fe-Ni and Fe-Ni-P systems below 900 C: Metallurgical Transactions A, v. 17, no. 7, p. 1131-1138.

Esbensen, K. H., Buchwald, V. F., Malvin, D. J., and Wasson, J. T., 1982, Systematic compositional variations in the Cape York iron meteorite: Geochimica et Cosmochimica Acta, v. 46, no. 10, p. 1913-1920.

Fleet, M., Liu, M., and Crocket, J., 1999, Partitioning of trace amounts of highly siderophile elements in the Fe–Ni–S system and their fractionation in nature:

Geochimica et cosmochimica acta, v. 63, no. 17, p. 2611-2622.

Fukami, Y., Kimura, J., Irisawa, K., Yokoyama, T., and Hirata, T., Mass-Dependent Fractionation of Tungsten Isotopes in IIIAB Iron Meteorites and Main-Group Pallasites, in Proceedings Lunar and Planetary Science Conference2010, Volume 41, p. 1649.

Goldstein, J., Scott, E., and Chabot, N., 2009a, Iron meteorites: Crystallization, thermal history, parent bodies, and origin: Chemie der Erde-Geochemistry, v. 69, no. 4, p. 293-325.

Goldstein, J. I., Scott, E. R. D., and Chabot, N. L., 2009b, Iron meteorites: Crystallization, thermal history, parent bodies, and origin: Chemie der Erde - Geochemistry, v. 69, no. 4, p. 293-325.

Haack, H., and McCoy, T., 2003, Iron and Stony-iron Meteorites: Treatise on Geochemistry, v. 1, p. 711.

Haack, H., and Scott, E. R., 1993, Chemical fractionations in group IIIAB iron meteorites: Origin by dendritic crystallization of an asteroidal core: Geochimica et Cosmochimica Acta, v. 57, no. 14, p. 3457-3472.

Haack, H., Scott, E. R., Love, S. G., Brearley, A. J., and McCoy, T. J., 1996, Thermal histories of IVA stony-iron and iron meteorites: Evidence for asteroid fragmentation and reaccretion: Geochimica et Cosmochimica Acta, v. 60, no. 16, p. 3103-3113.

Herr, W., Hoffmeister, W., Hirt, B., Geiss, J., and Houtermans, F., 1961, Versuch zur datierung von eisenmeteoriten nach der rhenium-osmium-methode: Zeitschrift für Naturforschung A, v. 16, no. 10, p. 1053-1058.

Hin, R. C., Burkhardt, C., Schmidt, M. W., Bourdon, B., and Kleine, T., 2013, Experimental evidence for Mo isotope fractionation between metal and silicate liquids: Earth and Planetary Science Letters, v. 379, p. 38-48.

Hin, R. C., Fitoussi, C., Schmidt, M. W., and Bourdon, B., 2014, Experimental determination of the Si isotope fractionation factor between liquid metal and liquid silicate: Earth and Planetary Science Letters, v. 387, p. 55-66.

Hirt, B., Herr, W., and Hoffmeister, W., 1963, Age determinations by the rhenium-osmium method: Radioactive Dating, p. 35-43.

Hopp, T., Fischer-Gödde, M., and Kleine, T., Ruthenium Isotope Fractionation During Planetesimal Core Crystallization, in Proceedings Lunar and Planetary Science Conference2016, Volume 47, p. 1231.

Hsu, W., Huss, G. R., and Wasserburg, G. J., 2000, Ion probe measurements of Os, Ir, Pt, and Au in individual phases of iron meteorites: Geochimica et Cosmochimica Acta, v. 64, no. 6, p. 1133-1147.

Huang, S., and Humayun, M., Osmium isotope anomalies in group IVB irons: cosmogenic or nucleosynthetic contributions, in Proceedings Lunar and Planetary Science Conference2008, Volume 39, p. 1168.

Jana, D., and Walker, D., 1997, The impact of carbon on element distribution during core formation: Geochimica et Cosmochimica Acta, v. 61, no. 13, p. 2759-2763.

Jones, J. H., and Drake, M. J., 1983, Experimental investigations of trace element fractionation in iron meteorites, II: The influence of sulfur: Geochimica et Cosmochimica Acta, v. 47, no. 7, p. 1199-1209.

Jones, J. H., and Malvin, D. J., 1990, A nonmetal interaction model for the segregation of trace metals during solidification of Fe-Ni-S, Fe-Ni-P, and Fe-Ni-SP alloys: Metallurgical transactions B, v. 21, no. 4, p. 697-706.

Kelly, W. R., and Larimer, J. W., 1977, Chemical fractionations in meteorites—VIII. Iron meteorites and the cosmochemical history of the metal phase: Geochimica et Cosmochimica Acta, v. 41, no. 1, p. 93-111.

Kracher, A., Kurat, G., and Buchwald, V., 1977, Cape York: The extraordinary mineralogy of an ordinary iron meteorite and its implication for the genesis of III AB irons: Geochemical Journal, v. 11, no. 4, p. 207-217.

Luck, J.-M., Birck, J.-L., and Allegre, C.-J., 1980, 187Re–187Os systematics in meteorites: early chronology of the Solar System and age of the Galaxy.

McCoy, T., Walker, R., Goldstein, J., Yang, J., McDonough, W., Rumble, D., Chabot, N., Ash, R., Corrigan, C., and Michael, J., 2011, Group IVA irons: New constraints on the crystallization and cooling history of an asteroidal core with a complex history: Geochimica et Cosmochimica Acta, v. 75, no. 22, p. 6821-6843.

McCoy, T. J., Mittlefehldt, D. W., and Wilson, L., 2006, Asteroid differentiation: Meteorites and the early solar system II, p. 733-745.

Morgan, J. W., Horan, M. F., Walker, R. J., and Grossman, J. N., 1995, Rheniumum concentration and isotope systematics in group IIAB iron meteorites: Geochimica et Cosmochimica Acta, v. 59, no. 11, p. 2331-2344.

Morgan, J. W., Walker, R. J., and Grossman, J. N., 1992, Rhenium-osmium isotope systematics in meteorites I: Magmatic iron meteorite groups IIAB and IIIAB: Earth and Planetary Science Letters, v. 108, no. 4, p. 191-202.

Mullane, E., Alard, O., Gounelle, M., and Russell, S., 2004, Laser ablation ICP-MS study of IIIAB irons and pallasites: constraints on the behaviour of highly siderophile elements during and after planetesimal core formation: Chemical geology, v. 208, no. 1, p. 5-28.

Olsen, E., and Fredriksson, K., 1966, Phosphates in iron and pallasite meteorites: Geochimica et Cosmochimica Acta, v. 30, no. 5, p. 459IN1461-460470.

Olsen, E. J., Kracher, A., Davis, A. M., Steele, I. M., Hutcheon, I. D., and Bunch, T., 1999, The phosphates of IIIAB iron meteorites: Meteoritics & Planetary Science, v. 34, no. 2, p. 285-300.

Papanastassiou, D., Shen, J., and Wasserburg, G., 1995, Re-Os in FeNi, sulfide, and phosphide: The possible determination of internal isochrons for iron meteorites: Meteoritics, v. 30.

Papanastassiou, D., Wasserburg, G., and Shen, J., Re-Os diffusion into massive schreibersite and possible internal isochrons for iron meteorites, in Proceedings Lunar and Planetary Science Conference1996, Volume 27.

Pepperhoff, W., and Acet, M., 2001, Engineering Materials.

Pernicka, E., and Wasson, J. T., 1987, Ru, Re, Os, Pt and Au in iron meteorites: Geochimica et Cosmochimica Acta, v. 51, no. 6, p. 1717-1726.

Poitrasson, F., Levasseur, S., and Teutsch, N., 2005, Significance of iron isotope mineral fractionation in pallasites and iron meteorites for the core–mantle differentiation of terrestrial planets: Earth and Planetary Science Letters, v. 234, no. 1–2, p. 151-164.

Randich, E., and Goldstein, J., 1978, Cooling rates of seven hexahedrites: Geochimica et Cosmochimica Acta, v. 42, no. 3, p. 221-233.

Rasmussen, K. L., Malvin, D. J., Buchwald, V. F., and Wasson, J. T., 1984, Compositional trends and cooling rates of group IVB iron meteorites: Geochimica et Cosmochimica Acta, v. 48, no. 4, p. 805-813.

Rasmussen, K. L., Malvin, D. J., and Wasson, J. T., 1988, Trace element partitioning between taenite and kamacite; relationship to the cooling rates of iron meteorites: Meteoritics, v. 23, no. 2, p. 107-112.

Rasmussen, K. L., Ulff-Møller, F., and Haack, H., 1995, The thermal evolution of IVA iron meteorites: Evidence from metallographic cooling rates: Geochimica et Cosmochimica Acta, v. 59, no. 14, p. 3049-3059.

Richter, F. M., Dauphas, N., and Teng, F.-Z., 2009, Non-traditional fractionation of non-traditional isotopes: evaporation, chemical diffusion and Soret diffusion: Chemical Geology, v. 258, no. 1, p. 92-103.

Richter, F. M., Davis, A. M., DePaolo, D. J., and Watson, E. B., 2003, Isotope fractionation by chemical diffusion between molten basalt and rhyolite: Geochimica et Cosmochimica Acta, v. 67, no. 20, p. 3905-3923.

Roskosz, M., Luais, B., Watson, H. C., Toplis, M. J., Alexander, C. M. D., and Mysen, B. O., 2006, Experimental quantification of the fractionation of Fe isotopes during metal segregation from a silicate melt: Earth and Planetary Science Letters, v. 248, no. 3, p. 851-867.

Roy-Barman, M., 1993, Mesure du rapport 187Os-186Os dans les basaltes et les péridotites: contribution à la systématique 187Re-187Os dans le manteau [Thesis: Université de Paris VII.

Sakakibara, N., Takahashi, Y., Okumura, K., Hattori, K. H., Yaita, T., Suzuki, K., and Shimizu, H., 2005, Speciation of osmium in an iron meteorite and a platinum ore specimen based on X-ray absorption fine-structure spectroscopy: Geochemical Journal, v. 39, no. 4, p. 383-389.

Schauble, E. A., 2004, Applying stable Isotope fractionation theory to new systems: Reviews in Mineralogy and Geochemistry, v. 55, p. 65-111.

Scott, E. D., 1972, Chemical fractionation in iron meteorites and its interpretation: Geochimica et Cosmochimica Acta, v. 36, no. 11, p. 1205-1236.

Scott, E. R., and Wasson, J. T., 1975, Classification and properties of iron meteorites: Reviews of Geophysics, v. 13, no. 4, p. 527-546.

Shahar, A., Hillgren, V. J., Young, E. D., Fei, Y., Macris, C. A., and Deng, L., 2011, High-temperature Si isotope fractionation between iron metal and silicate: Geochimica et Cosmochimica Acta, v. 75, no. 23, p. 7688-7697.

Shahar, A., Ziegler, K., Young, E. D., Ricolleau, A., Schauble, E. A., and Fei, Y., 2009, Experimentally determined Si isotope fractionation between silicate and Fe metal and implications for Earth's core formation: Earth and Planetary Science Letters, v. 288, no. 1, p. 228-234.

Shen, J. J., Papanastassiou, D. A., and Wasserburg, G. J., 1996, Precise Re Os determinations and systematics of iron meteorites: Geochimica et Cosmochimica Acta, v. 60, no. 15, p. 2887-2900.

Shirey, S. B., and Walker, R. J., 1995, Carius tube digestion for low-blank rhenium-osmium analysis: Analytical Chemistry, v. 67, no. 13, p. 2136-2141.

Smoliar, M. I., Walker, R. J., and Morgan, J. W., 1996, Re-Os Ages of Group IIA, IIIA, IVA, and IVB Iron Meteorites: Science, v. 271, no. 5252, p. 1099-1102.

Ulff-Møller, F., 1998, Effects of liquid immiscibility on trace element fractionation in magmatic iron meteorites: A case study of group IIIAB: Meteoritics & Planetary Science, v. 33, no. 2, p. 207-220.

Urey, H. C., 1947, The thermodynamic properties of isotopic substances: Journal of the Chemical Society (Resumed), p. 562-581.

van Acken, D., Humayun, M., Brandon, A. D., and Peslier, A. H., 2012, Siderophile trace elements in metals and sulfides in enstatite achondrites record planetary differentiation in an enstatite chondritic parent body: Geochimica et Cosmochimica Acta, v. 83, p. 272-291.

Walker, R. J., 2012, Evidence for homogeneous distribution of osmium in the protosolar nebula: Earth and Planetary Science Letters, v. 351–352, p. 36-44.

Walker, R. J., McDonough, W. F., Honesto, J., Chabot, N. L., McCoy, T. J., Ash, R. D., and Bellucci, J. J., 2008, Modeling fractional crystallization of group IVB iron meteorites: Geochimica et Cosmochimica Acta, v. 72, no. 8, p. 2198-2216.

Walker, R. J., Morgan, J. W., Beary, E. S., Smoliar, M. I., Czamanske, G. K., and Horan, M. F., 1997, Applications of the 190Pt 186Os isotope system to geochemistry and cosmochemistry: Geochimica et Cosmochimica Acta, v. 61, no. 22, p. 4799-4807.

Wasson, J., and Richardson, J., 2001, Fractionation trends among IVA iron meteorites: Contrasts with IIIAB trends: Geochimica et Cosmochimica Acta, v. 65, no. 6, p. 951-970.

Wasson, J. T., 1967, The chemical classification of iron meteorites: I. A study of iron meteorites with low concentrations of gallium and germanium: Geochimica et cosmochimica acta, v. 31, no. 2, p. 161-180.

Wasson, J. T., 1999, Trapped melt in IIIAB irons; solid/liquid elemental partitioning during the fractionation of the IIIAB magma: Geochimica et Cosmochimica Acta, v. 63, no. 18, p. 2875-2889.

Wasson, J. T., Huber, H., and Malvin, D. J., 2007, Formation of IIAB iron meteorites: Geochimica et Cosmochimica Acta, v. 71, no. 3, p. 760-781.

Watson, H. C., Richter, F., Liu, A., and Huss, G. R., 2016, Iron and nickel isotope fractionation by diffusion, with applications to iron meteorites: Earth and Planetary Science Letters, v. 451, p. 159-167.

Weyer, S., Anbar, A. D., Brey, G. P., Münker, C., Mezger, K., and Woodland, A. B., 2005, Iron isotope fractionation during planetary differentiation: Earth and Planetary Science Letters, v. 240, no. 2, p. 251-264.

Williams, H. M., and Archer, C., 2011, Copper stable isotopes as tracers of metal–sulphide segregation and fractional crystallisation processes on iron meteorite parent bodies: Geochimica et Cosmochimica Acta, v. 75, no. 11, p. 3166-3178.

Williams, H. M., Markowski, A., Quitté, G., Halliday, A. N., Teutsch, N., and Levasseur, S., 2006, Fe isotope fractionation in iron meteorites: New insights into metal-sulphide segregation and planetary accretion: Earth and Planetary Science Letters, v. 250, no. 3–4, p. 486-500.

Willis, J., and Goldstein, J. I., 1982, The effects of C, P, and S on trace element partitioning during solidification in Fe-Ni alloys: Journal of Geophysical Research: Solid Earth, v. 87, no. S01.

Wittig, N., Humayun, M., Brandon, A. D., Huang, S., and Leya, I., 2013, Coupled W–Os–Pt isotope systematics in IVB iron meteorites: In situ neutron dosimetry for W isotope chronology: Earth and Planetary Science Letters, v. 361, p. 152-161.

Wood, B. J., Walter, M. J., and Wade, J., 2006, Accretion of the Earth and segregation of its core: Nature, v. 441, no. 7095, p. 825-833.

Wood, J. A., 1964, The cooling rates and parent planets of several iron meteorites: Icarus, v. 3, no. 5-6, p. 429-459.

Yang, C.-W., Williams, D., and Goldstein, J., 1996, A revision of the Fe-Ni phase diagram at low temperatures (< 400 C): Journal of phase equilibria, v. 17, no. 6, p. 522-531.

Yang, J., and Goldstein, J. I., 2006, Metallographic cooling rates of the IIIAB iron meteorites: Geochimica et Cosmochimica Acta, v. 70, no. 12, p. 3197-3215.

Yang, J., Goldstein, J. I., Michael, J. R., Kotula, P. G., and Scott, E. R. D., 2010, Thermal history and origin of the IVB iron meteorites and their parent body: Geochimica et Cosmochimica Acta, v. 74, no. 15, p. 4493-4506.

Yang, J., Goldstein, J. I., and Scott, E. R., 2008, Metallographic cooling rates and origin of IVA iron meteorites: Geochimica et Cosmochimica Acta, v. 72, no. 12, p. 3043-3061.

Young, E. D., Manning, C. E., Schauble, E. A., Shahar, A., Macris, C. A., Lazar, C., and Jordan, M., 2015, High-temperature equilibrium isotope fractionation of non-traditional stable isotopes: Experiments, theory, and applications: Chemical Geology, v. 395, no. 0, p. 176-195.

− CHAPTER 5 −

Synthesis and Outlook

SYNTHESIS AND OUTLOOK

Over recent years there has been a significant expansion of geochemical tools. Nevertheless, fundamental questions pertaining to planetary differentiation, core solidification, and the early evolution of the Earth remain unanswered. To that end, this thesis has explored, for the first time, the mass-dependent fractionation of stable isotopes of osmium in a variety of terrestrial and extra-terrestrial systems. Osmium has several chemical characteristics that make it distinct from other elements. It is a highly siderophile and highly refractory element, that is chalcophile under the conditions that prevail in Earth's mantle, and compatible during mantle melting. Osmium is, therefore, potentially a powerful element for understanding processes associated with planetary differentiation, core formation, and for examining the formation, differentiation, and early history of planetary bodies. Prior to this study, Os has been considered in terms of its abundance, radiogenic isotopes, and mass-independent stable isotope variation, but mass-dependent variations have not yet been considered, largely due to the high mass of Os. This high mass, in turn, led to the expectation that any mass-dependent variations in Os isotopes would be minor and difficult to detect with current analytical capabilities because the extent of stable isotope variation usually diminishes with increasing mass. However, the detection of stable isotope variation in other high mass elemental systems, such as U and Tl, suggests that there is potential for high mass stable isotope systems to be used as geochemical tools.

CHAPTER 2 - In Chapter 2, the first objective of this thesis was addressed; namely, the development of a method to obtain high-precision Os stable isotope compositions of natural samples. The new method developed here uses a double spike technique to correct for non-natural mass-dependent fractionation induced during chemical purification or analysis. The most optimal spike isotope and sample:spike ratio, a ^{188}Os-^{190}Os spike, mixed with sample in a 55:45 ratio, were determined. Repeat measurement of the reference standard DROsS demonstrated that stable osmium isotope measurements can be obtained to a precision of ~0.01‰ amu^{-1} and with an external reproducibility of ~0.02‰ amu^{-1}. This is in good agreement with a calculated theoretical error based on current analytical capabilities. A similar precision and reproducibility were obtained for geological reference materials, i.e., peridotites, chromitites, chondrites. The method was developed for both MC-ICP-MS and N-TIMS, to permit measurement of samples over a large range of concentrations. For example, analysis by MC-ICP-MS is optimal for samples having ≥ 200 ng natural Os, whereas N-TIMS analyses are better for samples with lower Os abundances. This is because, at lower Os abundances, MC-ICP-MS analyses are not only less precise, but are also more sensitive to background effects. The N-TIMS provided accurate data when analyses were performed at total Os beam intensities of >1V, which was regularly achieved for sample loads of ≥5 ng natural Os. Following establishment of a reliable method, this new geochemical tool was used to examine a number of high-temperature settings, as discussed in Chapter 4 and 5 and below.

For future studies, it may be beneficial to utilize more sensitive resistors (i.e., 10^{12} or 10^{13} Ω) for N-TIMS analyses. This could allow the study of samples with lower quantities of Os, as the main limitation at the

moment is the uncertainty that is introduced by the oxygen correction when total Os beam intensities drop below 1 V. A potential study area of interest would be to determine the stable Os isotope composition of sulphides, to trace down inter-mineral fractionation. This could provide information about partial melt depletion or metasomatic events. Where this thesis has focused on high-temperature processes, the method could also be applied for studying the fractionation of Os during many low temperature processes. Considering that the degree of mass-dependent fractionation is inversely correlated with temperature, the variation in stable osmium isotope fractionation as a consequence of low-temperature processes may well be substantial. For example, to quantify the degree of alteration, to examine redox processes in oceanic shales resulting from meteorite impacts, or for application to oceanography by studying Fe-Mn nodules.

CHAPTER 3 - Chapter 3 presented the first ever study to consider stable Os isotope fractionation in geological materials. The main aim was to better constrain the abundance of highly siderophile elements (HSE) in the Earth's mantle. Furthermore, the aim was to better understand the timing and extent of late accreted meteoritic material, as well as how this subsequently mixed into the mantle. An extensive set of ordinary, enstatite, and carbonaceous chondrites was shown to possess a homogeneous stable Os isotope composition. This indicates that the bulk composition of the solar nebula is likely homogeneous, and, thus, that secondary processes such as oxidative loss of oxides, did not significantly affect stable Os isotope systematics. Samples from the Earth's mantle, including four reference materials and xenoliths from Kilbourne Hole, showed larger variability in the mass-dependent Os isotopic compositions, with resolvable variations within samples from Kilbourne Hole. This was interpreted to represent inter-mineral fractionation either during melt depletion or late-stage alteration of sulphides. However, taking an average of all mantle samples analysed within this study, the Earth's mantle samples yield a stable Os isotope composition within analytical uncertainty of that of chondrites. This either implies that metal-silicate segregation did not result in Os stable isotope fractionation, or that a signature as a result of core formation was overprinted by late-accreted material with a broadly chondritic bulk composition. If the latter is the case, preliminary results for Archean samples argue for efficient mixing of Os derived from late-accreted material into the mantle.

For future studies, it would be of interest to better constrain the extent of Os stable isotope fractionation as a consequence of metal-silicate differentiation. Achondrites would be a good candidate, as these rocks are thought to represent bodies that have undergone variable degrees of metal-silicate segregation (e.g., Warren et al., 2006). When investigating these rocks, attention should be paid to the extent of alteration that samples have experienced. This is because the Kilbourne Hole xenoliths indicate that the breakdown of phases and subsequent removal of the oxidized material during alteration of rocks at the Earth's surface might be a source of fractionation. Another way to examine the effect of metal-silicate segregation, would be to undertake a metal-silicate experimental study. However, the preferential partitioning of Os into the metal phase, combined with the general small size of these experiment will make such a study challenging.

The mantle samples studied for this study provide a first estimate of the stable Os isotope composition of Earth's mantle. For future studies, it would be useful to expand the range of terrestrial samples by

incorporating different mantle rock types. For example, abyssal peridotites to characterize the depleted MORB (mid-oceanic ridge basalts) mantle (DMM). It would also be interesting to investigate a larger sample set of Archean mantle rocks covering a wider range of ages. This could provide some insight into the efficiency of mixing of late veneer material. The samples used by Maier et al. (2009) may be good targets for such a study. In working with these samples it is of importance to consider supergene weathering. Breakdown of sulphides to sulphates could potentially fractionate Os isotopes and drive an original primary signature to lighter value. A mineral-scale study should be performed to examine if inter-mineral fractionation may have taken place. With the current analytical capacities, the low Os concentrations could be a limitation. One option to overcome this would be to manually select different populations, and combine these for a single measurement.

CHAPTER 4 - The objective of the study reported in Chapter 4 was to better understand processes associated with planetary core solidification. To this end, iron meteorites that are thought to represent the cores of differentiated parent bodies that have experienced fractional crystallization were investigated. Two of these groups, the IIAB and IIIAB iron meteorites, display significant stable Os isotope variation ($\delta^{190/188}$Os ranging from 0.05 - 0.49‰), relative to chondrites. On the basis of the observations here, it was concluded that the formation of troilite and schreibersite, or the exsolution of kamacite from taenite did not affect the Os isotopic system substantially. However, it is necessary to quantify this in the future by determining the isotopic signature of schreibersite and troilite, and by performing transects in the metal adjacent to non-metal phases. For kamacite and taenite, a similar study could be accomplished. Potentially, this could provide valuable information on diffusion and cooling rates in metallic systems. The observed variations are likely related to multiple processes that occurred during core solidification, including fractional crystallization, that created mass-dependent stable Os isotope fractionation. The new data, along with simple fractional crystallization models, require that the IIAB irons experienced a more complex crystallization history than previously proposed. For the IIIAB iron meteorite group, the data and fractional crystallization modelling provide evidence for mixing of early crystallized solids with more evolved melt. The data for the IVA and IVB iron groups, on the other hand, indicate that the limited Os isotope fractionation might be associated with the lower S abundance in these parent bodies. That the isotopic fractionation factors, deduced from the models, display a negative correlation with S content support this hypothesis. This suggest that stable Os isotopes can be used as a proxy of the S content. To examine this in more detail, an experimental study of coexisting liquid and solid metal under different physical and chemical conditions could provide more clarity.

To conclude, this thesis illustrates the first steps taken to develop and utilize mass-dependent stable Os isotope variations within geo- and cosmo-sciences. This new analytical method provides data of sufficiently high precision that small variations may be detected. The Os stable isotope system, therefore, further contributes to our understanding of processes that have and are acting in our solar system, although there are many open questions and avenues for future research. As analytical techniques and capabilities are improved upon, a wide range of geo- and cosmo-chemical problems could be addressed using the mass-dependent stable Os isotope system.

REFERENCES

Maier, W. D., Barnes, S. J., Campbell, I. H., Fiorentini, M. L., Peltonen, P., Barnes, S.-J., and Smithies, R. H., 2009, Progressive mixing of meteoritic veneer into the early Earth/'s deep mantle: Nature, v. 460, no. 7255, p. 620-623.

Warren, P. H., Ulff-Møller, F., Huber, H., and Kallemeyn, G. W., 2006, Siderophile geochemistry of ureilites: A record of early stages of planetesimal core formation: Geochimica et Cosmochimica Acta, v. 70, no. 8, p. 2104-2126.

− The END −

"EXCELLENT"